Development of optogenetic approaches to modulate synaptic plasticity in the postsynaptic cells

Agnieszka Mirosława Zbela

MSc

Submitted in fulfilment of the requirements for
the degree of Doctor of Philosophy (Medical Studies)

School of Medicine

University of Tasmania

April 2019

Declaration of Originality

This thesis contains no material which has been accepted for a degree or diploma by the University or any other institution, except by way of background information and duly acknowledged in the thesis, and to the best of my knowledge and belief no material previously published or written by another person except where due acknowledgement is made in the text of the thesis, nor does the thesis contain any material that infringes copyright.

Agnieszka Zbela
December 2018

Authority of Access

This thesis may be made available for loan and limited copying and communication in accordance with the Copyright Act 1968.

Agnieszka Zbela
December 2018

Statement of Ethical Conduct

The research associated with this thesis abides by the international and Australian codes on human and animal experimentation, the guidelines by the Australian Government's Office of the Gene Technology Regulator and the rulings of the Safety, Ethics and Institutional Biosafety Committees of the University.

Agnieszka Zbela
December 2018

Acknowledgements

My sincere gratitude goes to my supervisors, Dr John Lin, Dr David Gell and Prof. Lisa Foa, who gave me the opportunity to carry out this project. Thank you for being the exemplary advisors and mentors over these years. Your ever-present support and advice have been the valuable parts of this project. Thanks to this project you light up my life (literally). John, you taught me how to be more independent and how to collaborate with scientists from all around the world. You always encouraged me to present my work at conferences and to receive a scientific training from the experts in the field. David, you trusted in my skills and gave me the chance to become a researcher. I thank you for endless stimulating discussions. Lisa, you showed me how to tell a scientific story. You always pointed positive things when my criticism turned into pessimism. Thank you!

I wish to thank our collaborators, Prof. Gavan McNally and Dr Zayra Millan from the University of New South Wales, who helped to check the expression of my photoactivatable system *in vivo*. Thank you for hosting me in your laboratory and teaching stereotactic surgery.

My warm thanks go to Dr Macarena Pavez, who helped with the experiment of growth cone turning. Thank you for being a wonderful and supportive friend.

Many thanks go out to current and former members of the Foa/Small/Young/Lin groups. I was lucky to work with friendly and supportive people, who were always ready to share their knowledge and expertise. Special thanks to Jenny Smith for your skilful technical assistance and many science-free chats. Thanks to all marvellous and talented friends, whom I have met: Elise Devenish, Jayde Lockyer, Andrew Reading, Silvia Vicenzi, Solene Ferreira, Yilan Zhen, Raphael Ricci. I shared many memorable moments with you!

My loving thanks go to my husband Konrad. You are my most significant result from the high school. Thank you for being there when my gel went wrongly or cells behaved badly. Your support and patiance have been valuable, especially during the grand finale. You have always reminded me that there is life outside of the lab. Thanks to you, I am in the right place!

I would like to thank my mum Anna and my dad Mirosław for your love and great faith in me. My warm thanks belong to my brother Sebastian, his fiancée Asia and their adorable daughter Karolcia for brightening my life with great photos. Many thanks go to my grandparents and in-law family for your constant support and encouragement.

Table of contents

List of abbreviations

AAV	Adeno-associated virus
AKT	Protein kinase B
AMPAR	α-amino-3-hydroxy-5-methyl-4-isoxazolepropionic acid receptor
BDNF	Brain-derived neurotrophic factor
BphP1-Q-PAS1	Near-infrared light-induced heterodimerizing system
CAAX	C-terminal prenylation tag to localized proteins in membrane
CaMKII	Ca^{2+}/calmodulin-dependent protein kinase II
ChR-2	Channelrhodopsin-2
CIB1	Light-dependent Cry2-interacting protein
CID	Chemically induced dimerizer
CLICR	Clustering Indirectly using Cryptochrome 2
CPH1S	Cyanobacterial phytochrome 1 from *Synechocystis*
Cry2	Cryptochrome 2 from *Arabidopsis thaliana*
DAG	Diacylglycerol
DRG	Dorsal root ganglion neurons
EPSC	Excitatory postsynaptic current
EPSP	Excitatory postsynaptic potential
ERK1/2	Extracellular signal-regulated kinase 1/2
FAD	Flavin adenine dinucleotide
FBS	Fetal bovine serum
FGF	Fibroblast growth factor
FGFR1	Fibroblast growth factor receptor 1
$FKBP_{F36v}$	FK506 binding protein domain
FMN	Flavin mononucleotide
FRS2	Fibroblast growth factor receptor substrate 2
GAB1	GRB-associated binder-1
GRB2	Growth factor receptor-bound protein 2
GTPase	Guanosine triphosphate hydrolase enzymes
HEK293A/T	Human embryonic kidney cells
HeLa	Human cell line from cervical cancer
HR	Halorhodopsin

iLID/SspB	Blue light-induced heterodimerizing system
Ins(1,4,5)P_3 or IP_3	Inositol-1,4,5-trisphosphate
iRFP682	Near-infrared fluorescent protein
ITR	Inverted terminal repeat
kbp	Kilobase pairs
LOV	Light-oxygen-voltage sensing domain
LTD	Long-term depression
LTP	Long-term potentiation
mA	milliampere
MAPK	Mitogen-activated protein kinase
MEK	Mitogen-activated protein kinase kinase
mEPSC	Miniature excitatory postsynaptic current
mW/cm^2	milliwatt per square centimetre
MYR	N-terminal myristoylation tag to localized proteins in membrane
NGF	Nerve growth factor
NIH 3T3	Mouse embryo fibroblast
NLS	Nuclear localisation signal
NMDAR	N-methyl-D-aspartate receptor
NSC	Adult neural stem cells
NT-3	Neurotrophin-3
NT-4	Neurotrophin-4
O-GECO1	Orange fluorescent genetically encoded calcium indicator 1
optoTrkB	Light-activated full-length TrkB
p75	Pan-neurotrophin receptor
paAIP2	Photoactivatable autocamtide inhibitory peptide 2
PAK	Ser/Thr-protein kinase
PC12	Rat pheochchromocytoma cell line
PCB	Tetrapyrrole phycocyanobillin
PDGFRβ	Platelet-derived growth factor receptor β
PDPK1	3-phosphoinositide-dependent protein kinase 1
PH	Pleckstrin homology domain
PHR	Photolyase-homologous region domain of Cry2
PI3K	Phosphatidylinositol 3-kinase

PKC	Protein kinase C
PKMζ	Protein kinase M zeta
PLCγ1	Phospholipase C-γ1
pMag/nMag	Blue light-induced heterodimerizing system called Magnet
poly(A)	Polyadenylation signal
PSD95	Postsynaptic density protein 95
PtdIns(4,5)P_2 or PIP_2	Phosphatidylinositol-4,5-bisphosphate
Rac1	Small GTPase
Raf	Rapidly Accelerated Fibrosarcoma
Ras	Small GTPases
RTKs	Receptor tyrosine kinases
SAP97	Synaptic associated protein 97
SH2	Src homology 2 domain
SHC	(Src homology 2 domain)-containing proteins
SOS	Son of sevenless
STIM1	Stromal interaction molecule 1
T2A	“Self-cleaving” peptide derived from thosea asigna virus 2A
TrkA/B/C	Tyrosine receptor kinase A/B/C
TRPC3	Transient receptor potential cation channel 3
U73122	Inhibitor of PLC
WPRE	Woodchuck hepatitis virus posttranscriptional regulatory element

List of illustrations and tables

List of illustrations

Chapter 2

Chapter 3

Chapter 4

List of tables

Chapter 2

Chapter 3

Appendix

Abstract

Over the last few decades, learning and memory processes have been extensively studied from a variety of perspectives. Long-term potentiation (LTP), the long lasting strengthening of synaptic communications, is a key cellular event associated with learning at the organism level. Even now, 45 years since the first reported LTP recording, a precise molecular mechanism of LTP is still not fully elucidated. Understanding the cellular basis of learning and memory formation is important for the development of novel therapeutic approaches for patients with Alzheimer's disease or post-traumatic stress disorder, or even development of effective education curricula. LTP and its connection with learning have been studied using genetic, pharmaceutical and electrophysiological methods that provided valuable understanding of these processes. An optogenetic approach, that can manipulate the specific biochemical signalling associated with LTP with higher temporal and spatial precision in a genetically defined neuronal population, can provide a better causal and correlative link between LTP and learning. The main goal of this thesis is to generate a new optogenetic tool, which can be ultimately used to influence LTP, utilizing our current knowledge of the molecular mechanisms involved in LTP.

The cellular signalling, targeted in this thesis optogenetically, is the one associated with receptor tyrosine kinase B (TrkB), the receptor for brain-derived neurotrophic factor (BDNF). BDNF and TrkB are implicated in LTP and learning; therefore, optogenetic manipulation of these proteins could directly alter LTP and possibly animal behaviour. TrkB is a typical tyrosine kinase receptor that is located in the plasma membrane and activated through the receptor dimerization (mediated by the extracellular domain upon BDNF binding) and autophosphorylation (mediated by the intracellular kinase domain). TrkB activates three main signalling enzymes: phospholipase C-γ1 (PLCγ1), extracellular signal-regulated kinase (ERK) and AKT kinase. To trigger TrkB signalling in living cells upon blue light stimulation, the kinase domain of TrkB (TrkB(kd)) was attached to a photoreceptor, cryptochrome 2 (Cry2), as a freely diffusive cytosolic recombinant protein. Upon blue light illumination, Cry2 forms homo-oligomers and hetero-oligomers with its binding partner, CIB1. CIB1 was tethered to the plasma membrane. In this design, the intention was to trigger the oligomerization of TrkB(kd)-Cry2 and its recruitment to the membrane via Cry2/CIB1 heterodimerization upon blue light exposure. This led to the activation of TrkB(kd) and consequently initiated biochemical signalling cascades at the plasma membrane.

In this thesis, the designed two-component TrkB system was shown to trigger PLCγ1, ERK and AKT signalling pathways in non-neuronal HEK293 cells as well as in cultured neurons in a light-dependent manner. During the validation process, I discovered that, without the membrane-tethered CIB1 component, TrkB(kd)-Cry2 alone activated ERK and AKT signalling without elevation of intracellular Ca^{2+} that is related to the functional activation of PLCγ1. Additionally, a mutation was introduced in TrkB(kd) that prevented activation of PLCγ1, but still allowed ERK and AKT pathways to be triggered upon light stimulation. These two observations might have a practical application for dissecting biochemical signalling by TrkB, which is still not completely understood in LTP. Preliminary experiments in DRG neurons demonstrated that varying the amount of light caused contradictory responses of a growth cone, attraction or repulsion, when TrkB(kd)-Cry2 and CIB1 were used. The TrkB(kd)-Cry2 component alone was not able to change the growth cone turning in DRG neurons. These results suggest important roles of PLCγ1 and Ca^{2+} in axon steering over short timescales (minutes), but minimal effects of ERK and AKT on these timescales. Finally, the TrkB system was successfully introduced into the amygdala region of a freely behaving rat.

In this study, the process of designing and validating the optogenetic TrkB tool is presented as a part of broad project that ultimately aims to manipulate LTP and learning. This new photoactivatable TrkB system has several advantages over previously published optogenetic tools, which make it unique for *in vivo* applications in subsequent studies. This tool (1) can be packaged into recombinant adeno-associated viral vectors (AAV), (2) cannot be activated by endogenous BDNF due to the lack of TrkB extracellular domain, (3) provide separate controls of different biochemical pathways when used without membrane-tethered CIB1 or when specific mutation is introduced into TrkB(kd). Together this provides an exciting new approach to investigate how manipulation of BDNF/TrkB signalling affects learning and memory in awake behaving animals.

Chapter 1

Introduction and literature review

1.1 Basis of learning and memory formation

One of the most fascinating functions of the brain is the ability to acquire, store and retrieve information. Over the last few decades, learning and memory processes at the systematic, cellular and molecular levels remain the focus of intense research. Learning is the act of acquiring new information, whereas memory refers to recall of learned information.

Human memory is often categorized based on qualitatively different systems of information storage. According to this classification, there are two major memory systems in the brain: declarative (explicit) and non-declarative (implicit or procedural). Declarative memory can be defined as conscious storage of information about events and facts, such as people, places or objects. This type of memory can be verbalized. Establishing new declarative memories requires the medial temporal lobe structures (especially the hippocampus). In contrast, non-declarative memory includes motor skills, habits, procedures and any other information for which acquisition and retrieval do not depend on a conscious effort. Implicit memory involves different brain structures depending on the type of learning, for instance, cerebellum, amygdala or cortex (Mayford et al., 2012; Purves, 2004). The clinical case studies of Henry G. Molaison (known as Patient H.M.) provided valuable insights into the memory organization in the brain. H.M. had suffered from disabling epileptic seizures and was subject to a bilateral temporal medial lobe resection (including the hippocampus). After the surgery, H.M. was unable to form new declarative memories, whereas his ability to form procedural memories was intact (Annese et al., 2014; Lombroso and Ogren, 2009; Purves, 2004). This clinical case provided the important classification of memory as well as the localization of memory storage in the brain. However, the study did not provide insight into molecular mechanisms of memory.

In addition to the declarative and non-declarative classification of memories, memory can be also categorized according to the length of time that information is retained. These temporal categories of memory include short-term (immediate), working and long-term memory (Purves, 2004). Short-term memory is the routine ability to retain information for a brief moment (a memory of ongoing experiences). Working memory is the ability to hold information in mind for a period of time required for a cognitive process. For instance, the

performance of a simple mathematical calculation requires the information to be temporarily retained, utilized and then discarded (Slaughter, 2002). Finally, long-term memory is the storage of information in more permanent form for days, weeks or lifetime (Purves, 2004). This type of memory is created when short-term memories are converted into long-term ones in a process known as consolidation, which involves the hippocampus. The role of the hippocampus in consolidation was discovered from the studies on patient H.M., who was able to recall old memories without the ability to consolidate new ones into long-term memories (Annese et al., 2014).

In neuroscience, a general hypothesis postulates that long-term memory storage requires long-lasting changes in neurons. Synapses, the subcellular structures that mediate the communications between two neurons, have been proposed to be the cellular site of memory storage (Mayford et al., 2012). In 1949, Donald Hebb proposed the mechanism of neuronal adaptation during learning and memory formation. He argued that synaptic connections could be considered as the basis of mental associations (Hebb, 1949). His theoretical concept suggested that the modulation of synaptic connectivity is a key property of the mechanism of learning and memory. The objective of this chapter is to overview what is known about the cellular and molecular mechanisms underlying learning and memory formation, especially as relates to Hebbian plasticity.

1.1.1 Hebbian theory of synaptic plasticity

The Hebbian theory explains the basic mechanism for synaptic plasticity, which is defined as a change in the efficiency in synaptic signalling. The Hebbian plasticity theory proposes that memories are formed through increasing the efficiency of synaptic transmission called "synaptic strength" (Hebb, 1949; Vitureira and Goda, 2013). As a general rule, this synaptic transmission is initiated at presynaptic termini of synapses and involves neurotransmitter release. The released neurotransmitters diffuse across synaptic clefts and bind to the neurotransmitter receptors on the surface of postsynaptic cells (Vitureira and Goda, 2013). Synaptic efficiency is controlled by the neurotransmitter release probability (the likelihood of neurotransmitter exocytosis from the presynaptic neuron upon arrival of an action potential) and the number of available neurotransmitter receptors in the postsynaptic neuron (Del Castillo and Katz, 1954; Vitureira and Goda, 2013). According to the Hebbian theory, the long-lasting stimulation of a synapse, for instance during a learning process, may increase the efficiency of that synapse. Considering changes to parameters mentioned

previously, how can synaptic connections become strengthened as we learn? Firstly, when the neurotransmitter release probability is higher, then more glutamate (neurotransmitter) may be released from the presynaptic neuron. Secondly, the number of available neurotransmitter receptors on the postsynaptic site may be increased. Finally, these receptors may be more responsive to glutamate which may lead to the longer period of their open state and to the higher influx of ions to the postsynaptic cell (Lombroso and Ogren, 2009). These mechanisms can mediate a stronger response to a prolonged stimulation.

Moreover, the increased synaptic efficiency seems to correlate with an increased size of synapse. On the postsynaptic neurons, dendritic spines, small protrusions from dendritic branches, underwent enlargement upon repetitive glutamate uncaging protocol, known to induce structural synaptic plasticity (Matsuzaki et al., 2004). These results suggest that spines can be critical sites for memory storage. Showing that stimulated spines displayed long-lasting changes follows the Hebbian concept of learning.

In Hebbian plasticity, three critical features can be highlighted: synapse specificity, associativity and cooperativity. The induction of Hebbian plasticity is synapse specific and associative because strengthening of a presynaptic input onto a postsynaptic cell is possible when both pre- and postsynaptic neurons are coactivated at the same time to become associated (Mayford et al., 2012; Vitureira and Goda, 2013). In other words, Hebbian plasticity generates positive feedback which means that when a synapse is activated once, it can undergo further potentiation with greater ease (Vitureira and Goda, 2013). Association also refers to the process when a weak input is coupled with strong one and as a result of this, the weak input alone can become strengthened (Mayford et al., 2012). Finally, Hebbian plasticity is cooperative because numerous inputs have to be activated simultaneously to depolarize the adjacent postsynaptic neuron (Mayford et al., 2012). These features also describe durable forms of Hebbian synaptic plasticity, including long-term potentiation (LTP) and long-term depression (LTD). This chapter discusses mostly LTP as a model of changes in the strength of synaptic effects during learning and implicated in the memory formation.

A particularly challenging question in neuroscience has been: how do synaptic changes take place during learning? A crude, but very effective, approach to reveal the brain regions responsible for specific learning and memory formation is a controlled lesion in rodents, akin to the clinical case of H.M. (Elgersma and Silva, 1999). However, this approach does not reveal how learning processes change the connection between neurons. In 1970s, Eric Kandel and his colleagues made direct observations of synaptic changes during learning in the sea slug *Aplysia californica*. They described two forms of synaptic plasticity in this organism.

Touching the animal's siphon resulted in the gill withdrawal, but after repeated occurrences of this stimulation, the slug's response exhibited habituation such that the gill withdrawal became weaker. In the next experiment, touching the siphon was paired with an electrical stimulation to the animal's tail which triggered the strong gill withdrawal once again. This synaptic plasticity is called sensitization (Carew et al., 1971; Castellucci et al., 1978). The Kandel's group identified the set of synapses involved in the gill withdrawal behaviour. Moreover, their results provided an explanation for short- and long-term changes in synapses underlying associative and non-associative learning in a simple invertebrate system.

The direct observations of synaptic plasticity during mammalian learning are difficult because of the complexity of a brain. Nevertheless, there is strong evidence that synaptic plasticity is associated with emotional (fear) learning in amygdala in animals and humans (Adolphs et al., 1994; Davis et al., 1994). In these studies, fear conditioning, as a model for emotional learning in animals, was used. Measurements of synaptic strength in amygdala slices from fear-conditioned rats showed synaptic alterations induced by whole-animal emotional learning in comparison with naïve animals (McKernan and Shinnick-Gallagher, 1997). Similar observations were made in freely behaving rats that underwent fear-conditioning (Rogan et al., 1997). Interesting data were published by Johansen and colleagues in 2014 who provided evidence that Hebbian mechanism is necessary, but not sufficient, to generate synaptic plasticity in the lateral amygdala of rats under moderate training conditions. Direct manipulations of amygdala pyramidal cells (important for storing aversive memories) using light suggested that another form of synaptic plasticity has to be co-activated to form associative and aversive memories (Johansen et al., 2014). These results displayed the existence of different forms of synaptic plasticity. They showed that the direct relationship between synaptic plasticity and memory formation is more complex than a simple correspondence. Synaptic plasticity is not a unitary process which means that it can be seen as many processes harmonizing together during learning to create memories.

1.2 Synaptic mechanism of learning and memory

The Hebbian theory highlights that synapses are the critical sites for memory induction and storage. This synaptic hypothesis represents a concept that the creation of memories and their retention is associated with alterations in the strength of individual synapses between neurons. Two electrophysiological phenomena, LTP and LTD, are thought to occur to generate changes in synapse strength (Malenka and Nicoll, 1999; Slaughter, 2002).

LTP is a long-lasting enhancement of synaptic activity, classically evoked by brief high-frequency electrical stimulation of synapse. In contrast to LTP, LTD can be described as a long-term reduction of synaptic activity that is classically induced by low-frequency prolonged stimulation (Bear and Malenka, 1994). LTP is now used as a model of synaptic changes during learning and memory formation, is studied extensively. For example, a simple PubMed search with the keywords "long-term potentiation" retrieves more than 16,000 scientific articles. This section aims to summarize the existing understanding of LTP and its relationship with learning and memory formation.

1.2.1 Long-term potentiation as a neurobiological model of learning and memory

The first official report of LTP (then called long-lasting potentiation) was published in 1973. This paper highlighted immediately the possible role of LTP in the explanation of learning and memory processes (Bliss and Lomo, 1973). One of these authors described how LTP was discovered "by chance, not by pursuit of an idea. I happened to be in the right labs at the right time, presented with experimental preparations hiding secrets ready to be uncovered with the methods at hand" (Lomo, 2015). The experiments in question were conducted in the dentate gyrus of the hippocampal formation in anaesthetized rabbits. The recording electrode was placed beneath the molecular layer of the dentate area to record excitatory postsynaptic potentials (EPSPs) in granule cells evoked by the electrical stimulation of perforant fibres (Bliss and Lomo, 1973). When brief bursts of high-frequency electric stimulation (known as tetanus) of the perforant path were done, the amplitude of the recorded EPSP in granule cells increased for a very long period, sometimes up to ten hours after the last train (Bliss and Lomo, 1973; Lomo, 2015). The occurrence of LTP was subsequently confirmed in the dentate gyrus in rats (Douglas and Goddard, 1975) and *in vitro* in hippocampal slices from guinea pigs (Schwartzkroin and Wester, 1975). The terminology long-term potentiation (instead of "long-lasting") and the acronym LTP were then standardized in the field (Alger and Teyler, 1976; Douglas and Goddard, 1975; Lomo, 2015).

LTP has common features related to Hebbian synaptic plasticity: associativity and cooperativity (as explained in Section 1.1.1). The obvious characteristic of LTP is its duration, which can be hours, days or probably even a lifetime. LTP is also input-specific which means that the increase in synaptic strength is confined to active synapses (Malenka and Nicoll, 1999; Vitureira and Goda, 2013).

As more aspects of LTP have been studied, different phases of LTP have now been defined: an early phase, that is dependent on short-term second messenger alterations, and a late phase which involves the alterations in gene transcription and *de novo* protein synthesis (Luscher and Malenka, 2012). By altering the stimulation conditions, either electrically or chemically, it is possible to manipulate the phases of LTP (Molnar, 2011). The synaptic changes during LTP evolve in overlapping stages that require specific molecular events. Firstly, an LTP-inducing stimulus activates necessary molecular players within approximately one minute (induction) (Murakoshi et al., 2017). The initiated changes in the synapse recruit additional processes to ensure their durability (expression lasting for minutes to hours) and finally, these changes need to be maintained (maintenance lasting for days) (Luscher and Malenka, 2012). The main purpose of the next section is to describe the molecular mechanisms involved in the induction, expression and maintenance of LTP.

1.2.2 Molecular mechanism of LTP

The precise molecular mechanisms underlying the induction, expression and maintenance of the different forms of LTP have been the focus of thousands of research groups around the world. Understanding the molecular changes associated with LTP and memory formation and storage have significant implication for the development of therapeutic approaches. This might be especially relevant in treatment of patients with Alzheimer's disease and drug addiction, two conditions where LTP is disrupted (Crary J. F. et al., 2006; Luscher and Malenka, 2011).

Of the different forms of LTP that have been studied (Malenka and Bear, 2004), the N-methyl-D-aspartate receptor (NMDAR)-dependent LTP at CA1 hippocampal excitatory synapses is one of the most well-characterized forms of LTP and is more common in CNS synapses (Malenka and Bear, 2004; Nicoll, 2003). The molecular mechanism of this type of LTP, as a prototypical form of synaptic plasticity, is presented in this section.

The NMDAR-dependent LTP is induced and expressed in the postsynaptic neurons (Luscher and Malenka, 2012; Nicoll, 2003). The coincidence detection of presynaptic glutamate release and strong depolarization of postsynaptic cells is involved in the induction of NMDAR-dependent LTP. This coincidence detection leads to a rise of intracellular Ca^{2+} in postsynaptic spines. Three simultaneous events are required to trigger LTP: (1) NMDAR activation (Collingridge et al., 1983); (2) large rise in postsynaptic Ca^{2+} (Lynch et al., 1983); (3) depolarization of postsynaptic cells (Malinow and Miller, 1986). This coincident activity

is mostly accomplished by NMDAR and also α-amino-3-hydroxy-5-methyl-4-isoxazolepropionic acid receptor (AMPAR), the two main types of ionotropic ligand-gated ion channels for glutamate.

The excitatory neurotransmitter, glutamate, is released from synaptic vesicles in the presynaptic terminal into the synaptic cleft (Errington et al., 2003). Then, glutamate diffuses and reaches the postsynaptic membrane where it binds to NMDA and AMPA-type glutamate receptors (NMDARs and AMPARs) (Dingledine et al., 1999). AMPARs are permeable to monovalent cations (Na^+ and K^+) and upon activation Na^+ influx is favoured leading to the depolarization of the postsynaptic neuron (Malinow and Miller, 1986). AMPARs are tetrameric and may be composed of one subunit type, or a mixture of four subunit types: GluA1, GluA2, GluA3 and GluA4. (Luscher and Malenka, 2012; Madden, 2002). The composition of subunits in AMPARs, especially the presence of GluA2, has an influence on biophysical properties of AMPARs (Anggono and Huganir, 2012). These receptors can be also permeable to Ca^{2+} (Liu and Zukin, 2007). NMDARs are voltage-dependent glutamate receptors that allow Na^+ and Ca^{2+} to enter the postsynaptic cells (Ascher and Nowak, 1988). Similarly to AMPARs, NMDARs are tetramers composed of two GluN1 subunits and two additional GluN2 or GluN3 subunits (Paoletti et al., 2013). NMDARs have slower kinetics than AMPARs, but higher affinity for glutamate (Luscher and Malenka, 2012). The activation of NMDARs requires two simultaneous events: binding of glutamate to the receptor and strong depolarization of postsynaptic membrane. Strong depolarization is necessary because at near-resting membrane potentials, Mg^{2+} blocks the ion pore of NMDAR to prevent ion conductance. The Mg^{2+} block of the channel is relieved when the membrane is depolarized (Nowak et al., 1984).

The significance of NMDARs in the LTP induction is supported by experiments in which specific antagonists, such as AP5 or CPP, completely inhibited the generation of LTP (Collingridge et al., 1983). In a typical LTP paradigm, LTP is induced when Na^+ influx through AMPARs leads to depolarization of the postsynaptic cells, which relieves the Mg^{2+} block of NMDARs leading to high level of Ca^{2+} influx. This increase in Ca^{2+} concentration within the dendritic spines triggers the activation of intracellular cascades responsible for LTP confined to this specific synapse (Lombroso and Ogren, 2009; Luscher and Malenka, 2012; Malenka and Bear, 2004).

After the influx of Ca^{2+}, the activation of Ca^{2+}/calmodulin dependent protein kinase II (CaMKII), particularly isoform α, is an important event associated with LTP induction (Lisman et al., 2002). It has been shown that approximately one minute of CaMKIIα activity

is sufficient for LTP induction (Murakoshi et al., 2017). CaMKIIα is found in high concentrations in the postsynaptic density (Lee and Yasuda, 2009). X-ray crystallography studies and single particle electron microscopy have revealed that CaMKIIα is a large supramolecular structure consisting of 10–14 subunits (Chao et al., 2011; Kanaseki et al., 1991; Myers et al., 2017). Each subunit comprises an N-terminal catalytic kinase domain followed by a regulatory segment (or autoinhibitory domain), which is characteristic for calmodulin-regulated protein kinases, and C-terminal association (or hub) domain. The regulatory segment contains the regulatory phosphorylation site Thr286 (R1), the intramolecular clamp segment (R2) and the calmodulin-recognition motif (R3) (Chao et al., 2010; Chao et al., 2011). The intramolecular clamp segment fastens the regulatory segment to the kinase domain when CaMKIIα is autoinhibited. Finally, the association domain is responsible for the oligomerization process which helps subunits assemble into a large holoenzyme (Chao et al., 2010; Chao et al., 2011; Lisman et al., 2012). CaMKIIα is activated by binding Ca^{2+}-bound calmodulin (CaM) that displaces the autoinhibitory domain. One of the key substrates of the catalytic domain of CaMKIIα is the Thr286 residue on CaMKIIα itself. The phosphorylation of Thr286 prevents the autoinhibitory domain from binding to the catalytic kinase domain. Hence, the partial activation of CaMKIIα by Ca^{2+}-bound CaM can lead to autophosphorylation of CaMKIIα, at which point the complex becomes constitutively active without further stimulation (Miller and Kennedy, 1986). A point mutation at T286A in CaMKIIα, that blocked autophosphorylation, led to LTP inhibition (Giese et al., 1998). Several genetic manipulations were developed to investigate the physiological function of CaMKIIα in LTP, as follows. The injection of a truncated and constitutively active form of CaMKIIα into CA1 hippocampal pyramidal cells enhanced excitatory postsynaptic currents (EPSCs) (Lledo et al., 1995). In contrast, the application of inhibitory peptides (CN27, CN21, CN19) derived from a fragment of an endogenous inhibitor of CaMKIIα reversed LTP in hippocampal slices (Coultrap and Bayer, 2011; Sanhueza et al., 2011). The activated open form of CaMKIIα was shown to bind NMDARs (Leonard et al., 1999). This interaction was inhibited by the above mentioned inhibitory peptides *in vitro* (Vest et al., 2007).

CaMKIIα is thought to increase AMPAR-mediated transmission during LTP (Lisman et al., 2012). It can occur through two mechanisms. Firstly, the conductance of AMPARs is increased by phosphorylation at Ser831 of the GlaA1 subunit by CaMKIIα (Benke et al., 1998). Secondly, the AMPAR-mediated transmission can be enhanced by the insertion of AMPARs into a synapse. It was revealed that this insertion is mediated by an auxiliary subunit of AMPARs, stargazin. The phosphorylation of stargazin by CaMKIIα allows

AMPARs to bind to the postsynaptic density protein 95 (PSD-95) (Opazo et al., 2010). The synaptic associated protein 97 (SAP97) is believed to be involved in AMPARs exocytosis to the postsynaptic membrane during LTP because SAP97 interacts with GluA1 subunit and is transported into dendritic spines upon phosphorylation by CaMKIIα (Mauceri et al., 2004).

In comparison to the induction process of LTP, the maintenance of LTP is not well understood. LTP is maintained for a long period of time and this process requires protein synthesis. The autonomous activity of CaMKIIα was thought to be involved in maintenance of LTP. However, the inhibition of CaMKIIα by CN21 inhibitory peptide, used in rat hippocampal slices, prevented the induction of LTP, but not LTP maintenance (Buard et al., 2010). Another kinase, protein kinase M zeta (PKMζ), has been recognized as a protein which can be responsible for LTP maintenance (Ling et al., 2002). Once again, the role of PKMζ in LTP maintenance has been questioned by a genetic study, in which PKMζ knock-out mice exhibited intact LTP (Volk et al., 2013). Many gene knock-outs seem to impact LTP maintenance (Korte et al., 1998; Nagy et al., 2006; Oikawa et al., 2012) and suggest the overall process is complex.

The brain-derived neurotrophic factor (BDNF) and its receptor, tyrosine receptor kinase B (TrkB), have emerging roles in both early and late LTP (Lin et al., 2018; Mei et al., 2011). As BDNF/TrkB signalling is a pathway of interest in my thesis, its implication in LTP is discussed in the next section.

1.2.3 BDNF/TrkB signalling in LTP

In canonical signalling, TrkB is activated by BDNF-induced dimerization, which leads to autophosphorylation of tyrosine residues in TrkB kinase domains (Cunningham and Greene, 1998; Cunningham et al., 1997). As a consequence of the TrkB activation, three main signalling pathways are triggered: the phospholipase C-γl (PLCγ1)-Ca^{2+} pathway, the Ras/extracellular signal-regulated kinase (ERK) and phosphatidylinositol 3-kinase (PI3K)/AKT signalling pathways (Kaplan and Miller, 2000). The full-length TrkB receptor consists of extracellular, transmembrane and intracellular domains. Two alternatively spliced variants, TrkB.T1 and TrkB.T2, which do not contain the entire intracellular kinase domain, have been identified (Klein et al., 1990; Middlemas et al., 1991). The full-length TrkB structure and the action of this receptor are described in more detail in Chapter 2 (see Section 2.1). Even though neurotrophins and their receptors have been indentified in some invertebrates as reviewed by Bothwell (2006), bona fide genes encoding TrkB or BDNF were

not identified in *Drosophila melanogaster* and *Caenorhabditis elegans* (Beck et al., 2004; Benito-Gutierrez et al., 2006). The full-length TrkB as well as truncated TrkB.T1 and TrkB.T2 are abundantly expressed in a mammalian brain (Escandon et al., 1994; Otani et al., 2017). The full-length and truncated TrkB receptors are expressed in pre- and post-synaptic compartments of neurons (Kryl et al., 1999). In the excitatory neurons, TrkB colocalizes with NMDAR in dendrites, whereas in axons TrkB overlaps with synaptic vesicle proteins (Gomes et al., 2006). TrkB was also coimmunoprecipitated with NR2B subunit of NMDAR (Mizuno et al., 2003). Moreover, BDNF was shown to enhance phosphorylation of NR1 and NR2B subunits leading to increased NMDAR activity in hippocampal neurons (Levine et al., 1998; Lin et al., 1998). As mentioned in Section 1.2.2, NMDAR plays a crucial role in LTP expression, suggesting that BDNF/TrkB signalling is implicated in LTP. TrkB and BDNF have been indeed proven to play a significant role in mediating and modulating synaptic plasticity (as extensively reviewed by Korte and Schmitz (2016)).

The early evidence implicating of TrkB-mediated signalling in LTP has been deduced from the BDNF studies. The level of mRNA encoding BDNF was increased in CA1 neurons from hippocampal slices at 4 h after stimulation with an electrical paradigm inducing LTP (Patterson et al., 1992). The experiments on homozygous and heterozygous BDNF knock-out mice revealed a strong impairment of LTP in those animals (Korte et al., 1995). Moreover, this severe reduction in LTP expression could be restored by viral expression of BDNF in CA1 region or treatment of slices from BDNF-deficient mice with recombinant BDNF (Korte et al., 1996; Patterson et al., 1996). The local application of BDNF to mature dentate granule cells in hippocampal slices, with the concomitant weak burst of synaptic stimulation, induced robust LTP (Kovalchuk et al., 2002). These results suggested that BDNF can facilitate LTP induction. Taken together, the above evidence demonstrates the involvement of BDNF in LTP so, by the extrapolation, TrkB, as a receptor for BDNF, is thought to play a role in LTP.

Using a rabbit polyclonal antiserum, recognizing TrkB specifically and preventing TrkB-activated signalling, Kang et al. (1997) demonstrated that TrkB is involved in an early and late phase of LTP. Mice in which *trkB* gene was knocked-out conditionally in the forebrain during postnatal development exhibited impaired LTP in CA1 region (Minichiello et al., 1999). Contrary to the knock-out approach, the knock-in method allowed researchers to create two transgenic mouse lines with targeted mutations in TrkB: one in a site responsible for PLCγ1 activation and second in a site mediating ERK and AKT activation. The hippocampal LTP induction was reduced in mice with mutated PLCγ1-docking site, whereas in mice with mutated ERK/AKT-docking site LTP was unaltered (Minichiello et al., 2002).

These results were confirmed by Gruart et al. (2007) and Korte et al. (2000). The inhibition of TrkB-mediated PLCγ1 signalling in hippocampal CA1 and CA3 regions by virus encoding a pleckstrin homology (PH) domain of PLCγ1 caused the significant reduction of LTP (Gartner et al., 2006). Mice with a mutated PLCγ1-docking site in the kinase domain of TrkB, but normal ERK/AKT-docking site, showed impaired LTP at amygdalar synapses (Musumeci et al., 2009). The genetic mouse models, described above, provided solid evidence implicating TrkB in LTP. However, using knock-out or knock-in approaches can have long-term or developmental impacts that may overshadow a role of the specific pathway in LTP.

The studies mentioned above on transgenic mice highlighted the importance of a PLCγ1-docking site in LTP, but do not eliminate the involvement of TrkB-mediated ERK and AKT activation in LTP. It was shown that PLCγ1 signalling plays roles in the early and late phase of hippocampal LTP (Minichiello et al., 2002). The ERK inhibitor, PD 098059, attenuated the induction of LTP in the CA1 area of hippocampal slices, whereas the expression of established LTP was not affected (English and Sweatt, 1997). These results were supported electophysiologically in freely behaving adult rats (Ying et al., 2002). In the dentate gyrus, local application of ERK inhibitor, U0126, blocked LTP maintenance and Arc protein expression, suggesting that the ERK pathway has a role in the late phase of LTP, which is dependent on the protein synthesis (Panja et al., 2009). AMPAR insertion is crucial for hippocampal LTP (see Section 1.2.1). The BDNF/TrkB signalling was shown to be involved in this process (Zhang et al., 2018), possibly through activation of the PI3K pathway (Man et al., 2003). The existing evidence provides a strong correlation between BDNF/TrkB signalling and the process of LTP. Nevertheless, it is unclear whether TrkB activity itself is sufficient to induce LTP (Kang and Schuman, 1995; Kovalchuk et al., 2002). Additionally, the precise TrkB-mediated downstream signalling implicated in the early or late stages of LTP is not well-understood, nor is it understood whether this key action is pre- or post-synaptic site.

TrkB is present at pre- and post-synaptic sites (Kryl et al., 1999). The early results on cultured hippocampal neurons indicated that BDNF can enhance synaptic transmission and they suggested a presynaptic action of BDNF. The application of BDNF to cultured hippocampal neurons increased the frequency of mEPSCs, but not the amplitude, suggesting the presynaptic action of BNDF (Lessmann et al., 1994; Paul et al., 2001). The early evidence on the role of BDNF/TrkB signalling in synaptic transmission might have pointed to the presynaptic action of these proteins in LTP. Xu et al. (2000) showed that a deletion of TrkB

from hippocampal CA1 postsynaptic cells did not affect induction of LTP, indicating the presynaptic function of TrkB. Presynaptic BDNF was also implicated in the presynaptic component of LTP at hippocampal Schaffer collateral synapses (Zakharenko et al., 2003). The field potential recording in hippocampal CA3 presynaptic cells from BDNF knock-out mouse slices demonstrated reduction in LTP at mossy fiber synapses, suggesting that presynaptic component plays a role in LTP (Schildt et al., 2013). Finally, at corticostriatal synapses, axonal NMDARs are involved in LTP induction by stimulating a secretion of presynaptic BDNF (Park et al., 2014). However, Levine et al. (1995) reported that application of BDNF to cultured hippocampal neurons could increase the frequency and amplitude of EPSCs, suggesting pre- and postsynaptic action of BDNF/TrkB signalling. The postsynaptic function of BDNF in LTP was also postulated by Kovalchuk et al. (2002), who showed the induction of LTP in postsynaptic cells by BDNF. At the thalamo-amygdala synapses in heterozygous BDNF knock-out mice, LTP was abolished, suggesting a postsynaptic site of BDNF action (Meis et al., 2012). The pre- and postsynaptic site of BDNF/TrkB action in LTP was shown by the inhibition of their downstream target, PLCγ1. Blocking PLCγ1 signalling at both sites reduced LTP (Gartner et al., 2006); however, this interpretation assumes that PLCγ1 was exclusively activated by BDNF/TrkB under this condition. A recent systematic approach of conditional BDNF and TrkB knock-out in hippocampal CA1 and CA3 regions revealed distinct roles of pre- and postsynaptic BNDF/TrkB signalling in LTP. Most recently it has been shown that presynaptic BDNF and postsynaptic TrkB are responsible for LTP induction, whereas either presynaptic or postsynaptic TrkB, as well as postsynaptic BDNF are implicated in LTP maintenance (Lin et al., 2018).

The postsynaptic action of BDNF/TrkB is likely to be associated with structural LTP (sLTP), the structural changes in spines after LTP induction. After LTP induction, spine enlargement is widely observed in addition to the functional electrical changes in synapses (Matsuzaki et al., 2004). Two-photon glutamate uncaging, which mimics synaptic stimulation occurring during LTP induction, revealed TrkB activation in an individual dendritic spine. Moreover, this activation was dependent on NMDAR, CaMKII and postsynaptically secreted BDNF (Harward et al., 2016).

The presented literature provides solid connections between BDNF/TrkB signalling and LTP. Nevertheless, a lack of a tool that can manipulate biochemical processes in a fast timescale in defined pre- or postsynaptic cells means that many aspects cannot be easily addressed. BNDF/TrkB signalling appears to have both pre- and postsynaptic functions during LTP and it is difficult to precisely dissect these actions at each site. As it was

demonstrated that BDNF can decrease inhibitory postsynaptic currents (Frerking et al., 1998), it would be of interest to investigate the roles of excitatory neurons and the inhibitory cells in LTP. Finally, a direct causal link, showing the connection between a specific BDNF/TrkB downstream pathway, LTP and a specific behavioural paradigm, remains to be resolved. To address these controversies, this thesis presents a novel tool that can be used to activate TrkB signalling in defined cells with temporal resolution.

It is noteworthy that in addition to LTP phenomenon, BDNF/TrkB signalling plays many diverse roles in different cell types of the nervous system. TrkB has been shown to mediate axon outgrowth and to support the survival of rat sympathetic neurons (Atwal et al., 2000). BDNF/TrkB has been demonstrated to play a role in axon elongation and a growth cone formation in motoneurons (Dombert et al., 2017). Finally, BDNF acts as a chemotropic guidance cue so the growing axon of *Xenopus* spinal neuron has been attracted toward the concentration gradient of BDNF (Ming et al., 1997). The role of BDNF/TrkB in axon guidance has been described elaborately by Cohen-Cory et al. (2010) and by Thiede-Stan and Schwab (2015). These diverse implications of BDNF/TrkB signalling in different functions of the nervous system suggest that the tool developed in this project might have potential broader applications beyond LTP and memory formation. Nevertheless, the manipulation of synaptic plasticity by controlling BDNF/TrkB signalling in a high spatiotemporal manner is the main rationale behind designing the new TrkB-based approach.

1.3 Relationship between LTP and animal learning and memory

Despite strong theoretical implication of LTP for the behavioural aspects of learning, it has been technically challenging to demonstrate the direct link between LTP and learning/memory either correlatively or causally. One of the significant obstacles to observe LTP expression during behavioural training is a difficulty in localizing particular synapses in a brain that underwent potentiation during learning. In this section, a few examples that provide evidence for LTP and learning correlation are listed.

Rogan et al. (1997) discovered that LTP-like procsess, measured as field potentials, was evoked in the amygdala *in vivo* after a fear conditioning paradigm in freely behaving rats. The fear conditioning is a common paradigm for studying associative learning, in which animals usually learn to associate a foot shock (an aversive unconditioned stimulus, US) with a tone (a neutral conditioned stimulus, CS) that leads to stereotypical fear behaviour - freezing (a toned-driven conditioned response, CR) (Maren, 1999). The fear conditioning

evoked the synaptic potentiation in a similar manner to the high-frequency electrical stimulation (Maren and Fanselow, 1995; Rogan and LeDoux, 1995; Rogan et al., 1997). Similarly, Whitlock et al. (2006) detected LTP induction in the hippocampus of rats that underwent an inhibitory avoidance paradigm, in which animals learn to pair a foot shock with a dark place. In this study, the inhibitory avoidance training increased the phosphorylation at Ser831 of GluA1 subunit of AMPAR and increased a surface expression of GluA1 and GluA2, processes occurring during LTP expression (Lee et al., 2000). Although these examples are consistent with the hypothesis that LTP is the cellular mechanism of learning, they only suggest a correlation between LTP and learning without providing any causal links between these two events.

In 2014, a group of researchers from the University of California, San Diego examined LTP in fear learning with the utility of optogenetic methods (Nabavi et al., 2014). This study showed that the expression of fear behaviour was eliminated by an optogenetic LTD induction protocol that reversed LTP. The fear behaviour was reinstated by an optogenetic LTP induction protocol. These results, which are discussed in detail in Section 1.4.2, provided a more direct causal link between LTP/LTD and leaning processes, but still raise questions of a molecular mechanism involved in these processes.

1.3.1 BDNF/TrkB signalling in learning and memory

Since BNDF/TrkB signalling is involved in structural and functional LTP, many studies have been searching how this signalling influences learning and memory processes. One of the most extensive studies has been performed to link BNDF/TrkB signalling with hippocampal-dependent learning. The spatial learning, using a radial arm maze task, increased the level of BNDF mRNA in mouse hippocampus. Moreover, the reduction of BDNF expression by antisense oligonucleotides impaired acquisition and retention of spatial memories (Mizuno et al., 2000). The same task induced phosphorylation of TrkB, tyrosine kinase Fyn and NR2B subunit of NMDAR in the hippocampus (Mizuno et al., 2003). Using a tyrosine kinase inhibitor, the acquisition of spatial memories was delayed (Mizuno et al., 2003). Mice that underwent treadmill training exhibited enhancement in hippocampus-related aversive learning and this was also accompanied by increase in TrkB expression (Liu et al., 2008b). The homozygous conditional knock-out mice of TrkB showed impaired spatial learning (Minichiello et al., 1999). The heterozygous knock-in mice, carrying the mutation in PLCγ1-docking site of TrkB, exhibited disrupted acquisition of associative learning, which

suggested that PLCγ1 pathway is implicated in this type of learning (Gruart et al., 2007). Other transgenic mice overexpressing TrkB.T1, a dominant-negative receptor which acts as the inhibitor of full-length TrkB, showed an impairment in spatial memory (Saarelainen et al., 2000). Finally, heterozygous mice, overexpressing the full-length TrkB, displayed an improvement in spatial learning (Koponen et al., 2004).

In addition to the numerous studies on the role of BDNF/TrkB in hippocampal learning, a correlation between BDNF/TrkB and amygdalar learning has been unveiled. The application of TrkB inhibitor, K252a, and the dominant-negative isoform, TrkB.T1, resulted in the inhibition of acquisition of fear memories (Rattiner et al., 2004). Blocking normal function of the full-length TrkB by TrkB.T1 in the amygdala impaired the extinction of learned fear memories (Chhatwal et al., 2006). In addition to these results, the inhibition of TrkB anterograde axonal transport disrupted fear memory extinction, suggesting the presynaptic role of TrkB (Li et al., 2017). The conditional BDNF knock-out and sequestering TrkB function by the dominant-negative TrkB.T1 in the amygdala affected consolidation of appetitive and aversive emotional learning (Heldt et al., 2014). Knock-in studies revealed that mice carrying the mutation in PLCγ1-docking site of TrkB displayed the impairment in acquisition of fear memories, whereas mice with the mutation in ERK/AKT-docking site exhibited the disruption during consolidation (Musumeci et al., 2009). This reveals differential effects of the distinct TrkB signalling pathways on learning phases that could not be observed with LTP measurement in brain slices. This observation deserves further investigation with other approaches.

1.4 Optogenetics as a novel approach to investigate learning and memory processes

Optogenetics refers to the combination of genetics and optics to control processes in specific cells within living tissue (Deisseroth, 2011), achieving high spatial and temporal manipulation of a genetically-defined population of neurons. Optogenetics can be described as the expression of light-sensitive proteins in living cells, resulting in the ability to modulate cell behaviours with light. Many years before the introduction of this technique, Francis Crick made an observation that “a method by which all neurons of just one type could be inactivated, leaving the others more or less unaltered” is needed (Crick, 1979) and “the ideal signal would be light, probably at an infrared wavelength to allow the light to penetrate far enough” (Crick, 1999). Optogenetics can overcome several limitations of the current genetic, pharmacological and electrophysiological approaches. Moreover, optogenetics can

complement the classical techniques to acquire a comprehensive investigation of neural functions.

Various optogenetic tools, such as opsins, phototropins or cryptochromes, for manipulating neuronal behaviours and functions are presented in the next section.

1.4.1 Optogenetic tools for neuronal and biochemical control

Most modern optogenetic experiments utilize the light-inducible microbial opsins such as channelrhodopsin-2 (ChR-2) and halorhodopsin (HR) (Boyden et al., 2005; Johansen et al., 2014; Nabavi et al., 2014; Zhang et al., 2007). These opsins transport ions across the membrane either as ion channels or transporters (ion pumps) to directly control the membrane excitability by depolarization or hyperpolarization (Zhang et al., 2007). These tools serve as a valuable approach for mapping circuits and detecting connectivity in a nervous system. However, they do not contribute to our understanding of the cellular and molecular biochemical pathways that affect animal behaviour. For such types of investigation, alternative optogenetic tools have been developed over the past decade.

To manipulate biochemical pathways, other natural photosensors, such as Light, Oxygen or Voltage sensing domains (LOV), phytochrome and cryptochrome have been utilized (Kennedy et al., 2010; Pham et al., 2011; Reichhart et al., 2016). The first LOV domains were discovered in plant phototropins, photoreceptor threonine/serine kinases that utilize a flavin mononucleotide (FMN) cofactor as a chromophore (Christie et al., 1999; Huala et al., 1997). Although FMN is the common chromophore, LOV domains binding a flavin adenine dinucleotide (FAD) are also known in the literature (Losi et al., 2018). Both FMN and FAD are ubiquitously present in cells. Phototropins in plants regulate numerous processes including phototropism, chloroplast relocation and leaf movement (Kagawa et al., 2001; Sakai et al., 2001). Blue light illumination triggers the structural rearrangements in LOV domains (Harper et al., 2003). This leads to the activation of an effector protein tethered with LOV (Pham et al., 2011; Wu et al., 2009). The LOV2-Jα, a photosensor domain from *Avena sativa*, is an attractive optogenetic tool due to its solubility, small size, ubiquity of the cofactor that is present in most cell types and its reversible action (Christie et al., 2012). LOV2-Jα in fusion with other protein domains and peptides has been used to control biochemical processes. Wu et al. (2009) designed a recombinant protein by fusing LOV2-Jα with a small GTPase, Rac1, which resulted in a photoactivatable Rac1 that increased cell motility upon illumination. The LOV-Jα domain was used to generate a local Ca^{2+} signal at

the plasma membrane by attaching LOV-Jα to a fragment of stromal interaction molecule 1 (STIM1) which interacts with Orai1 to activate store-operated calcium entry (Pham et al., 2011; Varnai et al., 2009). LOV2-Jα was applied to control a protein translocation to the nucleus and, consequently, to control gene transcription (Yumerefendi et al., 2015).

Cryptochromes are another extensively studied group of blue-light photoreceptors. They are photolyase-like proteins that regulate circadian rhythm in *Drosophila* and floral initiation in a plant, *Arabidopsis thaliana* (Emery et al., 1998; Liu et al., 2008a). Cryptochromes consist of two domains: a photolyase-homologous region (PHR) domain and a C-terminal extension domain. PHR binds non-covalently to FAD (Brautigam et al., 2004; Liu et al., 2011). It has been shown that the photoexcited cryptochrome 2 (Cry2) from *Arabidopsis thaliana* can interact with a cryptochrome-interacting basic-helix-loop-helix protein (CIB1) (Liu et al., 2008a). This dimerization between Cry2 and CIB1 was used by Kennedy et al. (2010) to induce protein translocation, transcription and DNA recombination in mammalian cells upon light illumination. They also observed that the isolated PHD domain of Cry2 is sufficient to dimerize with the full-length and truncated CIB1 (Kennedy et al., 2010). In addition to light-mediated heterodimerization between Cry2 and CIB1, Cry2 oligomerizes upon blue light illumination (Bugaj et al., 2013). The latest versions of Cry2/CIB1 were designed to reduce dark activity, change lifetime of the excited state and affinity of dimerization (Taslimi et al., 2016). The heterodimerization of Cry2/CIB1 was used to activate Raf1 and neurite outgrowth in PC12 cells (Zhang et al., 2014), to activate AKT (Katsura et al., 2015) and recruit CaMKII and AMPAR to the postsynaptic density in hippocampal neurons (Sinnen et al., 2017). The self-oligemerization of Cry2 was used to activate receptor tyrosine kinases (RTKs) and to manipulate intracellular Ca^{2+} in hippocampal neurons (Kyung et al., 2015).

With the development of these light-responsive domains, it is possible to create an optogenetic tool to control cellular signalling implicated in learning and memory formation.

1.4.2 Optogenetics in studying learning and memory

The application of optogenetic techniques, surpassing the limited temporal resolution of genetic manipulations such as knock-in and knock-out, and the lack of genetic selectivity associated with electrical and pharmacological approaches, can provide more direct causal link between cellular events and behavioural consequences. Investigating learning and memory processes with optogenetic approaches in behaving animals can complement

existing knowledge on brain functions. For instance, recent studies have provided a strong connection between LTP and learning or between structural changes in dendritic spines and learning/memory formation *in vivo* (Hayashi-Takagi et al., 2015; Nabavi et al., 2014).

One of the interesting studies aimed to test a correlation between synaptic plasticity in the lateral amygdala and production of aversive memories in freely behaving rats (Johansen et al., 2014). The authors hypothesized that during threat conditioning in rats, the presynaptic activity evoked by conditioned stimulus (tone) and paired with convergent depolarization of the pyramidal neurons of the lateral amygdala, should generate synaptic plasticity in the postsynaptic pyramidal neurons and produce aversive memories. To address this hypothesis, the optogenetic inhibition of membrane excitability of the pyramidal neurons in the lateral amygdala was applied during learning process. This significantly reduced learning-induced plasticity and memory formation in rats (Johansen et al., 2014).

Strong evidence that the formation of aversive memories *in vivo* is associated with LTP was provided by Professor Roberto Malinow's group using optogenetic control of presynaptic termini (Nabavi et al., 2014). These experiments used a chimeric variant of ChR-2 to control the presynaptic termini projecting to the amygdala from the auditory cortex and medial geniculate nucleus. Optical control of vesicular release at the axonal termini in the lateral amygdala was used to induce LTP or LTD depending on the stimulation frequency and duration (Nabavi et al., 2014). An optical conditioned stimulus was paired with an aversive unconditioned stimulus (foot shock) which resulted in a conditioned response in freely behaving rats (freezing). In the same animals, LTD, evoked optogenetically, caused that animals did not display freezing. One day later, animals were exposed to an optical LTP protocol, after which rats exhibited freezing. Taken together, the aversive memories could be inhibited with LTD and reactivated with LTP (Nabavi et al., 2014). Thus far, this provides the strongest causal link between LTP and memory.

A study with *in vivo* two photon imaging and optogenetic approach established links between structural synaptic plasticity and motor learning in the cortex (Hayashi-Takagi et al., 2015). In this set of experiments, a photoactivatable Rac1 (described in Section 1.4.1.) was injected in the cortical layer II/III of the mouse primary motor cortex to induce single-spine shrinkage upon blue light illumination (Hayashi-Takagi et al., 2015). These data suggested that motor learning in mice increased spine volume. The photoactivation of Rac1 decreased this volume and erased the acquired motor skills in behaving mice (Hayashi-Takagi et al., 2015). This report described, for the first time, how learning and memory formation can initiate the structural rearrangements in individual spines.

By using optoSTIM1 (see Section 1.4.1) to elevate intracellular Ca^{2+} in neurons, it was demonstrated that the light-stimulated mice exhibited approximately two-fold increase in freezing behaviour, indicating that the light-activated Ca^{2+} signal can reinforce contextual fear memories (Kyung et al., 2015). This provided more causal connection between Ca^{2+} responses and learning/memory processes.

Another recent elegant study used light to release a CaMKII inhibitory peptide, paAIP2 (Murakoshi et al., 2017). Upon light activation, paAIP2 was able to impair the acquisition of inhibitory avoidance learning in the amygdala of freely behaving mice. Interestingly, CaMKII inhibition by paAIP2 had no effect after the initial phase of memory acquisition, contradictory to some existing literature on CaMKII functions in memory (Lisman et al., 2012). Although more investigation is necessary to confirm and interpret these results, they supported our understanding of CaMKII activation and memory formation *in vivo*.

1.5 Aims of the study

While it has been shown that BDNF/TrkB signalling plays an important role in modulating synaptic plasticity, a direct link between BNDF/TrkB signalling, LTP and memory processes remains to be investigated in the intact adult brain. The numerous studies employing BDNF or TrkB knock-out or knock-in mice highlighted the importance of BDNF/TrkB in synaptic plasticity and learning/memory processes, although there are concerns that developmental abnormalities in the genetically altered animals can affect synaptic plasticity at different stages and, consequently, affect animal behaviour. Moreover, it is technically difficult to influence BNDF/TrkB expression in a defined neuronal population with knock-out or knock-in approaches. Other difficulties arise from the lack of a targeted method for dissecting BNDF/TrkB-mediated signalling pathways with a spatiotemporal resolution.

To investigate a role of BDNF/TrkB signalling in LTP and learning in the adult nervous system of rodents, this study undertook an optogenetic approach to manipulate TrkB activity with light. To achieve the final goal, this project has two principal research aims:

1. Develop a light-inducible TrkB system which can evoke canonical TrkB-mediated signalling pathways.
2. Validate whether the tool can mimic TrkB action in living cells upon light stimulation.

In this thesis, a workflow for developing the photoactivatable TrkB system is presented. In Chapter 2, the generation of the TrkB system, its different configurations and ability to recapitulate the activation of TrkB-mediated signalling pathways in non-neuronal cells upon light are described. In Chapter 3, the utility of the initially validated TrkB system in neurons is presented. Finally, in Chapter 4, potential propositions of the TrkB system's application *in vivo* are made.

Chapter 2

Development of a photoactivatable TrkB system in non-neuronal cells

2.1 Introduction

Like other members of receptor tyrosine kinases (RTKs), TrkB possesses an N-terminal extracellular domain, a transmembane region and a C-terminal intracellular kinase domain. The extracellular domain is organized into five sub-domains. Domains 1 and 3 are cysteine-rich and flank the leucine-rich domain 2. Domains 4 and 5 are immunoglobulin-like regions, with domain 5 being responsible for ligand-binding specificity. The kinase domain is flanked by the juxtamembrane region and the C-terminal tail (Bertrand et al., 2012; Middlemas et al., 1991; Schneider and Schweiger, 1991).

The activation of TrkB is mediated through binding with neurotrophins: BDNF, NT-4 and to a lesser extent, with NT-3 (Ip et al., 1992; Klein et al., 1991). According to the model based on early studies of the tyrosine receptor kinase A-nerve growth factor (TrkA-NGF) complexes, and the structural similarity to other RTKs, TrkB is activated by dimerization upon ligand binding (Cunningham and Greene, 1998; Cunningham et al., 1997). However, the exact mechanism of BDNF-induced activation of TrkB at the molecular level remains still under discussion (Shen and Maruyama, 2012; Zahavi et al., 2018). Nevertheless, it has been shown that the homodimerized TrkB receptors autophosphorylate their tyrosine residues (Y701, Y705, Y706) within a structurally flexible activation loop that leads to conformational changes in their kinase domains making them easily accessible to substrates (Ahmed and Hristova, 2018; McCarty and Feinstein, 1998). Other phosphotyrosines within the intracellular kinase domain provide docking sites for effector proteins. A phosphorylated tyrosine 515 (Y515) at a juxtamembrane position of TrkB serves as a binding site for SHC (Src homology 2 domain) adaptor proteins to trigger Ras/ERK (extracellular signal-regulated kinase) and PI3K (phosphatidylinositol 3-kinase)/AKT signalling pathways (Minichiello et al., 1998; Stephens et al., 1994). A phosphotyrosine 816 (Y816) in the C-terminal tail of the intracellular domain is a binding site for phospholipase C-γl (PLCγ1) (Middlemas et al., 1994). Figure 2.1 shows a simplified schematic of the structural organization of TrkB and the canonical signalling pathways activated by TrkB.

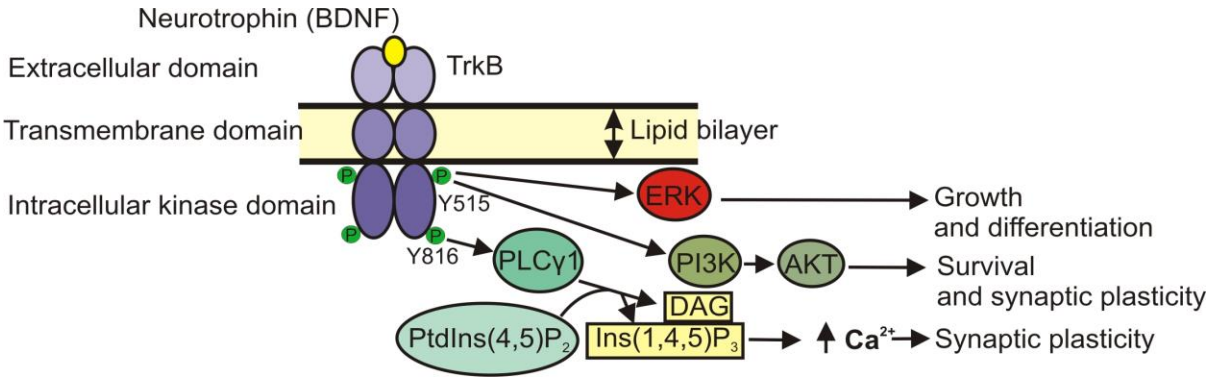

Figure 2.1 The canonical signalling pathways activated by TrkB. TrkB, a member of the tyrosine kinase family, can activate three main intracellular pathways upon binding brain-derived neurotrophic factor (BDNF). Recruitment of adaptor proteins to tyrosine 515 (Y515) triggers Ras/ERK (extracellular signal-regulated kinase) and PI3K (phosphatidylinositol 3-kinase)/AKT signalling pathways, which promote differentiation, growth, survival and synaptic plasticity in neuronal cells. Phosphorylation of TrkB tyrosine 816 leads to activation of phospholipase C-γl (PLCγ1), which catalyzes the hydrolysis of phosphatidylinositol-4,5-bisphosphate (PtdIns(4,5)P_2) to inositol-1,4,5-trisphosphate (Ins(1,4,5)P_3) and diacylglycerol (DAG). Ins(1,4,5)P_3 can promote the release of Ca^{2+} from the internal store and DAG can activate protein kinase C (PKC). These pathways are thought to be involved in synaptic plasticity. Figure was adapted from Minichiello (2009).

The involvement of RTKs in many important processes from development to maintenance of the central and peripheral nervous system has increased the interest in creating a tool to achieve precise control of neurotrophin activity. Such approach might provide better understanding of RTKs signalling and, if well-designed, a form of therapy, e.g. to induce axon outgrowth in neurodegenerative disease and spinal cord injury. Alfa et al. (2009) activated TrkA receptor by using a small chemically induced dimerizer (CID). In this approach, the intracellular domain of TrkA between 1410 and 2458 nucleotides (NCBI Reference Sequence: NM_021589), containing the juxtamembrane and activation loop region, was fused to an N-terminal myristoylation sequence for membrane localization and to two tandem FK506 binding protein domains ($FKBP_{F36V}$). In a CID system, two copies of $FKBP_{F36V}$ were brought together via a chemical inducer, AP20187 (Lin et al., 2013). The dimerization of the chimeric intracellular domains of TrkA by using AP20187 activated the PI3K/AKT and ERK1/2 cascades in PC12 cells. This meant that the effect of AP20187-induced dimerization was the same as when NGF binds to the full-length TrkA. The CID-TrkA approach was independent from the native ligand activation as the extracellular domain of TrkA was not present in this construct (Alfa et al., 2009). A similar CID system was also used to activate another RTK, fibroblast growth factor receptor 1 (FGFR1), in a fibroblast growth factor (FGF)-independent manner (Welm et al., 2002). Although the CID strategy could mimic the action of NGF on TrkA and FGF on FGFR1, it exhibits a few drawbacks:

(1) CID is practically irreversible as a chemical stimulus cannot be removed easily and fast; (2) pulse application of a chemical activator is difficult; (3) the delivery of CID to specific regions of tissue *in vivo* or to an individual cell is problematic (lack of spatial resolution); (4) the action of CID on signalling pathway is limited by diffusion of a chemical compound (lack of temporal control) (Leopold et al., 2018).

To overcome some of the disadvantages arising from the CID approach, an optogenetic strategy has been developed to control proteins optically. In this section, previous achievements using light-activated RTKs are discussed. The summary of the main strategies applied for RTK activation with light is presented in Figure 2.2. Chang et al. (2014) utilized the homodimerization properties of cryptochrome 2 (Cry2) from *Arabidopsis thaliana* upon blue light illumination to activate TrkA, TrkB and TrkC signalling (Fig. 2.2 A). Their main focus was on the photoactivatable TrkB (optoTrkB). In this system, the intracellular domain of full-length TrkB was linked to the N-terminus of a truncated version of Cry2 (498 amino acid-long photolyase homology region, PHR). The chimeric construct was visualized by monomeric yellow fluorescent protein, mCitrine, fused to the C-terminus of Cry2. It was shown that the resulting optoTrkB could activate the canonical TrkB signalling pathways upon light illumination in a reversible manner in HeLa and PC12 cell lines (Chang et al., 2014). Nevertheless, the extracellular domain of optoTrkB remained intact so the chimeric receptor could be still stimulated by the endogenous BDNF in addition to light stimulation. A very high expression level of optoTrkB in a cell membrane may result in light- or BDNF-independent activation of receptor molecules due to limited space (artefacts caused by RTKs overexpression were described by (Dikic et al., 1994; Traverse et al., 1994)). This stimulus-independent activity of optoTrkB was evident in HeLa cells, where the background activity of ERK signalling was increased in the dark. Interestingly, in PC12 cells the background activity of ERK was not elevated in the dark, which demonstrates that the action of optoTrkB may be expression level-dependent in different cell types (Chang et al., 2014). The optoTrkB approach for *in vivo* application is also limited by the size of the chimeric receptor (4.683 kilobase pairs (kbp) for the full-length TrkB-Cry2(PHR)-mCitrine insert only without any additional elements required for viral expression), which excludes the use of the recombinant adeno-associated virus (rAAV) for optoTrkB delivery due to packaging limit of rAAV (4.7 kbp – 5.2 kbp between 5' and 3' inverted terminal repeats (ITR)) (Choi et al., 2014; Holehonnur et al., 2015). Although other viral vectors can be used to deliver optogenetic tools *in vivo*, the use of rAAV is the most common and advantageous because of its long

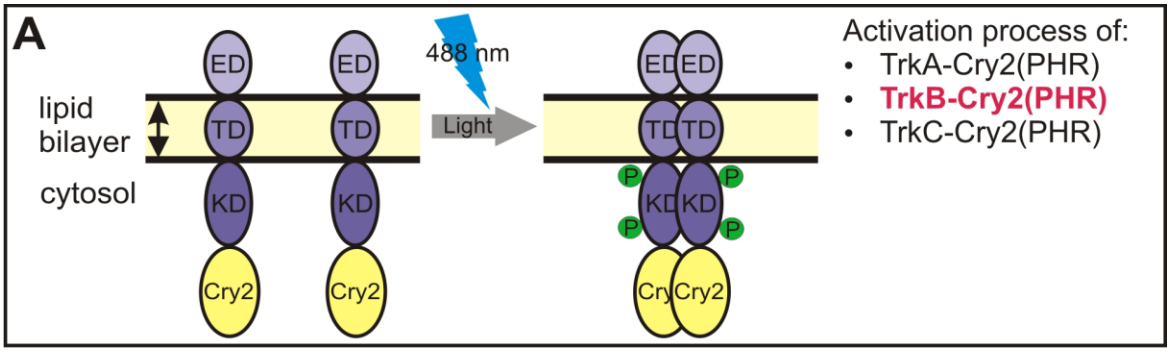
A
lipid bilayer
cytosol
ED
TD
KD
Cry2
488 nm
Light
P
Activation process of:
• TrkA-Cry2(PHR)
• TrkB-Cry2(PHR)
• TrkC-Cry2(PHR)

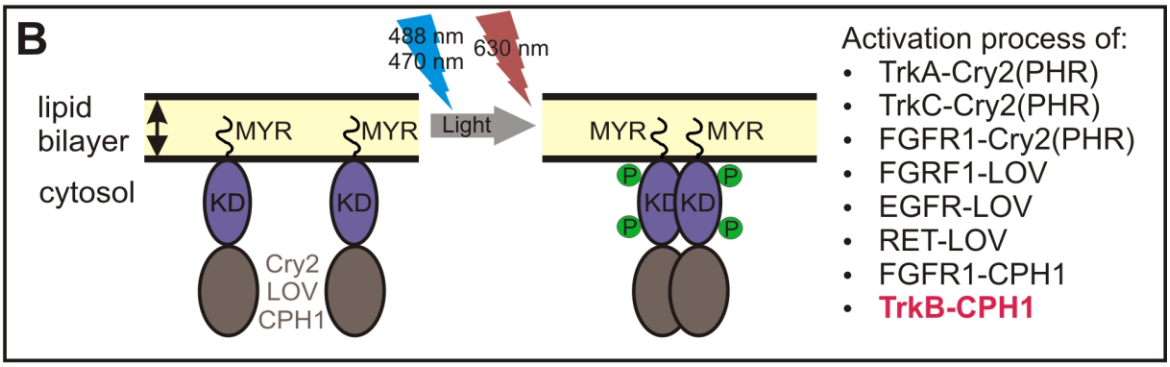
B
lipid bilayer
cytosol
MYR
KD
Cry2
LOV
CPH1
488 nm
470 nm
630 nm
Light
P
Activation process of:
• TrkA-Cry2(PHR)
• TrkC-Cry2(PHR)
• FGFR1-Cry2(PHR)
• FGRF1-LOV
• EGFR-LOV
• RET-LOV
• FGFR1-CPH1
• TrkB-CPH1

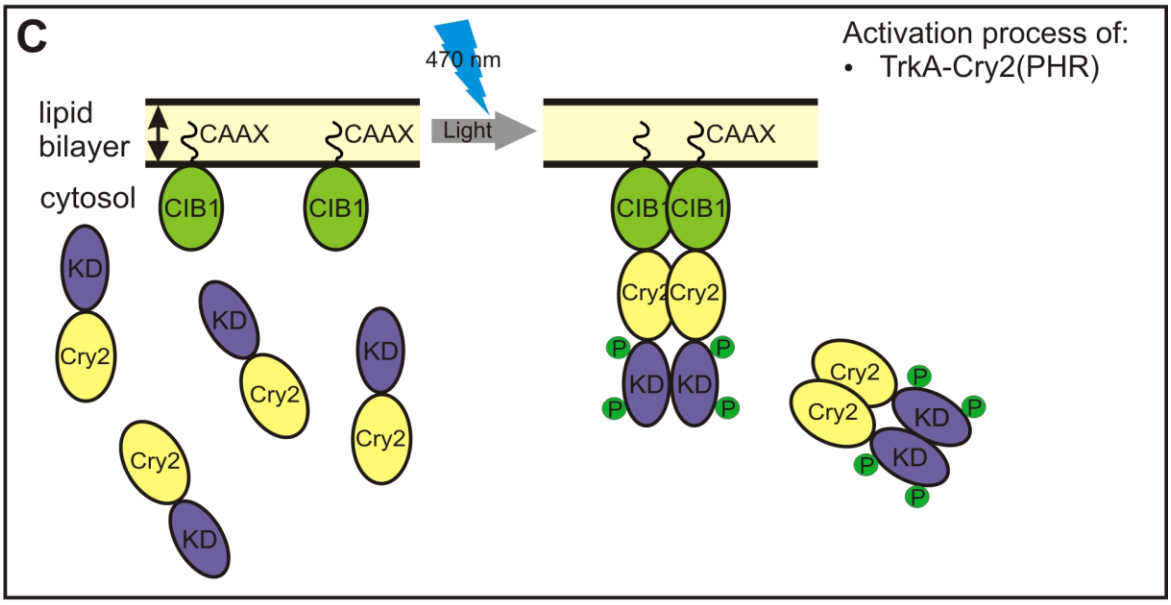
C
lipid bilayer
cytosol
CAAX
CIB1
KD
Cry2
470 nm
Light
P
Activation process of:
• TrkA-Cry2(PHR)

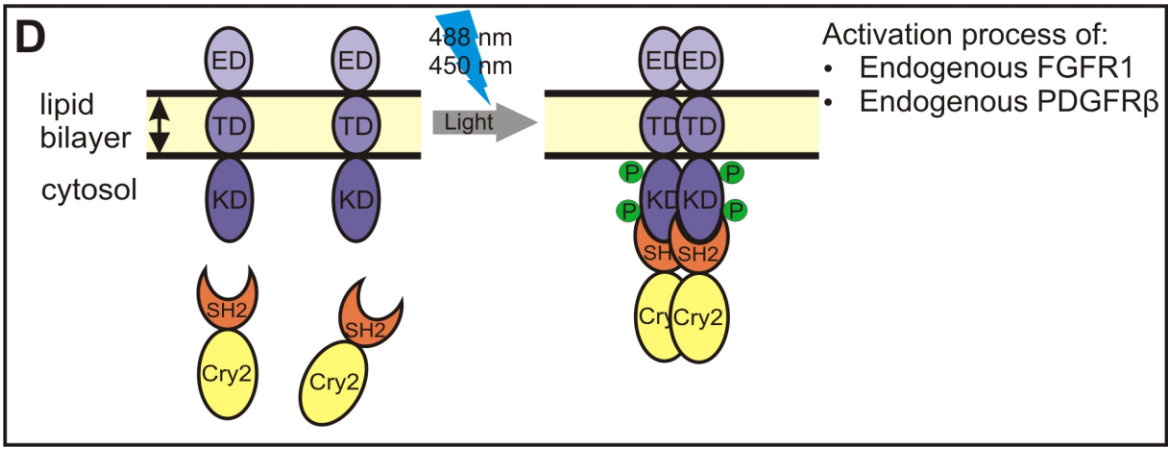
D
lipid bilayer
cytosol
ED
TD
KD
SH2
Cry2
488 nm
450 nm
Light
P
Activation process of:
• Endogenous FGFR1
• Endogenous PDGFRβ

Figure 2.2 The main strategies applied for the activation of receptor tyrosine kinases (RTKs). **(A)** TrkA, TrkB and TrkC receptors were activated with blue light illumination due to the fusion of each full-length receptor to the photolyase homology region of cryptochrome 2 (Cry2(PHR)) (Chang et al., 2014). **(B)** The intracellular kinase domains (KD) of RTKs in membrane were attached to Cry2(PHR) or a light-oxygen-voltage domain (LOV) for the activation mediated by blue light (Duan et al., 2018; Grusch et al., 2014; Han et al., 2016; Kim et al., 2014). To create the red-light inducible RTKs, their kinase domains were linked to the cyanobacterial phytochrome 1 (CPH1) (Reichhart et al., 2016). **(C)** In another strategy, the kinase domain of TrkA was fused to Cry2(PHR) and the activation by blue light was achieved by the oligomerization of TrkA-Cry2(PHR) in the cytosol or by the translocation of TrkA-Cry2(PHR) to the membrane where a Cry2-binding protein (CIB1) was targeted (Duan et al., 2018). **(D)** The clustering process of endogenous RTKs by using a Src homology 2 domain (SH2) linked to Cry2(PHR) was used to activate pathways with blue light (Bugaj et al., 2015). This approach was called CLICR (Clustering Indirectly using Cryptochrome 2). The specific strategies of TrkB activation were marked in red. Abbreviations: ED, extracellular domain; TD, transmembrane domain; KD, kinase domain; P, phosphorylation sites to mark activation of RTKs (does not represent the exact numbers of phosphotyrosines in a kinase domain after activation); MYR, myristoylation tag; CAAX, prenylation tag.

lasting transgene expression efficiency and lack of inflammatory or immune response in an infected animal (Holehonnur et al., 2015).

Since the development of optoTrkB by Chang et al. (2014), and during the realization of this research project, many light-inducible RTKs have been developed. Grusch et al. (2014) created an optogenetically-activated FGFR1 (optoFGFR1) by linking the intracellular catalytic domain to an N-terminal myristoylation signal (for membrane localization) to create a chimeric receptor that was insensitive to an endogenous ligand (Fig. 2.2 B). The C-terminus of FGFR1 was fused to a light-oxygen-voltage (LOV) domain from the yellow-green alga *Vaucheria frigida*. Blue light-induced dimerization of optoFGFR1 led to the activation of ERK, AKT and PLCγ1 pathways in HEK293 cells (Grusch et al., 2014). The similar photoactivatable FGFR1, using Cry2(PHR) as a photodimerizer, was developed and tested in HeLa cells by Kim et al. (2014) (Fig. 2.2 B). In both approaches, the photoactivatable FGFR1 was still localized in membrane and could potentially contribute to light-independent dimerization of the receptors when the expression level is high.

Similarly, another group employed the homooligomerization feature of Cry2 to activate endogenous RTKs in three different cell types: HEK293T, NIH 3T3 fibroblasts and rat hippocampal adult NCSs (Bugaj et al., 2015). The strategy was called CLICR (Clustering Indirectly using Cryptochrome 2). In this approach, a Src homology 2 domain (SH2) from PLC, which serves as a binding protein towards RTKs, was fused with the N-terminus of mCherry-Cry2 (‘m’ stands for monomeric fluorescent protein) (Fig. 2.2 D). Upon blue light illumination, it was hypothesized that SH2-mCherry-Cry2 could bind weakly activated RTKs

and cause their clustering and activation. Two RTKs: FGFR1 and a platelet-derived growth factor receptor β (PDGFRβ) were activated with light by using SH2-mCherry-Cry2 oligomerization (Bugaj et al., 2015). Thanks to this approach, unregulated activation of RTKs due to overexpression could be avoided as 3T3 cells expressing SH2-mCherry-Cry2 did not exhibit elevated signal activation in comparison with wild-type cells (Bugaj et al., 2015). Nevertheless, SH2 lacks specificity so SH2-mCherry-Cry2 can activate a broad range of RTKs upon light stimulation.

The strategies described above utilized blue light illumination at 470 or 488 nm to induce dimerization of LOV domain from *Vaucheria frigida* or Cry2 (Bugaj et al., 2015; Grusch et al., 2014; Kim et al., 2014). In the next studies, a red-light induced homodimerization domain was developed and applied to activate FGFR1 and TrkB in HEK293 cells (Reichhart et al., 2016). The cyanobacterial phytochrome 1 from *Synechocystis* (CPH1S) was linked to the C-terminus of the intracellular domain of TrkB (Fig. 2.2 B). The extracellular domain of TrkB was replaced by the myristoylation sequence to ensure membrane localization of the chimeric receptor. Red light illumination at 630 nm was sufficient to activate TrkB-CPH1S and trigger ERK and AKT signalling pathways. The advantage arising from this approach is that red light illumination can penetrate more deeply than blue light so this tool seems to be more suitable for *in vivo* application. However, using CPH1S for protein activation *in vivo* upon red light has a significant limitation. This is a requirement for supplementation with the tetrapyrrole phycocyanobillin (PCB), the chromophore for CPH1S, which is not synthesized by mammalian cells (Reichhart et al., 2016).

The next two studies developed photoactivatable TrkC and TrkA by using Cry2 oligomerization. Han et al. (2016) generated optoTrkC to examine whether intracellular signalling triggered by TrkC is responsible for synapse development. The blue-light inducible optoTrkC was created as a fusion of the cytoplasmic region of mouse TrkC (between 454 and 825 amino acid) to the N-terminus of Cry2(PHR) (Fig. 2.2 B). The membrane insertion of optoTrkC was achieved by the N-terminal myristoylation sequence and the chimeric receptor was visualized by the near-infrared fluorescent protein (iRFP682). The activation of optoTrkC was studied by its ability to activate three canonical pathways: ERK, AKT and PLCγ1 in cultured hippocampal neurons (Han et al., 2016). The action of TrkC was inert to the endogenous ligand, NT-3, but optoTrkC was still localized in the membrane, which could increase the background signalling. Very recent designs for optical activation of TrkA have been published (Duan et al., 2018) while this thesis was being written. In these studies, three

different strategies utilizing Cry2 system were compared to achieve the light-inducible activation of TrkA. The first approach is the same as that described by Chang et al. (2014) and involved the full-length TrkA linked to the N-terminus of Cry2 (Fig. 2.2 A). Secondly, they used a similar design to the chemical induction of TrkA (Alfa et al., 2009). However, instead of using two tandem FK506 domains for TrkA dimerization, Cry2 was fused to the C-terminus of the intracellular domain of TrkA and this chimeric receptor was localized to the membrane by the myrisoylation tag (Fig. 2.2 B). The final tool, which is very similar to the approach developed in this PhD project, involved the co-expression of two components: (1) the intracellular domain of TrkA fused to Cry2 (without any membrane tag), and (2) a membrane-targeted Cry2 interaction partner, CIB1 (Fig. 2.2 C). The efficiency of these three strategies were evaluated in PC12 cells to check neurite growth upon blue light illumination and in cultured dorsal root ganglion (DRG) cells to examine whether blue light can promote neuronal survival. According to these results from PC12 and DRG cells, it was shown that the kinase domain of TrkA-Cry2 + CIB1 strategy is the most effective to mimic the activity of NGF (Duan et al., 2018). Thus, the results obtained by Duan et al. (2018) support the data described in this thesis.

The studies described above highlight the increasing interest in optical activation of RTKs to evoke biological responses, such as: neuronal survival (Duan et al., 2018), neurite outgrowth (Chang et al., 2014; Duan et al., 2018) or synaptic development (Han et al., 2016). Inspired by the design of optoTrkB, in which the full-length TrkB was clustered by Cry2 upon blue light illumination (Chang et al., 2014), this project aimed to develop a photoactivatable TrkB system that could be used *in vivo*, and particularly, to examine its usefulness for controlling learning and memory processes in behaving animals. In my approach, a two component system was created where the kinase domain of TrkB without any membrane-localization signal was attached to the N-terminus of Cry2 (denoted as TrkB(kd)-Cry2) and the second component, CIB1, was targeted to the plasma membrane. In principle, blue light illumination should cause the aggregation of TrkB(kd)-Cry2 and its recruitment to CIB1 in the plasma membrane to activate the canonical signalling cascades on membrane. The general idea of this system's action is depicted in Figure 2.3. The approach has several potential advantages: (1) the activity is independent from the endogenous BDNF; (2) the stimulus-independent activation of TrkB(kd)-Cry2 is avoided as it is not attached to the membrane; (3) the system can be packaged into rAAV when split, or into lentiviral vectors as a single insert when a "self-cleaving" T2A peptide is used.

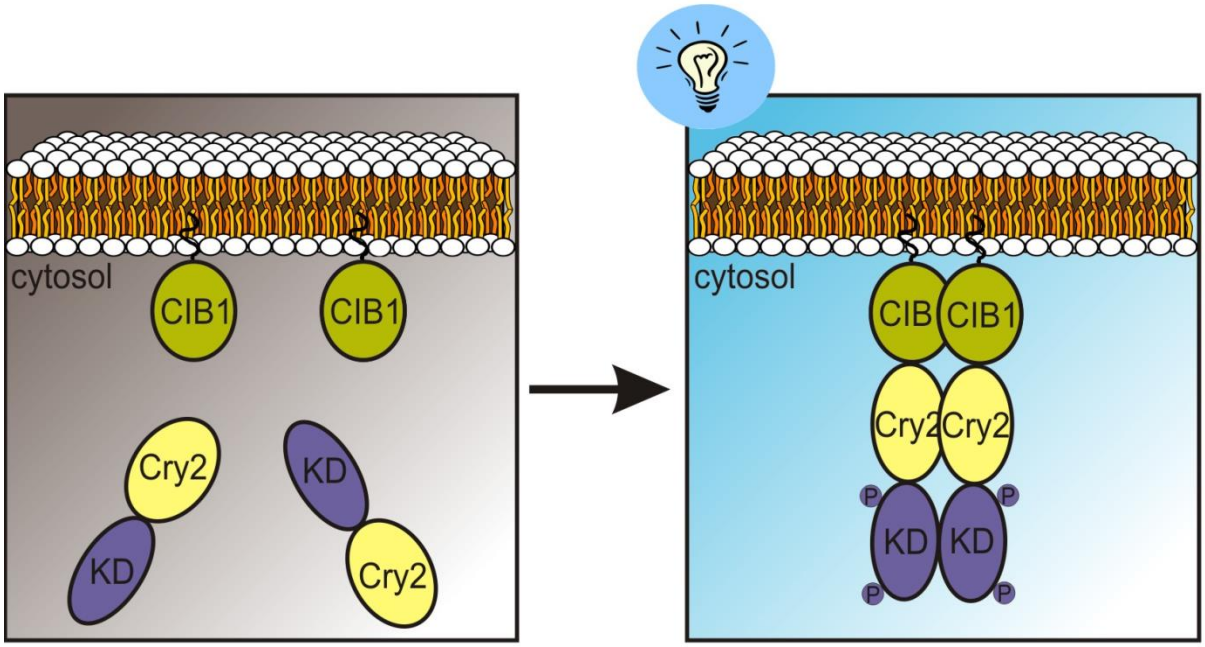

Figure 2.3 The schematic of the design developed and described in this thesis. The figure shows the predicted action of the photoactivatable TrkB. Blue light illumination is used to aggregate Cry2 fused to the C-terminus of the kinase domain (kd) of TrkB and to recruit TrkB(kd)-Cry2 to the membrane-localized CIB1 protein. This light-induced reaction leads to activating TrkB-mediated signalling at the plasma membrane.

As reviewed by Leopold et al. (2018), the process of designing a photoactivatable kinase usually starts from the choice of a target protein and a rational method for engineering this protein, and then, an appropriate optogenetic system needs to be selected. In the next step, the responsiveness of the opto-protein system should be validated using multiple tests. For this reason, the aim of this chapter is to show how a new light-inducible TrkB was created and subsequently, validated in non-neuronal cells, HEK293A and HeLa cell lines. The first validation was performed using an orange genetically encoded calcium indicator (O-GECO1) to assess the activation of PLCγ1 pathway upon blue light illumination. The determination of ERK and AKT pathway activation was fulfilled using ERK1-mCherry and mCherry-AKT1$_{PH}$ sensors upon blue light. Afterwards, the results were confirmed by western blotting using phospho-specific antibodies which can distinguish between non-activated and activated states of PLCγ1, ERK and AKT. The results obtained from these experiments showed that signalling by the new photoactivatable TrkB system was strictly regulated by light illumination.

2.2 Materials and methods

2.2.1 Materials

A summary of key resources used to develop and examine the photoactivatable TrkB system in non-neuronal cells is presented in Table A1 in Appendix.

Water for the preparation of buffers and solutions was purified through Milli-Q Water Purification System (Millipore). Buffers/solutions were sterilized through mixed cellulose ester and polyethersulfone filters with 0.2 µm pore size.

The standard LB broth was made based on a following recipe: 10 g/l tryptone, 5 g/l yeast extract, 10 g/l NaCl (and for the solid agar plate: 14 g/l agar). LB broth was autoclaved at 121°C for 20 min. Ampicillin was added to the cooled LB at final concentration of 100 µg/ml.

2.2.2 RNA extraction and cDNA synthesis

To obtain cDNAs for the kinase domain of TrkB, full-length ERK1 and PH domain of AKT1, total cellular RNA was prepared with Tri-Reagent (Sigma-Aldrich) using manufacturer provided protocol. Briefly, RNA was extracted from adult female Sprague-Dawley rat brain homogenized in Tri-Reagent (1 ml per 50 – 100 mg of tissue) in IKA 3737001 T10 basic ULTRA-TURRAX Homogenizer system 115VAC (Cole-Parmer). After centrifugation of the homogenate at 12,000 × g for 10 min at 4°C, 0.2 ml of chloroform was added per 1 ml of the supernatant. The mixture was shaken for 15 s and incubated for 5 min at RT. The subsequent centrifugation step at 12,000 × g for 15 min at 4°C separated the resulting mixture into 3 phases. The upper aqueous solution contained RNA. The isolated RNA was precipitated by adding 0.5 ml of isopropanol per 1 ml of Tri-Reagent, incubated for 10 min at RT and spun at 12,000 × g for 10 min at 4°C. The pellet of RNA was washed once using 70% ethanol (1 ml of ethanol per 1 ml of Tri-Reagent) and subsequently, air-dried for 10 min. Finally, RNA was resuspended in 20 µl RNase-free water and its purity was checked using NanoDrop (ND-1000 Spectrophotometer, Thermo Fisher Scientific). Aliquoted RNA was stored at -80°C.

In the experiments, which aimed to assess presence or absence of TrkB in HEK293A and HeLa cells, RNeasy Mini Kit (Qiagen) was used for the total RNA extraction and a

procedure of purification was provided by the manufacturer. After the quality check, RNA was stored at -80°C.

Construction of cDNA libraries was performed by using the isolated RNAs and Maxima H Minus First Strand cDNA Synthesis Kit (Thermo Scientific). In each experiment, 1 µg of RNA was used for a first strand cDNA synthesis. The mixture of RNA and the components of the cDNA Synthesis Kit were incubated for 30 min at 50°C. The reaction was terminated by heating at 85°C for 5 min. The reverse transcription reaction products were used directly in PCR or stored at -20°C.

2.2.3 Plasmid construction

2.2.3.1 Molecular cloning a photoactivatable TrkB system

The whole list of constructs created for the purpose of this chapter is included in Section 2.3.1 (see Table 2.4). The amino acid sequences of two main components of the photoactivatable TrkB are enclosed in Appendix (see Table A2).

Briefly, generation of the required DNA constructs was performed by standard molecular biology techniques: polymerase chain reaction (PCR) and 2-step overlapping PCR to introduce point mutations, digestion with restriction enzymes, ligation of a desired insert into a plasmid, transformation of DH5α bacterial strain and checking sequences by Sanger sequencing method (Sambrook et al., 1989).

The cDNA of TrkB kinase domain (TrkB(kd) region between nucleotides 1359 and 2463 in the sequence of the full-length TrkB (NCBI Reference Sequence NM_012731.2) was amplified from the rat brain cDNA library by PCR using following oligonucleotides:
BamHI-ClaI-TrkB_kinase_5F: 5'-ccggatccatcgatatgaagttggcgagacattccaagtttg-3';
TrkB_kinase-AgeI-stop-XbaI_3RC: 5'-ggtctagactaaccggtgcctaggatgtccaggtagacg-3'.

The amplified product of TrkB(kd) (~ 1.1 kbp) was fused with 5'-end of the codon-optimized photolyase homology region (PHR) of cryptochrome 2 (Cry2(498); comprising 498 amino acid residues from Cry2) through a flexible 27-base pair (bp) linker. The TrkB(kd)-Cry2(498) DNA frament was cloned into pcDNA3.1H vector, resulting in pcDNA3.1H-CMV-TrkB(kd)-Cry2(498). In addition, Cry2(498) was attached to the 5'-end of TrkB(kd) through a flexible 33-bp linker and inserted into pcDNA3.1H to create: pcDNA3.1H-CMV-Cry2(498)-TrkB(kd)). Both TrkB chimeric constructs contain a cytomegalovirus promoter (CMV).

Subsequently, a bicistronic lentiviral expression vector with TrkB(kd)-Cry2(498) and a membrane-localized CIB1 (CIB1(170)-eGFP-CAAX) under regulation of CMV promoter was created (pLenti-CMV-TrkB(kd)-Cry2(498)-T2A-CIB1(170)-eGFP-CAAX). In this vector, the first gene containing 5'-TrkB(kd)-Cry2(498)-3' was inserted at a 5'-end of a "self-cleaving" peptide (T2A, 54 bp) (Liu et al., 2017). The second gene containing 5'-CIB1(170 amino acids)-eGFP-prenylation CAAX motif-3' was cloned at 3' end of T2A.

The following constructs: pcDNA3.1H-CMV-TrkB(kd)-Cry2(498); pcDNA3.1H-CMV-Cry2(498)-TrkB(kd); pLenti-CMV-TrkB(kd)-Cry2(498)-T2A-CIB1(170)-eGFP-CAAX; pcDNA3.1H-CMV-CIB1(170)-eGFP-CAAX and pcDNA3.1H-CMV-CIB1(81)-eGFP-CAAX were prepared by Dr John Lin.

In the next cloning step, the insert: TrkB(kd)-Cry2(498)-T2A-CIB1(170)-eGFP-CAAX from the lentiviral expression plasmid was transferred into pcDNA3 vector for efficient expression in HEK293A cells. The construct: pcDNA3-CMV-TrkB(kd)-Cry2(498)-T2A-CIB1(170)-eGFP-CAAX served as a template for further cloning. To create a bicistronic construct, in which Cry2(498) is fused to the N-terminal end of TrkB(kd), 5'-Cry2(498)-TrkB(kd)-3' was PCR-amplified from pcDNA3.1H-CMV-Cry2(498)-TrkB(kd) with the following oligonucleotides:

HindIII-BamHI-Nlinker_5F: 5'-cccaagcttggatccggcaccggcagcacc-3';

TrkB-K-no stop-NheI_3RC: 5'-aaagctagcgcctaggatgtccaggtagacg-3'.

This PCR product was used to replace 5'-TrkB(kd)-Cry2(498)-3' from the bicistronic construct, resulting in the generation of pcDNA3-CMV-Cry2(498)-TrkB(kd)-T2A-CIB1(170)-eGFP-CAAX.

To test different versions of Cry2-CIB1dimerization system, longer Cry2(535) (1 – 535 amino acids of Cry2) and truncated CIB1(81) (1 – 81 amino acids of CIB1), described by Taslimi et al. (2016), were cloned into the construct: pcDNA3-CMV-TrkB(kd)-Cry2(498)-T2A-CIB1(170)-eGFP-CAAX. For this purpose, Cry2(535) flanked by the flexible linkers was PCR-amplified using the following primers:

AgeI-N-linker_5F: 5'-gcaaccggtggcggcag-3';

C-Linker-no stop-NheI_3RC: 5'-tccgctagctcccgcgcctcctcc-3'.

Subsequently, 5'-CIB1(81)-eGFP-CAAX-3' was PCR-amplified from pcDNA3.1H-CMV-CIB1(81)-eGFP-CAAX using:

BsiWI-N-linker_5F: 5'-aaacgtacgggcggcagtggtggc-3';

CAAX_stop_EcoRI_3RC: 5'-cccgaattcttacataattacacactttgtctttgacttctttttcttc-3'.

The PCR products of Cry2(535) and CIB1(81) were inserted into the corresponding sites in the bicistronic vector, resulting in: pcDNA3-CMV-TrkB(kd)-Cry2(535)-T2A-CIB1(81)-eGFP-CAAX.

To examine whether different orientation of Cry2(535)/CIB1(81) may result in better performance of the dimerizing system, a N-myristoylated CIB1(81) (MYR-CIB1(81)) was produced and inserted at 5'-end of T2A, whereas 5'-TrkB(kd)-Cry2(535)-3' was fused to 3'-end of T2A, resulting in: pcDNA3-CMV-MYR-CIB1(81)-eGFP-T2A-TrkB(kd)-Cry2(535).

To create a bicistronic control construct with eGFP, the 5'-eGFP-3' insert was cloned at 3'-end of T2A, that led to tgeneration of pcDNA3-CMV-TrkB(kd)-Cry2(535)-T2A-eGFP.

2.2.3.2 Introducing mutations into TrkB kinase domain and Cry2

The site-directed mutagenesis of TrkB kinase domain and Cry2 was performed by two-step overlap extension PCR. The sequences of the oligonucleotides used for introducing mutations into TrkB kinase domain (Y515F, K571A, Y816F) and Cry2 (W349R, D387A, E490G) are listed in Table 2.1 and Table 2.2, respectively. All mutated inserts were sequenced to confirm the presence of the intended point mutation.

Table 2.1 The oligonucleotides for mutagenesis of TrkB kinase domain.

Mutation	Name of oligonucleotide	Sequence 5' → 3'
Y515F	TrkB-Y515F_5F	gaaaacccccagtTcttcggtatc
	TrkB-Y515F_3RC	gataccgaagAactgggggttttc
	BamHI-ClaI-TrkB_kinase_5F	ccggatccatcgatatgaagttggcgagacattccaagtttg
	TrkB_kinase-AgeI-stop-XbaI_3RC	ggtctagactaaccggtgcctaggatgtccaggtagacg
K571A	TrkB-K571A_5F	gtgGCgacgctgaaggac
	TrkB-K571A_3RC	gtccttcagcgtcGCcac
	BamHI-ClaI-TrkB_kinase_5F	ccggatccatcgatatgaagttggcgagacattccaagtttg
	TrkB_kinase-AgeI-stop-XbaI_3RC	ggtctagactaaccggtgcctaggatgtccaggtagacg
Y816F	BamHI-ClaI-TrkB_kinase_5F	ccggatccatcgatatgaagttggcgagacattccaagtttg
	TrkB-Y816F-AgeI-stop-XbaI_3RC	ggtctagactaaccggtgcctaggatgtccaggAagacg

Table 2.2 The oligonucleotides for mutagenesis of Cry2(535).

Mutation	Name of oligonucleotide	Sequence 5' → 3'
W349R	CRY2-W349R_5F	ggagctgCgggccacg
	CRY2-W349R_3RC	cgtggcccGcagctcc
	AgeI-N-linker_5F	gcaaccggtggcggcag
	C-Linker-no stop-NheI_3RC	tccgctagctcccgcgcctcctcc
D387A	CRY2-D387A_5F	cacgctgctggCcgctgac
	CRY2-D387A_3RC	gtcagcgGccagcagcgtg
	AgeI-N-linker_5F	gcaaccggtggcggcag
	C-Linker-no stop-NheI_3RC	tccgctagctcccgcgcctcctcc
E490G	CRY2-E490G_5F	ctaggacacgggGggcccaaattatg
	CRY2-E490G_3RC	cataatttgggccCcccgtgtcctag
	AgeI-N-linker_5F	gcaaccggtggcggcag
	C-Linker-no stop-NheI_3RC	tccgctagctcccgcgcctcctcc

2.2.3.3 Generating reporters: ERK1, AKT1PH and O-GECO1

The of full-length ERK1 cDNA (NCBI: NM_017347.2) and a pleckstrin homology domain ($AKT1_{PH}$; amino acid 1 – 147) of AKT1 (NCBI: NM_033230.2) were amplified from rat brain cDNA library with the following primers:

BamHI-Erk1_5F: 5'-aaaggatccatggcggcggcgg-3';

Erk1-nostop-ClaI_3RC: 5'-gggatcgatgggggcctctggtgcc-3'.

NotI-Akt1-PH_5F: 5'-cgggcggccgcatgaacgacgtagccattgtgaag-3';

Akt1-PH-stop-XbaI_3RC: 5'-gattctagactacatggtcacacggtgcttgg-3'.

Subsequently, the amplified products were ligated into pcDNA3.1H vector in a frame with mCherry at the C (ERK1) or N ($AKT1_{PH}$) termini of the proteins.

The orange fluorescent genetically encoded calcium indicator (O-GECO1) was obtained from Addgene (Wu et al., 2013). The region encoding O-GECO1 was transferred into pLenti-CMV vector between BamHI and EcoRI sites. This construct (pLenti-CMV-O-GECO1) was created by Dr John Lin.

2.2.4 Sanger sequencing of prepared plasmids

The sequences for all subcloned cDNAs were confirmed by sequencing analyses. The Sanger sequencing was performed on site using 3500 Series Genetic Analyzer (Applied Biosystems) and Big Dye Terminator chemistry version 3.1 (Applied Biosystems) followed by the Agencourt CleanSEQ sequencing reaction clean-up system (Beckman Coulter). For each sequencing reaction, 250 ng of plasmid DNA was used. Compositions of sequencing reactions, conditions of sequencing cycle and purification of sequencing mixtures were performed as described by manufacturer instructions. The on-site sequencing usually allowed 600 – 850 bp of a good-quality readout.

The Sanger sequencing of difficult templates or for single reads longer than 850 bp was performed at the Australian Genome Research Facility (AGRF) in Sydney. The sample preparation information is available at: www.agrf.org.au.

2.2.5 Cell cultures and transfection

HEK293A (Invitrogen) and HeLa (American Type Culture Collection, ATCC) cells were cultured in Dulbecco's Modified Eagle Medium (DMEM; Gibco) supplemented with 8% fetal bovine serum (FBS; Gibco) and 1% Penicillin-Streptomycin solution (Sigma-Aldrich) at 37°C in a humidified 5% CO_2 environment. A routine subculturing was performed by washing cells with 5 ml of Dulbecco’s Phosphate Buffered Saline (DPBS; Sigma-Aldrich) supplemented with 20 mM HEPES and 1 mM EDTA and final pH adjusted to 7.4. Cells were trypsinized with TrypLE Express (Gibco) and subcultured in 10-cm dishes every 3 – 4 days.

The HEK293A cells stably expressing O-GECO1 (O-GECO1-HEK293A) were prepared by lentiviral infection of HEK293A. For this purpose, lentiviral particles containing O-GECO1 gene were produced by transient transfection of HEK293A cells in a 10-cm dish using X-tremeGENE 9 (Roche). X-tremeGENE 9 reagent was mixed with DNA (7.55 µg combined total of pLenti-CMV-O-GECO1, pMD2.G, psPAX2) in 2:1 ratio volume:weight (2 µl of X-tremeGENE per 1 µg of DNA) and added to cells (~90% confluent in the day of transfection). The crude medium containing viral particles was collected 24 h and 48 h after transfection. This crude medium with lentivirus was used to infect HEK293A resulting in O-GECO1-HEK293A stable cell line.

Two methods of transfection of HEK393A, O-GECO1-HEK293A and HeLa cells were used: polyethylenimine (PEI) and X-tremeGENE 9 transfection. In brief, for live cell imaging, HEK293A, O-GECO1-HEK293A or HeLa cells were seeded on glass coverslips (ø 13 mm, Thermo Fisher Scientific) in a 24-well plate ~24 h before transfection. For HEK293A and O-GECO1-HEK293A, coverslips were coated with poly-L-lysine (PLL; at a final concentration of 50 µg/ml) and collagen (at a final concentration of 500 µg/ml). Cells were transfected at ~50% confluency. Then, 0.1 µg of total DNA for HEK293A/O-GECO1-HEK293A (0.05 µg of each DNA in cotransfection experiments) and 0.2 µg of total DNA for HeLa (0.1 µg of each DNA in cotransfection experiments) per well of a 24-well plate were used. DNA was mixed with 0.1 M PEI (pH 7.0) in 2:1 ratio (e.g., 0.2 µg DNA + 0.1 µl PEI). The DNA:PEI mixture was incubated for 15 min at RT and added to cells in FBS-free medium. The cells had medium replaced with FBS-containing DMEM after 3 h from the addition of DNA:PEI. In X-tremeGENE transfection method, DNA was mixed with X-tremeGENE reagent in 1:3 ratio (e.g., 0.1 µg DNA + 0.3 µl X-tremeGENE) and incubated for 20 min at RT. Then, DNA:X-tremeGENE mixture was dropped to cells and medium was not replaced. Cells were placed in the incubator under aluminium foil to protect from light. In each method of transfection, cells were imaged ~48 h after transfection. The light stimulation experiments were performed in HEK293A cells with similar transfection efficiency of vectors expressing the TrkB system. The conditions of transfection were kept the same for each TrkB vector and enabled to achieve the transfection efficiency estimated at 50% to 70% of GFP-positive cells. The transfection efficiency was kept at this level as non-transfected cells within a field of view during imaging experiments could serve as an internal control to ensure that only GFP^+ cells could be activated under light stimulation.

For immunoblot analysis, 1.7×10^5 HEK293A cells were seeded into a 3.5-cm dish. The transfection was performed ~24 h after seeding by mixing 0.75 µg DNA per plate with X-tremeGENE in 1:3 ratio weight:volume. The DNA and transfection reagent complex was incubated for 20 min at RT and after this time, it was added to cells. The incubation of cells under aluminium foil in the incubator was continued for ~48 h.

2.2.6 Live-cell imaging, photostimulation and data acquisition

Light activation of the chimeric TrkB system was examined by the observation of PLCγ1, ERK1/2 and AKT1 signalling pathways using the genetically encoded sensors: O-

GECO1, ERK1-mCherry and mCherry-AKT1$_{PH}$, respectively. Cells transfected with the required sensor and the photoactivatable TrkB system were imaged at RT.

Live-cell imaging was performed using an Olympus BX51WI fluorescent microscope equipped with a Scientific CMOS camera and the water immersion objectives: 40×/NA0.8 (Olympus) and 20×/NA0.5 (Zeiss). A white light LED (X-Cite 110LED, Excelitas Technologies) was the fluorescence light source. GFP (excitation at 470 nm) images were taken using a GFP filter cube: 472/30, FF495-Di03, FF01-520/35, whereas O-GECO1 (excitation at 543 nm) and mCherry (excitation at 587 nm) were detected using a second filter cube: FF01-543-22, 562-Di03, FF01-593/40. Micro-Manager 1.4.22 software was used for microscope image acquisition. For blue light activation of Cry2-CIB1 and Cry2-Cry2 interactions, a customized LED (Luxeon Star) was placed next to the recording chamber. The stimulation mode of the LED device was controlled by LED Driver Control Panel V3.1.0 (Mightex). The light intensity and duration of light stimulation are stated in the text or in the figure legends. Figure 2.4 illustrates how live-cell imaging with blue light stimulation was performed.

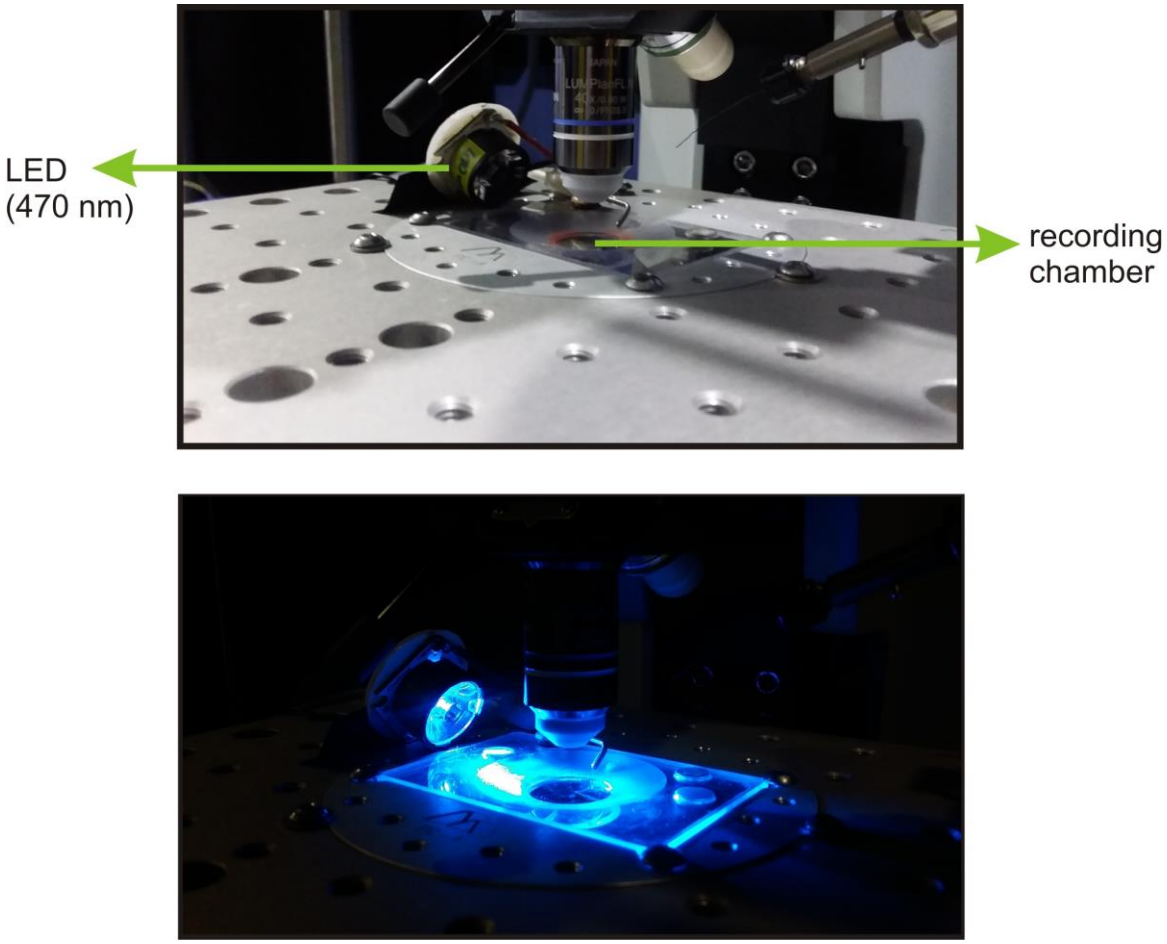

Figure 2.4 A customized LED device for blue light stimulation during live-cell imaging. The light intensity and duration of illumination were set via LED Driver Control Panel V3.1.0 (Mightex). Blue light was irradiated from the side of the recording chamber not to disrupt imaging.

2.2.6.1 Calcium imaging with O-GECO1 sensor

The O-GECO1-HEK293A stable cell line transfected with the photoactivatable TrkB system was imaged at ~48 h post-transfection. Cells seeded on 13 mm-coverslips were transported in extracellular solution (ECS) in a dish wrapped in aluminium foil. The ECS was of the following composition: 140 mM NaCl, 2.8 mM KCl, 10 mM HEPES, 1 mM $MgCl_2$, 2 mM $CaCl_2$, 10 mM D-glucose, pH 7.4, osmolarity between 290 and 310 mOsm/l. This ECS also served as recording solution in the microscope recording chamber. The O-GECO1, intensiometric fluorescent protein-based Ca^{2+} indicator, has an excitation maximum at 543 nm and emission at 564 nm in Ca^{2+}-bound state, which enables the imaging of Ca^{2+} changes independent from activation of Cry2-CIB1 dimerization with blue light (470 nm) (Wu et al., 2013). Calcium imaging was performed using the O-GECO1/mCherry filter cube and either 40× or 20× objectives. Images were obtained at a frame rate of 1 Hz and acquisition parameters were the same for all groups of cells to be compared. Blue light stimulation of 1 s pulse duration at 36.8 mW/cm^2 (100 mA LED current) was delivered at 0.5 min from the beginning of the imaging timecourse (unless stated otherwise). The expression of the photoactivatable TrkB, visualized through the GFP filter cube, was checked at the end of each imaging session. Calcium imaging experiments in HeLa cells, co-transfected transiently with O-GECO1 and the photoactivatable TrkB constructs, were performed as described for HEK293A cells.

In an experiment testing PLCγ1 inhibitor, U73122 (Sigma-Aldrich), the transfected O-GECO1-HEK293A cells were pre-incubated with 2.5 µM U73122 diluted in ECS for 10 min at 37°C. After this time, cells were imaged as described above in ECS containing 2.5 µM U73122 for another 5 min at RT. The control cells were incubated with the same volume of DMSO (at final concentration of 0.125% v/v) for 10 min at 37°C.

Calcium imaging in a nominally calcium-free solution was carried out as described above. ECS did not contain 2 mM $CaCl_2$ and its osmolarity was 290 mOsm/l. In this experiment images were taken at a frame rate of 0.5 Hz and blue light (1 s pulse at 36.8 mW/cm^2) was irradiated at 5.5 min of the time-lapse.

Calcium imaging data were analyzed in ImageJ. In each experiment, only GFP-positive cells (expressing chimeric TrkB constructs) were quantified. Ca^{2+} levels in GFP-positive cells were calculated as a change in O-GECO1 fluorescence intensity normalized to the baseline fluorescence (before blue light stimulation). Number of replicates/cells and statistical tests to assess significance were stated in the text or in the figure legends. Statistical analyses were performed in OriginPro 8.

2.2.6.2 ERK1 and $AKT1_{PH}$ translocation assay

The HEK293A and HeLa cells co-transfected with the photoactivatable TrkB system and ERK1-mCherry were imaged ~48 h after transfection. Cells were transported and imaged in the same ECS as for calcium imaging (Section 2.2.6.1). Images were collected every 30 s through the O-GECO1/mCherry filter cube and 40× objective. Blue light pulse (1 s at 36.8 mW/cm^2) was delivered at 3 min of a timecourse. The expression of the photoactivatable TrkB was validated at the end of each experiment and only GFP-positive cells were analyzed. The ERK1 translocation from cytosol to nucleus was calculated as a ratio between nuclear and cytosolic ERK1 intensities normalized to the background before light exposure. The formula to determine this ratio is: ratio = $(I_{nucleus} - I_{background}) / (I_{cytosol} - I_{background})$ where "I" is the average pixel intensity. The average pixel intensity was measured in a circular ROI covering the nucleus or in an elliptical ROI covering the cytoplasm. The average pixel intensity for background was measured from ROI outside cells. Statistical analyses were performed using OriginPro 8. Number of replicates/cells and statistical tests to assess significance were stated in the text or in the legends of figures.

The HEK293A and HeLa cells co-transfected with the photoactivatable TrkB system and the mCherry-$AKT1_{PH}$ sensor were imaged in the exactly same manner as cells expressing the ERK1-mCherry sensor. The translocation of mCherry-$AKT1_{PH}$ from cytosol to membrane was not analyzed quantitatively.

2.2.7 Harvesting cells, SDS-PAGE and western blotting

Around 48 h post-transfection, HEK293A cells were illuminated with blue light. The LED (470 nm) used for illumination was customized and controlled by LED Driver Control Panel V3.1.0 (Mightex). Blue light intensity was measured using an optical power meter (Thorlabs, model S121C) by Dr John Lin and Ms Elise Devenish. Cells were illuminated

with continuous blue light set with an LED current of 100 mA (36.8 mW/cm^2) for 30 s at RT. Figure 2.5 shows how cells plated into a 3.5-cm dish were subjected to blue light illumination. Control cells were kept on a disabled LED for 30 s at RT (dark condition). Cells were transported from an incubator to LED in a dark container and room lights remained off during experiments. After the incubation on the LED, cells were returned to the incubator and harvested after 10 min.

Non-transfected cells were treated with BDNF (Invitrogen) at final concentration of 100 ng/ml for 10 min. The control non-transfected cells were treated with a vehicle (in this case, with Molecular Biology Grade Water, Sigma-Aldrich) for 10 min.

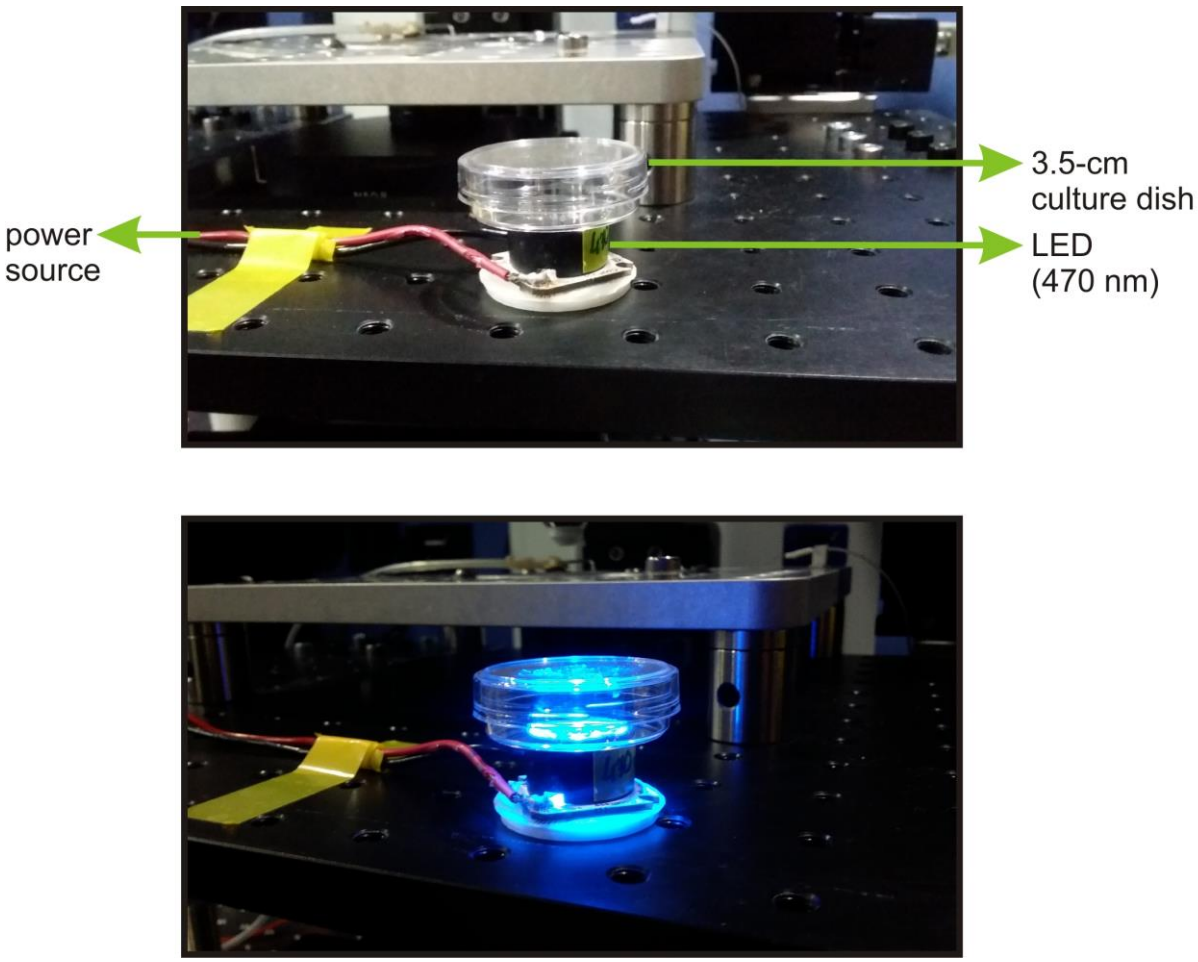

Figure 2.5 A customized LED device for activation of cells grown on a 3.5-cm dish. The light intensity can be controlled via LED Driver Control Panel V3.1.0 (Mightex). As shown, light from LED was irradiated from the bottom of the dish and was not distributed evenly across the bottom of the dish.

After desired treatment, cells were washed twice with ice-cold PBS and lysed in 200 µl of RIPA buffer (50 mM Tris-HCl, 150 mM NaCl, 1% NP-40, 1% sodium deoxycholate, 0.1% SDS, protease inhibitor cocktail (Roche), phosphatase inhibitor cocktail (Roche)) in the dark. Collected lysates were frozen in liquid nitrogen and stored at -80°C until use. Thawed lysates were clarified by centrifugation at 13,000 rpm (Heraeus Rotor 3325B), 4°C for 10 min. Then,

Table 2.3 Primary and secondary antibodies used for immunoblotting analysis in HEK293A cells.

Antibody	Epitope	Isotype	Concentration used
Primary antibody			
Anti-Phospho-Akt	Phospho-Ser473	Rabbit monoclonal	1:2,000
Anti-Akt	C-terminus of Akt	Rabbit polyclonal	1:1,000
Anti-Phospho-p44/42 MAPK (Erk1/2)	Phospho-Thr202/Tyr204	Mouse monoclonal	1:2,000
Anti-p44/42 MAPK (Erk1/2)	C-terminus of p44 MAPK	Rabbit polyclonal	1:1,000
Anti-Phospho-PLCγ1	Phospho-Tyr783	Rabbit polyclonal	1:1,000
Anti-PLCγ1	Residues surrounding Leu1220 of PLCγ1	Rabbit monoclonal	1:1,000
Secondary antibody			
Anti-Mouse/HRP	-	Goat polyclonal	1:10,000
Anti-Rabbit/HRP	-	Goat polyclonal	1:10,000

supernatants were aspired and a Lowry-based assay (DC Protein Assay, Bio-Rad) was carried out to assess protein concentrations. The lysates were mixed with Bolt LDS Sample Buffer (Invitrogen) supplemented with DTT and denatured at 70°C for 10 min. 10 µg of total proteins for anti-ERK/anti-AKT antibodies and 20 µg of total proteins for anti-PLCγ1 antibodies were resolved on Bolt 4 – 12% Bis-Tris Plus gels (Invitrogen) (two separate gels for phospho- and total-antibody to avoid stripping of the membrane when quantification was required) using a Mini Gel Tank (Life Technologies, cat#A25977). Proteins were transferred to a polyvinylidene fluoride (PVDF) membrane (Bio-Rad) using a Mini Blot Module (Life Technologies, cat#B1000) at 20 V, 4°C for 60 min. After transfer, the PVDF membranes

were incubated for 60 min at RT in 5% (w/v) non-fat dry milk in TBS buffer supplemented with 0.05% (v/v) Tween-20 (Sigma-Aldrich). Subsequently, the membranes were probed with primary antibodies diluted in 5% non-fat dry milk + TBS buffer + 0.05% Tween-20. Incubation was carried out overnight at 4°C. This was followed by an incubation for 60 min at RT with the appropriate horseradish peroxidase conjugated secondary antibody diluted in 1% non-fat dry milk + TBS buffer + 0.05% Tween-20. The concentrations of primary and secondary antibodies used for immunoblotting are listed in Table 2.3 and ordering details are in Table A1 (see Appendix). Proteins were detected by using Immobilon Western Chemiluminescent HRP Substrate (Millipore) and scanned by Amersham Imager 600 (GE Healthcare).

2.3 Results

2.3.1 The design of a light-activated TrkB system

As illustrated in Figure 2.3, a light-inducible TrkB system, developed for the purpose of this project, consists of two components necessary for its activation. One component contains an intracellular kinase domain with the juxtamembrane and C-tail of TrkB linked to a photolyase homology region (PHR) of Cry2 (referred to as TrkB(kd)-Cry2 from here in). The sequence of TrkB(kd) corresponds to the sequence of TrkB between amino acids 454 and 821 published (UniProtKB Q63604-1; TrkB isoform GP145-TrkB). The second component of the TrkB system is composed of a truncated CIB1 attached to an enhanced green fluorescent protein and a membrane localization sequence (referred to as CIB1-eGFP). Blue light illumination induces interactions between Cry2 and CIB1, and the expression of this dimerization module is not toxic for cells (Kennedy et al., 2010). Moreover, the activities of target proteins can be controlled with light when they are fused to Cry2/CIB1 (Chang et al., 2014; Duan et al., 2018; Katsura et al., 2015; Kennedy et al., 2010; Taslimi et al., 2016). My two-component TrkB system is designed so that upon light illumination, TrkB(kd)-Cry2 can be recruited to CIB1-eGFP, which is localized in the membrane, and simultaneously, TrkB(kd)-Cry2 can oligomerized in the membrane through Cry2-Cry2 interactions. As described below, this process can activate downstream signalling pathways in a light-dependent manner.

To test the system in non-neuronal cells, TrkB(kd)-Cry2 and CIB1-eGFP were cloned into the mammalian expression vector pcDNA3.1H or pcDNA3, under transcriptional control

Table 2.4 Generated DNA constructs for non-neuronal studies.

#	The full name of construct
DNA constructs encoding the sensor proteins	
1	pLenti-CMV-O-GECO1
2	pcDNA3.1H-CMV-ERK1-mCherry
3	pcDNA3.1H-CMV-mCherry-AKT1$_{PH}$
DNA constructs serving as templates for further cloning	
4	pcDNA3.1H-CMV-CIB1(170)-eGFP-CAAX
5	pcDNA3.1H-CMV-CIB1(81)-eGFP-CAAX
6	pcDNA3.1H-CMV-MYR-CIB1(81)-eGFP
7	pcDNA3.1H-CMV-TrkB(kd)-Cry2(498)
8	pcDNA3.1H-CMV-Cry2(498)-TrkB(kd)
9	pLenti-CMV-TrkB(kd)-Cry2(498)-T2A-CIB1(170)-eGFP-CAAX
DNA constructs with wild-type TrkB(kd) and different Cry2 and CIB1	
10	pcDNA3-CMV-TrkB(kd)-Cry2(498)-T2A-CIB1(170)-eGFP-CAAX
11	pcDNA3-CMV-Cry2(498)- TrkB(kd)-T2A-CIB1(170)-eGFP-CAAX
12	pcDNA3-CMV-TrkB(kd)-Cry2(535)-T2A-CIB1(81)-eGFP-CAAX
13	pcDNA3-CMV-MYR-CIB1(81)-eGFP-T2A-TrkB-Cry2(535)
14	pcDNA3-CMV-TrkB(kd)-Cry2(535)-T2A-eGFP
DNA constructs with a point mutation within TrkB(kd)	
15	pcDNA3-CMV-**TrkB(kd)-Y816F**-Cry2(498)-T2A-CIB1(170)-eGFP-CAAX
16	pcDNA3-CMV-**TrkB(kd)-Y515F**-Cry2(498)-T2A-CIB1(170)-eGFP-CAAX
17	pcDNA3-CMV-**TrkB(kd)-K571A**-Cry2(498)-T2A-CIB1(170)-eGFP-CAAX
DNA constructs with a point mutation within Cry2(535)	
18	pcDNA3-CMV-TrkB(kd)-**Cry2(535)-D387A**-T2A-CIB1(81)-eGFP-CAAX
19	pcDNA3-CMV-TrkB(kd)-**Cry2(535)-E490G**-T2A-CIB1(81)-eGFP-CAAX
20	pcDNA3-CMV-TrkB(kd)-**Cry2(535)-W349R**-T2A-CIB1(81)-eGFP-CAAX

pLenti, pcDNA3.1H (H = hygromycin B antibiotic resistance) and pcDNA3 are the plasmid backbones. By using these backbones, the expression of required proteins is controlled under the cytomegalovirus promoter (CMV). CAAX, C-terminal prenylation signal (GKKKKKKSKTKCVIM); MYR, N-terminal myristoylation signal (MGCIKSKRKDNLN); T2A, "self-cleaving" peptide derived from thosea asigna virus 2A (EGRGSLLTCGDVEENPGP).

of CMV promoter. The different truncations and combinations of Cry2 PHR domains (498 vs 535 amino acids) and CIB1 (170 vs 81 amino acids) were tested (Kennedy et al., 2010;

Taslimi et al., 2016). The exact truncated form is acknowledged in a bracket from here in (e.g. TrkB(kd)-Cry2(498)). Moreover, two orientations of Cry2 to TrkB(kd) were examined, in which TrkB(kd) was fused to the N- or C-terminus of Cry2. Three amino acid point mutations in Cry2 (D387A, E490G, W349R) were investigated to determine their effects on the kinetics of TrkB signalling activation. To study whether the upregulation of canonical TrkB signalling is mediated through kinase activity specifically, the point mutations in TrkB(kd) (Y816F, Y515F, K571A) were introduced. For the attachment of CIB1 to the membrane, the N-terminal MYR and C-terminal CAAX tags were both tested. In most of the experiments, bicistronic constructs with a T2A sequence were used to promote equal levels of co-expression of Cry2 and CIB1 components. The T2A sequence is a "self-cleaving" peptide derived from a viral genome (T2A; thosea asigna virus 2A) (Szymczak and Vignali, 2005). The "self-cleaving" is achieved by skipping the formation of a glycyl-prolyl peptide bond at the C-terminus of T2A by ribosome and when successful, it results in translation of two proteins (Donnelly et al., 2001; Liu et al., 2017). From here in, the application of the bicistronic vector is pointed by adding "T2A" between each component in the photoactivatable TrkB system. The list of created DNA constructs is presented in Table 2.4.

2.3.2 Light-mediated activation of canonical TrkB pathways in HEK293A cells

2.3.2.1 Light activation of optogenetic TrkB increases cytosolic calcium through PLCγ1 signalling

The phosphorylation of TrkB at Y816 provides a docking site for PLCγ1, which leads to the phosphorylation of PLCγ1 and its activation (Kim et al., 1991; Middlemas et al., 1994). Subsequently, activated PLCγ1 can cause Ca^{2+} to be released from the internal store (see Fig. 2.1) (Berridge and Irvine, 1984; Disatnik et al., 1994; Widmer et al., 1993) and Ca^{2+} influx through a subsequent activation of a transient receptor potential cation channel 3 (TRPC3) (Amaral and Pozzo-Miller, 2007).

Monitoring Ca^{2+} changes was used as a surrogate for PLCγ1 activity. A HEK293A cell line stably expressing the Ca^{2+} biosensor, O-GECO1, was transfected with the different variants of the TrkB tools. The cells transfected with pcDNA3-TrkB(kd)-Cry2(498)-T2A-CIB1(170)-eGFP-CAAX, encoding both Cry2 and CIB1 components, showed the elevation of intracellular Ca^{2+} upon a single blue light pulse of 1 s (470 nm) (Fig. 2.6 A, B). Blue light illumination activated only eGFP positive cells, which indicated the expression of this TrkB

tool. The light-provoked Ca^{2+} increase was transient and returned to the baseline within 5 min (Fig. 2.6 B, black trace). The CIB1(170)-eGFP-CAAX component or TrkB(kd)-Cry2(498) alone was not sufficient to elevate intracellular Ca^{2+} in response to the blue light stimulation (Fig. 2.6 B, blue and red trace, respectively). A previous reported photoactivation of O-GECO1 (Wu et al. (2013); Fig. 4 C) was not observed under our conditions of stimulation.

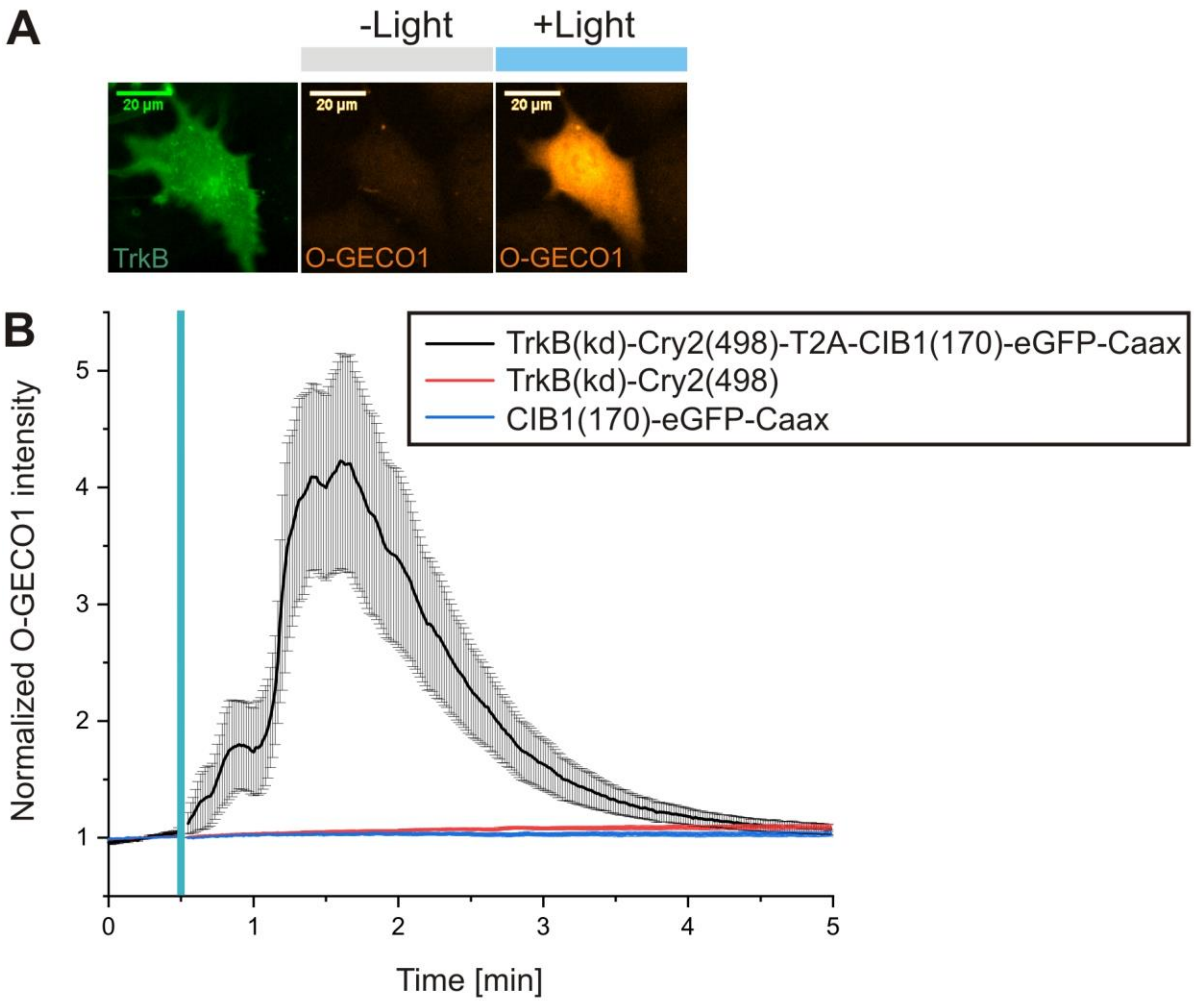

Figure 2.6 Light activates the photoactivatable TrkB system. (A) In O-GECO1-HEK293A stable cell line co-expressing TrkB(kd)-Cry2(498) and the membrane-anchored CIB1(170), light illumination led to the elevation of intracellular Ca^{2+}, as visualized with the orange fluorescent genetically encoded calcium indicator (O-GECO1), which is consistent with the activation of PLCγ1. The images show an example of a cell expressing TrkB(kd)-Cry2(498)-T2A-CIB1(170)-eGFP-CAAX which responded to blue light illumination. **(B)** The graph shows that both components (TrkB(kd)-Cry2(498) and CIB1(170); black line) were necessary to elevate intracellular Ca^{2+} in cells. Either TrkB(kd)-Cry2(498) or CIB1(170)-eGFP-CAAX component alone was not sufficient to evoke Ca^{2+} transients. Intracellular Ca^{2+} changes were quantified as O-GECO1 fluorescence intensity normalized to the baseline fluorescence before blue light stimulation delivered at 0.5 min after the initiation of imaging (represented as a blue line). Results are presented as mean ± SEM calculated from one independent experiment performed in triplicates. The total numbers of cells used for quantification are as follows: 19 cells for TrkB(kd)-Cry2(498)-T2A-CIB1(170)-eGFP-CAAX; from 27 cells for TrkB(kd)-Cry2(498); from 30 cells for CIB1(170)-eGFP-CAAX.

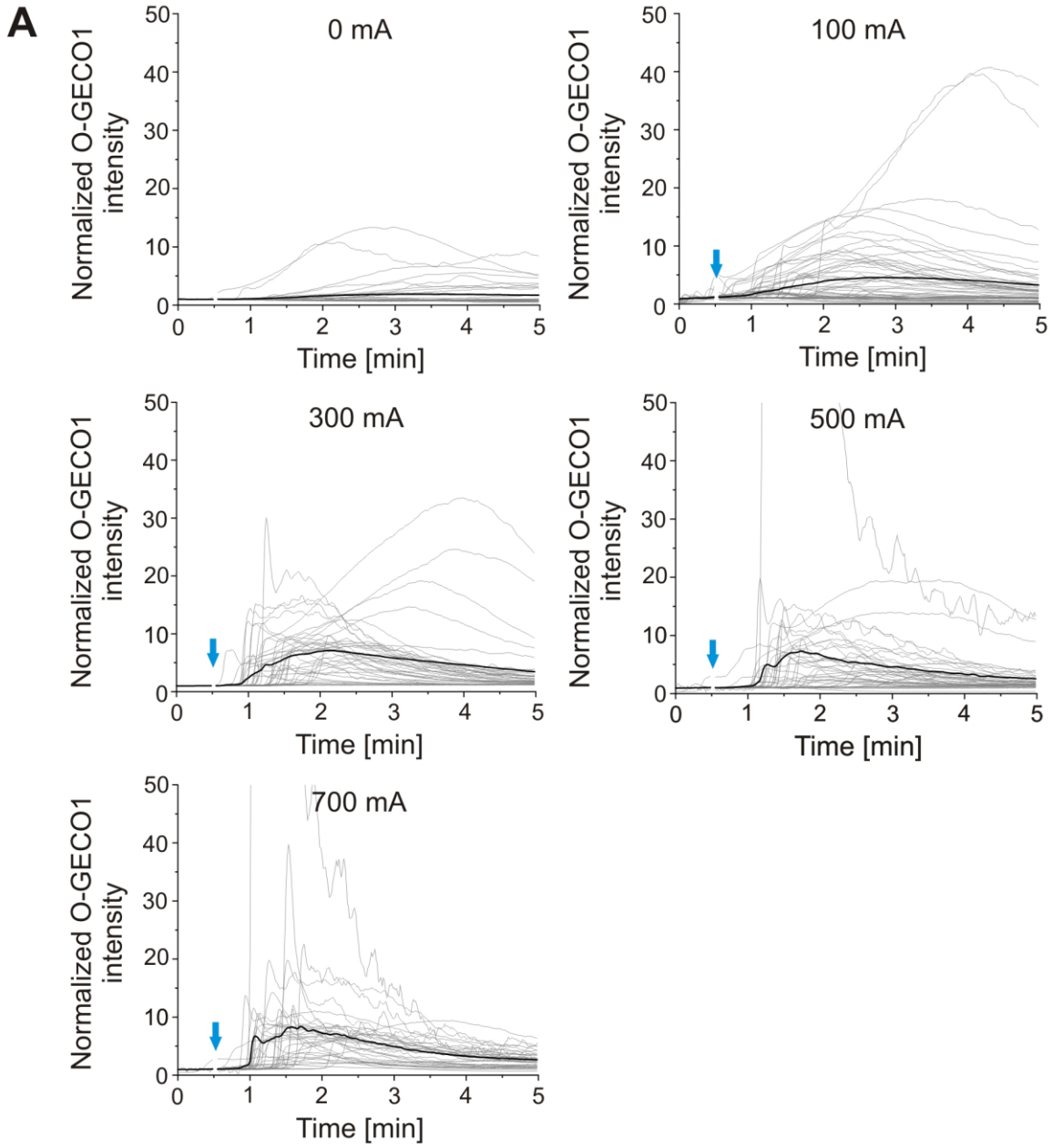
A
0 mA
100 mA
300 mA
500 mA
700 mA
Normalized O-GECO1 intensity
Time [min]

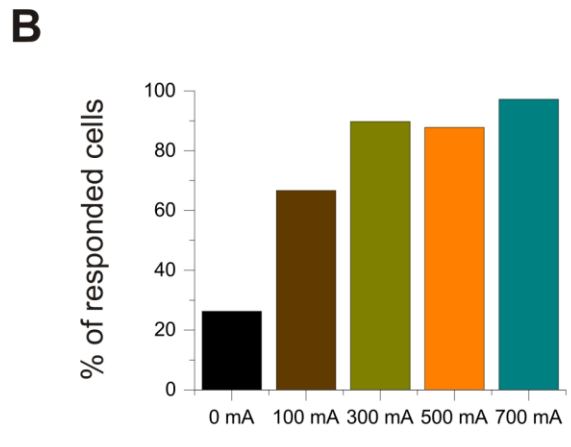
B
% of responded cells
0 mA
100 mA
300 mA
500 mA
700 mA

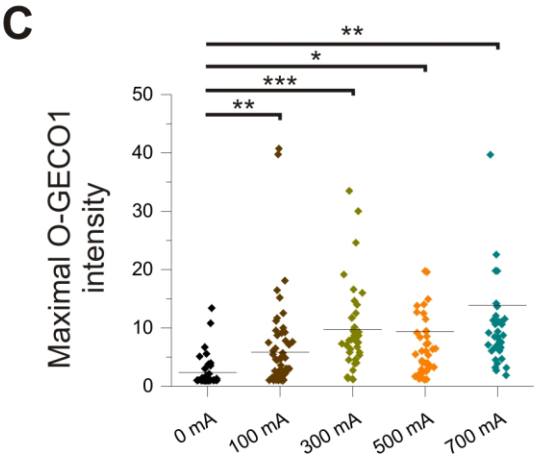
C
Maximal O-GECO1 intensity
**
*
***
**
0 mA
100 mA
300 mA
500 mA
700 mA

Figure 2.7 The effect of increasing LED light intensities on Ca^{2+} responses in O-GECO1-HEK293A cells transfected with TrkB(kd)-Cry2(498)-T2A-CIB1(170)-eGFP-CAAX. (A) Graphs represent raw Ca^{2+} transients in the individual cells (grey lines) and the mean (black lines) upon the increasing light intensities of 470 nm LED (36.8 mW/cm^2 at 100 mA, 95.6 mW/cm^2 at 300 mA, 148.1 mW/cm^2 at 500 mA, 191.8 mW/cm^2 at 700 mA) delivered as a 1-s pulse. The light stimulation is indicated as a blue arrow. **(B)** Bar graph represents the percentage of TrkB system-positive cells, which responded upon the increasing powers of the blue light. 26% of non-stimulated cells responded upon the conditions of imaging (0 mA). This response was considered as a background activity of the system. However, more cells responded upon blue light stimulation (67% for 100 mA; 90% for 300 mA; 88% for 500 mA; 97% for 700 mA). **(C)** Graph represents the peak values of Ca^{2+} transients for individual cells within each group showed in (A). The 100 mA current was the lowest intensity tested that gave the significant increase in the amplitude of Ca^{2+} in comparison to non-stimulated cells with blue light. Two cells, one in the 500 mA group and second in the 700 mA group, reached the intensiometric changes of 117× and 149×, respectively (not shown in the graph). This magnitude of changes is possible for O-GECO1 as described by Wu et al. (2013). Significance was compared between the response for 0 mA and the responses for the increasing blue light powers (100 mA, 300 mA, 500 mA and 700 mA, respectively). The individual dot represents a maximal O-GECO1 intensity for a single cell (line = mean; ***P<0.001, **P<0.01, *P<0.05, unpaired Student's t-test). The total number of cells tested from one independent experiment performed in triplicates is as follows: 38 cells for 0 mA; 60 cells for 100 mA; 39 cells for 300 mA; 41 cells for 500 mA; 36 cells for 700 mA.

Four different blue light (470 nm) intensities were tested. Each population of transfected cells was exposed to a 1-s light pulse with the LED current set at 0 mA (background activity caused by a live-imaging light and without blue light stimulation), at 100 mA, 300 mA, 500 mA and 700 mA (Fig. 2.7). The estimated light intensities at each LED current were as follows: 36.8 mW/cm^2 at 100 mA, 95.6 mW/cm^2 at 300 mA, 148.1 mW/cm^2 at 500 mA, 191.8 mW/cm^2 at 700 mA. The green light applied during the live-cell imaging without the exposure of blue light evoked the activation of Ca^{2+} signalling in 26% of cells expressing the photoactivatable TrkB system (Fig. 2.7 B). Nevertheless, the delivery of blue light at increasing intensities activated 67%, 90%, 88%, 97% for 100 mA, 300 mA, 500 mA and 700 mA, respectively (Fig. 2.7 B). Moreover, the lowest blue light intensity, which gave the significant increase in the mean peak value of Ca^{2+} responses over the background activity (at 0 mA), was 100 mA (Fig. 2.7 C). The LED settings at 100 mA were used as default for the blue light stimulation.

To test whether the Ca^{2+} transients can be evoked repeatedly, the 1-s blue light pulses were delivered three times to the same cells separated by 20 min intervals. Light-induced Ca^{2+} was detected in all instances in spite of smaller responses in second and third stimulation (Fig. 2.8). The 20 min between blue-light stimulation was sufficient to allow Cry2-CIB1 to come back to the unbound state because the reversal time of Cry2-CIB1 has

been reported as ~12.5 min (Kennedy et al., 2010). The activation of the TrkB system could therefore be controlled in a recurrent manner.

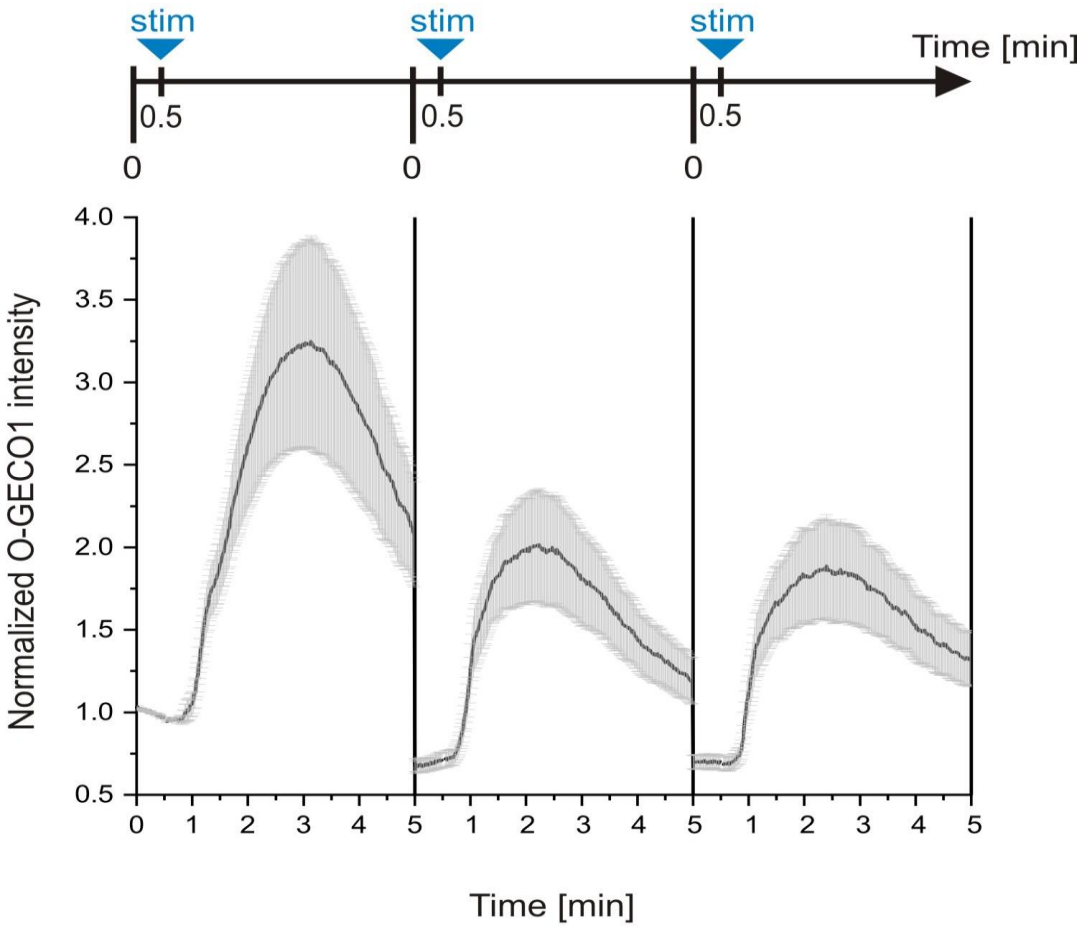

Figure 2.8 Ca^{2+} transients can be controlled in a reversible manner with light. Delivery of three 1-s light pulses with 20-min interstimulus intervals evoked Ca^{2+} transients repetitively in O-GECO1-HEK293A cells expressing TrkB(kd)-Cry2(498)-T2A-CIB1(170)-eGFP-CAAX. The results are presented as mean ± SEM calculated from 25 cells. All responses were normalized to the baseline fluorescence before first light stimulation at 0.5 min.

By using a correlation analysis, the existence of a relationship between the expression level of the photoactivatable TrkB system and the magnitude of Ca^{2+} transient was investigated. The O-GECO1-HEK293A cells were transfected with pcDNA3-CMV-TrkB(kd)-Cry2(498)-T2A-CIB1(170)-eGFP-CAAX and the standard Ca^{2+} imaging with the 1-s blue light stimulation was performed as described before. The expression of photoactivatable TrkB was determined by measuring fluorescence intensity of eGFP. The expression level was correlated with the peak value of Ca^{2+} signal upon the blue light stimulation. Using a Pearson's correlation coefficient (Pearson's r), it was shown that expression level was a poor predictor of the magnitude of Ca^{2+} signal (although the negative

sign of the regression slope was significant at P = 0.00015 (< 0.05); Fig. 2.9). In the same experiment, it was assessed that 76% of cells, expressing the TrkB system, responded to the blue light stimulation.

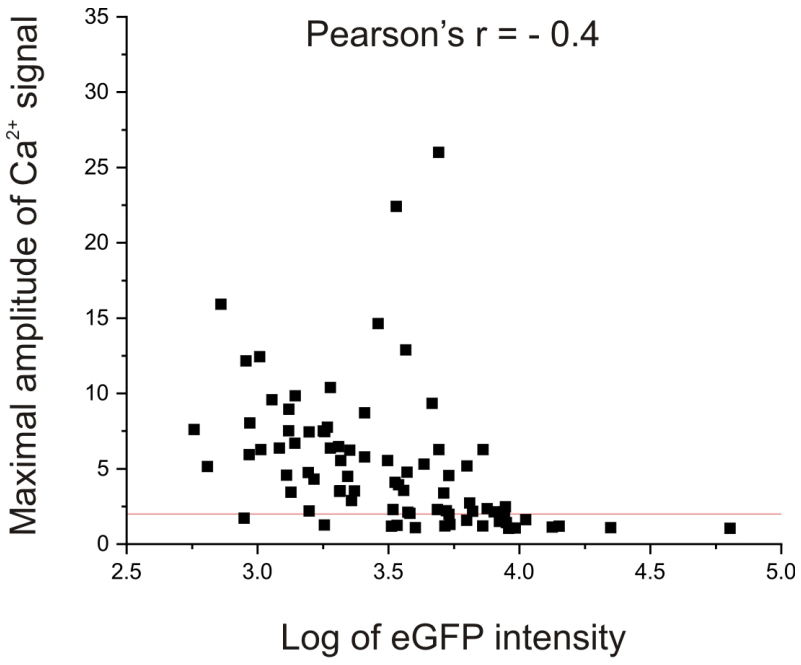

Figure 2.9 The relationship between the expression level of TrkB system and the amplitude of Ca^{2+} response upon blue light illumination. In O-GECO1-HEK293A cells expressing TrkB(kd)-Cry2(498)-T2A-CIB1(170)-eGFP-CAAX, the expression of the photoactivatable TrkB system (measured as the intensity of eGFP fluorescence) was a poor predictor of the magnitude of Ca^{2+} signal (Pearson's r = -0.407; n = 82 cells; P = 0.00015). The horizontal line at 2 separates cells with the amplitudes lower than 2, which were considered as non-responesive cells. 76% of cells responded to the light stimulation above this threshold.

The order of domains in the fusion between TrkB(kd) and Cry2(498) appears to influence the effectiveness of this system. When Cry2(498) was linked to the N-terminus of TrkB(kd), the Ca^{2+} transients were evoked less efficiently upon blue light. Only 6% of the cells expressing the TrkB system in this order responded compared to 76% when Cry2(498) was linked to the C-terminus of TrkB(kd) (Fig. 2.10).

To determine if the observed stimulatory effect of blue light is mediated through the specific PLCγ1 signalling cascade, the O-GECO1-HEK293A cells expressing TrkB(kd)-Cry2(498)-T2A-CIB1(170)-eGFP-CAAX were treated with an aminosteroid inhibitor of PLC receptors (U73122) prior performing Ca^{2+} imaging. The U73122 inhibitor blocks PLC-catalyzed evolution of DAG and Ins(1,4,5)P_3 (Bleasdale et al., 1990). Consequently, U73122

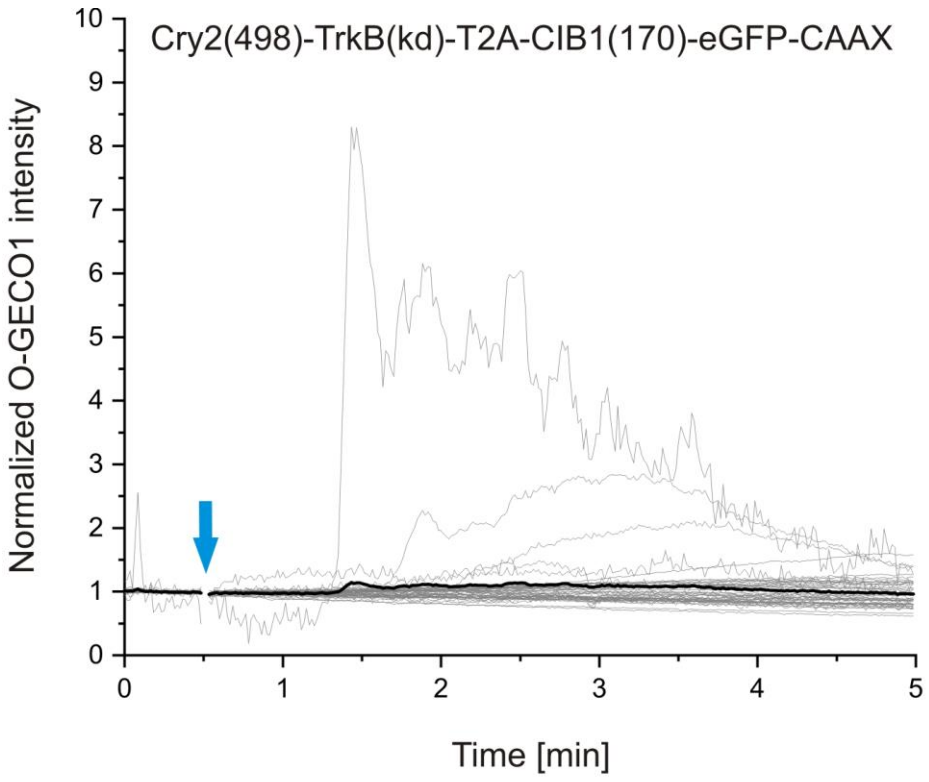

Figure 2.10 The fusion of Cry2(498) to the N-terminus of TrkB(kd) is less effective at elevating Ca^{2+}. When TrkB(kd) was fused to C-terminus of Cry2 (498) (Cry2(498)-TrkB(kd)) only 6% of the cells expressing these proteins responded to the 1-s light stimulation compared to 76% of the cells with TrkB(kd) fused to the N-terminus of Cry2(498). Grey lines represent the Ca^{2+} traces for single cells, whereas black line represents the mean measured from 47 cells pooled from two independent experiments each performed in duplicates. Blue arrow shows the blue light delivery.

inhibits Ca^{2+} mobilization from intracellular stores associated with PLC activation (Jin et al., 1994). The pre-incubation of O-GECO1-HEK293A cells expressing TrkB(kd)-Cry2(498)-T2A-CIB1(170)-eGFP-CAAX with 2.5 µM U73122 for 10 min abolished light-evoked Ca^{2+} responses (Fig. 2.11, compare A and B). These results suggest that PLC-mediated production of $Ins(1,4,5)P_3$ is an essential step for the light-induced elevation of the intracellular Ca^{2+}.

To investigate the source of intracellular Ca^{2+}, cells were incubated and imaged in a Ca^{2+}-free solution. The Ca^{2+}-free solution had the similar composition to ECS described in Section 2.2.6.1, but it did not contain 2 mM $CaCl_2$. The transfected O-GECO1-HEK293A cells were imaged in this solution for 10 min at 0.5 Hz and 1-s blue light pulse was delivered at 5.5 min of the time-lapse. The results shown in Figure 2.12 A indicated that without 2 mM extracellular Ca^{2+}, the Ca^{2+} transients could be still activated with blue light, suggesting that

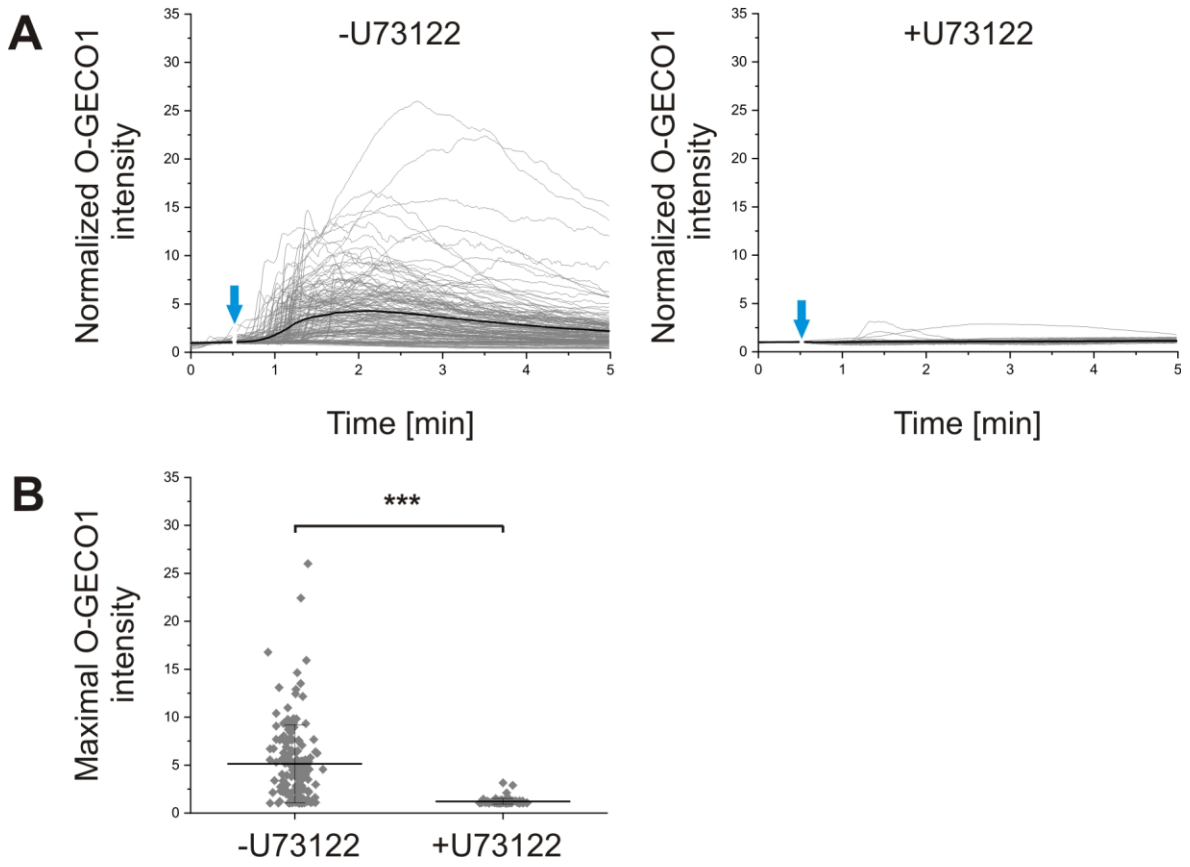

Figure 2.11 Light activation of TrkB signalling is consistent with PLCγ1-mediated Ca^{2+} increase. (A) In O-GECO1-HEK293A cells transfected with TrkB(kd)-Cry2(498)-T2A-CIB1(170)-eGFP-CAAX, blue light delivered at 0.5 min of a timecourse (arrow) led to the elevation of intracellular Ca^{2+} (left graph). Pre-treatment of cells with PLC inhibitor U73122 at the final concentration of 2.5 µM for 10 min reduced light-evoked Ca^{2+} signals (right graph). Ca^{2+} transients were quantified as changes in O-GECO1 fluorescence intensity normalized to the baseline fluorescence prior photostimulation. The grey lines are responses of the individual cells and the mean is shown in black. **(B)** The column scatter graph shows the peak responses of individual cells (grey dots) represented in the panel A for non-treated cells (-U73122; n = 154) and cells treated with the inhibitor (+U73122; n = 105). Central line and error bars represent mean ± SD; ***P<0.001, unpaired Student's t-test.

Ca^{2+} was released from the internal store. Interestingly, Ca^{2+} responses in the Ca^{2+}-free solution were more transient and recovered to the baseline within 1.5 min, whereas in the normal ECS, these responses came back to the baseline within 2.5 min (Fig. 2.12 A, B). This might suggest that in addition to the mobilization of the internal store, a different Ca^{2+} source can be involved in the light-mediated Ca^{2+} signalling when the extracellular Ca^{2+} is present.

To investigate whether the elevation of Ca^{2+} signalling upon blue light requires the kinase activity of the photoactivatable TrkB, three different point mutations were introduced into TrkB(kd). Firstly, a mutation from tyrosine to phenylalanine at 515 amino acid of TrkB(kd) (TrkB_Y515F) was introduced as described in the literature (Easton et al., 1999).

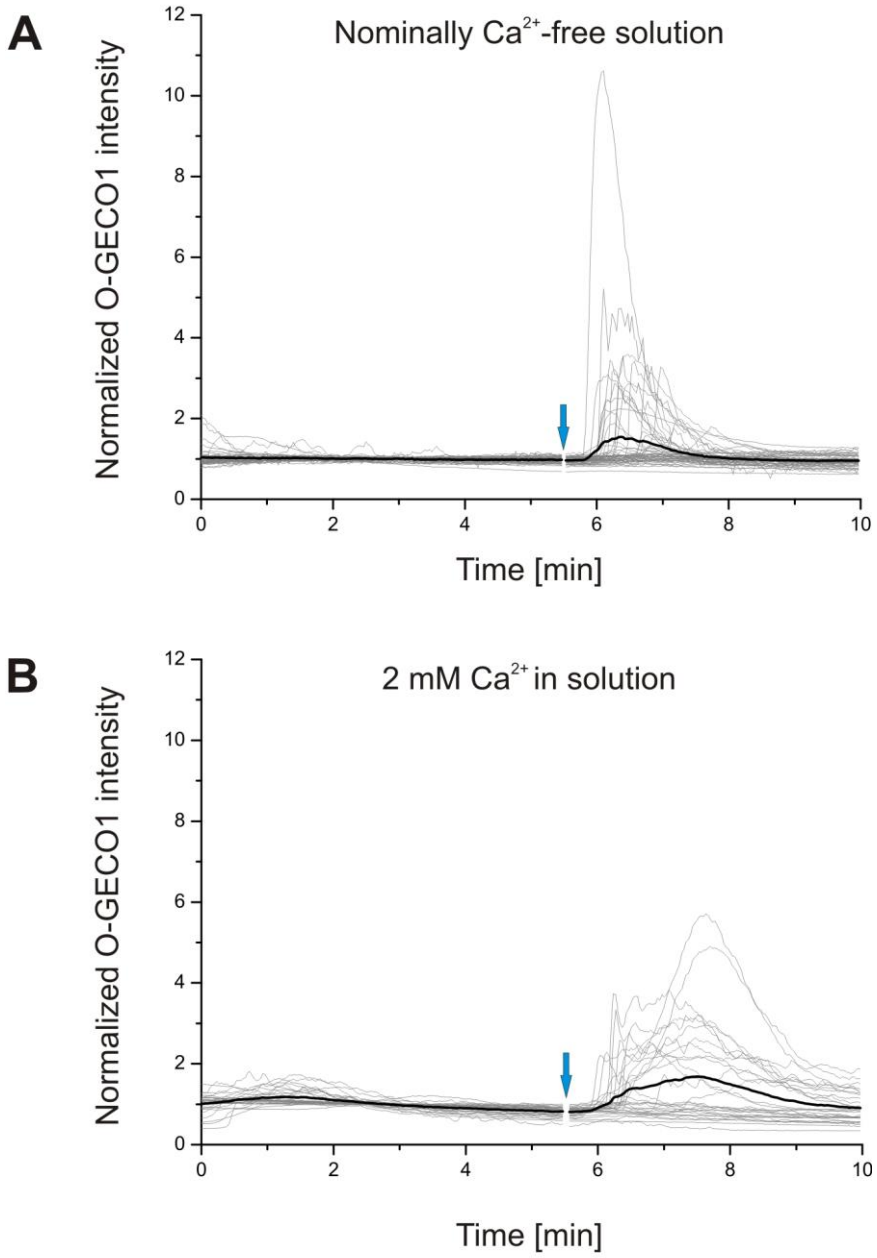

Figure 2.12 Blue light mediates Ca^{2+} mobilization from an intracellular store. O-GECO1-HEK293 cells, expressing TrkB(kd)-Cry2(498)-T2A-CIB1(170)-eGFP-CAAX, responded to blue light stimulation in the Ca^{2+}-free solution **(A)**. In panel **(B)**, Ca^{2+} traces upon blue light stimulation in the Ca^{2+}-containing solution are presented. Grey lines represent a Ca^{2+} traces for a single cell, whereas black lines represent means quantified from 51 cells for **(A)** and from 30 cells for **(B)** from one independent experiment in triplicate and duplicate, respectively. Blue arrow shows the point of blue light delivery.

The Y515 site lies within a juxtamembrane region of TrkB(kd) that binds to the SHC adapter proteins and consequently leads to the activation of AKT and ERK signalling pathways (Atwal et al., 2000; McCarty and Feinstein, 1998). Therefore, the TrkB_Y515F mutant was

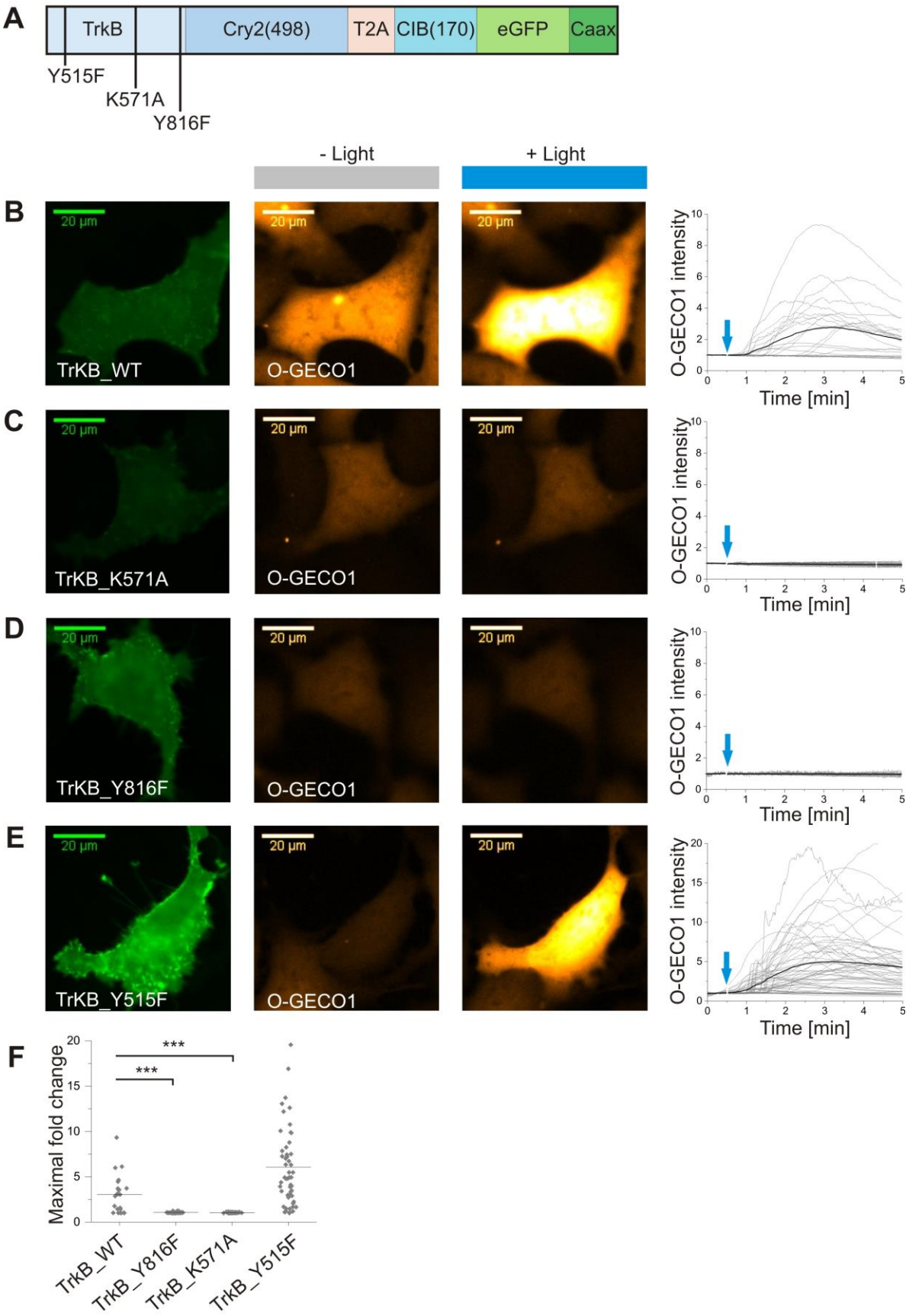
A
TrkB
Cry2(498)
T2A
CIB(170)
eGFP
Caax
Y515F
K571A
Y816F
- Light
+ Light
B
C
D
E
20 µm
TrKB_WT
TrKB_K571A
TrKB_Y816F
TrKB_Y515F
O-GECO1
O-GECO1 intensity
Time [min]
F
Maximal fold change
***
***
TrkB_WT
TrkB_Y816F
TrkB_K571A
TrkB_Y515F

Figure 2.13 Ca^{2+} responses are abolished by the mutations in TrkB kinase domain. (A) The outline represents DNA constructs consisting of mutated TrkB kinase domain in TrkB(kd)-Cry2(498)-T2A-CIB1(170)-eGFP-CAAX. **(B)** In this panel, the example of a O-GECO1-HEK293A cell expressing the wild-type TrkB kinase domain (TrkB_WT) fused to the photoactivatable system is shown. Blue light illumination evoked Ca^{2+} transients, which was measured by the increase in the O-GECO1 fluorescence. The graph shows the Ca^{2+} responses from 23 cells expressing the TrkB_WT system. **(C)** The substitution K to A at 571 aa of TrkB kinase domain (TrkB_K571A) caused the photoactivatable system to be incapable of activating PLCγ1 pathway, which was seen as a lack of Ca^{2+} responses evoked by blue light (as shown in the graph, n = 43 cells expressing TrkB_K571A system). **(D)** Similarly to TrkB_K571A results, introducing Y816F mutation in TrkB kinase domain (TrkB_Y816F) abolished light-evoked Ca^{2+} transients in cells expressing TrkB_Y816F (as seen in the graph, n = 42 cells). **(E)** A mutation Y515F, which is known to affect SHC phosphorylation leading to supression of Erk and Akt pathways, did not change Ca^{2+} responses in cells expressing TrkB_Y515F (as shown in the graph, n = 54 cells). Cells shown in B-E were obtained from one independent experiment in triplicate (total number of cells per condition was ≥10). **(F)** This graph summarises the peak Ca^{2+} responses upon blue light stimulation in each group of cells expressing various TrkB(kd) mutants (line = mean; ***P<0.001, unpaired Student's t-test). Means were calculated from second independent experiment performed in triplicates. Overall, the experiment was performed as two independent experiments: first imaging session under 40× objective and second one under 20× objective. Cells from "20× objective" experiment were quantified and shown in graphs B-F.

expected to attenuate the initiation of AKT and ERK pathways, but not to alter PLCγ1 signalling. The second substitution was introduced at a lysine 571 which serves as a consensus ATP binding site within an active site of TrkB(kd) (Guiton et al., 1994). The mutation to alanine (TrkB_K571A) has been reported to abolish all kinase activity of TrkB as it completely eliminates a phosphoryl transfer (McCarty and Feinstein, 1998). The TrkB_K571A mutant was considered as a "kinase-dead" mutant so it was predicted to block the activity of the photoactivatable TrkB completely. Finally, a mutation of tyrosine 816, a residue previously identified to interact with PLCγ1 (Atwal et al., 2000; Middlemas et al., 1994), to phenylalanine (TrkB_Y816F) was expected to abolish the light-mediated Ca^{2+} increase, whereas the induction of AKT and ERK pathways should not be disturbed.

As predicted, light did not evoke Ca^{2+} elevation in TrkB_K571A (kinase-dead) and TrkB_Y816F (unable to interact with PLCγ1) mutants (Fig. 2.13 C, D). The TrkB_Y515F mutant did not alter Ca^{2+} signalling (Fig. 2.13 E). These results indicate that the observed Ca^{2+} increase upon light requires the kinase activity of TrkB domain and is mediated through interaction with PLCγ1.

Taking advantage of the recent development of a second generation Cry2-CIB1 dimerizer with reduced background binding (Taslimi et al., 2016), a new Cry2-CIB1 pair was tested in the context of my TrkB system. In this new system, the Cry2 domain was truncated

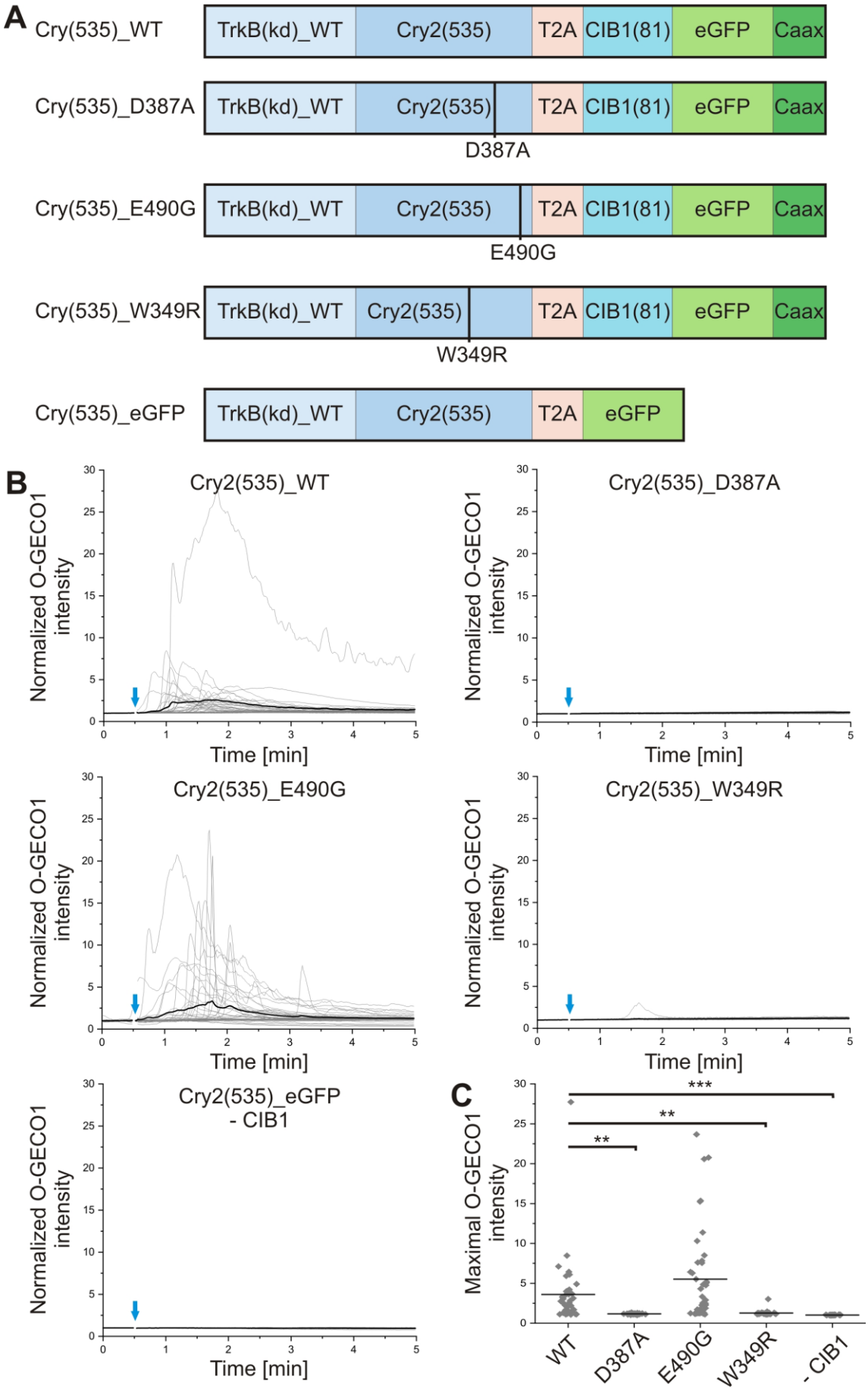
A
Cry(535)_WT
TrkB(kd)_WT
Cry2(535)
T2A
CIB1(81)
eGFP
Caax
Cry(535)_D387A
D387A
Cry(535)_E490G
E490G
Cry(535)_W349R
W349R
Cry(535)_eGFP
B
Cry2(535)_WT
Cry2(535)_D387A
Cry2(535)_E490G
Cry2(535)_W349R
Cry2(535)_eGFP
- CIB1
Normalized O-GECO1 intensity
Time [min]
C
Maximal O-GECO1 intensity
***
**
**
WT
D387A
E490G
W349R
- CIB1

Figure 2.14 Ca^{2+} responses can be evoked by TrkB system fused to different Cry2 and CIB1 variants. (A) The schematic representations of chimeric proteins show a wild type TrkB kinase domain (TrkB(kd)) fused to 535 aa-long Cry2 mutants and 81 aa-CIB1 attached to eGFP-Caax. Cry2(535) component is connected with CIB1(81) by T2A sequence. The amino acid substitutions prepared in this project are presented within Cry(535) sequence. **(B)** The graphs show the Ca^{2+} traces in O-GECO1-HEK293A expressing different Cry(535) mutants upon blue light pulse. A wild type Cry2(535) as well as Cry2(535)_E490G (oligomerisation) mutant could trigger Ca^{2+} elevation upon light stimulation. A light-insensitive mutant (Cry2(535)_D387A), a fast-cycling mutant (Cry2(535)_W349R) and the Cry2(535) system without CIB1(81) (Cry2(535)_eGFP) component failed to trigger Ca^{2+} responses. Grey lines represent traces of individual cells, whereas black lines are means. **(C)** The column scatter plot represents Ca^{2+} peak responses for each Cry2(535) mutant. Grey dots are responses of single cells. Black line is mean (***P<0.001, **P<0.01, unpaired Student's t-test). (n = 38 cells for Cry2(535)_WT; n = 50 cells for Cry2(535)_D387A; n = 42 cells for Cry2(535)_E490G; n = 37 cells for Cry2(535)_W349R; n = 35 cells for Cry2(535)_eGFP). All cells were pooled from one independent experiment performed in triplicate.

to 535 amino acids (Cry2(535)), whereas CIB1 was truncated to 81 amino acids (CIB1(81)) as opposed to the initial pair of Cry(498) and CIB1(170). Taslimi et al. (2016) showed that Cry2(535) exhibited lower self-association in dark, while its interaction in light condition was still substantial. They also described new mutations affecting Cry2(535) photocycle kinetics, including a fast short-cycling W349R variant (Cry2535_W349R) with a half-life of 2.5 minutes (Taslimi et al., 2016). In a separate study, a mutation E490G within Cry2 domain was shown to enhance a light-dependent clustering of Cry2, while retains binding to CIB1(170) (Taslimi et al., 2014). A light-insensitive mutant of Cry2 (D387A) was also created. The D387 is a part of FAD-binding pocket and once mutated, it interrupts the light-dependent interaction between Cry2 and CIB1 (Liu et al., 2008a). These mutants were assessed in my standardized Ca^{2+} assay.

When the new Cry2(535)/CIB1(81) was used in the place of the original Cry2(498)/CIB1(170), a blue light pulse could still trigger Ca^{2+} elevation (Fig. 2.14 B). Interestingly, this response lasted ~1.5 min and seemed to be more transient that the response compared to the Cry2(498)/CIB1(170) pair (see Fig. 2.6 B). This observation was also confirmed when the light stimulation was delivered to the cells after longer baseline period (Fig. 2.15). The Cry2(535)_E490G mutant was able to trigger Ca^{2+} responses (Fig. 2.14 B and C). The light insensitive Cry2(535)_D387A as well as the short-cycling Cry2(535)_W349A failed to evoke Ca^{2+} transients (Fig. 2.14 B and C). Similarly, Cry2(535) without CIB1(81) in the membrane did not show any elevation of Ca^{2+} signal (Fig. 2.14 B and C).

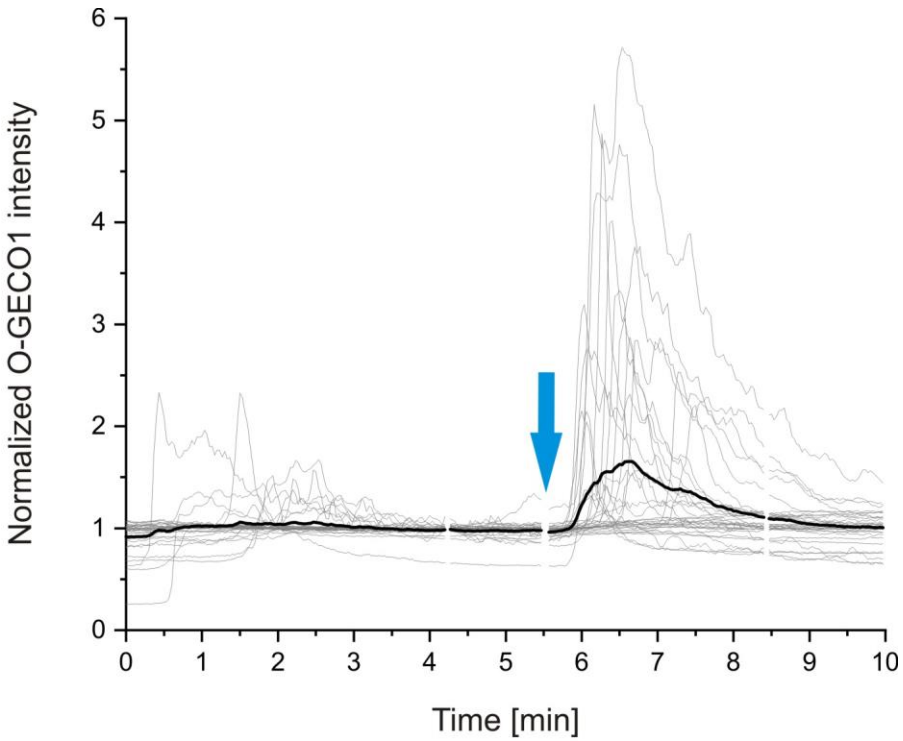

Figure 2.15 Cry2(535) and CIB1(81) pairs evokes transient Ca^{2+} response. O-GECO1-HEK293A cells, expressing TrkB(kd)-Cry2(535)-T2A-CIB1(81)-eGFP-CAAX, responded to blue light stimulation delivered after 5.5 min of imaging. Grey line represents a Ca^{2+} trace for a single cell, whereas black line represents the mean quantified from 32 cells pooled from one independent experiment in duplicate. Blue arrow shows the point of blue light delivery.

Similar to the results presented in Figure 2.9, the association between the expression level of TrkB(kd)-Cry2(535)-T2A-CIB1(81)-eGFP-CAAX (measured as fluorescence intensity of eGFP) and magnitude of Ca^{2+} was correlated by using Pearson's r. There was no significant linear relationship between the expression of the TrkB system with Cry2(535)/CIB1(81) and the amplitude of Ca^{2+} responses as the Pearson's r equalled 0.072 and $P > 0.05$ (Fig. 2.16). In this assay, it was assessed that 77% of the transfected O-GECO1-HEK293A cells responded upon blue light illumination, which is consistent with the results obtained for TrkB(kd)-Cry2(498)-T2A-CIB1(170)-eGFP-CAAX construct (refer to Fig. 2.9).

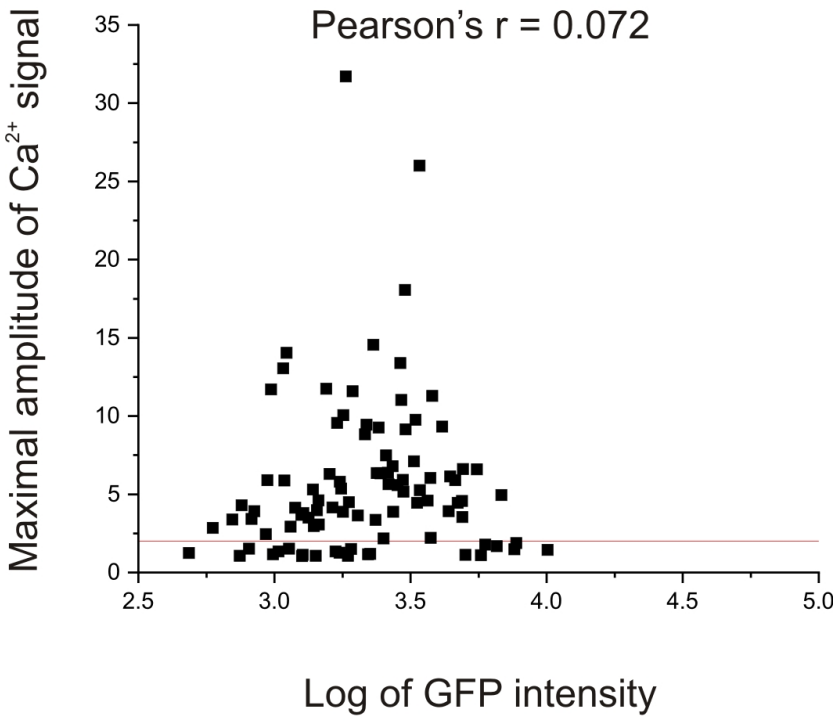

Figure 2.16 The relationship between the expression level of TrkB system with Cry2(535)-CIB1(81) and the amplitude of Ca^{2+} response upon blue light illumination. In O-GECO1-HEK293A cells, expressing TrkB(kd)-Cry2(535)-T2A-CIB1(81)-eGFP-CAAX, the expression level was not significantly related to the amplitude of Ca^{2+} signal (Pearson correlation coefficient, r = 0.072; n = 94 cells; P = 0.49). The horizontal line at 2 shows the cells with the amplitude lower than 2, which were considered as non-responsive cells. Having this threshold, it can be seen that 77% of cells responded to the light stimulation.

The PLCγ1 inhibitor, U73122, reduced the light-induced Ca^{2+} elevation in O-GECO1-HEK293A cells expressing TrkB(kd)-Cry2(535)-T2A-CIB1(81)-eGFP-CAAX (Fig. 2.17). These results are in agreement with observations for Cry2(498)/CIB1(170) pair (refer to Fig. 2.11). It confirms that the light-triggered Ca^{2+} increase is mediated through the PLCγ1 pathway in both cases.

I also tested whether changing the membrane C-terminal lipidation anchor of CIB1(81) for a N-myristoylation tag (denoted as MYR) could also activate the signalling effectively. To achieve this, TrkB(kd)-Cry2(535) now had to be inserted after the T2A sequence. This configuration (MYR-CIB1(81)-eGFP-T2A-TrkB(kd)-Cry2(535)) did not activate Ca^{2+} signalling upon the 1-s blue light pulse (Fig. 2.18).

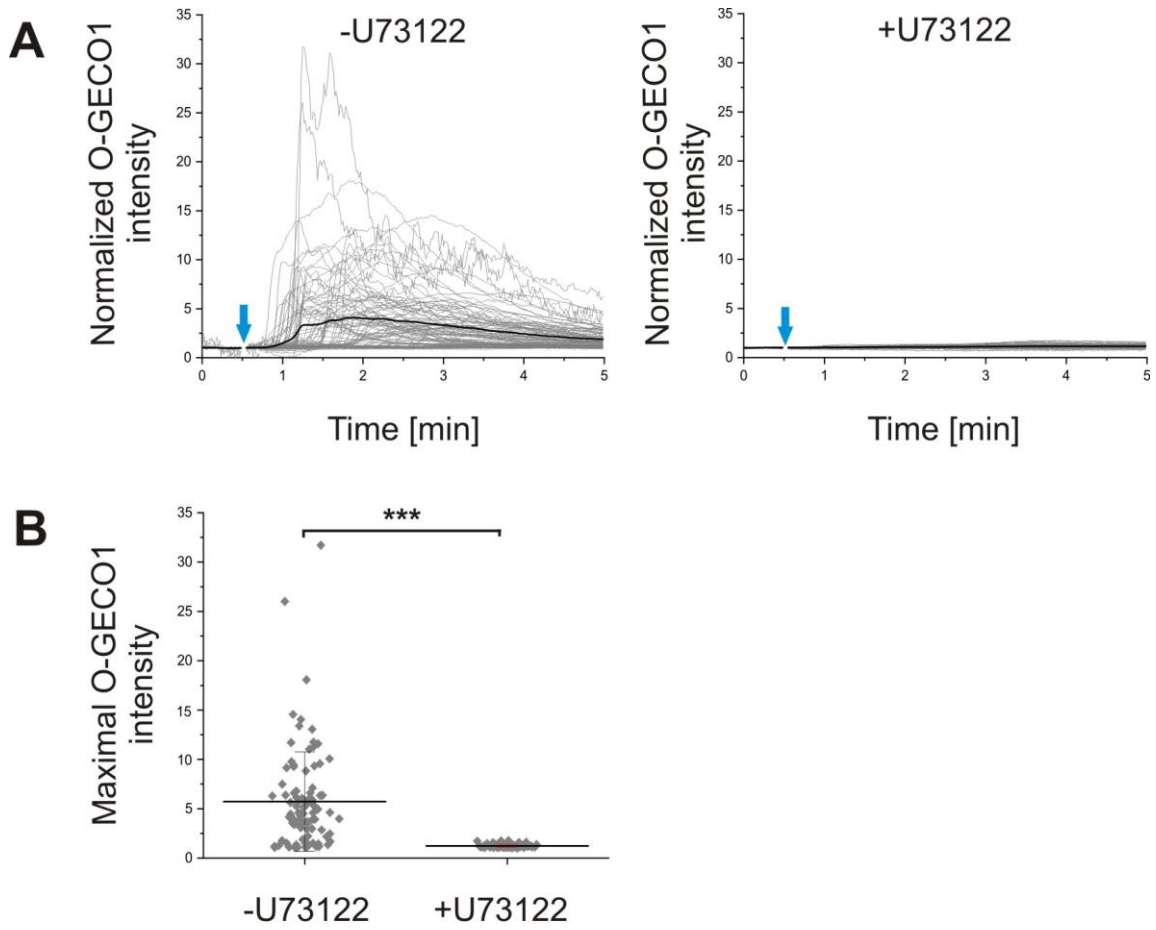

Figure 2.17 Light activation of TrkB(kd)-Cry2(535) with CIB1(81) is consistent with PLCγ1-mediated Ca^{2+} increase. (A) In O-GECO1-HEK293A cells, transfected with TrkB(kd)-Cry2(535)-T2A-CIB1(81)-eGFP-CAAX, blue light delivered at 0.5 min of a timecourse (arrow) led to the elevation of intracellular Ca^{2+} (left graph). Pre-treatment of cells with PLC inhibitor U73122 at the final concentration of 2.5 µM for 10 min reduced light-evoked Ca^{2+} signals (right graph). **(B)** The graph shows the peak responses of individual cells (grey dots) represented in the panel A for non-treated cells (-U73122; n = 94) and cells treated with the inhibitor (+U73122; n = 98). Central line and error bars represent mean ± SD; ***P<0.001, unpaired Student's t-test.

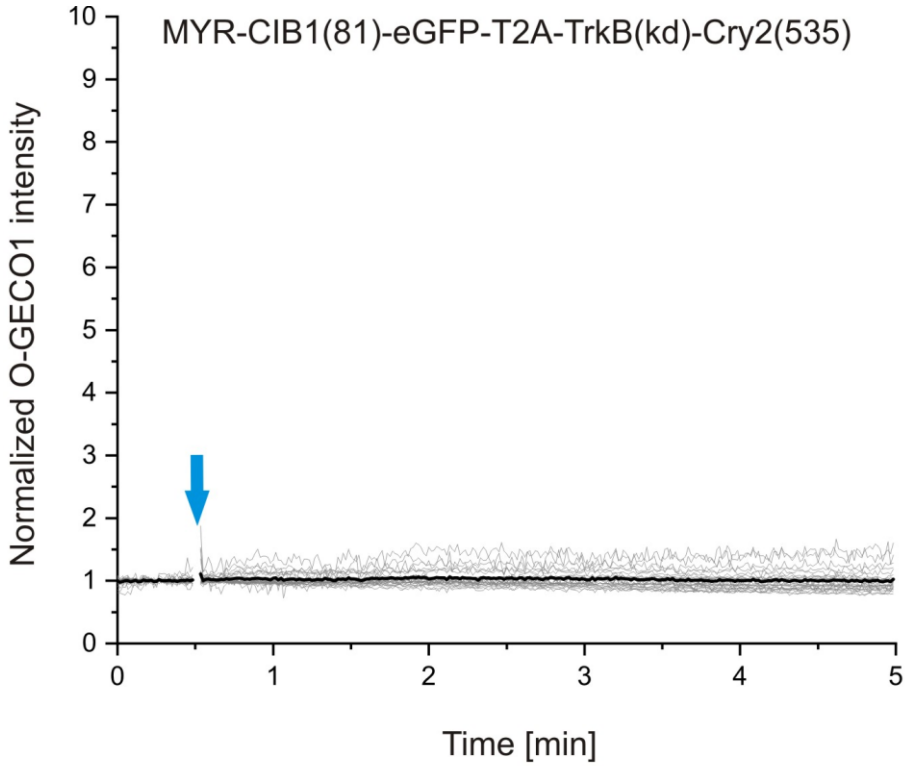

Figure 2.18 Changing order of CIB1(81) and TrkB(kd)-Cry2(535) in the bicistronic construct disrupts functional expression of chimeric proteins. O-GECO1-HEK293 cells, expressing CIB1(81) attached to N-myristoylation signal and TrkB(kd)-Cry2(535) (MYR-CIB1(81)-eGFP-T2A-TrkB(kd)-Cry2(535)) did not respond to blue light stimulation as robustly as cells, expressing TrkB(kd)-Cry2(535)-T2A-CIB1(81)-eGFP-CAAX. Grey lines represent the Ca^{2+} traces for single cells, whereas black line represents the mean measured from 25 cells from one independent experiment performed in duplicate. Blue arrow shows the point of blue light delivery.

2.3.2.2 Light activation of TrkB leads to the translocation of a cytosolic ERK1 to nucleus

The autophosphorylation of TrkB at Y515 within its juxtamembrane region leads to recruitment of SHC adaptor proteins and subsequent activation of the Ras-mitogen-activated protein kinase (Ras-MAPK) signalling pathway (McCarty and Feinstein, 1998; Stephens et al., 1994). In a simplistic linear pathway model, the phosphorylated SHC adapters engage the binding of growth factor receptor-bound protein 2 (GRB2) and son of sevenless (SOS), allowing thus Ras activation (Egan et al., 1993). Subsequently, Ras activation causes the recruitment and activation of Raf (Rapidly Accelerated Fibrosarcoma) in the membrane (Vojtek et al., 1993). The phosphorylated Raf leads to the activation of mitogen-activated protein kinase kinase (MEK), which, consequently, phosphorylates MAPK (Kyriakis et al.,

1992). The most characterized MAPKs are extracellular signal-regulated kinases 1 and 2 (ERK1 and ERK2). For the full activity, ERK1 and ERK2 have to be phosphorylated at threonine 202 and tyrosine 204 within their activation loops (Burack and Sturgill, 1997). Both ERK1 and ERK2 are activated in the cytoplasm and then translocated to the nucleus allowing the phosphorylation of their targets in this cell compartment (Khokhlatchev et al., 1998). The nuclear translocation of ERK2 attached to GFP was examined by Horgan and Stork (2003) to reveal the mechanism of this movement.

To assay ERK1/2 translocation from the cytoplasm to the nucleus upon ERK activation, ERK1-mCherry sensor was generated (refer to Table 2.4). Live-cell imaging to study ERK1-mCherry translocation upon blue light was performed in HEK293A cells by delivering a 1-s light pulse after 3 min of baseline imaging. This assay was used to test whether my photoinducible TrkB system can activate ERK-mediated signalling.

Cells expressing ERK1-mCherry, but not the TrkB system, did not show detectable changes in ERK1 localization upon blue light stimulation (Fig. 2.19 A). In cells expressing the light-activated TrkB system, the transport of ERK1-mCherry to the nucleus could be seen upon light stimulation within ~10 min (Fig. 2.19 B). The TrkB_Y816F mutant (no interaction with PLCγ1) was still capable of inducing the translocation of ERK1-mCherry to the nucleus, suggesting ERK activation remained intact, as predicted (Fig. 2.19 C). The elimination of the kinase activity through the TrkB_K571A mutant abolished completely the translocation of ERK1-mCherry (Fig. 2.19 D). It was expected that the mutation at Y515 might attenuate the phosphorylation of ERK1 as described by Easton et al. (1999). Interestingly, the TrkB_Y515F mutant remained capable of triggering the translocation of ERK1-mCherry to the nucleus (Fig. 2.19 E) and there was no significant difference between responses obtained for TrkB_WT and TrkB_Y515F (Fig. 2.19 F, $p = 0.66$, unpaired Student's t-test). The results for TrkB_Y515F suggest that TrkB can activate ERK1 independently of the Y515 site. Taken together, the photoactivatable TrkB system can activate a signalling pathway leading to ERK1 activation in a light-dependent manner.

As it was shown in Figure 2.7 A and B, the imaging light (filtered with a 543-22 interference filter) without the specific blue light stimulation caused the photoexctitation of Cry2/CIB1 in 26% of O-GECO1-HEK293A cells. Hence, the same question was asked for the ERK1-mCherry translocation upon imaging conditions. In this experiment, HEK293A cells were co-transfected with ERK1-mCherry and either TrkB-Cry2(498)-T2A-CIB1(170)-eGFP-CAAX or TrkB-Cry2(535)-T2A-CIB1(81)-eGFP-CAAX. The Cry2(535)/CIB1(81)

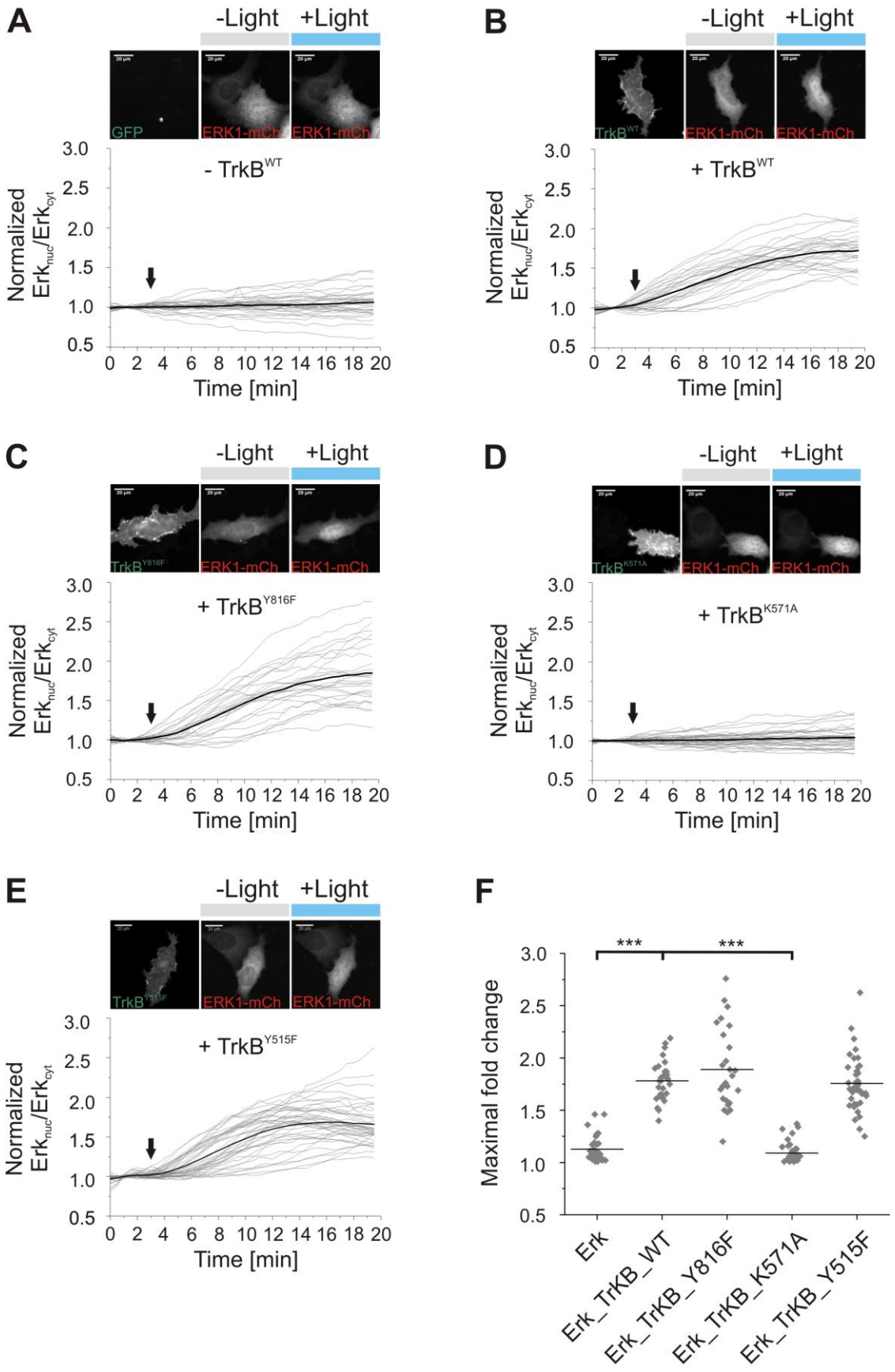
A
-Light
+Light
GFP
ERK1-mCh
ERK1-mCh
- TrkB^WT
Normalized Erk_nuc/Erk_cyt
Time [min]
B
TrkB^WT
+ TrkB^WT
C
TrkB^Y816F
+ TrkB^Y816F
D
TrkB^K571A
+ TrkB^K571A
E
TrkB^Y515F
+ TrkB^Y515F
F
Maximal fold change
***
***
Erk
Erk_TrKB_WT
Erk_TrKB_Y816F
Erk_TrKB_K571A
Erk_TrKB_Y515F

Figure 2.19 Light activation of TrkB leads to ERK1 translocation to the nucleus in HEK293 cells. The graphs represent a time-lapse of translocation of ERK1-mCherry (ERK1-mCh) to nucleus upon blue light stimulation. The images show the cells co-transfected with ERK1-mCh and TrkB-Cry2(498)-T2A-CIB1(170)-eGFP-CAAX constructs with different mutations in TrkB(kd) (refer to Table 2.4) before and after blue light stimulation (left panels are the examples of an expression of the photoactivatable TrkB constructs). The cells transfected with ERK1-mCh alone did not undergo nuclear translocation upon light stimulation **(A)**. In cells co-transfected with the photoactivatable systems with TrkB_WT **(B)**, TrkB_Y816F mutant **(C)** and TrkB_Y515F mutant **(E)**, light illumination led to the translocation of cytosolic ERK1-mCh to the nucleus, which is known to be associated with the phosphorylation of ERK1 by TrkB receptor. Elimination of the kinase activity with K571A mutation **(D)** did not lead to the translocation of ERK1-mCh to the nucleus. **(F)** The graph summarises the maximum responses of ERK1-mCh translocated to the nucleus within each group of cells **(A-E)** (each grey diamond represents an individual cell; line = mean; ***P<0.001, unpaired Student's t-test). For each condition n cells were tested: n = 33 cells for (A); n = 29 cells for (B); n = 27 cells for (C); n = 37 cells for (D); n = 41 cells for (E) and data were pooled from two independent experiments each performed in duplicates. For (A-E), grey lines are responses of individual cells and the average is shown in black. These responses were measured as ratios of nuclear and cytoplasmic ERK1 normalized to the baseline before blue light stimulation. A single blue light pulse of 1 s was delivered at t = 3 min of a timecourse (arrow). Scale bars, 20 µm.

pair was included as it has been shown to have lower background activity in the literature (Taslimi et al., 2016). Both Cry2(498)/CIB1(170) (Fig. 2.20 B) and Cry2(535)/CIB1(81) (Fig. 2.20 D) could trigger the activation of ERK1 as demonstrated by ERK1-mCherry recruitment to the nucleus. The light insensitive mutant of Cry2 (TrkB-Cry2(535)_D387A-T2A-CIB1(81)-eGFP-CAAX) was also tested in the same configuration. This light insensitive construct, co-transfected with ERK1-mCherry sensor, did not cause ERK1 translocation to the nucleus upon simultaneous imaging light and blue light illumination (Fig. 2.21 B). These results suggest that under our imaging condition, some fraction of Cry2/CIB1 in the cell can be activated, leading to detectable ERK translocation.

In a previous Ca^{2+} imaging experiment (refer to Fig. 2.6 B and 2.14 B), the photoactivatable TrkB system without the membrane-tethered CIB1 component was not sufficient to initiate Ca^{2+} response in O-GECO1-HEK293A cells. Nevertheless, the effect of the TrkB system without CIB1 component (TrkB-Cry2(535)-T2A-eGFP) was tested in ERK1 translocation assay. Intriguingly, TrkB-Cry2(535)-T2A-eGFP triggered the ERK1-mCherry translocation to the nucleus upon light irradiation (Fig. 2.22). Comparing the average maximum value for ERK1 translocation measured as a ratio of nuclear to cytoplasmic fractions for TrkB-Cry2(535)-T2A-eGFP (1.40 ± 0.34; n = 52; Fig. 2.22) and TrkB-Cry2(535)-T2A-CIB1(81)-eGFP-CAAX (1.71 ± 0.31; n = 23; Fig. 2.21 A) suggests that the response evoked without CIB1 component is considerably lowered. Taken together, the

photoactivatable TrkB system without CIB1 component can activate ERK translocation upon light stimulation.

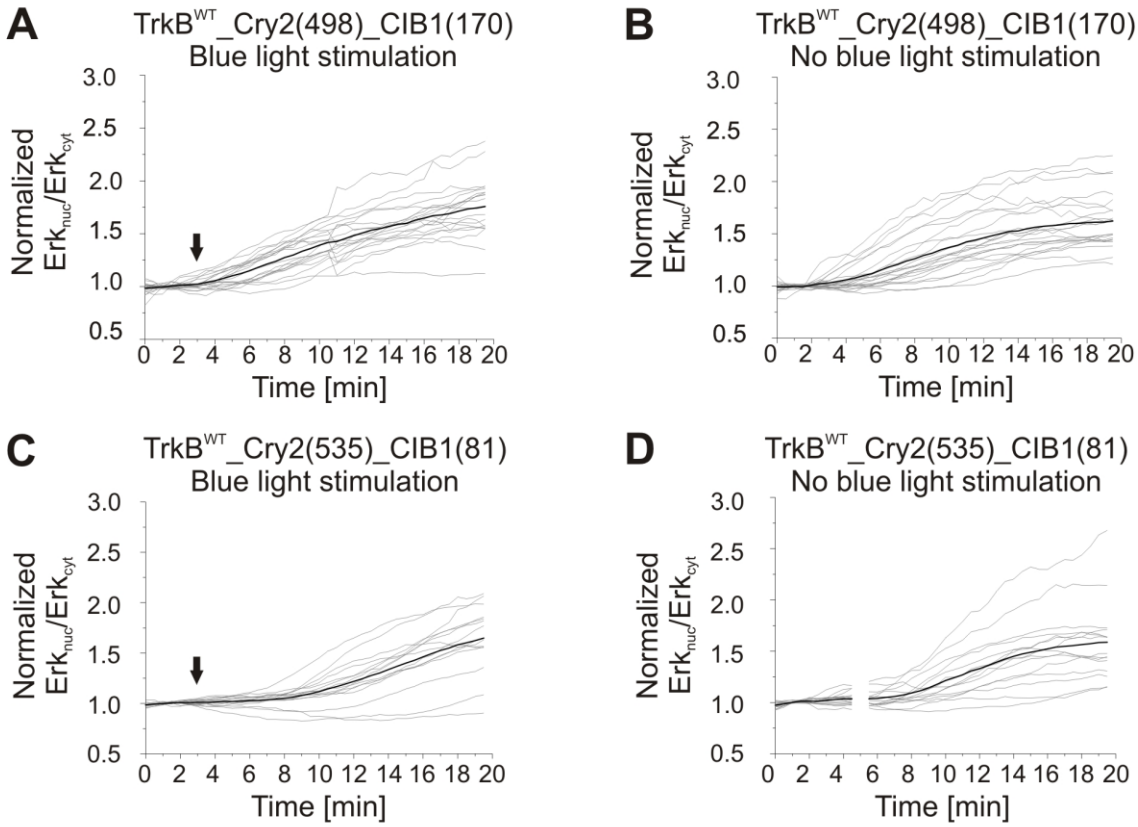

Figure 2.20 Imaging light is sufficient to induce ERK1 translocation to the nucleus in HEK293A cells co-expressing the photoactivatable TrkB and ERK1-mCherry. The graphs represent a time-lapse of translocation of ERK1-mCherry to the nucleus upon blue light stimulation **(A, C)** as well as without blue light stimulation (**B, D)**. The graphs **(A)** and **(B)** show the cells co-transfected with ERK1-mCherry and TrkB-Cry2(498)-T2A-CIB1(170)-eGFP-CAAX constructs. In these cells, imaging light caused the activation of the TrkB system and triggered the ERK1 transport to the nucleus. In the next step, Cry2(535) and CIB1(81) pair, which is known to have lower background activity, was examine with and without blue light illumination **(C, D)**. The imaging light sill caused the ERK1 translocation in the cells transfected with TrkB-Cry2(535)-T2A-CIB1(81)-eGFP-CAAX. For each condition the following numbers of cells were tested: n = 20 cells for A; n = 22 cells for B; n = 15 cells for C; n = 15 cells for D. The data were pooled from one independent experiment in duplicate. Grey lines are responses of individual cells and the average is shown in black. A single blue light pulse of 1 s was delivered at t = 3 min of a timecourse (arrow) **(A, C)**. A gap in panel D represents the frame at 5 min which was removed due to a visually detected artefact leading to the distorted image of cells within this frame.

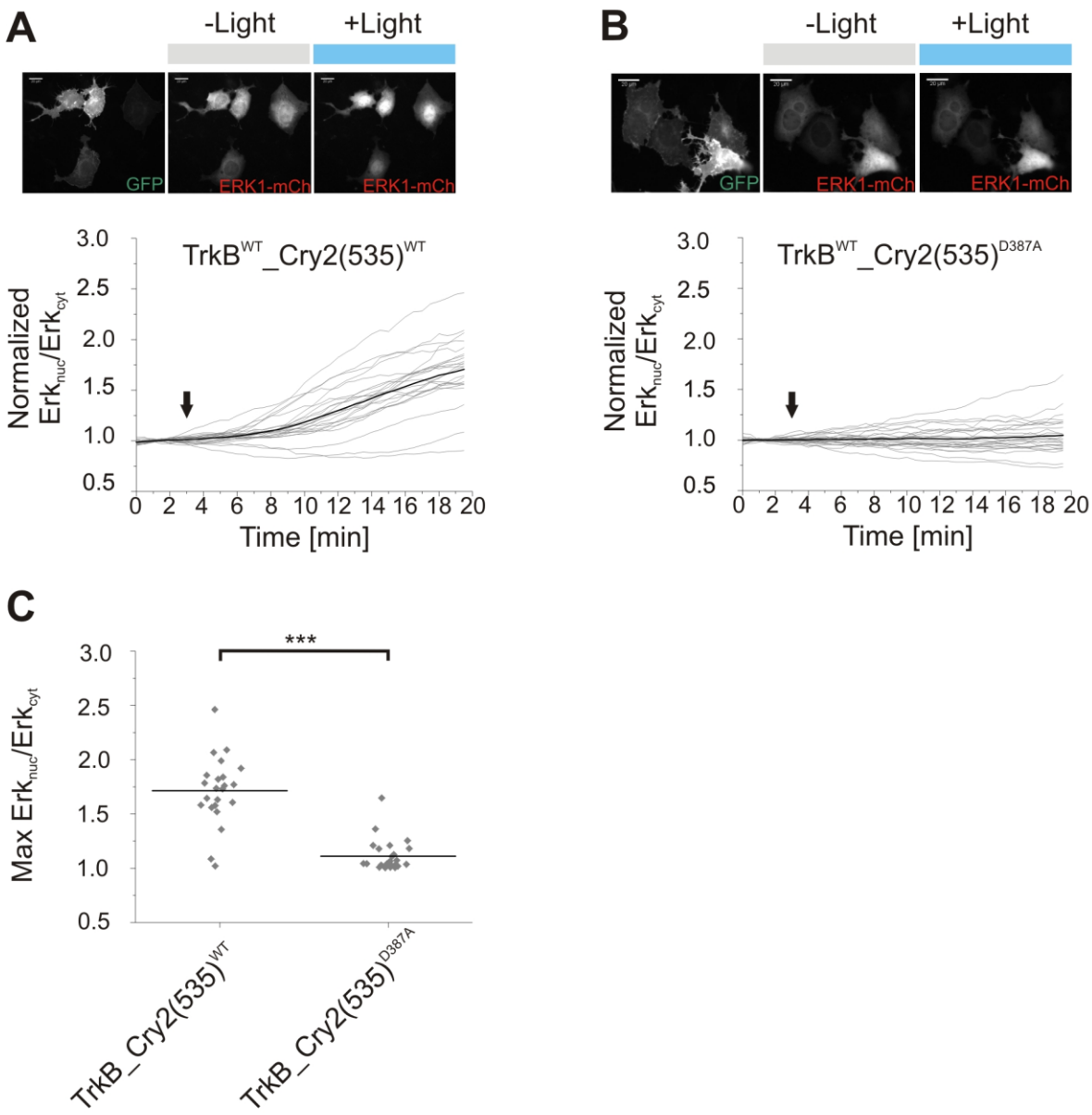

Figure 2.21 ERK1 translocation to the nucleus is mediated by the photoactivation of Cry2/CIB1 system because the light-insensitive mutant of Cry2(535)_D387A failed to cause ERK1 translocation. The graphs represent a time-lapse of translocation of ERK1-mCherry (ERK1-mCh) to nucleus upon blue light stimulation when cells were co-transfected with the light-responsive TrkB-Cry2(535)_WT-T2A-CIB1(81)-eGFP-CAAX **(A)** or the light-insensitive mutant TrkB-Cry2(535)_D387A-T2A-CIB1(81)-eGFP-CAAX **(B).** The examples of cells in which ERK1 underwent light-dependent translocation are shown above each graph. The left photos are the examples of the expression of the constructs (labelled as "GFP"). The graph **(C)** represents the maximum response for individual cells from each group of cells shown in **(A)** and **(B)**. For each condition the following numbers of cells were tested: n = 23 cells for A; n = 25 cells for B. The data were pooled from two independent experiments. Grey lines are responses of individual cells **(A, B)**. The average response is shown in black **(A, B)**. A single blue light pulse of 1 s was delivered at t = 3 min of a timecourse (arrow) **(A, B)**. Grey diamonds are the peak values for the individual cells and the line represents mean (***P<0.001, unpaired Student's t-test). Scale bar, 20 µm.

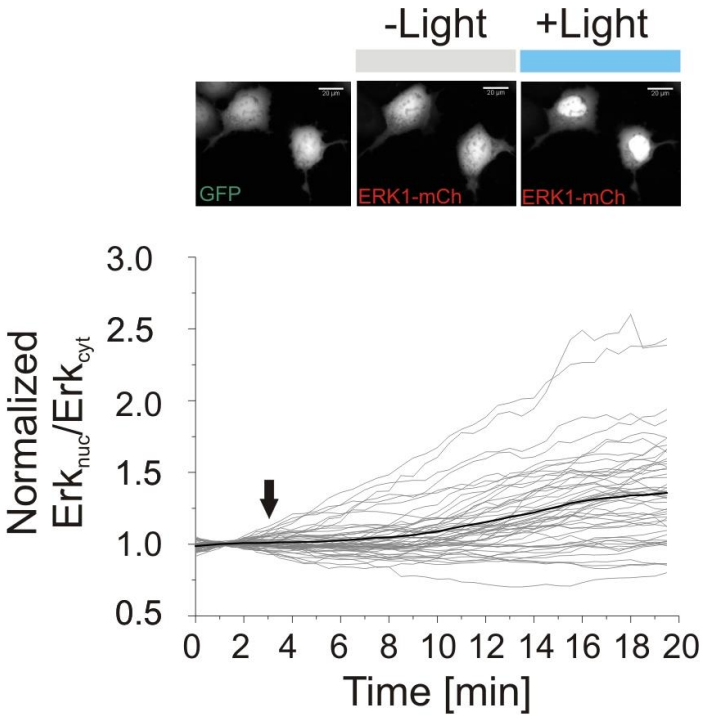

Figure 2.22 The photoactivatable TrkB system, which consists of Cry2(535) without CIB1 component in the membrane, can still activate ERK1 pathway in HEK293A cells.
The graph represents a time-lapse of translocation of ERK1-mCherry (ERK1-mCh) to nucleus upon blue light stimulation when cells were co-transfected with the ERK1-mCh and TrkB^{WT}-Cry2(535)-T2A-eGFP. The examples of cells in which ERK1 underwent light-dependent translocation are shown above the graph. The left photo is the example of the expression of the construct (labelled as "GFP"). In this experiment, 52 cells were analyzed and pooled from two independent experiments each performed in triplicate and in quadruplicate. Grey lines are responses of individual cells, whereas the average response is shown in black. A single blue light pulse of 1 s was delivered at t = 3 min of a timecourse (arrow). Scale bar, 20 μm.

2.3.2.3 Light activation of TrkB causes AKT1$_{PH}$ membrane accumulation

The third canonical pathway that is activated by TrkB involves the phosphorylation of phosphatidylinositol 3-kinase (PI3K) and AKT (Zheng et al., 2008). As is the case for stimulation of MAPK by TrkB, neither PI3K nor AKT interacts directly with TrkB. The SHC adaptors, bound to the phosphorylated Y515 of TrkB on one site and to GRB2 on the other site, allow, for instance, the association of GRB-associated binder-1 (GAB1) to GRB2 (Holgado-Madruga et al., 1997). This leads to the activation of PI3K, 3-phosphoinositide-dependent protein kinase 1 (PDPK1) and finally, AKT (Holgado-Madruga et al., 1997; Zheng et al., 2008). In the classical model of AKT regulation, AKT is translocated to the plasma membrane where it is subsequently phosphorylated at S473 within

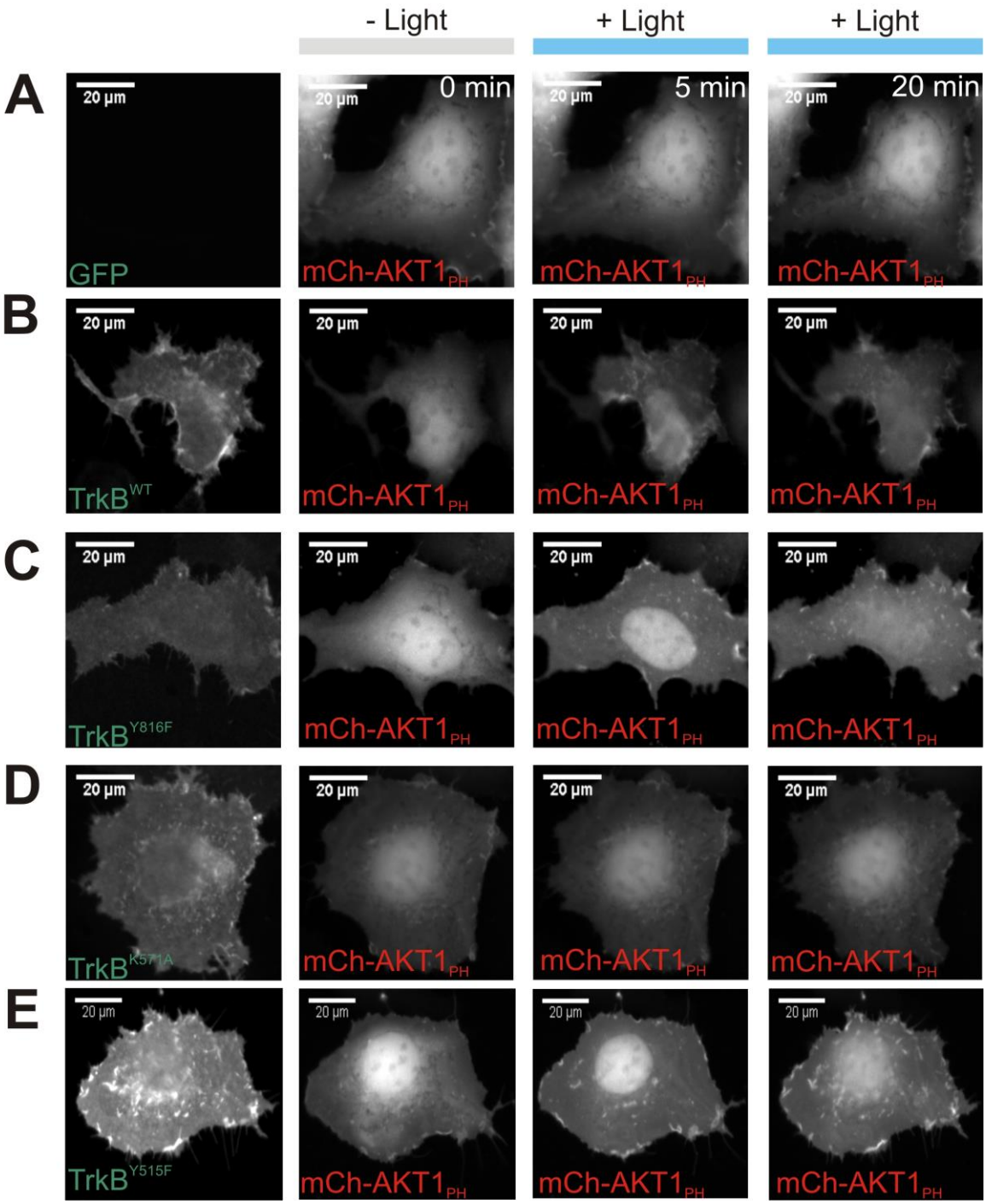

Figure 2.23 Light activation of TrkB signalling leads to $AKT1_{PH}$ membrane accumulation. Light-mediated activation of TrkB signalling induced the relocation of mCherry tagged pleckstrin homology (PH) domain of AKT1 protein (mCh-$AKT1_{PH}$) to the plasma membrane **(B)**, which is consistent with the signalling associated with TrkB receptor. Such effect was still evident in TrkB_Y816F mutant **(C)**, confirming the sole association of Y816 to PLCγ1 activation and not AKT1. The K517A mutation abolished the kinase activity and $AKT1_{PH}$ relocation was not observed **(D)**. The $AKT1_{PH}$ translocation was not seen in cells expressing $AKT1_{PH}$ alone **(A)**. However, this transport was still present in cells co-expressing $AKT1_{PH}$ and TrkB_Y515F mutant **(E)**, similarly to the results when ERK1-mCherry translocation was examined. Experiments were performed in

HEK293A cells co-expressing mCherry-AKT1$_{PH}$ and TrkB-Cry2(498)-T2A-CIB1(170)-eGFP-CAAX with different mutations in TrkB kinase domain (refer to Table 2.5). For each condition n > 10 cells were tested. A single blue light pulse of 1 s was delivered at t = 3 min of a timecourse. From the left images show eGFP fluorescence indicating the expression of the TrkB system; then images of mCherry-AKT1$_{PH}$ at 0 min of the time-lapse (before blue light stimulation); third images of mCherry-AKT1$_{PH}$ at 5 min of the timecourse (and 2 min after blue light pulse); finally images of mCherry-AKT1$_{PH}$ at 20 min (the end of the time-lapse). Cells are representative of cells from three independent experiments each performed in duplicates.

C-terminal tail and at T308 within activation loop (Chu et al., 2018). It has been shown that PI3K activation can cause the translocation of an isolated N-terminal pleckstrin homology domain (PH) of AKT fused to a fluorescent protein to the membrane (Yang et al., 2012). The fluorescent-tagged AKT1$_{PH}$ has been useful for optogenetic application (Chang et al., 2014; Han et al., 2016). Therefore, the translocation of mCherry-AKT1$_{PH}$ to the membrane can be used as an assay for AKT activation.

Following co-transfection of HEK293A cells with mCherry-AKT1$_{PH}$ and the photoactivatble TrkB system containing the wild-type or mutated TrkB(kd), blue light illumination caused an mCherry-AKT1$_{PH}$ fusion to be transported to the membrane in TrkB_WT, TrkB_Y816F mutant and TrkB_Y515F mutant (Fig. 2.23 B, C, E, respectively). The mutation Y816F within a kinase domain can abolish PLCγ1 activity without inhibiting the activitity of AKT and ERK, as expected. Similarly to the results from the ERK translocation assay (see Fig. 2.19 E), TrkB_Y515F showed that Y515 site was not necessary for the activation of AKT1$_{PH}$. The kinase-dead mutant, TrkB_K571A, did not induce AKT1$_{PH}$ relocation (Fig. 2.23 D), demonstrating that AKT actication was dependent on TrkB kinase activity.

The imaging light conditions were shown to trigger Ca^{2+} responses in 26% of tested cells (Fig. 2.7) and to induce ERK1 translocation from the cytoplasm to the nucleus (Fig. 2.20). Similarly, the imaging conditions used for AKT1$_{PH}$ translocation could relocate the mCherry-AKT1$_{PH}$ fusion from the cytoplasm to the membrane (Fig. 2.24 B and D). However, the utilization of the TrkB system with the light-insensitive Cry2 mutant (TrkB-Cry2(535)_D387A-T2A-CIB1(81)-eGFP-CAAX) did not evoke significant mCherry-AKT1$_{PH}$ translocation upon blue light stimulation (Fig. 2.25 B), indicating this process requires Cry2/CIB1 interaction.

Interestingly, mCherry-AKT1$_{PH}$ translocated to the plasma membrane upon light stimulation was observed to occupy similar microdomains as compared to CIB1(170)-eGFP-CAAX or CIB1(81)-eGFP-CAAX components. This co-localization can be clearly seen in

Figure 2.23 (Panels B, E), Figure 2.24 (Panels A, C) and Figure 2.25 (Panel A) when the photos on the left-hand side, representing the expression of TrkB systems, are compared with the photos on the right-hand side, showing $AKT1_{PH}$ translocation at 20 min of timecourses.

Similarly to the results presented in Figure 2.22 for the ERK1 translocation, the $AKT1_{PH}$ transport can occur in the absence of the membrane-anchored CIB1 component, and light-induced Cry2(535) oligomerization is sufficient to activate TrkB(kd) which consequently can lead to $AKT1_{PH}$ relocation to the membrane (Fig. 2.26).

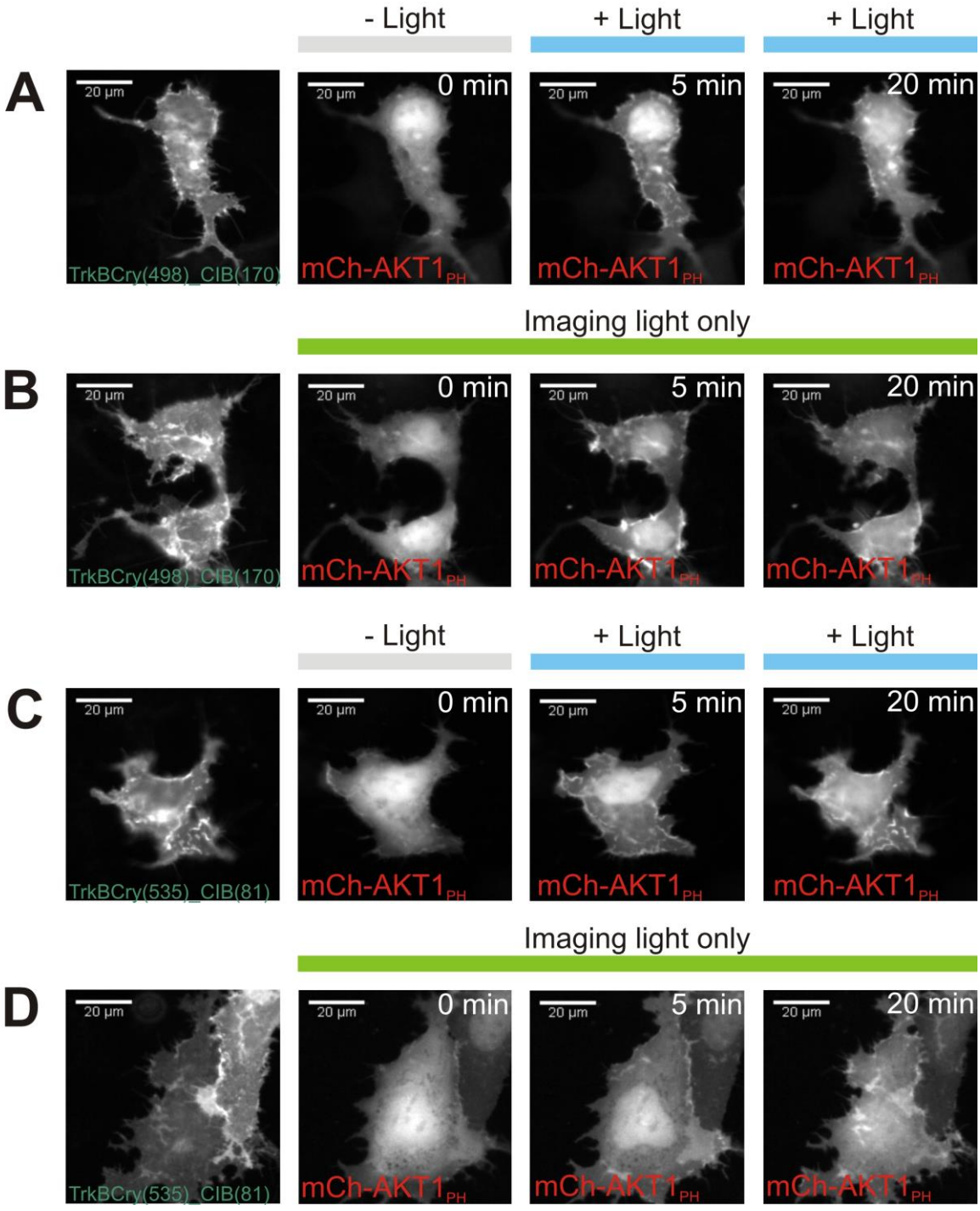

Figure 2.24 Imaging conditions lead to $AKT1_{PH}$ translocation to the membrane. The panels represent a time-lapse of translocation of mCherry-$AKT1_{PH}$ (mCh-$AKT1_{PH}$) to the membrane upon blue light stimulation **(A, C)** as well as upon live-imaging conditions without blue light stimulation **(B, D)**. The left photos show the expression of indicated constructs. The images (**A)** and (**B)** show the cells co-transfected with mCherry-$AKT1_{PH}$ and TrkB-Cry2(498)-T2A-CIB1(170)-eGFP-CAAX constructs. In these cells, imaging light caused the activation of the the mCherry-$AKT1_{PH}$ transport to the membrane. In the next step, Cry2(535) and CIB1(81) pair (TrkB-Cry2(535)-T2A-CIB1(81)-eGFP-CAAX), which is known to have lower background activity, was examined with and without blue light illumination **(C, D, respectively)**. The TrkB photoactivatable system with this pair still caused the mCh-$AKT1_{PH}$ translocation upon imaging light. For each condition n > 10 cells were tested. A single blue light pulse of 1 s was delivered at t = 3 min of a timecourse **(only for A, C)**. Photos show the cells at 0 min, 5 min and 20 min of the time-lapse. Cells are representative from two independent experiments each performed in duplicates.

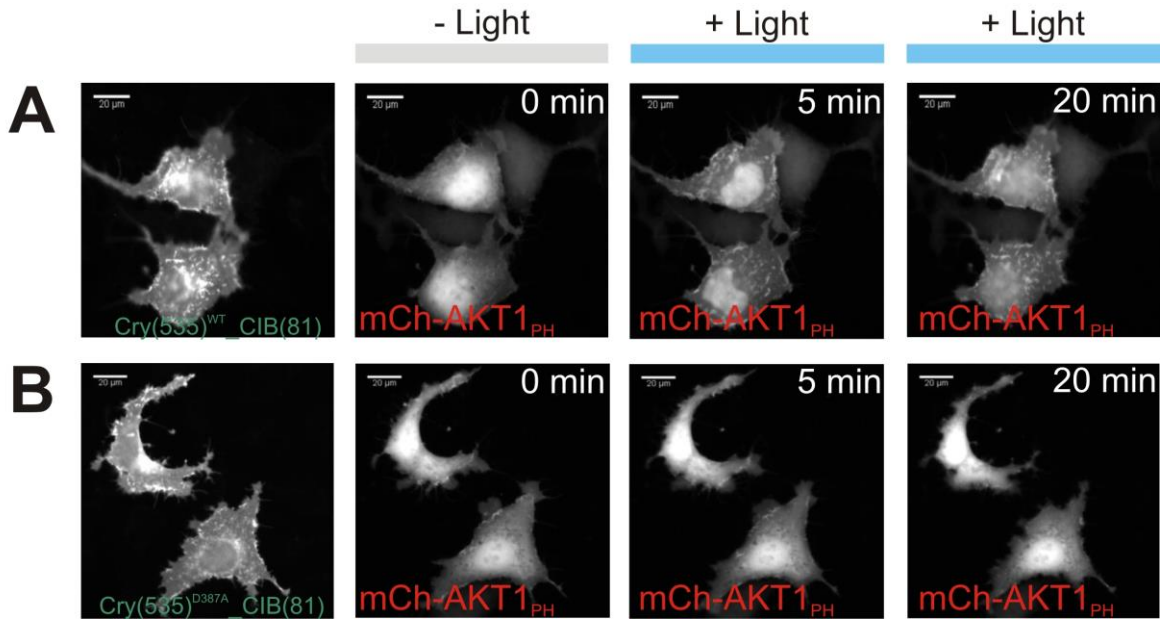

Figure 2.25 $AKT1_{PH}$ translocation to the membrane is caused by the activation of the photoactivatable TrkB system upon the imaging light conditions. The photos represent a time-lapse of the mCherry-$AKT1_{PH}$ translocation to the membrane upon blue light stimulation when cells were co-transfected with the light-responsive Cry2(535)_WT **(A)** or the light-insensitive mutant Cry2(535)_D387A **(B)** in the TrkB system. According to these examples, $AKT1_{PH}$ underwent light-dependent translocation as shown in the photos when Cry2(535)_WT is in the system **(A)**, whereas the translocation was abolished when Cry2(535)_D387A was used. The left photos are the examples of the expression of the constructs. For each condition n > 10 cells were tested from two independent experiments each performed in duplicates.

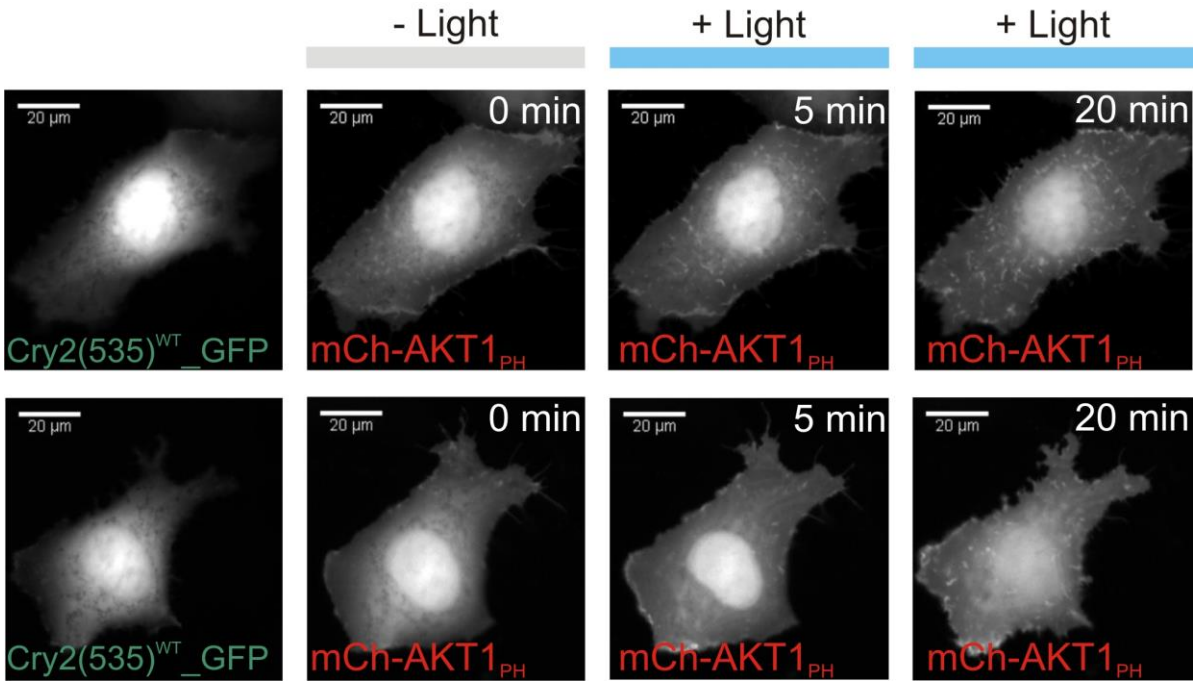

Figure 2.26 The photoactivatable TrkB system, which consists of Cry2(535) without CIB1 component in the membrane, can still activate AKT1 pathway in HEK293A cells. The panels show two examples of the mCherry-AKT1$_{PH}$ translocation to the membrane upon blue light stimulation when cells were co-transfected with the mCherry-AKT1$_{PH}$ and TrkB^{WT}-Cry2(535)-T2A-eGFP. The left photos show the expression of the construct (labelled as "Cry2(535)^{WT}_GFP"). The examples of mCHerry-AKT1$_{PH}$ translocation are shown at 0 min, 5 min and 20 min of the time-lapse. In this experiment, n > 10 cells were analyzed from one independent experiment in triplicate. A single blue light pulse of 1 s was delivered at t = 3 min of a timecourse.

2.3.2.4 Biochemical confirmation of ERK and PLCγ1 activation by western blotting analyses

Upon activation by TrkB, its downstream targets, PLCγ1, ERK and AKT, are phosphorylated (see Section 2.3.2.1, 2.3.2.2 and 2.3.2.3, respectively). Changes in phosphorylation states of these proteins upon a blue light exposure were assayed by western blotting. After 48 h post-transfection, the cells were stimulated by continuous and global exposure to blue light at 36.8 mW/cm^2 for 30 s or were kept on a disabled LED source in dark. Then, the whole cell lysates were collected at 10 min after light termination. The endogenous ERK, PLCγ1, AKT proteins were analyzed using specific phospho-antibodies (see Table 2.3).

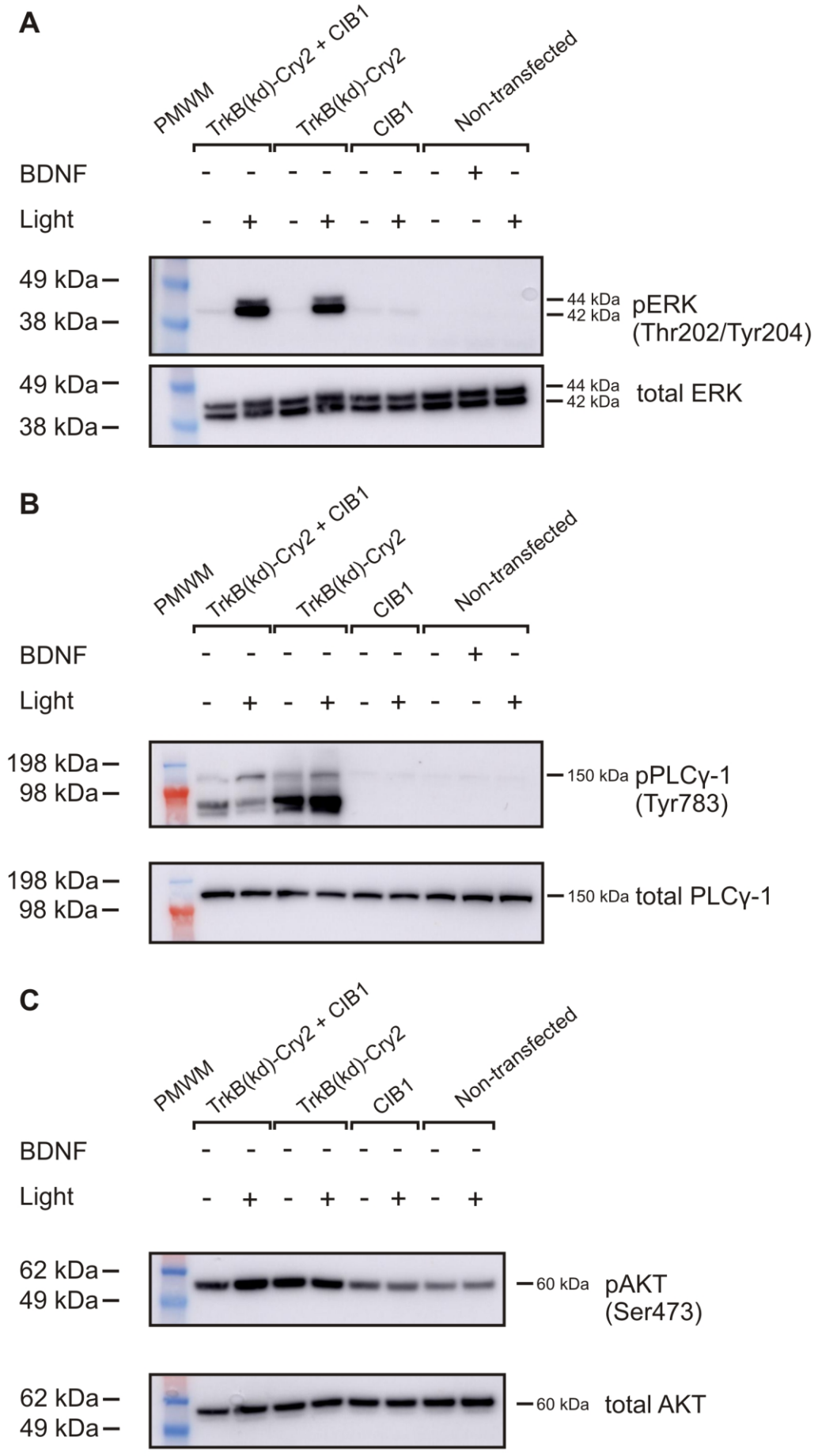
A
PMWM
TrkB(kd)-Cry2 + CIB1
TrkB(kd)-Cry2
CIB1
Non-transfected
BDNF
Light
49 kDa
38 kDa
44 kDa
42 kDa
pERK
(Thr202/Tyr204)
total ERK
B
198 kDa
98 kDa
150 kDa
pPLCγ-1
(Tyr783)
total PLCγ-1
C
62 kDa
49 kDa
60 kDa
pAKT
(Ser473)
total AKT

Figure 2.27 Immunoblot analyses of endogenous ERK, PLCγ1 and AKT proteins in HEK293A cells transfected with the photoactivatable TrkB system. (A) The two-component TrkB(kd) system consisting of Cry2(535) and CIB1(81) proteins as well as a single-component system with TrkB(kd)-Cry2(535) activated endogenous ERK proteins upon blue light stimulation. The activation of ERK was measured by using antibody against phospho-ERK when phosphorylated at Thr202 and/or Tyr204. Phospho-ERK was examined in presence and absence of 30-s blue light stimulation. Total ERK is given to ensure that the total protein level remains unchanged. Representative images from one independent experiment. **(B)** The two-component TrkB(kd) system consisting of Cry2(535) and CIB1(81) proteins as well as the single-component system with TrkB(kd)-Cry2(535) activated endogenous PLCγ1 upon blue light stimulation. The PLCγ1 activity was examined by checking the level of phosphorylated protein at Tyr783 in presence and absence of 30-s blue light stimulation. Unfortunately, the phospho-PLCγ1 antibody detected unspecific bands below required 150 kDa band in HEK293A cells. Total PLCγ1 level was checked. Representative images from two independent experiments. **(C)** The two-component TrkB(kd)-Cry2(535) + CIB1(81) system could activate insignificantly endogenous AKT measured by the level of its phosphorylation at Ser473, whereas the one component TrkB(kd)-Cry2(535) system could not. The phospho-AKT was studied in presence and absence of 30-s blue light stimulation. Total AKT level was examined. Representative images from one independent experiment. In each experiment, phospho-proteins were examined 10 min after the 30-s light stimulation at 470 nm. Non-transfected cells were used as a control and as a further confirmation that they do not express endogenous TrkB. PMWM – protein molecular weight marker.

Upon blue light stimulation of the cell population transfected with pcDNA3-CMV-TrkB-Cry2(535)-T2A-CIB1(81)-eGFP-CAAX, the level of phosphorylated ERK at T202/Y204 was increased approximately 29-fold compared to cells not illuminated with blue light (Fig. 2.27 A). The cells transfected with pcDNA3-CMV-TrkB-Cry2(535)-T2A-eGFP also exhibited increased phospho-ERK (~21-fold compared to the non-illuminated cells) upon light stimulation. In non-transfected cells, neither blue light stimulation nor BDNF treatment did elicit the phospohorylation of ERK (Fig. 2.27 A). Lack of response upon BDNF indicates that HEK293A cells do not express the endogenous TrkB.

The same conditions were used to assess the phosphorylation level of PLCγ1 at Tyr783 upon light exposure. Consistent with previous observations from live-cell imaging, the cells transfected with pcDNA3-CMV-TrkB-Cry2(535)-T2A-CIB1(81)-eGFP-CAAX, when stimulated with light, showed 4.7-fold and 8.6-fold increase in phospho-PLCγ1 (data from two independent experiments) (Fig. 2.27 B). The transfection with pcDNA3.1H-CMV-CIB1(81)-eGFP-CAAX as well as BDNF treatment did not cause phosphorylation of PLCγ1. Intriguingly, without the membrane-anchored CIB1, the cytosolic TrkB-Cry2(535) alone could phosphorylate PLCγ1 upon blue light stimulation (from two independent experiments: 2.0-fold and 3.5-fold increase in the phosphorylation level compared to the unexposed cells). This observation was unexpected as no detectable Ca^{2+} elevation was observed in Ca^{2+}

imaging experiments, when cells expressing this construct were stimulated with blue light (refer to Fig. 2.14 B).

Finally, the phosphorylation state of AKT at Ser473 was examined upon blue light illumination. When cells were transfected with pcDNA3-CMV-TrkB-Cry2(535)-T2A-CIB1(81)-eGFP-CAAX or pcDNA3-CMV-TrkB-Cry2(535)-T2A-eGFP, the background phosphorylation in the dark was high in comparison with non-transfected cells or cells transfected with pcDNA3.1H-CMV-CIB1(81)-eGFP-CAAX alone (Fig. 2.27 C). Nevertheless, blue light exposure of cells expressing TrkB-Cry2(535)-T2A-CIB1(81)-eGFP-CAAX caused 1.6-fold increase in the phosphorylation level of AKT. The TrkB-Cry2(535) or CIB1(81) components, when used separately, did not raise the level of phospho-AKT above their baseline under blue light exposure (Fig. 2.7 C).

2.3.3 Light-mediated activation of TrkB signalling in HeLa cells

As it was shown in Figure 2.27 (Panels A, B) HEK293A cells did not respond to BDNF treatment, which suggests that endogenous TrkB receptors are not expressed, or are expressed at very low level, in this cell culture. Furthermore, it suggests that the photoactivatable TrkB system does not require endogenous TrkB for its action. To examine further whether the TrkB system acts completely independent from the endogenous expression of TrkB, a HeLa cell line was used as a model, as it is known from the literature that HeLa cells do not express the endogenous TrkB receptors (Chang et al., 2014). Using RNA sequencing data, deposited on The Human Protein Atlas website (www.proteinatlas.org), the TrkB transcript abundance in HEK293 and HeLa cells was estimated (Fig. 2.28 A). According to these results, TrkB was not expressed in HEK293 and HeLa cell lines. In an independent test, RT-PCR results obtained from RNA extracted from HEK293A and HeLa cells showed no band corresponding to the intracellular domain of TrkB (TrkB(kd)) in Hela (Fig. 2.28 A, lanes 2 and 3) and a faint band at the expected size for TrkB(kd) in HEK293A (Fig. 2.28 A, lanes 4 and 5).

Having established that HeLa cells do not express endogenous TrkB, the Ca^{2+} imaging in HeLa cells co-expressing O-GECO1 and TrkB(kd)-Cry2(498)-T2A-CIB1(170)-eGFP-CAAX demonstrated that the photoactivatable TrkB acts without the endogenous TrkB upon light illumination (Fig. 2.28 B). Similarly, ERK and AKT pathways could also be activated upon light exposure in HeLa cells (Fig. 2.28 C, D).

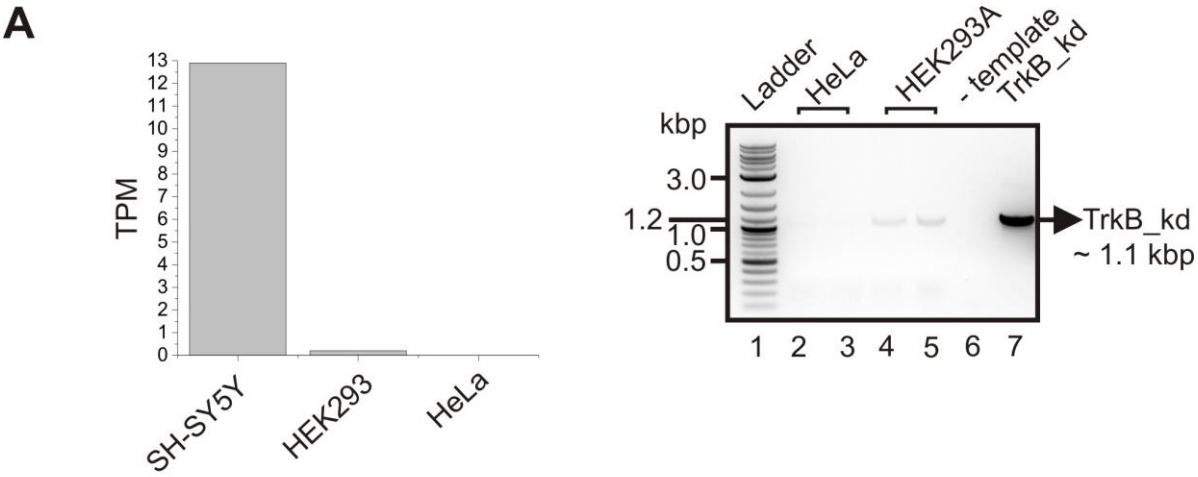
A
TPM
SH-SY5Y
HEK293
HeLa
Ladder
HeLa
HEK293A
- template
TrkB_kd
kbp
3.0
1.2
1.0
0.5
TrkB_kd
~ 1.1 kbp
1 2 3 4 5 6 7

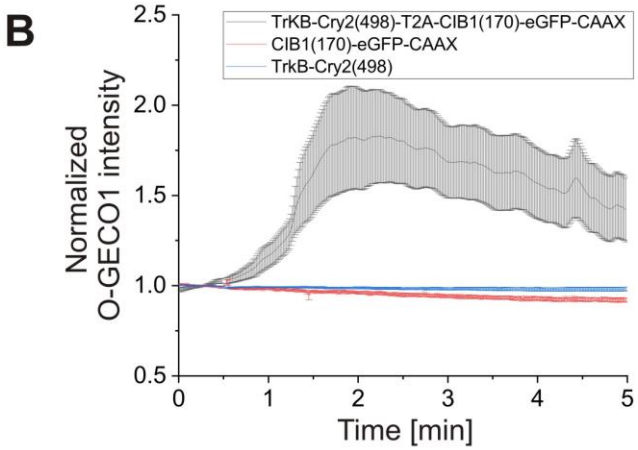
B
TrkB-Cry2(498)-T2A-CIB1(170)-eGFP-CAAX
CIB1(170)-eGFP-CAAX
TrkB-Cry2(498)
Normalized
O-GECO1 intensity
Time [min]

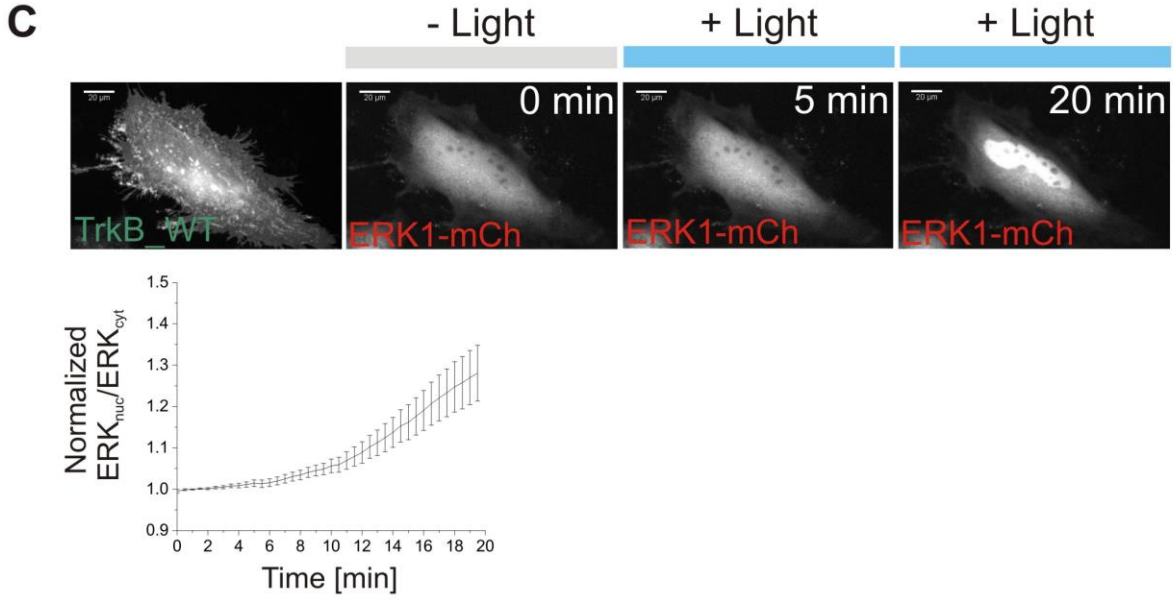
C
- Light
+ Light
+ Light
0 min
5 min
20 min
TrkB_WT
ERK1-mCh
ERK1-mCh
ERK1-mCh
Normalized
ERKnuc/ERKcyt
Time [min]

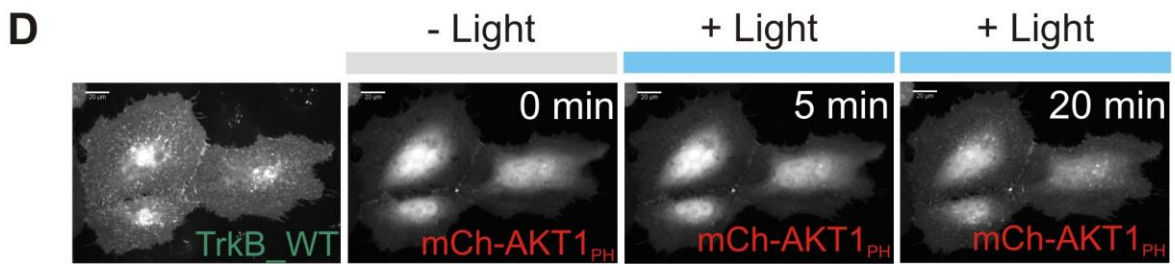
D
- Light
+ Light
+ Light
0 min
5 min
20 min
TrkB_WT
mCh-AKT1PH
mCh-AKT1PH
mCh-AKT1PH

Figure 2.28 The photoactivatable TrkB system works in HeLa cells. (A) The left graph represents RNA expression of TrkB gene in SH-SY5Y (shown as an example of the cell line which is enriched in TrkB expression), HEK293 and HeLa cell lines. The sequencing results are reported as Transcripts per Kilobase Million (TPM). The TPM of 1.0 is a threshold for expression of a gene that means that TrkB protein is expressed in SH-SY5Y but not in HEK293 and HeLa. Presented data were obtained from the Human Protein Atlas website available from https://www.proteinatlas.org/ENSG00000148053-NTRK2/cell#rna. The agarose gel photo (right) shows the results of RT-PCR using cDNA prepared from HeLa and HEK293A and primers against the intracellular domain of human TrkB. Lanes 2 and 3 are RT-PCR results from HeLa from two independent RNA extractions; lanes 4 and 5 from HEK293A from two independent RNA exptarctions; lane 6 is a negative control (no template control); lane 7 is a positive control (intracellular domain of TrkB) and this PCR product was used in the previous cloning experiments. **(B)** In HeLa cells co-expressing TrkB-Cry2(498)-T2A-CIB1(170)-eGFP-CAAX and O-GECO1, light illumination led to the elevation of intracellular Ca^{2+} (black line). TrkB-Cry2(498) or CIB1(170)-eGFP-CAAX component alone was not sufficient to evoke Ca^{2+} transients (blue and red lines, respectively). Intracellular Ca^{2+} changes were quantified as O-GECO1 fluorescence intensity normalized to the baseline fluorescence before blue light stimulation at 0.5 min. Results are presented as mean ± SEM calculated from 37 cells for TrkB(kd)-Cry2(498)-T2A-CIB1(170)-eGFP-CAAX; from 18 cells for TrkB-Cry2(498); from 17 cells for CIB1(170)-eGFP-CAAX from two independent experiments. **(C)** Light activation of TrkB led to ERK1 translocation to the nucleus in HeLa cells. Photos are the representative HeLa cell co-expressing ERK1-mCherry and TrkB(kd)-Cry2(498)-T2A-CIB1(170)-eGFP-CAAX before light illumination (0 min) and after light illumination (5 min and 20 min). The graph shows the average ratio of nuclear to cytosolic ERK1 upon light illumination from two independent experiments each performed in duplicates (mean ± SEM from n = 16 cells in total). 1-s light illumination was delivered at 3 min of the imaging. **(D)** Light activation of TrkB leads to $AKT1_{PH}$ translocation to the membrane in HeLa cells. Photos show a HeLa cell co-expressing mCherry-$AKT1_{PH}$ and TrkB(kd)-Cry2(498)-T2A-CIB1(170)-eGFP-CAAX before light illumination (0 min) and after light illumination (5 min and 20 min). Representative image from two independent experiments.

Taken together, these results proved that the action of the light-inducible TrkB can act independently from the endogenous expression of this protein. Whether the photoactivatable TrkB action can be affected by endogenous TrkB in other cell types still needs to be tested.

2.4 Discussion

The increasing interest in light-inducible RTKs dictates the necessity for the development of new optogenetic approaches. The data presented in this chapter prove that the photoactivatable TrkB system can be re-designed without considerable engineering of the receptor and genetically encoded dimerizers to achieve desired outcome. In this PhD thesis, a new two-component light-controllable TrkB was created by fusing TrkB(kd) to Cry2 and

localizing CIB1 to the membrane. This has added a new tool to the existing RTKs toolbox and introduced new possibilities.

This chapter aims to describe the photoactivatable TrkB system in non-neuronal cells, HEK293A and HeLa, prior proceeding with more complicated neuronal cells. The experimental results from HEK293A and HeLa cell lines confirm that the optogenetic TrkB system can activate signalling pathways associated with TrkB kinase activity, such as PLCγ1, ERK and AKT cascades, upon light illumination. The new TrkB system can be activated independently from its natural ligand, BDNF, as the extracellular domain of TrkB was excised. Removing the ligand-binding domain makes the system more suitable for *in vivo* application to ensure that any observed perturbations come from light rather than endogenous BDNF. Additionally, the new TrkB system consists of two components that can be used as a bicistronic system through a "self-cleaving" peptide, T2A, or as monocistronic vectors that can be packaged into recombinant viral AAV for *in vivo* studies. In this chapter, the utility of the bicistronic vectors was mostly presented.

As hypothesized, the expression of TrkB(kd)-Cry2(498)-T2A-CIB1(170)-eGFP-CAAX in cells can mimic native signalling, leading to the activation of PLCγ1, ERK and AKT proteins upon light (Table 2.5). In this system, the original truncated Cry2(498) (known in the literature as PHR domain) and the truncated CIB1(170) (known in the literature also as CIB1N) were utilized (Kennedy et al., 2010). Replacement of the original Cry2(498) and CIB1(170) with the second-generation dimerizers – a longer Cry2(535) and shorter CIB1(81), which were reported to lower background interactions (Taslimi et al., 2016) – results in constructs that can still activate the canonical signalling cascades mediated by the TrkB system. Interestingly, when the same 1-s light stimulation was used during live-cell imaging experiments, Ca^{2+} responses, triggered by TrkB(kd)-Cry2(535)-T2A-CIB1(81)-eGFP-CAAX, were more transient than those induced by TrkB(kd)-Cry2(498)-T2A-CIB1(170)-eGFP-CAAX. This observation can be possibly explained by lower affinity between Cry2(535) and CIB1(81). It has been reported that Cry2(535) shows weaker self-association and lower background interaction with CIB1 in dark (Taslimi et al., 2016), which might also translate to a weaker or more transient interaction between Cry2 and CIB1 in the light.

When the single component of CIB1(170 or 81)-eGFP-CAAX was tested without Cry2 using live-cell imaging or western blotting, it did not evoke light-dependent activation of the canonical pathways (Table 2.5). When TrkB(kd)-Cry2(498 or 535) or TrkB(kd)-Cry2(535) were used without CIB1, they failed to mobilize Ca^{2+} release in live-cell imaging

experiments. The same TrkB(kd)-Cry2(535), when tested by western blotting, caused the phosphorylation of PLCγ1 upon blue light exposure. The explanation of this inconsistency might be that PLCγ1 is a cytosolic enzyme and is known to become membrane-associated under EGF treatment (Todderud et al., 1990; Wahl et al., 1992; Wang and Wang, 2003). I have shown that TrkB(kd)-Cry2(535) can phosphorylate PLCγ1 in the cytosol, but without membrane anchored CIB1, TrkB might fail to localized PLCγ1 to the membrane. Consequently, PLCγ1 might not be able to cleave the membrane phospholipid PtdIns(4,5)P_2 to DAG and Ins(1,4,5)P_3, and Ca^{2+} elevation is prevented. This observation might be helpful in biochemical dissection of the TrkB-mediated signalling pathways upon light exposure.

Table 2.5 The activation of the canonical pathways by the photoactivatable TrkB system tested by live-cell imaging and western blotting.

Component of the system	PLCγ1	ERK	AKT
TrkB(kd)-Cry2(498)-T2A-CIB1(170)-eGFP-CAAX	✓LCI	✓LCI	✓LCI
TrkB(kd)-Cry2(498)	-LCI	NT	NT
CIB1(170)-eGFP-CAAX	-LCI	NT	NT
Cry2(498)-TrkB(kd)-T2A-CIB1(170)-eGFP-CAAX	-LCI	NT	NT
TrkB(kd)-Cry2(535)-T2A-CIB1(81)-eGFP-CAAX	✓LCI ✓WB	✓LCI ✓WB	✓LCI ✓WB
TrkB(kd)-Cry2(535)_D387A-T2A-CIB1(81)-eGFP-CAAX	-LCI	-LCI	-LCI
TrkB(kd)-Cry2(535)-T2A-eGFP	-LCI ✓WB	✓LCI ✓WB	✓LCI -WB
CIB1(81)-eGFP-CAAX	-WB	-WB	-WB
MYR-CIB1(81)-eGFP-T2A-TrkB(kd)-Cry2(535)	-LCI	-LCI	-LCI

✓activated pathway; - not activated pathway; LCI, tested by live-cell imaging; WB, tested by western blotting; NT, not tested.

It is noteworthy that different blue light durations were used between live-cell imaging (1 s) and immunoblotting (30 s), which could also affect the activation of PLCγ1. The light

dose-dependent activation of PLCγ1 pathway was reported previously by Han et al. (2016) with optoTrkC. In their system, PLCγ1-induced Ca^{2+} release associated with optoTrkC activity was only detected when higher blue light intensity (five 350-ms pulses at 32.47 mW/cm^2) was used (Han et al., 2016).

Consistently, either live-cell imaging with ERK1-mCherry sensor or western blotting showed that TrkB(kd)-Cry2(535) alone can trigger the signalling cascade leading to ERK activation (Table 2.5). In cells, expressing TrkB(kd)-Cry2(535), the live-cell imaging assay involving $AKT1_{PH}$ translocation showed that the PH domain of AKT1 can be relocated from the cytoplasm to the plasma membrane after light stimulation. However, TrkB(kd)-Cry2(535) alone did not cause the apparent increase in the level of AKT phosphorylation at Ser473 measured by immunoblotting (Table 2.5). It is noteworthy that the two-component TrkB system, even that it induced the robust light-dependent translocation of $AKT1_{PH}$, caused only ~1.6-fold increase of the endogenous AKT1 phosphorylation at Ser473 upon light stimulation. This lowered sensitivity of the immunoblotting assay might be due to the observation reported by Ebner et al. (2017), in which insulin promoted more sustain accumulation of mCherry-AKT_{PH} (longer than 20 min), whereas the full-length AKT retained in the membrane for approximately 10 min. This can suggest that the observed in this study relocation of mCherry-$AKT1_{PH}$ upon light illumination in the live-cell imaging experiment might have different kinetics than the endogenous full-length AKT1 tested by western blotting. Following that, the phosphorylation of the endogenous AKT1 might be transient and have a peak earlier than 10 min post-stimulation which was not therefore captured by the immunoblotting. The inconsistency between the action of TrkB(kd)-Cry2(535) component, when tested by the live-cell imaging and western blotting, suggests that CIB1 component in the membrane might be necessary for AKT1 activation upon light. As it was observed, mCherry-$AKT1_{PH}$ was retained in the similar membrane domains as CIB1-eGFP-CAAX upon light illumination. This can be supported by the observation that the activation of AKT is restricted to discrete membrane locations (Ebner et al., 2017; Lucic et al., 2018). Differently, TrkB(kd)-Cry2(535) alone upon light stimulation can trigger AKT1 relocation to the membrane without its full-activation. A recent report can provide an explanation by showing that the $AKT1_{PH}$ domain engagement to the membrane is not the only factor necessary for the full AKT1 activation, but also the phosphorylation at Ser473 is required (Chu et al., 2018). Taken together, TrkB(kd)-Cry2(535) alone leads to the AKT1 relocation to the membrane where AKT1 might not be further activated. Nevertheless, either the two-component or the one-component TrkB system elevated the baseline levels of phosphorylated

AKT1 in the dark, whereas a single CIB1 component did not (total AKT1 levels remained unchanged in each condition). This background elevation of AKT1 phosphorylation may be specific to the cell line used for the expression of the TrkB system as it has been shown by Chang et al. (2014) who reported that the full-length optoTrkB can cause increase in ERK phosphorylation in the dark state in HeLa, but not in PC12 cells.

The orientation of TrkB(kd)-Cry2 and CIB1 around T2A affect the performance of the light-inducible system

It has been shown in the literature that when Cry2/CIB1 pair is applied to activate a target protein, the orientation-specific effect should be taken into consideration (Che et al., 2015; Hallett et al., 2016; Kennedy et al., 2010). For instance, Cry2 localized in the membrane has been reported to affect the light-induced interaction with CIB1 (Kennedy et al., 2010).

For the purpose of this project, two bicistronic constructs were generated originally with the inserts: TrkB(kd)-Cry2(498)-T2A-CIB1(170)-eGFP-CAAX and Cry2(498)-TrkB(kd)-T2A-CIB1(170)-eGFP-CAAX. In these constructs, CIB1 component attached to the membrane by a C-prenylation tag, CAAX, was fused after the self-cleaving T2A sequence, whereas Cry2 and TrkB component in two orientations was linked before T2A peptide. Both of these constructs were tested to check their abilities to trigger Ca^{2+} responses upon light illumination (Table 2.5). In this assay, the TrkB(kd)-Cry2 orientation was more efficient than Cry2(498)-TrkB(kd) at activating the signalling cascade. Recently, it has been reported that the kinase domain of TrkA without the membrane-localization tag can be fused to the C-terminus of Cry2 and can successfully activate AKT and ERK pathways upon light (Duan et al., 2018). However, this design was used in a co-transfection experiment with CIB1-GFP-CAAX and without the self-cleaving peptide between Cry2 and CIB1. The differences in the actions between two constructs used in this project are likely due to the use of T2A sequence. The protein expressed upstream of the T2A peptide is linked to the complete sequence of T2A (except the C-terminal proline) (Donnelly et al., 2001; Liu et al., 2017). This suggests that the T2A peptide might block the availability of C-terminal Y816 within TrkB(kd) for its docking partner, PLCγ1, which consequently, might lead to the less efficient activation of Ca^{2+} signal. Consistent with the work published by Han et al. (2016), Cry2 is less sensitive to the presence of extra amino acids on its C-terminus. Moreover, it has

been shown that the peptide attached to C-terminal Cry2 can enhance the oligomerization of Cry2 (Park et al., 2017).

Finally, CIB1 was attached to the membrane through the N-terminal myristoylation tag and upstream of T2A, whereas TrkB-Cry2 was linked downstream of T2A (MYR-CIB1(81)-eGFP-T2A-TrkB(kd)-Cry2(535)). This orientation also failed to activate Ca^{2+} signalling (Table 2.5). It is possible due to three reasons: (1) N-terminus of CIB1 is involved in the membrane fusion; (2) eGFP as a quite bulky protein might act as a steric hindrance and block interaction between Cry2 and CIB1; (3) the expression of TrkB-Cry2 might not be sufficient. It is known that N-terminus of CIB1 is necessary for dimerization with Cry2 (Hallett et al., 2016). The myristoylation sequence has been used previously to localize CIB1 component to the membrane. However, the direct fusion between the myristoylation tag and a fluorescent protein was made to leave the N-terminus of CIB1 accessible (MYR-FP-CIB1) (Katsura et al., 2015). Furthermore, the utility of T2A might decrease the expression of the gene, which is downstream of T2A (here: TrkB(kd)-Cry2) (Liu et al., 2017).

The green-light imaging conditions can cause the photoexcitation of Cry2

In the live-cell imaging experiments, the TRITC filter set was used to visualize the O-GECO1/mCherry fluorescence changes caused by Ca^{2+}, ERK and AKT activation. Unfortunately, this filter set can transmit excitation light down to approximately 530 nm. Consistently with the absorption spectra for Cry2 (Banerjee et al., 2007), the longer wavelengths above 500 nm and up to 550 nm can cause the residual cryptochrome activity (Ahmad et al., 2002). This was confirmed by Kennedy et al. (2010) who observed Cry2-mCherry translocation to CIB1-Citrine under the high intensity illumination at 514 nm. Then, Tucker et al. (2014) reported that the illumination at 561 nm for prolonged period and at high intensity can excite Cry2/CIB1 interaction.

These observations are in agreement with the results obtained in this project that the green light is able to activate Cry2/CIB1 system. Consequently, the imaging conditions led to ERK and AKT translocations upon activation of the TrkB system. It is worth mentioning that these two pathways were activated more easily with imaging light in almost all cells, whereas Ca^{2+} responses did not (only in approximately 26% of cells), likely due to the higher intensity imaging light used during ERK/AKT translocation experiments than during Ca^{2+} imaging and also possibly due to the chain activation of multiple proteins leading to ERK and AKT phosphorylation. This has been shown in case of optoTrkC activation where lower light

intensity could trigger ERK and AKT pathways, but not Ca^{2+} release (Han et al., 2016). To overcome spectral overlap between the imaging conditions and the absorption spectrum of Cry2, a near-infrared fluorescent protein IFP1.4 (excitation at 684 nm) (Shu et al., 2009) can be attached to ERK1 and $AKT1_{PH}$ to create sensors. These sensors and an appropriate filter set might potentially eliminate the activation of the photoactivatable TrkB upon light imaging conditions leading to ERK/AKT translocation dependent on specific blue light illumination.

The stimulatory light effect is mediated through the kinase activity of TrkB

The point mutations in TrkB(kd) confirmed that the light-mediated activation of the canonical pathways is through the kinase activity. The K571A mutation, which was described previously to abrogate TrkB kinase activity (Guiton et al., 1994; McCarty and Feinstein, 1998), abolished Ca^{2+} increase as well as ERK and AKT translocation in the light state (Table 2.6). The mutation of Y816F inhibited the light-mediated Ca^{2+} increase, confirming the sole association of Y816 to PLCγ1 activation (Middlemas et al., 1994). Moreover, using the PLC inhibitor, U73122, suppressed light-triggered Ca^{2+} elevation, which also proved the involvement of PLCγ1 activity. The Y816F mutation did not block the activation of ERK and AKT pathways (Table 2.6).

Table 2.6 The activation of canonical pathways by the photoactivatable TrkB system with mutation in the kinase domain of TrkB.

Construct	PLCγ1	ERK	AKT
TrkB(kd)_WT-Cry2(498)-T2A-CIB1(170)-eGFP-CAAX	✓LCI	✓LCI	✓LCI
TrkB(kd)_Y816F-Cry2(498)-T2A-CIB1(170)-eGFP-CAAX	-LCI	✓LCI	✓LCI
TrkB(kd)_Y515F-Cry2(498)-T2A-CIB1(170)-eGFP-CAAX	✓LCI	✓LCI	✓LCI
TrkB(kd)_K571A-Cry2(498)-T2A-CIB1(170)-eGFP-CAAX	-LCI	-LCI	-LCI

✓ activated pathway; - not activated pathway; LCI, tested by live-cell imaging.

The mutation Y515F, previously identified to attenuate ERK and AKT phosphorylation (Easton et al., 1999), remained capable of the activation of ERK and AKT pathways upon light. Moreover, this mutant did not reduce the activation of ERK or AKT. As expected, Y515F did not alter Ca^{2+} responses in O-GECO1-HEK293A cells in light condition (Table

2.6). The ability to evoke ERK pathway by the Y515F mutant is in agreement with the previous studies showing BDNF-dependent activation of ERK signalling through fibroblast growth factor receptor substrate 2 (FRS2) which does not interact with Y515 and does not form a complex with SHC (Easton et al., 1999). Another study reported that the basal level of Ca^{2+}, not coupled with the Ca^{2+} elevation by PLCγ1, gates AKT signalling by BDNF treatment in cortical neurons (Zheng et al., 2008). Moreover, it has been shown recently that the activation of protein kinase C (PKC) requires BNDF-TrkB signalling (Colgan et al., 2018) and PLCγ1 is responsible for the PKC activation (Li et al., 2013). Furthermore, PKC has been indicated to trigger AKT and ERK pathways (Li et al., 2013; Shatos et al., 2009). As described, the crosstalk between the AKT, ERK and PLCγ1 pathways as well as the recruitment of distinct sets of effector proteins to TrkB could activate ERK and AKT independently from the Y515 site.

The photoactivatable TrkB system can work without endogenous TrkB

The experiments for the purpose of this chapter were conducted in HEK293A and HeLa cells, which do not express endogenous TrkB. In these cells, expressing the light-inducible TrkB, the exposure to light was sufficient to activate PLCγ1, ERK and AKT pathways. However, it remains still unclear whether there can be a trans-activation between the light-dependent TrkB and the endogenous TrkB in our testing conditions.

Taken together, the data presented in this chapter demonstrate the successful generation of the photoactivatable TrkB system. This chimeric receptor induced downstream TrkB signalling pathways upon light. The results are consistent with the activation of PLC, ERK and AKT signalling. The TrkB tool was controlled repeatedly. The introduction of Y816F mutation in TrkB(kd) abolished the activation of PLCγ1 while retaining the activities of ERK and AKT pathways, which can be used to dissect these cascades. Originally, the TrkB system was designed to work as a two-component tool; however, it was found that one component is sufficient to trigger signalling. This can be also used to dissect signalling. The developed tool acts independently from BDNF, which makes it attractive to *in vivo* applications. Finally, the approach can be generalized to other tyrosine kinase receptors, as confirmed by the optoTrkA design published by Duan et al. (2018).

Chapter 3

Validation of a photoactivatable TrkB in neuronal cells

3.1 Introduction

Many optogenetic tools have been successfully used for manipulation of specific biochemical processes in neuronal cells as reviewed by Zhou et al. (2015). Among these approaches, the optical control of RTKs has been applied in primary neurons. The optoTrkB, developed by Chang et al. (2014), was demonstrated to activate AKT pathway in hippocampal neurons upon light illumination. Thanks to this experiment, the light-mediated formation of lamellipodia and filopodia, actin-based structures, in perisomatic regions of illuminated neurons was observed. Following this, filopodia formation could be induced with spatially restricted precision within a single hippocampal cell upon focal light stimulation. Chang et al. (2014) could also increase the neurite length and the number of branch points in hippocampal neurons upon the activation of optoTrkB with light. Han et al. (2016) showed that optoTrkC could activate AKT, ERK and PLCγ1 pathways in cultured hippocampal neurons upon light illumination. Moreover, they used optoTrkC to regulate synapse development in a light intensity-dependent manner. Finally, the recent results provided by Duan et al. (2018) demonstrated that optoTrkA could support survival of DRG neurons without NGF supplementation, with light exposure mimicking NGF function.

The mentioned optoTrk receptors were introduced into cultured neurons by electroporation or liposome-based transfection without any further intention to apply them *in vivo* (Chang et al., 2014; Duan et al., 2018; Han et al., 2016). Conducting *in vivo* experiments on behaving animal requires the production of lentiviral or AAV vectors for transgene expression. Although the described optoTrk receptors were not packaged into any viral vectors, the wild-type TrkB receptors were delivered into specific brain regions by lentiviral or AAV infection. For instance, a lentiviral vector encoding a dominant-negative TrkB isoform (TrkB.T1) was constructed to infect the amygdala *in vivo* (Chhatwal et al., 2006; Heldt et al., 2014; Rattiner et al., 2004; Rattiner et al., 2005). The lentiviral vector was used to overexpress TrkB.T1, which lacks the entire kinase domain and acts as an inhibitor of BDNF signalling through native TrkB. This approach was applied to examine the involvement of TrkB in amygdala-dependent learning (Chhatwal et al., 2006; Heldt et al., 2014; Rattiner et al., 2004; Rattiner et al., 2005). The same truncated TrkB.T1, as well as the

full-length TrkB, were packaged into AAV serotype 2 and used to investigate the role of TrkB in motor neuron degeneration (De Wit et al., 2006). Another example of delivering TrkB via viral vector *in vivo* was the packaging of the full-length receptor into AAV serotype 7. This recombinant AAV7 was used to infect phrenic motoneurons for enhancing recovery after spinal cord injury (Martinez-Galvez et al., 2016). Finally, a bicistronic AAV2 encoding the full-length TrkB and mature BDNF was introduced in mouse retinal ganglion cells and this approach wasn believed to be useful as a gene therapy (Osborne et al., 2018). The mentioned approaches for *in vivo* studies utylized the intact full-length TrkB and this rceptor cannot be simply turned on or off with a temporal resolution. Moreover, the activation of TrkB relies on the availability of the endogenous BDNF (an exception is the tool provided by Osborne et al. (2018)). To overcome these limitations, the photoactivatable TrkB system, developed and described in Chapter 2, was therefore tested in neuronal cells.

To validate the photoactivatable TrkB system in neurons, this transgene was introduced into a recombinant AAV vector. Infection with viral particles enabled the expression of the light-activated TrkB in a high proportion of cultured primary neurons (see Section 3.3.2) and subsequent infection of a required brain region for *in vivo* studies (see Section 3.3.5). The photoactivatable TrkB provides for the possibility of activating canonical signalling pathways in neurons with a spatiotemporal resolution. Moreover, TrkB signalling can be induced independently of endogenous BDNF. As mentioned in Chapter 1 (Section 1.2.3), BDNF/TrkB signalling contributes to the axon pathfinding process. BDNF acts as an attractive guidance cue (Ming et al., 1997). The axon guidance in dorsal root ganglion neurons (DRG) was therefore used as a proof-of-concept experiment to validate the functionality of the photoactivatable TrkB to change the growth cone motility upon light. The aim of this chapter is to present results, demonstrating that the photoactivatable TrkB can be controlled in a light-dependent manner in neurons *in vitro*. Furthermore, this TrkB system can be successfully expressed in the brain region of freely behaving rats.

3.2 Materials and methods

3.2.1 Ethical declaration

The animal procedures were approved by the Animal Ethics Committee of the University of Tasmania (Ethics number: A0016936) and conformed to the requirements of the Australian code of practice for the care and use of animals for scientific purposes.

3.2.2 Materials

The resources and reagents used for creating and validating the photoactivatable TrkB system in primary neuronal cells are summarized in Table A1 in Appendix.

3.2.3 Plasmid construction

For generation of recombinant AAV virus, some of the constructs tested in Chapter 2 were cloned into an AAV transfer vector (Addgene #50977) (Lin et al., 2009) between two AAV2 inverted terminal repeat (ITR) sequences. Additional genetic elements were included for neuron-specific expression, which includes the sequence for human synapsin promoter (abbreviated as hSyn), woodchuck hepatitis virus posttranscriptional regulatory element (WPRE – full length or reduced length, see below) followed by a simian virus 40 (SV40) polyadenylation (poly(A)) signal. The hSyn promoter ensures neuron specific expression and WPRE increases the stability of the mRNA to enhance expression. In the TrkB plasmid, a truncated WPRE sequence (Choi et al.) was used to keep the insert below the packaging size-limit of AAV particles, whereas the full-length WPRE was used in CIB1-containing plasmids. The reduced WPRE sequence was synthesized by IDT DNA (Singapore) as a gBlock fragment. The generated constructs are listed in Table 3.1.

The sequences for all inserts were confirmed by sequencing analyses performed onsite or in AGRF in Sydney. Confirmed plasmids were purified on a midi- or maxi-scale.

Table 3.1 Generated DNA constructs for neuronal studies.

#	The full name of constructs	Sequence length between ITRs
All DNA constructs for neuronal studies		
1	AAV2-hSyn-CIB1(81)-eGFP-CAAX	2.811 kbp
2	AAV2-hSyn-CIB1(170)-eGFP-CAAX	3.081 kbp
3	AAV2-hSyn-TrkB(kd)-Cry2(535)-T2A-mCherry	4.878 kbp
4	AAV2-hSyn-TrkB(kd)-Y816F-Cry2(535)-T2A-mCherry	4.878 kbp
5	AAV2-hSyn-TrkB(kd)-Cry2(535)-D387A-T2A-mCherry	4.878 kbp
6	AAV2-hSyn-TrkB(kd)-Cry2(498)-T2A-mCherry	4.752 kbp
7	AAV2-hSyn-TrkB(kd)-Y816F-Cry2(498)-T2A-mCherry	4.752 kbp

DNA constructs used for the production of AAV particles		
8	AAV2-hSyn-CIB1(81)-eGFP-CAAX	2.811 kbp
9	AAV2-hSyn-TrkB(kd)-Cry2(535)-T2A-mCherry	4.878 kbp
10	AAV2-hSyn-TrkB(kd)-Cry2(535)-D387A-T2A-mCherry	4.878 kbp

The AAV2 backbone was used. The expression of required proteins was driven by a human synapsin promoter (hSyn). CAAX, C-terminal prenylation signal (GKKKKKKSKTKCVIM); T2A, "self-cleaving" peptide (EGRGSLLTCGDVEENPGP); ITRs, inverted terminal repeats.

3.2.4 AAV production and titration

The recombinant AAV (rAAV2/8) particles expressing the photoactivatable TrkB system were produced based on the protocol provided by Lin (2013). The summary of workflow for AAV preparation and validation is presented in Figure 3.1.

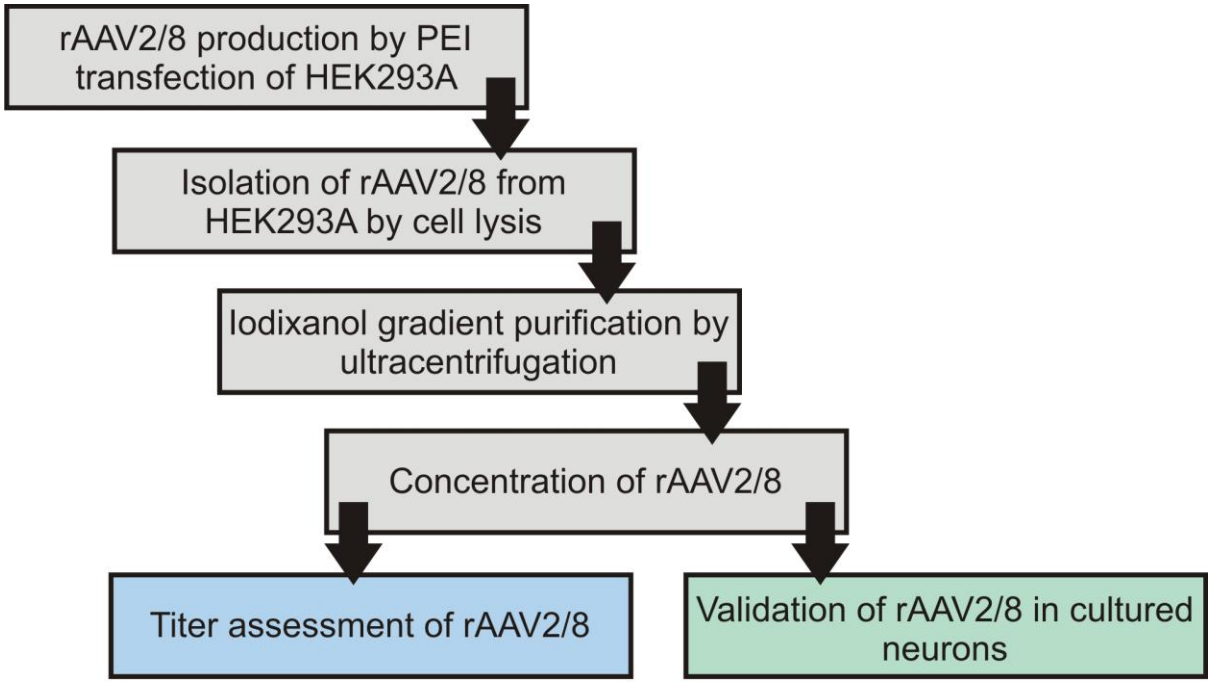

Figure 3.1 The steps of rAAV2/8 production for the expression of the photoactivatable TrkB system. This flow chart also represents the validation methods, which include measurement of AAV genome copies by qPCR and infection of cultured neurons in order to visualize the fluorescent proteins attached to components of the TrkB system. The figure was modified after Lin (2013).

In a first step of AAV production, HEK293A cells were plated in six 15-cm culture dishes per a single virus preparation. When cell reached ~90% confluency, they were transfected using PXR8, pXX6-80 and a desired transfer plasmid at 1:1:1 molar ratio using

the PEI method. PXR8 contains the AAV *rep*/*cap* genes and defines serotype 8. pXX6-80 contains *E2a*, *E4* and *VA* genes. A transfer plasmid contains the transgene of interest and other genetic elements between the AAV2 ITRs. The transfer plasmids were as follows: CIB1(81)-eGFP-CAAX, TrkB(kd)-Cry2(535)-T2A-mCherry or TrkB(kd)-Cry2(535)-D387A-T2A-mCherry as listed in Table 3.1. The transfected cells were harvested at approximately 72 h post-transfection and mechanically scraped off the culture dish in buffer containing: 10 mM Tris (pH 7.6), 150 mM NaCl, 10 mM $MgCl_2$ (0.5 ml per plate). The cells in suspension were lysed by freezing-thawing cycle and trituration through a 23-gauge needle. The cell lysate was then incubated with benzonase nuclease (1 µl per 5 ml of lysate) for 45 – 60 min at 37°C and was centrifuged at 4,000 rpm (Centurion Scientific Rotor BR5510) for 20 min at 4°C to remove cellular and solid debris. The supernatant containing rAAV2/8 particles was decanted into a fresh tube and further purified by using discontinuous iodixanol gradients. The gradient lyers were buffers with 15%, 25%, 40% and 58% iodixanol. The virus-containing supernatant was added on top of the 15% gradient buffer. The tubes with the gradients were then centrifuged at 48,000 rpm in a Beckman Type 70Ti rotor for 130 min at 18°C. After centrifugation, the rAAV2/8 particles were extracted from the 40% – 58% interface. Finally, the viral particles were concentrated by utilizing a 10 kDa or 50 kDa MW cut-off (MWCO) Amicon centrifuge filter (Millipore). The 10 kDa MWCO Amicon allowed rAAV2/8 to be concentrated to a volume of ~500 µl, whereas the 50 kDa MWCO Amicon allowed concentration down to ~200 µl. The purified rAAV2/8 particles were aliquoted and stored at -80°C.

The rAAV2/8 titration was performed by a quantitative polymerase chain reaction (qPCR) with primers targeting ITRs within the AAV2 vector. For this purpose, the AAV titration kit from Takara was used, and quantification of AAV genome copies was carried out (as described by the manufacturer) in the Corbett Rotor-Gene 6000. The titres of the generated rAAV2/8s are listed in Table 3.2.

3.2.5 Primary cortical culture

Cortical neurons were prepared as described by Southam et al. (2018) with some modifications in the protocol. The primary cortical cultures were obtained from cortices of embryonic day 18.5 (E18.5) rats (Sprague-Dawley). The dissected cortices were digested enzymatically in 0.025% (w/v) trypsin in HBSS for 5 min at 37°C. After this time, the solution was removed carefully and the tissue was washed once with 1 ml of Neurobasal

medium supplemented with 10% (v/v) FBS, 2% (v/v) B-27, 2 mM GlutaMAX and 1% (v/v) penicillin-streptomycin solution (neuronal plating medium). The supernatant was aspired and the tissue was triturated in 1 ml of neuronal plating medium. Number of cells was counted. Cortical cells were plated onto 13 mm-coverslips coated with poly-L-lysine in 24-well culture plates at a density of 5×10^4 cells per well containing neuronal plating medium. For western blotting analyses, cortical cells were plated onto 3.5-cm culture dishes coated with poly-L-lysine at a density of 2×10^5 cells per dish with neuronal plating media. After 24 h from plating cells, neuronal plating medium was replaced with the same medium but without FBS. For long-term cultures, neuronal medium lacking serum was refreshed every 3 – 5 days.

3.2.6 Transduction of neuronal cells in culture

The cortical neurons plated onto coverslips in 24-well plates were infected with the generated rAA2/8 particles to check the expression of transgenes. For this purpose, different volumes of viruses were added per one well: 10 µl, 5 µl, 3 µl, 2 µl and 1 µl. Cells were imaged at 48 h to 5 days post-infection. The expression of TrkB(kd)-Cry2(535) and TrkB(kd)-Cry2(535)-D387A was verified by checking mCherry fluorescence, whereas CIB1(81) was checked by eGFP fluorescence under an Olympus BX51WI fluorescent microscope.

The cortical neurons seeded onto 3.5-cm cultured dishes were co-infected with 5 µl rAAV2/8-CIB1(81)-eGFP-CAAX and 5 µl rAAV2/8-TrkB(kd)-Cry2(535)-T2A-mCherry or rAAV2/8-TrkB(kd)-Cry2(535)-D387A-T2A-mCherry when cells were at 9 DIV. For a single infection, 5 µl of each virus was added to neurons. After 6 days, and before harvesting cells for western blotting, the expression of mCherry and eGFP was validated under an Olympus IX73 fluorescence microscope.

3.2.7 Harvesting cells, SDS-PAGE and western blotting

The cortical neurons, transduced with rAAV2/8s, were harvested at 15 DIV for western blotting analyses. The overview of western blotting experiments on the infected neurons is presented in Figure 3.2. The protocol for treating neurons, harvesting them and western blotting is the same as for HEK293A (see section 2.2.7).

Before harvesting, the cortical neurons were exposed to continuous blue light illumination at 36.8 mW/cm^2 for the time duration as indicated in the figure legends in the result section 3.3. The cells were harvested in RIPA buffer 10 min after light termination.

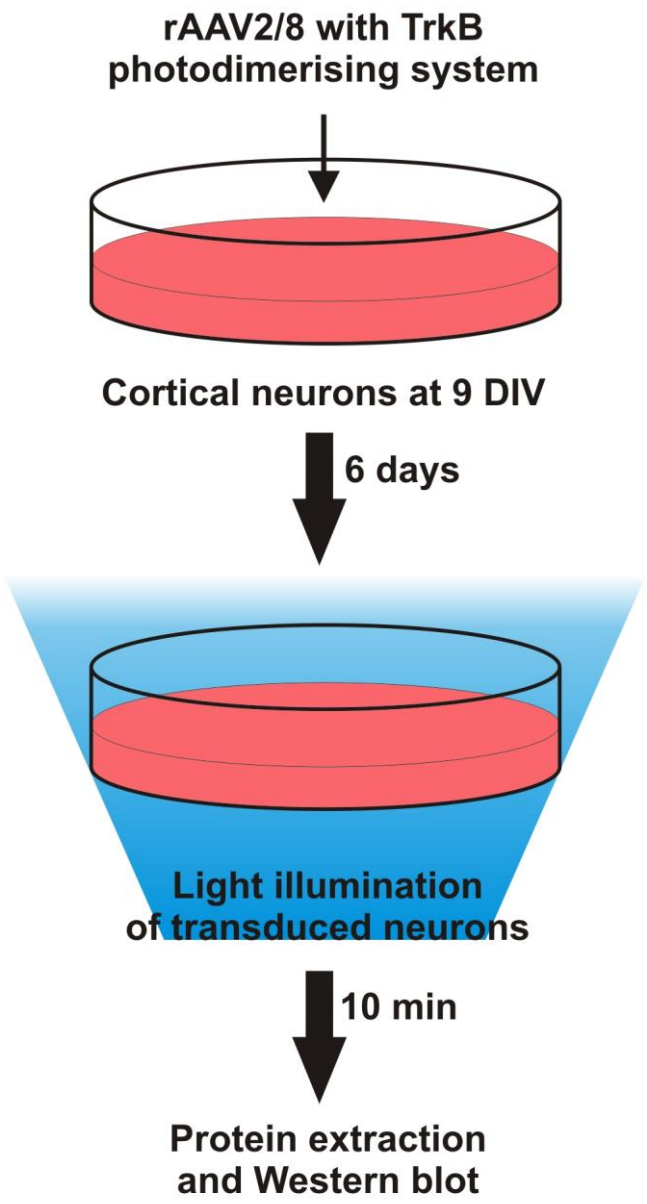

Figure 3.2 Functional expression of rAAV2/8 encoding the photoactivatable TrkB system in cultured cortical neurons. The diagram shows the steps for testing the functional expression of TrkB photodimerizing system in cortical neurons by western blotting. Neurons were infected at 9 DIV with rAAV2/8 carrying the photoactivatable TrkB. After 6 days, these transduced cells were treated with blue light. Subsequently, neurons were lysed and proteins were immunoblotted against phosphorylated ERK, AKT or PLCγ1 proteins, which served as the indicators of activation of canonical TrkB signalling pathways.

Non-infected cells were treated with BDNF (Invitrogen) at final concentration of 100 ng/ml for 10 min. The control non-infected cells were treated with a vehicle (Molecular Biology Grade Water) for 10 min.

After desired treatment, cells were lysed in 200 µl of RIPA buffer and protein concentrations were measured. 10 µg of total protein per lane was used for immunoblotting with anti-ERK/anti-AKT antibodies and 20 µg of total protein per lane was used for anti-PLCγ1 antibodies. Protein samples were resolved on Bolt 4 – 12% Bis-Tris Plus gels (Invitrogen). Proteins were then transferred to a PVDF membrane at 20 V, 4°C for 60 min. For more detailed protocol of immunoblotting see Section 2.2.7. The concentrations of primary and secondary antibodies used for western blotting are listed in Table 2.3 and their ordering details in Table A1 (see Appendix).

Densitometry analyses of chemiluminescence were performed using ImageJ. Statistical analyses were performed in OriginPro 8.

3.2.8 Stereotactic AAV injection into a basolateral amygdala

The stereotactic surgery to deliver virus, and immunohistochemistry to confirm the viral infection, were performed by Dr Zayra Millan from the School of Psychology at the University of New South Wales (UNSW). The procedures were approved by the UNSW Animal Care and Ethics Committee.

Naïve male Long-Evans rats received a unilateral injection into the basolateral amygdala (BLA) using the following coordinates from bregma: anteroposterior = -2.85 mm, mediolateral = -4.85 mm and from a flat-skull position: dorsoventral = -8.85 mm. The mix of both viruses (0.3 µl of each virus): rAAV2/8-hSyn-TrkB(kd)-Cry2(535)-T2A-mCherry (7.25×10^{10} copies/ml) and rAAV2/8-hSyn-CIB1(81)-eGFP-CAAX (3.07×10^{11} copies/ml) was infused at a rate of 0.1 µl/min via a 31-gauge needle. After surgery, rats were allowed to recover for 4 weeks. After this time, rats were perfused with paraformaldehyde and brains were fixed and sectioned to conduct immunofluorescence histochemistry for mCherry and eGFP detection in BLA.

3.2.9 Analyses of growth cone motility upon light illumination

The measurement of growth cone motility upon light illumination was performed by Dr Macarena Pavez from the School of Medicine at the University of Tasmania. In this

experiment, thoracic dorsal root ganglion neurons (DRG) were used as a common model for assessing axon pathfinding (Gasperini et al., 2009; Mitchell et al., 2012). The cells were prepared from rat (E16 – E18) embryos (Sprague-Dawley) based on the protocol described previously by Gasperini et al. (2009). The isolated DRG neurons were supplemented with NGF so their survival was mediated by TrkA. Dissociated DRG neurons were electroporated with the following DNA constructs: pcDNA3-CMV-TrkB(kd)-Cry2(535)-T2A-CIB1(81)-eGFP-CAAX, pcDNA3-CMV-TrkB(kd)-Cry2(535)-D387A-T2A-CIB1(81)-eGFP-CAAX, pcDNA3-CMV-TrkB(kd)-Cry2(535)-T2A-eGFP (see Table 2.4), the included CMV promoter can mediate stronger expression one day after transfection than the hSyn promoter (Kugler et al., 2003b). This was crucial as the growth cone turning experiments were conducted after overnight incubation. The electroporation was conducted according to the instructions provided with the Nucleofector Kit (Lonza, Switzerland). The transfected cells were plated onto laminin-coated coverslips and imaged using an oil-immersion objective (100×/NA0.95) and NIS-Elements AR 4.00.12 software (Nikon, Japan). Growth cones extending from the DRG neurons transfected with the TrkB system were stimulated with blue light (485 nm) using a digital mirror device (Mightex, USA), which restricted the illuminatation area to one side of the growth cone. The growth cones expressing TrkB(kd)-Cry2(535)-T2A-CIB1(81)-eGFP-CAAX were stimulated with two light protocols: 2-s pulse delivered every 5 min or 10-s pulse every 2 min. The growth cone turning experiment was conducted for 15 min. The angle of turning was measured between the initial and the final trajectories of the distal 10 µm of axon, as described previously (Gasperini et al., 2009). A positive angle represented turning towards illuminated side of the growth cone (attraction), whereas a negative angle represented turning away from the illuminated side (repulsion). The growth cone turning was analyzed using ImageJ and statistical analyses were performed in GraphPad Prism 6 (GraphPad Software Inc., USA).

3.3 Results

3.3.1 Design of rAAV vectors for neuronal expression of the photoactivatable TrkB system

Adeno-associated viral vectors have been described as efficient tools for gene delivery *in vitro* and *in vivo* into neuronal cells (Choi et al., 2014; Royo et al., 2008). To conduct further experiments in cultured neurons and, ultimately, in behaving animal models, the

photoactivatable TrkB system was inserted into an AAV2 transfer plasmid. For the expression of transgene in neurons, the total genomic material between the ITRs of the AAV vector cannot exceed 5.2 kbp including the necessary expression elements (e.g., promoter, transgene and poly(A) signal). For the promoter elements, the hSyn promoter was used, as it has small size (~0.4 kbp), is neuron specific and can maintain stable expression over time (Kugler et al., 2003a) compared to α-CaMKII promoter (specific for subset of neurons, 1.3 kbp in size), EF-1α promoter (not neuron specific, 1.2 kbp), CAG promoter (not neuron specific, 1.6 kbp) and CMV promoter (not neuron specific, 0.4 kbp).

The CIB1(81)-eGFP-CAAX or CIB1(170)-eGFP-CAAX components were inserted into the expression vector consisting of a non-modified WPRE and poly(A) (0.8 kbp in total). All AAV vectors encoding TrkB(kd)-Cry2 components possessed the truncated WPRE and poly(A) (0.4 kbp in total) (Choi et al., 2014) that permitted the larger TrkB(kd)-Cry2 to be packaged. The AAV vector designs with the necessary sequences are presented in Figure 3.3.

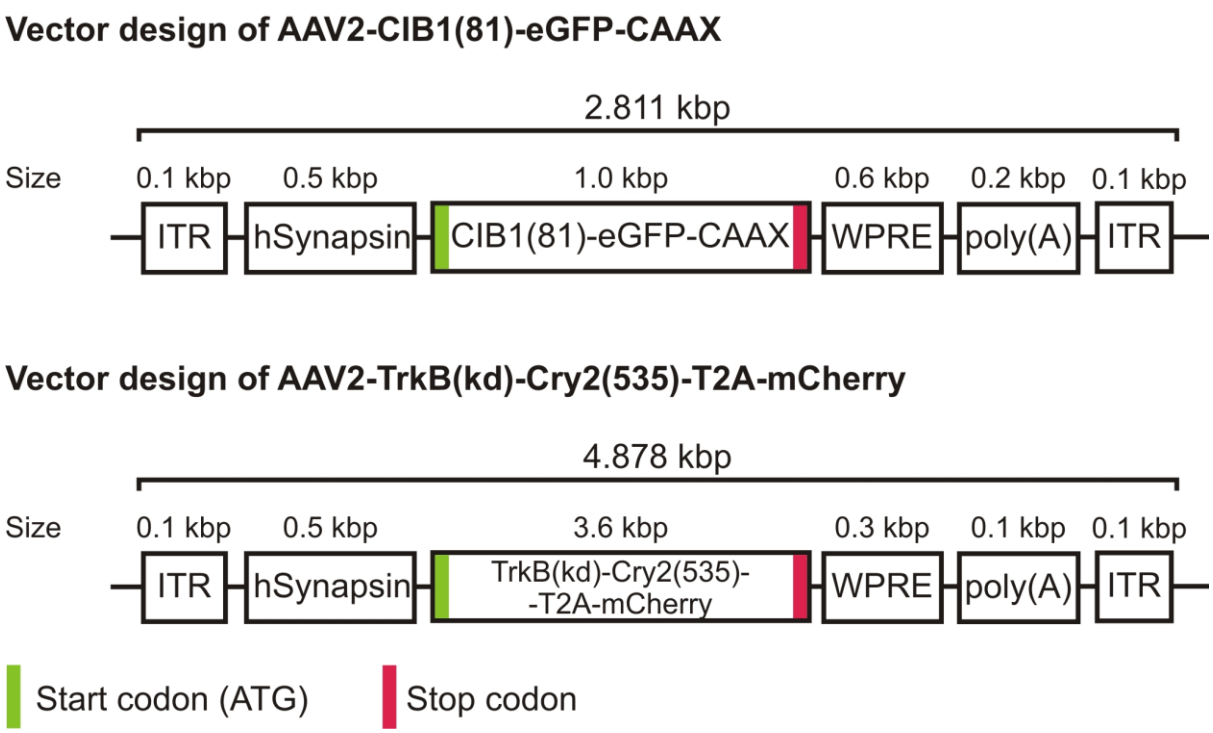

Figure 3.3 AAV viral vector designs for expressing the photoactivatable TrkB system in neurons. Each component of the photoactivatable TrkB system was generated as a separate AAV viral vector. The transgene, encoding CIB1(81)-eGFP-CAAX, was inserted between two ITRs in AAV2 which also contains: a human synapsin promoter, WPRE and poly(A). All these additional elements in AAV2-CIB1(81)-eGFP-CAAX vector derived from AAV2-oChIEF-tdTomato plasmid (Addgene #50977) (Lin et al., 2009). The transgene, encoding TrkB(kd)-Cry2(535)-T2A-mCherry, was also inserted into the backbone of AAV2-oChIEF-tdTomato vector but WPRE and poly(A)

cassettes were truncated to increase AAV packaging limit. Thanks to this truncation, the additional 0.4 kbp could be packaged. The shorter WPRE and poly(A) elements were synthesized as described by Choi et al. (2014) (based on pAAV-CW3SL-EGFP vector with KJ411916 accession number at GeneBank).

3.3.2 Expression of the light-activated TrkB system in cortical culture

Recombinant AAV particles (referred to as rAAV2/8 from here in) were generated using CIB1(81)-eGFP-CAAX, TrkB(kd)-Cry2(535)-T2A-mCherry and TrkB(kd)-Cry2(535)-D387A-T2A-mCherry as the expression cassettes (see Table 3.1 for the transfer plasmids) and capsid proteins from AAV serotype 8. The produced rAAV2/8s are compiled in Table 3.2. According to this table, the viruses made in batches no. 1 and 3 had lower concentrations than the corresponding viruses in batches no. 2 and 4. It is due to the concentration of the virus in the final step of purification. The viruses in batches no. 1, 3 and 5 were concentrated using 10 kDa MWCO Amicon filter, whereas the batches no. 2 and 4 were concentrated using 50 kDa MWCO filter, which enabled to achieve more concentrated samples.

Table 3.2 Generated rAAV2/8 particles encoding the photoactivatable TrkB system for *in vitro* neuronal studies and *in vivo* application.

Batch #	rAAV2/8 particles	Titer [copies/ml]
1	rAAV2/8-hSyn-CIB1(81)-eGFP-CAAX	3.07×10^{11}
2	rAAV2/8-hSyn-CIB1(81)-eGFP-CAAX	2.16×10^{12}
3	rAAV2/8-hSyn-TrkB(kd)-Cry2(535)-T2A-mCherry	7.25×10^{10}
4	rAAV2/8-hSyn-TrkB(kd)-Cry2(535)-T2A-mCherry	1.06×10^{12}
5	rAAV2/8-hSyn-TrkB(kd)-Cry2(535)-D387A-T2A-mCherry	8.63×10^{11}

The produced rAAV2/8 particles were validated in cultured primary cortical neurons. Each batch of virus was checked under a fluorescence microscope for expression of eGFP and mCherry proteins. All viruses successfully infected neurons in culture, as shown in Figure 3.4. The hSyn promoter was predicted to restrict expression of transgenes to neuronal cells, although the exclusive expression in neurons was not examined in detail.

rAAV2/8-hSyn-CIB1(81)-eGFP-CAAX

A

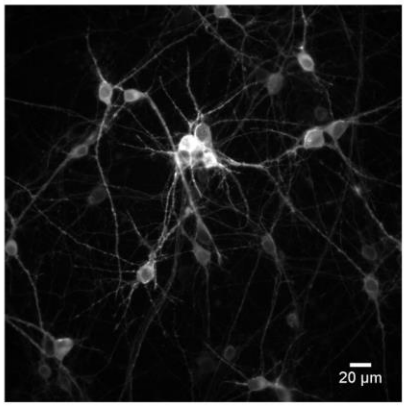

B

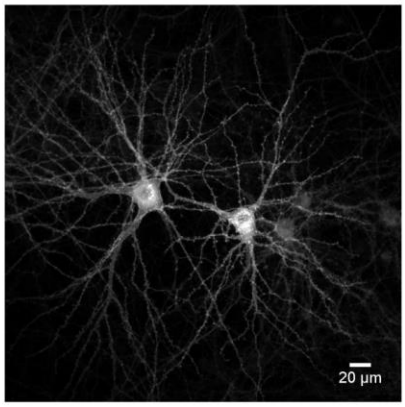

rAAV2/8-hSyn-TrkB(kd)-Cry2(535)-T2A-mCherry

C

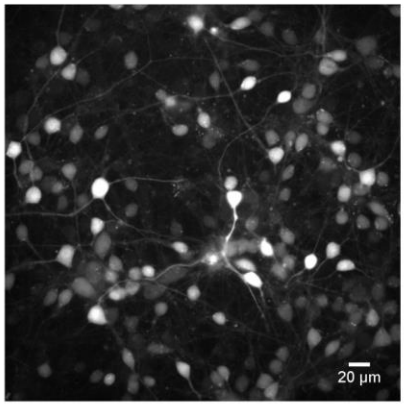

D

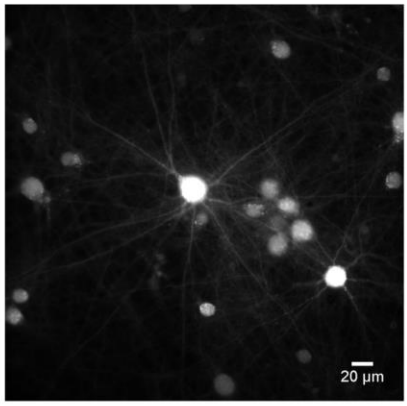

rAAV2/8-hSyn-TrkB(kd)-Cry2(535)-D387A-T2A-mCherry

E

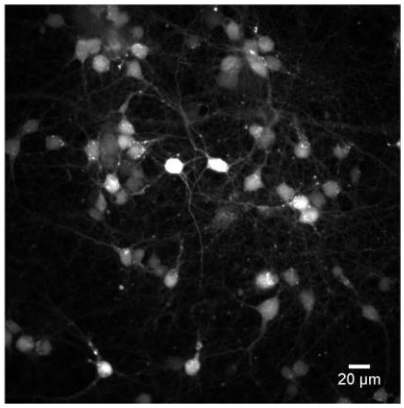

Figure 3.4 Validation of rAAV2/8 encoding the photoactivatable TrkB system in cultured cortical neurons. The figures **(A)** and **(B)** show cortical primary neurons infected with rAAV2/8-hSyn-CIB1(81)-eGFP-CAAX created in two separate batches. eGFP expression was validated and its expression was expected in the cell membrane. The figures **(C)** and **(D)** represent cortical neurons infected with two different batches of rAAV2/8-hSyn-TrkB(kd)-Cry2(535)-T2A-mCherry, whereas the figure **(E)** demonstrates neurons transduced with rAAV2/8-hSyn-TrkB(kd)-Cry2(535)-D387A-T2A-mCherry. Both rAAV2/8-hSyn-TrkB(kd)-Cry2(535)-T2A-mCherry and rAAV2/8-hSyn-TrkB(kd)-Cry2(535)-D387A-T2A-mCherry were validated based on mCherry fluorescence in cytosol. Cells were between 8 and 15 DIV and 48 h to 5 days post-infection.

3.3.3 The TrkB photodimerizing system activates canonical signalling pathways in cortical primary neurons upon blue light stimulation

As described in Chapter 2, the phosphorylation of ERK, AKT or PLCγ1 proteins can indicate the activation state of these proteins. To examine whether the photoactivatable TrkB system can activate the canonical signalling pathways in neurons upon light stimulation, the immunoblot analyses of endogenous ERK, AKT and PLCγ1 were performed. For this purpose, cortical neurons were infected with rAAV2/8 encoding TrkB(kd)-Cry2(535) or CIB1(81)-eGFP-CAAX, as presented in Section 3.2.6. Subsequently, a 30-s blue light stimulation was applied and cell lysates were blotted against suitable antibodies (see Section 3.2.7). The activity of ERK, AKT and PLCγ1 was quatified using densitometric analysis as a ratio between the optical density for a phosphorylated protein and for a total protein.

Firstly, the activation of ERK pathway was investigated. Upon exposure of a cortical cell population, co-infected with rAAV2/8s for both components (TrkB(kd)-Cry2(535) and CIB1(81)-eGFP-CAAX), to a 30-s blue light illumination, the level of phosphorylated ERK1/2 at T202/Y204 was increased 3.9 ± 0.7 times compared to the dark control (Fig. 3.5 A and B). Consistently with the results obtained from HEK293A cells (see Section 2.3.2.4), cortical cells expressing only a single component, TrkB(kd)-Cry2(535), exhibited light-mediated phosphorylation of ERK (4.4 ± 0.9 fold increase over the dark condition). The CIB1(81)-eGFP-CAAX component did not cause the elevation of ERK phosphorylation after light exposure. Non-infected neurons served as a control. These cells were treated with BDNF, which gave rise to the elevated phospho-ERK. The non-infected neurons exposed to the blue light stimulation did not display increased phosphorylation of ERK. Moreover, the viral infection did not lead to a significant increase in background ERK activity and did not cause changes in the expression level of total ERK (Fig. 3.5 B and C).

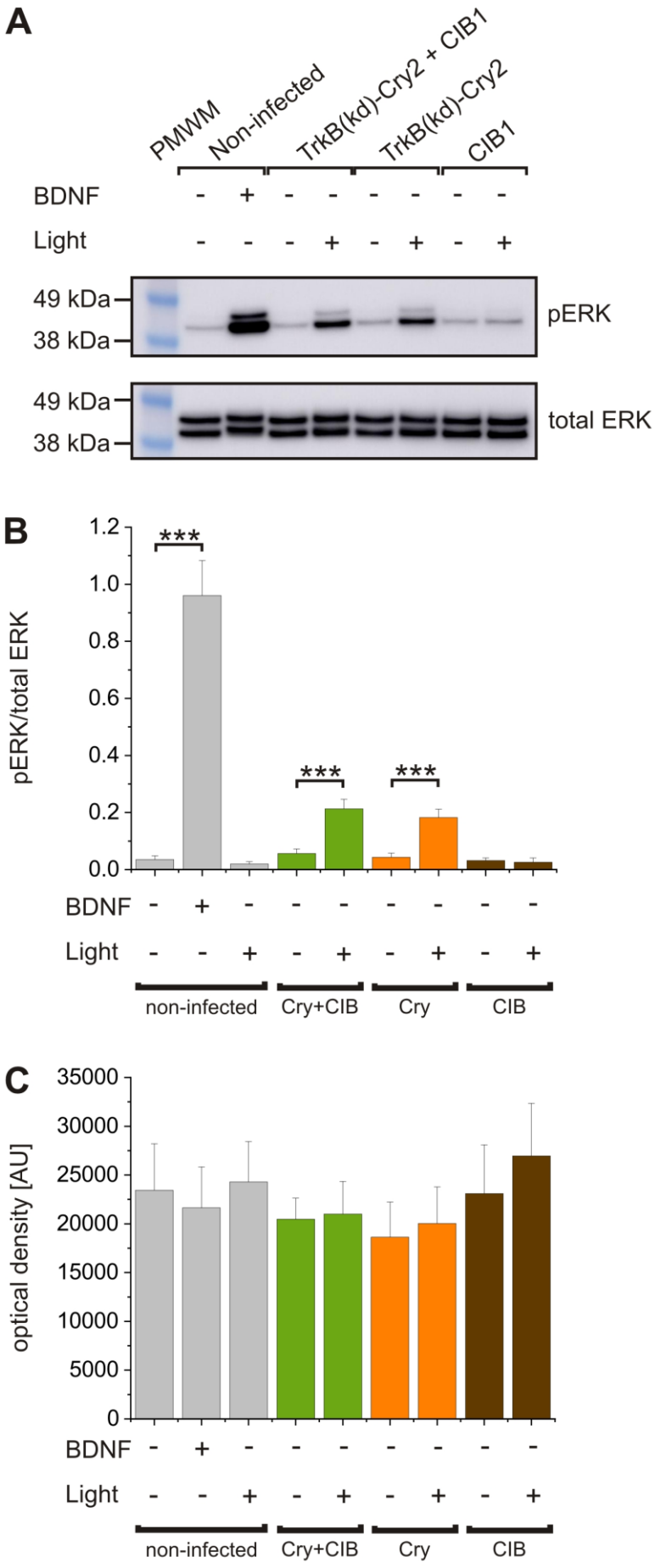
A
PMWM
Non-infected
TrkB(kd)-Cry2 + CIB1
TrkB(kd)-Cry2
CIB1
BDNF
Light
49 kDa
38 kDa
pERK
total ERK
B
pERK/total ERK
***
non-infected
Cry+CIB
Cry
CIB
C
optical density [AU]

Figure 3.5 Immunoblot analysis of endogenous ERK activity in primary cortical neurons expressing the photoactivatable TrkB system. (A) Representative immunoblot images show the level of level of phosphorylated protein (pERK) at Thr202/Tyr204 in the absence or presence of 30-s blue light illumination. The phosphorylation of ERK was examined 10 min after light exposure. To measure changes in total ERK, the antibody recognizing an epitope present in ERK1 and ERK2 independent of phosphorylation was used. Cortical neurons co-expressing both components: TrkB(kd)-Cry2(535)-T2A-mCherry and CIB1(81)-eGFP-CAAX (TrkB(kd)-Cry2 + CIB1) showed increased phosphorylation of ERK upon blue light illumination in comparison with non-stimulated cells. A single component: TrkB(kd)-Cry2(535)-T2A-mCherry (here as: TrkB(kd)-Cry2) also caused the elevation of phospho-ERK upon light irradiation. The CIB1(81)-eGFP-CAAX component (here as: CIB1) did not trigger phosphorylation of ERK in the light state. As a control, non-infected cortical neurons treated with 100 ng/ml of BDNF were compared to the level of phospho-ERK in non-treated neurons. PMWM stands for protein molecular weight marker. **(B)** The summary bar graph quantifies ERK activation as a ratio between phosphorylated ERK and total ERK in all tested conditions (see Sections 3.2.7 and 3.3.3). "Cry+CIB" means that neurons were co-infected with both components: TrkB(kd)-Cry2(535)-T2A-mCherry and CIB1(81)-eGFP-CAAX; "Cry" represents neurons infected with TrkB(kd)-Cry2(535)-T2A-mCherry component only, whereas "CIB" – neurons infected with CIB1(81)-eGFP-CAAX only. Data are shown as mean ± SD from four independent cell cultures. ***P<0.001, unpaired Student's t-test. **(C)** The bar graph represents the level of total ERK within each group presented in **(B)**. Results show no significant differences in total ERK levels between groups. Data are shown as mean ± SD from four independent cell cultures.

The same experimental conditions were applied to assess the phosphorylation state of AKT at Ser473 in cortical cells upon light. Although in cortical neurons co-expressing TrkB(kd)-Cry2(535) and CIB1(81)-eGFP-CAAX the difference in the phospho-AKT was approximately 1.4-fold between light and dark conditions, it was not significant (Fig. 3.6 A and B; P = 0.060, unpaired Student's t-test). When neurons were infected with rAAV2/8 encoding TrkB(kd)-Cry2(535), the phosphorylation of AKT was not elevated significantly upon light illumination (P = 0.065, unpaired Student's t-test). Similarly, the CIB1(81)-eGFP-CAAX component did not cause an increase in AKT phosphorylation in the light state. As expected, the BDNF treatment of cortical cells led to approximately 3-fold increase over non-treated control (Fig. 3.6 B). The overexpression of the photoactivatable TrkB did not elevate the background activity of AKT. Some changes in total AKT were observed across the different treatments (Fig. 3.6 C), but this was not investigated further.

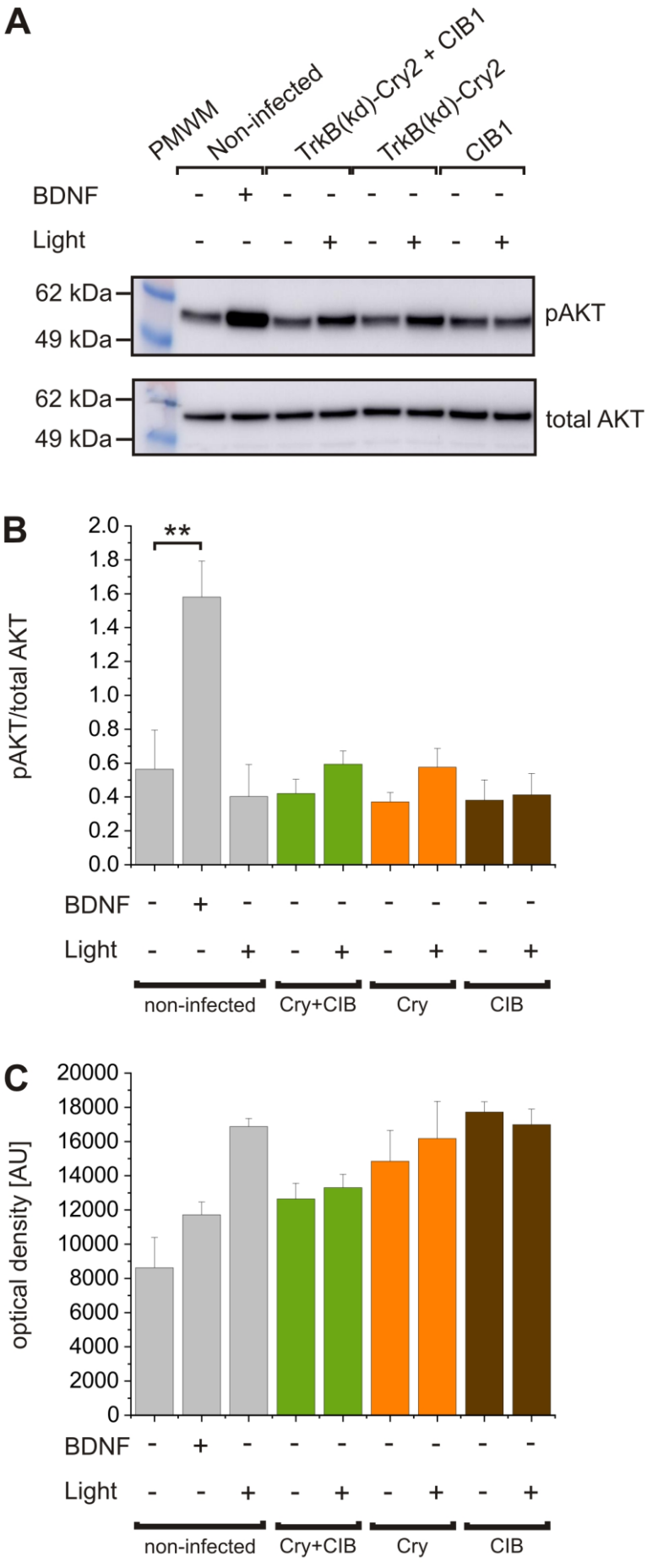
A
PMWM
Non-infected
TrkB(kd)-Cry2 + CIB1
TrkB(kd)-Cry2
CIB1
BDNF
Light
62 kDa
49 kDa
pAKT
62 kDa
49 kDa
total AKT
B
pAKT/total AKT
**
BDNF
Light
non-infected
Cry+CIB
Cry
CIB
C
optical density [AU]
BDNF
Light
non-infected
Cry+CIB
Cry
CIB

Figure 3.6 Immunoblot analysis of endogenous AKT activity in primary cortical neurons expressing the photoactivatable TrkB system. (A) Representative immunoblot images show a level of phosphorylated AKT at Ser473 in the absence or presence of 30-s blue light illumination. The phosphorylation of AKT was examined 10 min after light exposure. The antibody that recognizes AKT independently of phosphorylation state was used to check any changes in total amount of AKT. Abbreviation: PMWM - protein molecular weight marker. **(B)** The bar graph quantifies AKT activation as a ratio between phosphorylated AKT and total AKT in all tested conditions (see Sections 3.2.7 and 3.3.3). Cortical neurons expressing both components, TrkB(kd)-Cry2(535)-T2A-mCherry and CIB1(81)-eGFP-CAAX (TrkB(kd)-Cry2 + CIB1), did not exhibit a significant increase in AKT phosphorylation upon blue light illumination in comparison with non-stimulated cells ($P = 0.060$, unpaired Student's t-test). A single TrkB(kd)-Cry2(535)-T2A-mCherry (here as: TrkB(kd)-Cry2) or CIB1(81)-eGFP-CAAX component (here as: CIB1), when used separately, did not cause a significant elevation in the phosphorylation of AKT in the light state ($P = 0.065$ and $P = 0.77$, respectively; unpaired Student's t-test). As a control, non-infected cortical neurons treated with 100 ng/ml of BDNF were compared to the level of phospho-AKT in unstimulated neurons. The BDNF treatment led to the significant increase in AKT phosphorylation (**$P<0.01$, unpaired Student's t-test). Data are shown as mean ± SD from three independent experiments. **(C)** The bar graph represents levels of total AKT within each group presented in **(B)**. Data are shown as mean ± SD from three independent experiments.

Finally, the phosphorylation level of PLCγ1 at Tyr783 was investigated in neurons expressing both TrkB(kd)-Cry2(535) and CIB1(81)-eGFP-CAAX. When these cells were stimulated with a single 30-s pulse of blue light, the phospho-PLCγ1 increased 5.8 ± 2 times compared to the dark state (Fig. 3.7 A and B). Similarly, the TrkB(kd)-Cry2(535) component alone led to the PLCγ1 phosphorylation upon light illumination (approximately 6.5-fold increase). The CIB1(81)-eGFP-CAAX alone did not cause the elevation in phospho-PLCγ1. The control BDNF treatment of non-infected neurons evoked PLCγ1 phosphorylation (Fig. 3.7 A and B). The viral transduction did not change the baseline phosphorylation or the total level of PLCγ1 (Fig. 3.7 B and C).

In summary, the photoactivatable TrkB system activated ERK and PLCγ1 pathways in neurons upon blue light exposure, as judged by ERK/PLCγ1 phosphorylation. However, changes in AKT phosphorylation were not significant.

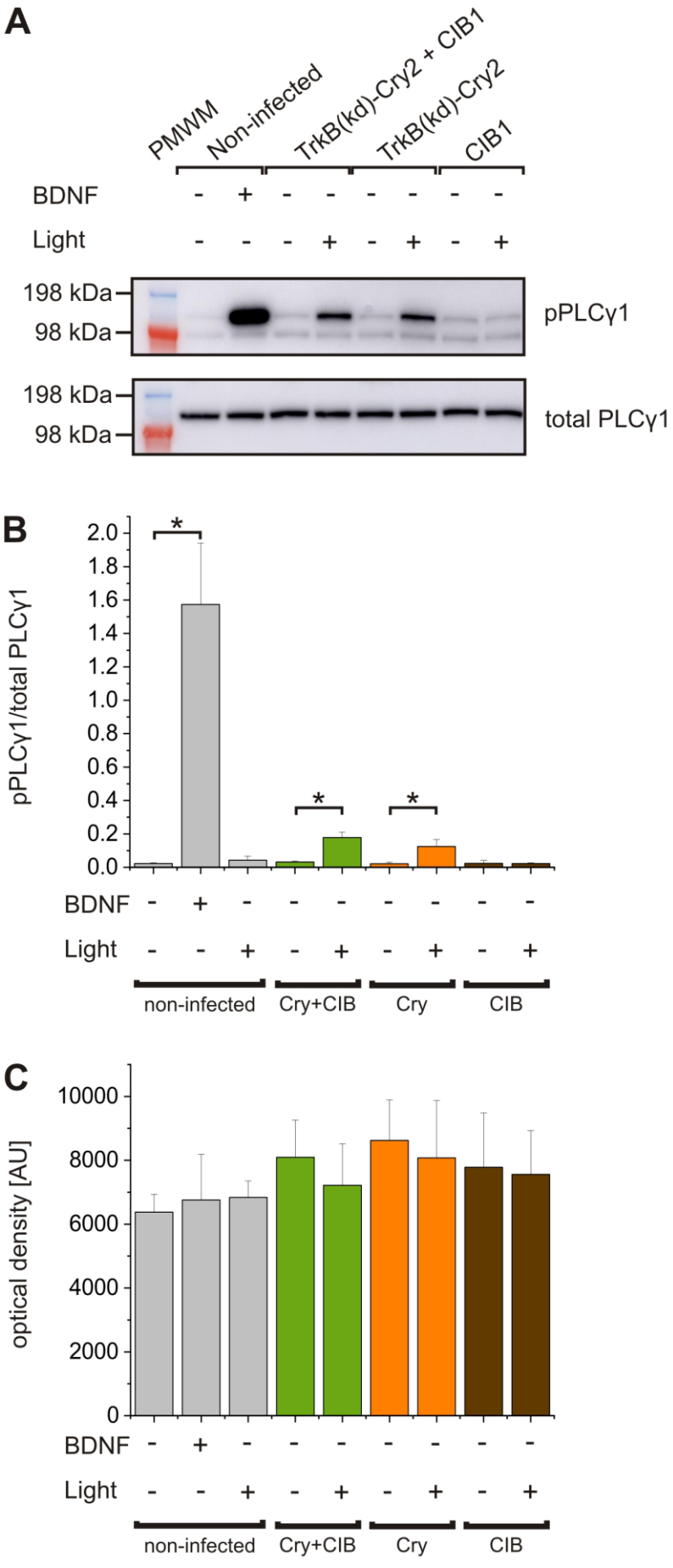
A
PMWM
Non-infected
TrkB(kd)-Cry2 + CIB1
TrkB(kd)-Cry2
CIB1
BDNF
Light
198 kDa
98 kDa
pPLCγ1
198 kDa
98 kDa
total PLCγ1
B
pPLCγ1/total PLCγ1
2.0
1.8
1.6
1.4
1.2
1.0
0.8
0.6
0.4
0.2
0.0
*
*
*
BDNF
Light
non-infected
Cry+CIB
Cry
CIB
C
optical density [AU]
10000
8000
6000
4000
2000
0
BDNF
Light
non-infected
Cry+CIB
Cry
CIB

Figure 3.7 Immunoblot analysis of endogenous PLCγ1 activity in primary cortical neurons expressing the photoactivatable TrkB system. (A) Representative immunoblot images show the level of phosphorylated PLCγ1 at Tyr783 in the absence or presence of 30-s blue light illumination. The phosphorylation of PLCγ1 was investigated 10 min after light exposure. The endogenous level of total PLCγ1 was also checked. Abbreviation: PMWM - protein molecular weight marker. **(B)** The bar graph quantifies PLCγ1 activation as a ratio between phosphorylated PLCγ1 and total PLCγ1 in all tested conditions (see Sections 3.2.7 and 3.3.3). Cortical neurons expressing both components, TrkB(kd)-Cry2(535)-T2A-mCherry and CIB1(81)-eGFP-CAAX (TrkB(kd)-Cry2 + CIB1), displayed a significant increase in PLCγ1 phosphorylation upon blue light illumination in comparison with non-stimulated cells. Light irradiation of cells expressing the single TrkB(kd)-Cry2(535)-T2A-mCherry component (here as: TrkB(kd)-Cry2) caused the significant elevation of phosphorylated PLCγ1 ($P = 0.047$, unpaired Student's t-test). Exposing cells infected with CIB1(81)-eGFP-CAAX component (here as: CIB1) to light illumination did not cause the increase in the phosphorylation of PLCγ1. As a positive control, the level of phospho-PLCγ1 in non-infected cortical neurons treated with 100 ng/ml of BDNF was compared to the level of phospho-PLCγ1 in unstimulated neurons. The BDNF treatment led to the significant increase in PLCγ1 phosphorylation. Data are shown as mean ± SD from three independent experiments. *$P<0.05$, unpaired Student's t-test. **(C)** The bar graph demonstrates levels of total PLCγ1 in each group presented in **(B)**. The results indicated no significant differences between total PLCγ1 between groups. Data are shown as mean ± SD from three independent experiments.

To investigate whether the phosphorylation of ERK and PLCγ1 upon light is mediated through a light-inducible interaction between Cry2-Cry2 and Cry2-CIB1, a rAAV2/8 with a light-insensitive Cry2 (Cry2_D387A) linked to TrkB(kd) was produced. Subsequently, this virus was tested in cortical neurons exposed to a single 30-s blue light pulse. The cortical cells expressing TrkB(kd)-Cry2_D387A alone or with CIB1(81)-eGFP-CAAX component did not exhibit the elevated phosphorylation of ERK (Fig. 3.8) and PLCγ1 (Fig. 3.9) after photostimulation, confirming that the activation of signalling pathways was triggered in response to light.

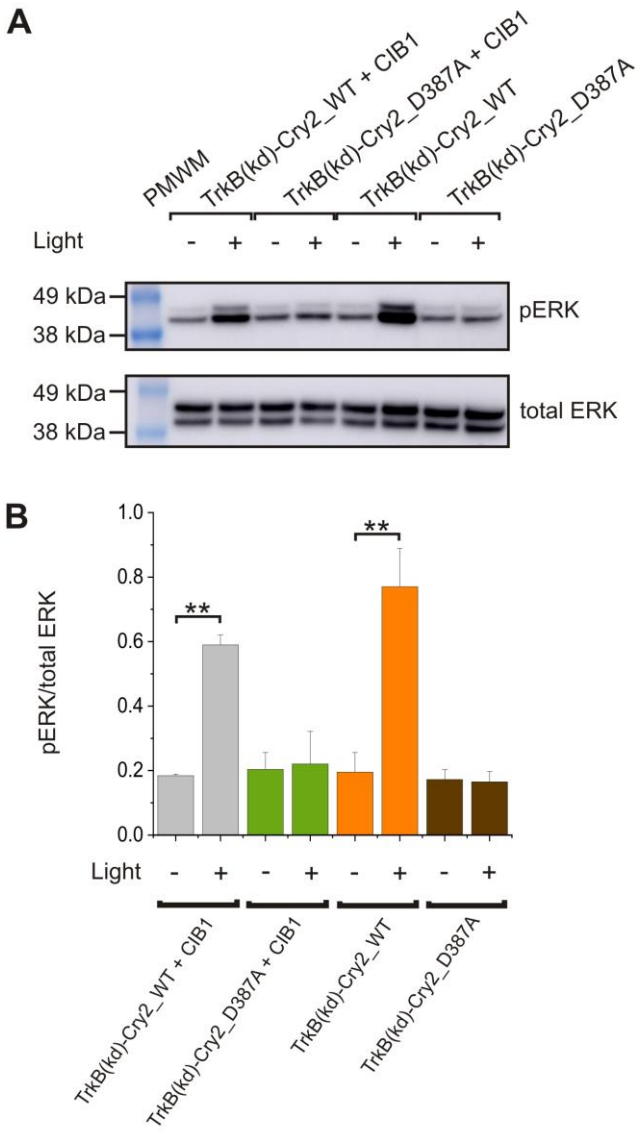

Figure 3.8 The light-insensitive Cry2 mutant (Cry2_D387A) in TrkB system failed to activate ERK signalling pathway upon light illumination in cortical neurons. (A) Representative immunoblot images show ERK phosphorylation in cortical neurons infected with the TrkB system with a wild-type Cry2(535) (TrkB(kd)-Cry2_WT) or with a light-insensitive mutant of Cry2(535) (TrkB(kd)-Cry2_D387A) in the absence or presence of 30-s blue light illumination. Cells were harvested 10 min after light exposure. The TrkB tool was tested as a two-component system (with CIB1(81)-eGFP-CAAX) or as a single-component system. To investigate changes in total ERK, an antibody that recognizes ERK1 and ERK2 independently of phosphorylation state was applied. PMWM stands for protein molecular weight marker. **(B)** The summary bar graph demonstrates the quantification of ERK activation as a ratio between phosphorylated ERK and total ERK in dark/light conditions (see Sections 3.2.7 and 3.3.3). Cortical neurons expressing both components, TrkB(kd)-Cry2(535)_WT and CIB1(81)-eGFP-CAAX (TrkB(kd)-Cry2_WT + CIB1), showed increased phosphorylation of ERK upon blue light illumination in comparison with non-stimulated cells. The single component: TrkB(kd)-Cry2(535)_WT also caused the elevation of phospho-ERK in light state. Neither two components, TrkB(kd)-Cry2_D387A + CIB1, nor TrkB(kd)-Cry2_D387A alone triggered phosphorylation of ERK upon light. Data are shown as mean ± SD from three independent experiments. **P<0.01, unpaired Student's t-test.

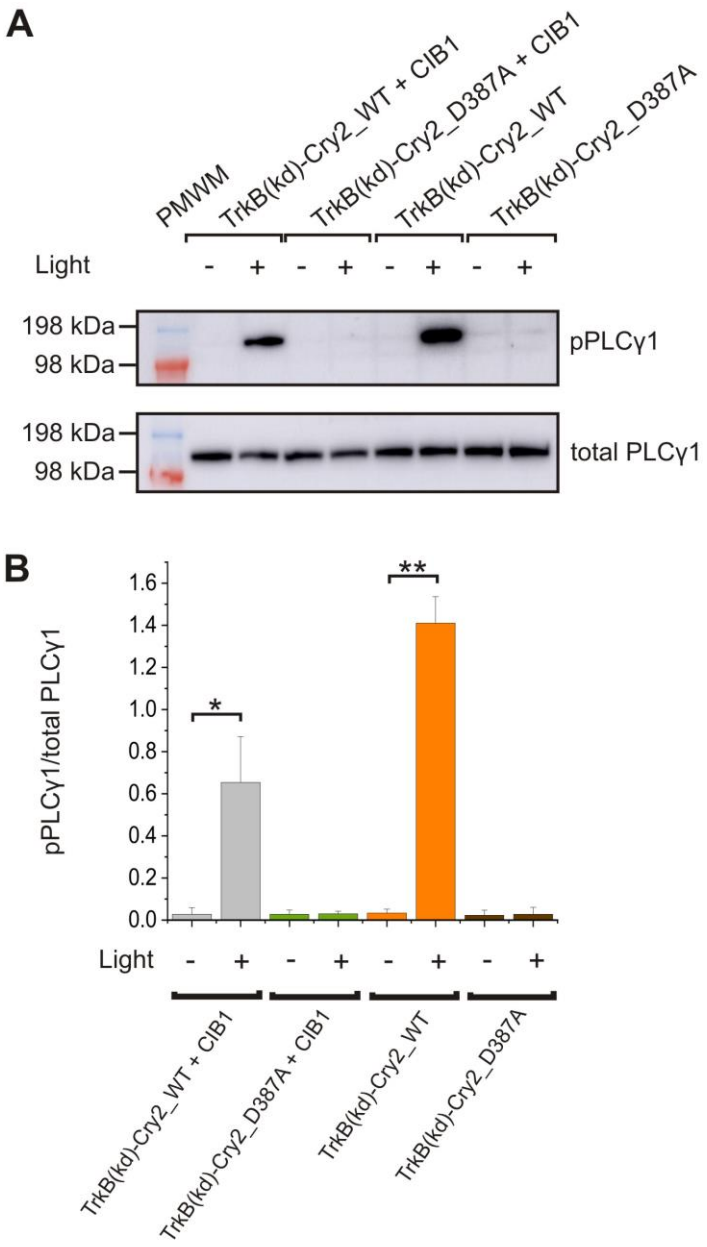

Figure 3.9 The light-insensitive Cry2 mutant (Cry2_D387A) in TrkB system failed to activate PLCγ1 upon light illumination in cortical neurons. (A) Representative immunoblot images show PLCγ1 phosphorylation in cortical neurons infected with the TrkB system with a wild-type Cry2(535) (TrkB(kd)-Cry2_WT) or with a light-insensitive mutant of Cry2(535) (TrkB(kd)-Cry2_D387A) in the absence or presence of 30-s blue light illumination. Cells were harvested 10 min after light exposure. PMWM - protein molecular weight marker. **(B)** The summary bar graph shows the quantification of PLCγ1 phosphorylation (see Sections 3.2.7 and 3.3.3). Cortical neurons expressing both components, TrkB(kd)-Cry2(535)_WT and CIB1(81)-eGFP-CAAX (TrkB(kd)-Cry2_WT + CIB1), showed elevated phosphorylation of PLCγ1 upon blue light illumination in comparison with non-exposed cells. The single component, TrkB(kd)-Cry2(535)_WT, also caused the increase of phospho-PLCγ1 in light state. Both the two-component system with D387A mutant and the one-component system with the same mutation did not trigger phosphorylation of PLCγ1 upon light. Data are shown as mean ± SD from three independent experiments. *P<0.05, **P<0.01, unpaired Student's t-test.

3.3.4 Effect of different blue light durations on the activation of ERK and PLCγ1 pathways

The light-mediated activation of ERK and PLCγ1 pathways was investigated in further experiments in which cortical neurons, transduced with rAAV2/8s encoding the TrkB system, were exposed to increasing durations of blue light. The intensity of stimulating LED light (36.8 mW/cm^2) remained unchanged, whereas a 1-s, 10-s and 30-s single light pulse was applied. Delivering these light pulses to cells gave rise to the increasing level of phospho-ERK (Fig. 3.10) and phospho-PLCγ1 (Fig. 3.11). This demonstrated that the activation of ERK and PLCγ1 pathways is dependent on light and can be modulated by different length of light stimulation. As presented in Figure 3.10 and Figure 3.11, the single 30-s pulse caused the robust phosphorylation of ERK and PLCγ1.

An inconsistency can be observed in Figure 3.11 B in which PLCγ1 was not significantly phosphorylated upon 30-s light illumination in neurons expressing both components of the TrkB system (TrkB(kd)-Cry2(535)-T2A-mCherry and CIB1(81)-eGFP-CAAX), compared to the results in Figure 3.7 and 3.9. In each replicate of the experiment shown in Figure 3.11, the increasing duration of light caused the increasing level of phospho-PLCγ1 in these neurons. However, when the data were pooled from these three independent experiments, no significant result was obtained for the stimulation of cells for 30 s ($P = 0.60$, using one-way ANOVA with Tukey's multiple comparison test). This is inconsistent with the results presented in Figure 3.7 B and Figure 3.9 B in which 30-s light illumination caused the significant increase in the phosphorylated PLCγ1 in neurons expressing both components of the photoactivatable TrkB. The lack of significance in Figure 3.11 might be due to a high variability of the assay in three experiments.

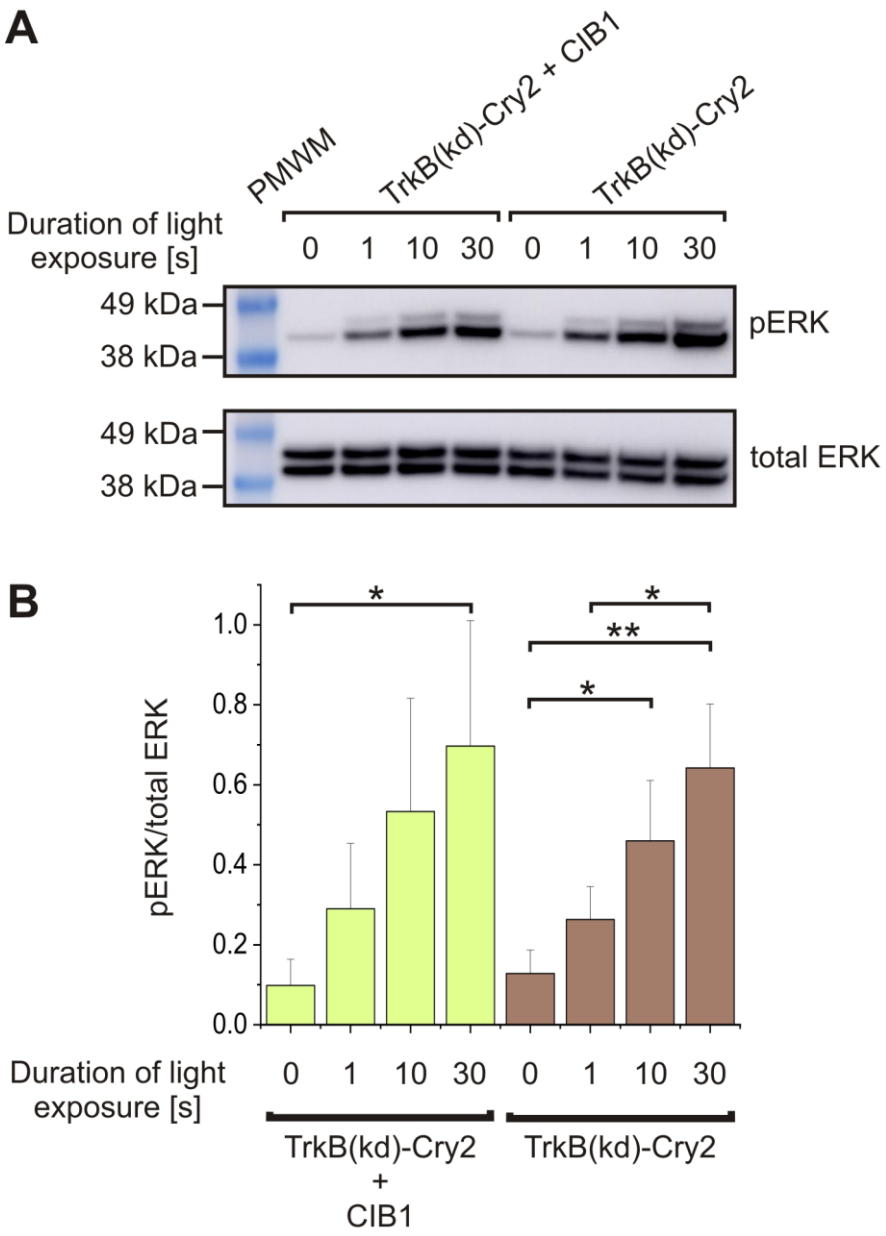

Figure 3.10 Effect of blue light duration on the activation of ERK pathway. Cortical neurons infected with two components, TrkB(kd)-Cry2(535)-T2A-mCherry and CIB1(81)-eGFP-CAAX, or with TrkB(kd)-Cry2(535)-T2A-mCherry alone, were exposed to different durations of blue light stimulation (0 s, 1 s, 10 s, 30 s). The blue light intensity remained the same for each group and was 36.8 mW/cm^2. The phosphorylation of ERK was examined 10 min after light exposure. **(A)** Representative western blot images show the phosphorylation of ERK and total ERK proteins with increasing duration of blue light illumination. Abbreviation: PMWM stands for protein molecular weight marker. **(B)** The bar graph summarizes results from three independent cultures. Neurons expressing both components of the photoactivatable TrkB system (TrkB(kd)-Cry2 + CIB1), when stimulated with a single 30-s light pulse, showed a significant increase in ERK phosphorylation compared to non-stimulated cells ($P = 0.0497$, one-way ANOVA with a Tukey post hoc test). Cortical neurons infected with only one component (TrkB(kd)-Cry2) exhibited significant ERK phosphorylation when illuminated for 10 s and 30 s (*$P<0.05$, **$P<0.01$, one-way ANOVA with a Tukey's post hoc test). Data are presented as mean ± SD from three independent experiments.

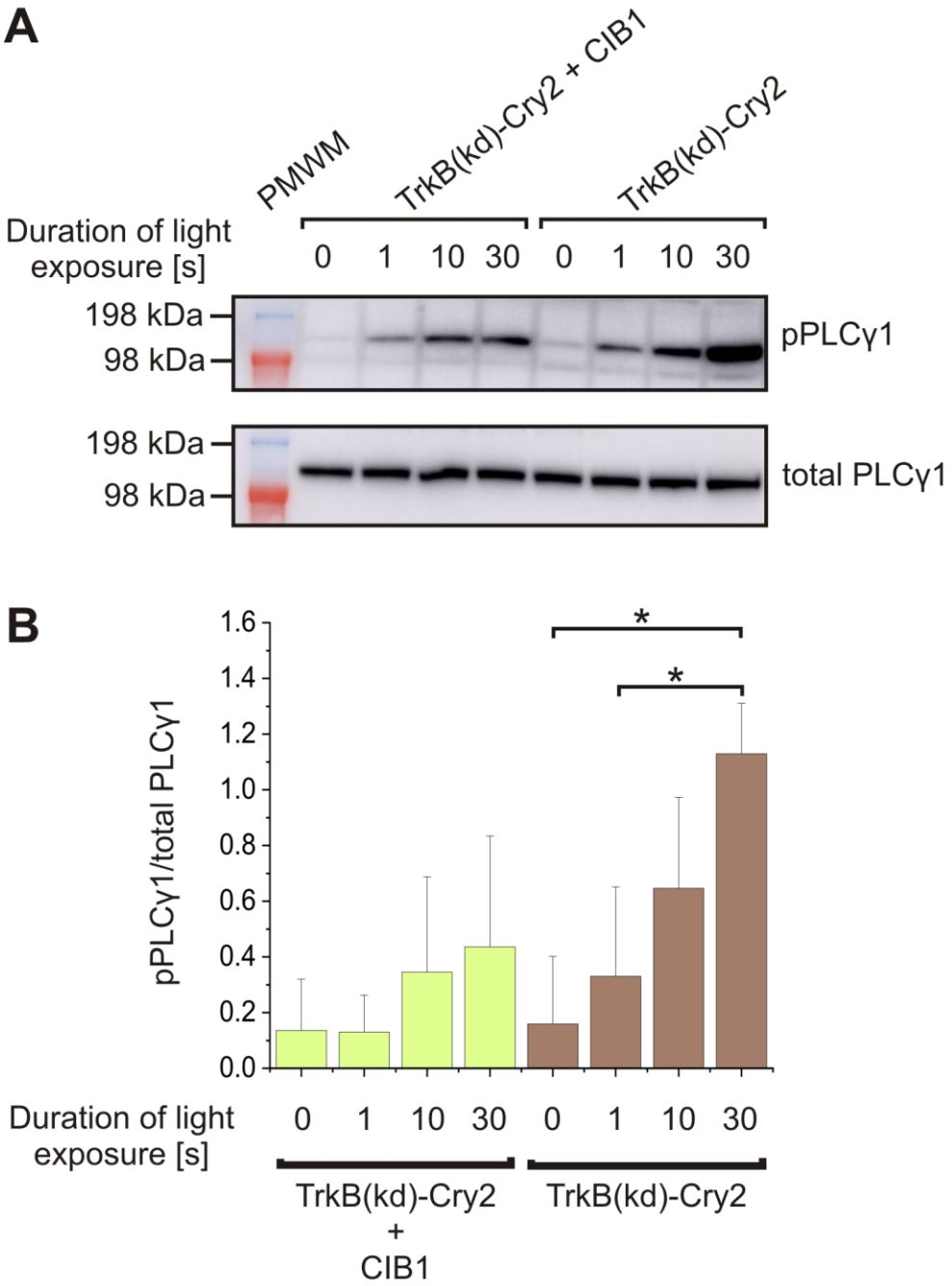

Figure 3.11 Effect of blue light duration on the activation of PLCγ1 pathway. Cortical neurons infected with two components, TrkB(kd)-Cry2(535)-T2A-mCherry and CIB1(81)-eGFP-CAAX, or with TrkB(kd)-Cry2(535)-T2A-mCherry alone, were exposed to different durations of blue light stimulation (0 s, 1 s, 10 s, 30 s). The blue light intensity remained the same for each group and was 36.8 mW/cm^2. The phosphorylation of PLCγ1 was examined 10 min after the light exposure. **(A)** Representative western blot images show the phosphorylation of PLCγ1 and total PLCγ1 with increasing duration of blue light illumination. PMWM - protein molecular weight marker. **(B)** The bar graph summarizes results from three independent cultures. Cortical neurons infected with only one component (TrkB(kd)-Cry2) exhibited significant PLCγ1 phosphorylation when were exposed to a 30-s light pulse (*P<0.05, one-way ANOVA with a Tukey's post hoc test). Data are presented as mean ± SD from three independent experiments.

3.3.5 The photoactivatable TrkB system can be expressed in the basolateral amygdala

As shown in Figure 3.12, rAAV2/8s, encoding the components of the TrkB system (see Table 3.2), successfully infected the basolateral amygdala (BLA) brain region of freely behaving rats. The expression of both transgenes was detected in BLA by mCherry fluorescence (TrkB(kd)-Cry2(535)-T2A-mCherry) and eGFP fluorescence (CIB1(81)-eGFP-CAAX). This validation was the first step to conduct *in vivo* behavioural studies which aim to modulate learning and memory processes.

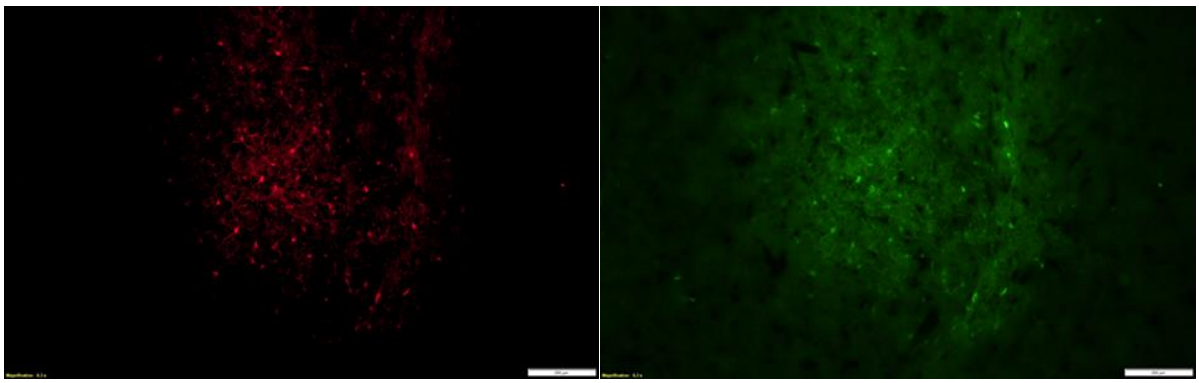

Figure 3.12 Validation of rAAV2/8s encoding the photoactivatable TrkB system in BLA. The mCherry fluorescence in BLA region indicated the successful expression of TrkB(kd)-Cry2(535)-T2A-mCherry (left panel), whereas the eGFP fluorescence demonstrated the expression of CIB1(81)-eGFP-CAAX component (right panel). The experiment was conducted by Dr Zayra Millan as described in Section 3.2.8.

3.3.6 The photoactivatable TrkB system can be used for controlling axon pathfinding upon light stimulation

To further validate the photoactivatable TrkB system, we used a growth cone turning assay, as BDNF is a strong attractive guidance cue in cultured *Xenopus* spinal neurons (Ming et al., 1997). Moreover, BDNF/TrkB signalling is responsible for the formation of growth cone in motoneurons (Dombert et al., 2017). We hypothesized that the photoactivatable TrkB system can steer the growth cone in response to light in a similar manner to the pharmacological application of BDNF.

DRG neurons were transfected with the photoactivatable TrkB system and used in the growth cone turning assay, as described in Section 3.2.9. The preliminary results suggested that the growth cones expressing the two-component TrkB system (TrkB(kd)-Cry2(535)-

T2A-CIB1(81)-eGFP-CAAX) exhibited either attractive or repulsive behaviour towards light (Fig. 3.13 C), dependent on the light stimulation protocol. More frequent and longer pulses (8 × 10-s pulse every 2 min) evoked attraction, whereas less frequent and shorter pulses (3 × 2-s pulse every 5 min) caused repulsion. As expected, the light insensitive mutant of Cry2 (TrkB(kd)-Cry2(535)-D387A-T2A-CIB1(81)-eGFP-CAAX) did not change the growth cone turning upon illumination (Fig. 3.13 C). The one-component TrkB system (TrkB(kd)-Cry2(535)-T2A-eGFP) also did not alter growth cone motility with light (Fig. 3.13 C). The axon extensions were not changed in response to any light stimulation patterns or expression of the transgenes (Fig. 3.13 D). Taken together, these data suggested that the photoactivatable TrkB system can be functionally expressed in DRG neurons to steer the growth cone turning with light.

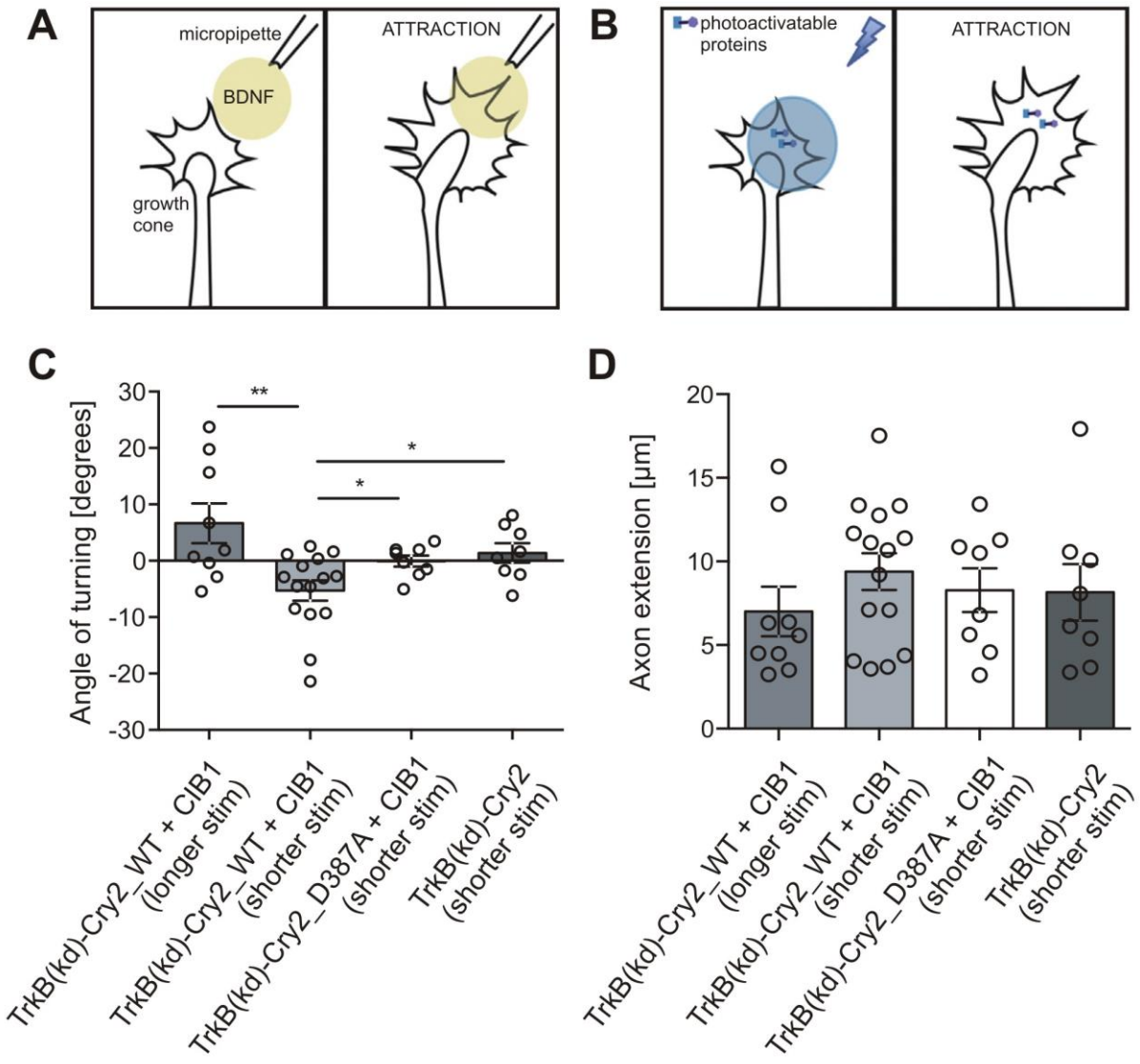

Figure 3.13 Growth cone turning can be steered by light. (A) The application of BDNF, an attractive guidance cue, can activate growth cone navigation towards the micropipette source of BDNF (Gasperini et al., 2009; Mitchell et al., 2012). This change in a trajectory of growth cone by BDNF is defined as an attraction, whereas the opposite behaviour is called a repulsion (not shown). **(B)** If the photoactivatable TrkB system can mimic the signalling pathway, we would expect that spatially limited light illumination can guide axon turning as well. Illustrations presented in A and B were adapted from Erdogan et al. (2016). **(C)** Axons sent out from DRG neurons, expressing TrkB(kd)-Cry2(535)-T2A-CIB1(81)-eGFP-CAAX (see Table 2.4; annotated in the figure as TrkB-Cry2_WT + CIB1) could be steered dependent on the parameters of light stimulation. The growth cones turned towards the light source when longer stimulation was applied (8 × 10-s pulse every 2 min), whereas they turned away from light when shorter stimulation was delivered (3 × 2-s pulse every 5 min). The attraction towards the light source is represented as a positive angle and the repulsion as a negative angle. The growth cones expressing either the light-insensitive TrkB system (TrkB(kd)-Cry2_D387A + CIB1) or the TrkB(kd)-Cry2 component did not show any preferential turning. The data are presented as mean ± SEM ($P<0.05$, $^{**}P<0.01$, Mann–Whitney U-test). **(D)** Light stimulation did not alter axon extension in DRG cells expressing the TrkB system in any of the test configurations. The data are shown as mean ± SEM. The experiments were conducted by Dr Macarena Pavez as described in Section 3.2.9.

3.4 Discussion

Controlling the activity of TrkB with light opens new possibilities for investigating the spatial and temporal dynamics of intracellular signalling pathways *in vivo*. Furthermore, it might allow us to test causal connections between biochemical events and animal behaviours. As presented in Chapter 2, the TrkB receptor was successfully manipulated with light in HEK293A and HeLa cell lines. To fulfil the requirements for using the photoactivatable TrkB *in vivo* as a final goal, testing this system in cultured neurons was the subsequent step.

To conduct experiments on cultured neurons and in behaving animals, the photodimerizing TrkB system was packaged into the rAAV2/8 vector. The AAV vector was chosen for several reasons: (1) it can transduce neurons *in vitro* and *in vivo* with low toxicity; (2) it can deliver transgene with high efficiency; (3) it enables a long-term transgene expression in neurons (Choi et al., 2014; Royo et al., 2008). Due to the limitation of DNA size that can be incorporated into AAV, the bicistronic vector with TrkB system (see Table 2.4) was split into two separate AAV vectors: one encoding CIB1 component and second encoding TrkB(kd)-Cry2 (see Table 3.1). The size of CIB1(81)-eGFP-CAAX component was below the packaging limit allowing it to be inserted into the AAV backbone, derived from AAV2-oChIEF-tdTomato (Lin et al., 2009), without any changes in the regulatory elements (WPRE and poly(A)). However, the size of TrkB(kd)-Cry2(535)-T2A-mCherry insert required a truncation of the expression cassettes to package this larger transgene without

compromising infection efficiency (Choi et al., 2014). Moreover, both components remained under control of the hSyn promoter, which is known to restrict the expression to neuronal cells (Kugler et al., 2003a; Lin, 2013). The rAAV2/8s encoding both components of the TrkB system successfully infected cortical neurons *in vitro*. Moreover, these two transgenes were also successfully delivered into neuronal cells in the BLA region of freely behaving rats. The *in vivo* validation of the photoactivatable TrkB expression is a first step for further behavioural studies, which are aiming to examine the roles of BDNF and TrkB in learning and memory processes.

Delivering the photoactivatable TrkB into cultured cortical neurons with high efficiency enabled us to assess the functional expression of the system upon light illumination. The western blotting analyses of phospho-ERK, phospho-AKT and phospho-PLCγ1 upon blue light in neurons, expressing the two-component TrkB system, revealed that both ERK and PLCγ1 signalling pathways can be manipulated with light. On the other hand, light exposure did not result in the significant elevation of phospho-AKT. However, AKT was still translocated to the membrane in HEK293A cells upon light illumination, as shown in Figure 2.23. Consistent with the results presented in Chapter 2, the light-dependent activation of TrkB(kd)-Cry2 alone led to the phosphorylation of ERK and PLCγ1 in cortical neurons. Moreover, the overexpression of the photoactivatable TrkB did not significantly increase background ERK, AKT and PLCγ1 activities in neurons, which is an important requirement for any *in vivo* activation. BDNF treatment of non-transduced neurons was used as a positive control for the activation of ERK, AKT and PLCγ1. In these experiments, BDNF exposure evoked a larger effect than light illumination in neurons expressing the photoactivatable TrkB. This could be partly due to the manner in which cells were exposed to BDNF or light: neurons were treated with BNDF continuously for 10 min, whereas they were exposed to a brief 30-s pulse of blue light and incubated in dark for another 10 min after light termination. It can be speculated that a longer duration of light stimulation might evoke a larger effect, and results from experiments shown in Figures 3.10 and 3.11 support this. Another reason for the larger effect of BDNF could be that light was not delivered evenly to all cells, due to the physical arrangement of the culture dish over the light source (see Figure 2.5). Hence some cells may have received insufficient light to fully activate Cry2. Finally, cultured neurons might also contain glia cells in which the effect of BDNF can be mediated by a pan-neurotrophin receptor p75 (Vignoli et al., 2016). The activation of p75 with BDNF was shown to trigger ERK1/ERK2 pathway in PC12 cells (Lad and Neet, 2003).

The photoactivatable TrkB system was able to alter the turning of the growth cone in cultured DRG neurons. Interestingly, we were able to steer growth cones to opposing directions with different amounts of light, with smaller 'dose' of light leading to repulsion and higher 'dose' leading to attraction. BDNF is generally regarded as an attractive guidance cue (Ming et al., 1997); therefore, it was expected that the photoactivatable TrkB, once activated with light, might steer the growth cone towards the light. The TrkB(kd)-Cry2 component without the membrane anchored CIB1 was unable to steer growth cones in this assay, suggesting the observed turning might require intracellular Ca^{2+} signalling since TrkB(kd)-Cry2 alone was able to phosphorylate ERK, PLCγ1 and to translocate AKT (see Figures 3.5, 3.7 and 2.26, respectively), but unable to evoke a rise in intracellular Ca^{2+} (see Figures 2.6 and 2.14). It is noteworthy that the activation of PKC by DAG, as the effect of PLCγ1 activity (not investigated in this project), might also play a role in the growth cone turning. It is speculated that the observed attraction and repulsion upon different light parameters might be associated with the magnitude of released Ca^{2+}. It has been demonstrated that transient high concentration of Ca^{2+} can promote the attraction (via CaMKII activation), whereas low concentration of Ca^{2+} can cause repulsion (via calcineurin activation) (Forbes et al., 2012; Sutherland et al., 2014; Wen et al., 2004). Similarly, the different polarities of growth cone responses have been shown to be dependent on the mean BDNF concentration in a microfluidics-based assay (Joanne Wang et al., 2008). Altogether this raises the interesting questions of the roles of ERK and AKT in BDNF mediated-axon guidance *in vivo*. I speculate in this context that the immediate Ca^{2+} increase might have more rapid effects on turning and that ERK and AKT might play roles in downstream, or slower, signalling pathways that are important for sustaining or maintaining axon navigation towards its appropriate target. To support this speculation, further experiments are necessary, for instance, with growth cone expressing the TrkB system with different mutations within the intracellular domain of TrkB.

Taken together, the results, presented in this chapter, show that the photoactivatable TrkB system can be delivered to neurons *in vitro* and *in vivo* through recombinant AAV vectors. This tool is functional in cultured neurons, either cortical or DRG, upon light exposure. However, it remains unclear whether endogenous TrkB in neuronal cells can compete or interfere with the signalling activated by the photoactivatable TrkB system. In the next step, it would be crucial to perform an immunoblotting experiment in which infected neuronal cells with the recombinant AAV vectors encoding the TrkB system will be stimulated with BDNF. This result will help to assess whether the photoactivatable TrkB can

disrupt the action of the endogenous receptors. Overall, these results suggest the possible application of this approach for investigating causal links between BDNF/TrkB signalling and learning/memory processes in behaving animals.

Chapter 4

Conclusions and future directions

The TrkB-mediated activation of signalling pathways has a vital role in many neurobiological functions including development, regeneration and repair, learning and memory (De Wit et al., 2006; Martinez-Galvez et al., 2016; Minichiello et al., 1999). BDNF and TrkB have been implicated in multiple facets of synaptic plasticity, especially LTP, learning and memory formation (Korte and Schmitz, 2016; Minichiello, 2009). The quickly growing interest in demonstrating causal connections between biochemical pathways, synaptic plasticity and behaviours *in vivo* dictates a necessity for new tools. A photoactivatable TrkB might serve as an appropriate tool to probe such a link. A previous optogenetic approach for controlling TrkB (optoTrkB) (Chang et al., 2014) has limitations to be overcome for investigating biological questions *in vivo*. OptoTrkB is composed of the full-length TrkB receptor with the intact extracellular domain that can still bind to endogenous BDNF, likely making cells hypersensitive to the endogenous ligand. Moreover, overexpression of optoTrkB in the membrane might cause the activation of receptors in the absence of stimulus (as stated by Chang et al. (2014) in Supplementary Figures 3a and 5a). Finally, the size of recombinant optoTrkB DNA limits the delivery methods into cells available for *in vivo* studies (Chang et al., 2014). To overcome these limitations, my thesis presents and validates a second-generation of the photoactivatable TrkB. This novel TrkB system was designed to be readily applicable *in vivo* for the manipulation of synaptic plasticity and animal behaviour in response to light.

My photoactivatable TrkB has been intended as a two-component system, consisting of a cytosolic TrkB(kd)-Cry2 and CIB1 localized at the plasma membrane. These smaller components were packaged into AAV viral vectors. Moreover, the extracellular domain of TrkB receptor was excised to prevent endogenous BDNF binding. My experimental data are consistent with a model that light illumination leads to the oligomerization of TrkB(kd)-Cry2 and the kinase domains can undergo autophosphorylation in a similar way to endogenous TrkB receptor upon BDNF binding (Fig. 4.1 A, B). The cytosolic TrkB(kd)-Cry2 is capable of phosphorylating TrkB downstream targets localized in the cytosol. The translocation of TrkB(kd)-Cry2 to the plasma membrane via the Cry2/CIB1 heterodimerization can activate further signalling via second messangers that are derived from the plasma membrane (IP_3 and

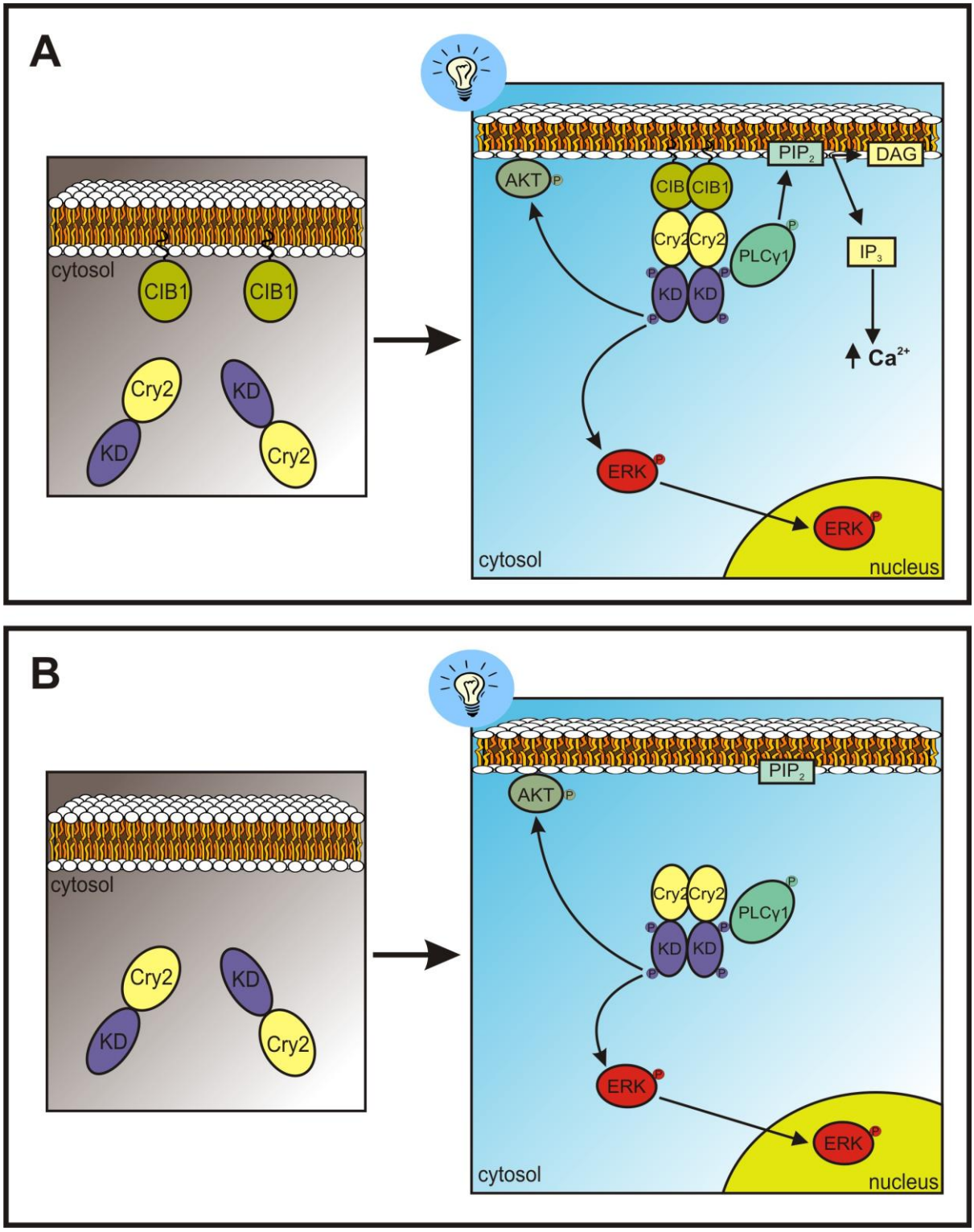

Figure 4.1 Models for the action of the photoactivatable TrkB upon light illumination. (A) The two-component TrkB system acts at the plasma membrane. This model features triggering three main TrkB signalling pathways, involving phosphorylation of PLCγ1, ERK and AKT proteins. Importantly, the Cry2/CIB1 interaction localizes TrkB(kd) to the membrane such that activated phospho-PLCγ1 is in close proximity to its lipid substrate and can generate IP_3, which can mobilize Ca^{2+} increase in cells. Phosphorylated ERK can be translocated from the cytoplasm to the nucleus.

AKT can be transported from the cytoplasm to the plasma membrane, where it might be phosphorylated (still to be investigated). **(B) The one-component TrkB acts in the cytosol.** In this model, TrkB-mediated phosphorylation of PLCγ1 and ERK occurs in the cytosol. Light stimulation can lead to functional responses of ERK and AKT (translocation), but although PLCγ1 is phosphorylated, it fails to evoke Ca^{2+} increase. Abbreviations: KD, kinase domain of TrkB; P, phosphorylation sites; PIP_2, phosphatidylinositol-4,5-bisphosphate; IP_3, inositol-1,4,5-trisphosphate; DAG, diacylglycerol.

DAG). Models showing how the photoactivatable TrkB system acts in the cytosol and membrane are presented in Figure 4.1. Consolidating my Ca^{2+} imaging and western blot data, both ERK and PLCγ1 were phosphorylated by TrkB(kd)-Cry2 in the cytosol, and AKT was translocated from the cytosol to the membrane. However, only TrkB(kd)-Cry2 that is targeted to the membrane through interaction with membrane-anchored CIB1 was capable of elevating intracellular Ca^{2+}, suggesting that PLCγ1 needs to be both phosphorylated and relocated to the membrane to exert its function. My results suggest that relocation is necessary for PLCγ1 to effectively access its substrate, PIP_2, in the inner leaflet of the plasma membrane (Berridge and Irvine, 1984). The action of the photoactivatable TrkB at the plasma membrane reflects better the signalling of endogenous TrkB.

Compared to the similar existing published work on an optogenetic system manipulating TrkA receptor (Duan et al., 2018) (see Fig. 2.2 C), the current work has provided more detailed insights into the mechanism of the tool's action, highlighting that both oligomerization of Cry2 and heterodimerization of Cry2/CIB1 are necessary to activate signalling cascades to reflect the activity of endogenous RTKs. The oligomerization of Cry2 is required for clustering RTK kinase domains to enable their autophosphorylation, whereas the Cry2/CIB1 heterodimerization restricts the activation of signalling to the membrane. This suggests that to control RTK signalling with other light-induced or chemical heterodimerizers that interact with 1:1 stoichiometry – such as the blue-light activated iLID/SspB (Guntas et al., 2015) and pMag/nMag (Kawano et al., 2015), the red-light activated BphP1-Q-PAS1 (Redchuk et al., 2017), the chemically-induced iDimerize system (Takara Bio) – a tandem repeat of one of the binding partner at the membrane would be necessary to recruit two RTKs kinase domains to the membrane and simultaneously, to induce their autophosphorylation. This would have strong implications for developing future systems as more light- and chemically-induced systems are generated.

This unexpected mode of action, in which both oligomerization and relocation of TrkB(kd)-Cry2 to the membrane is required for the intracellular Ca^{2+} elevation, brings the possibility of dissecting ERK, AKT and PLCγ1/Ca^{2+} signalling pathways. This is reflected in

our results on the growth cone turning, which showed that TrkB(kd)-Cry2 alone (ERK and AKT translocation, ERK and PLCγ1 phosphorylation, but no Ca^{2+} increase) was not sufficient to change the trajectory of growing axon (see Fig. 3.13). TrkB(kd)-Cry2 with the membrane CIB1 (ERK and AKT tranlocation, ERK and PLCγ1 phosphorylation, Ca^{2+} elevation) did steer a growth cone upon light illumination. This suggests that immediate turning of the growth cone requires Ca^{2+} signal, whereas ERK and AKT may have other functional effects, possibly sustained at a delay time point (Carlson et al., 2011).

This ability of dissecting specific signalling cascades of TrkB can be greatly beneficial for understanding the function of TrkB signalling during distinct phases of LTP and learning. Other useful tools include the TrkB kinase domain mutant that prevents PLCγ1 docking and Ca^{2+} elevation upon light illumination (see Fig. 2.13). Based on the growth cone behaviours observed in axon guidance upon light stimulation, a similar differential response in synapses could allow us to induce both LTP and LTD by simply using distinct light stimulation protocols and also to investigate roles of different signalling pathways in LTP.

There are some outstanding questions of the roles of BDNF/TrkB in LTP, learning and memory that might be addressed with the optogenetic tool described in the current thesis. For example, testing whether activation of TrkB in the postsynaptic cells is sufficient to initiate and maintain LTP. Another question concerns the functional roles of ERK/AKT/PLCγ1 in structural LTP within the synapse. With the utilization of a truncated postsynaptic density protein 95 (PSD95) (Hayashi-Takagi et al., 2015) or the PSD95-targeting fibronectin intrabodies (Gross et al., 2013), it is potentially possible to target the CIB1 component specifically to the postsynaptic site, restricting the action of the TrkB system within the dendritic spines. This can be further spatially restricted by using a two-photon excitation approach, which was shown to induce Cry2/CIB1 heterodimerization (Kennedy et al., 2010). Given the known involvement of TrkB in structural LTP (Harward et al., 2016), anchoring the TrkB system in dendritic spines might give a new insight into whether TrkB activity is sufficient to enlarge spines and if it can efficiently enhance learning in behaving animals. This potential experiment would test the theory of Hayashi-Takagi et al. (2015) that the major loci of memory traces are dendritic spines.

Enhancing BDNF/TrkB signalling potentially has a therapeutic potential, as a dysfunction of this signalling has been reported in Alzheimer's disease (Connor et al., 1997), Huntington's disease (Ferrer et al., 2000) and Parkinson's disease (Parain et al., 1999). Searching for a novel treatment is even more relevant due to the fact that BDNF does not cross the blood-brain barrier efficiently and has a short lifetime in blood so its delivery to

target regions is difficult (Pan et al., 1998; Pilakka-Kanthikeel et al., 2013). Another interesting aspect of learning and memory that could be investigated by using the photoactivatable TrkB system is extinction of fear memories. The BDNF/TrkB signalling pathway is involved in the mechanism underlying memory extinction (Li et al., 2017). It can have also potential therapeutic application in treatment of patients with post-traumatic stress disorder whose memory extinction is impaired (as reviewed by Andero and Ressler (2012)). Although there is a very long route to use the photoactivatable TrkB system as a therapeutic strategy, its application for studying learning and memory might improve our knowledge of these processes.

To summarize, the work presented in this thesis adds a new approach to the optogenetic toolkit. The photoactivatable TrkB system can act as a two-component or a single component system, enabling the investigation of the different biochemical pathways' functions. This approach activates the canonical signalling pathways in HEK cells and neuronal cells upon light stimulation. It can be expressed functionally in DRG neurons to steer growth cone turning with light. Finally, it can be packaged into recombinant AAV vectors for *in vivo* application. This opens new possibilities to examine processes connected with learning and memory as well as axon regeneration in behaving animals.

Appendix

Appendix I: Key resources and reagents used in experiments described in Chapter 2 and Chapter 3.

Table A1 Key resources and reagents to examine the photoactivatable TrkB system in non-neuronal and neuronal cells.

REAGENT OR RESOURCE	SOURCE	IDENTIFIER
Antibody		
Anti-Phospho-Akt (Ser473)	Cell Signaling Technology	Cat#4060 RRID:AB_2315049
Anti-Akt	Cell Signaling Technology	Cat#9272 RRID:AB_329827
Anti-Phospho-p44/42 MAPK (Erk1/2) (Thr202/Tyr204)	Cell Signaling Technology	Cat#9106 RRID:AB_331768
Anti-p44/42 MAPK (Erk1/2)	Cell Signaling Technology	Cat#9102 RRID:AB_330744
Anti-Phospho-PLCγ1 (Tyr783)	Cell Signaling Technology	Cat#2821S RRID:AB_330855
Anti-PLCγ1	Cell Signaling Technology	Cat#5690P RRID:AB_10691383
Anti-Mouse/HRP secondary antibody	Dako	Cat#P0447 RRID:AB_2617137
Anti-Rabbit/HRP secondary antibody	Dako	Cat#P0448 RRID:AB_2617138
Bacterial strain		
DH5α Competent Cells	Invitrogen	Cat# 18265-017
Chemicals and recombinant proteins		
Acetic acid	Sigma-Aldrich	Cat# 695092-2.5l
Agar bacteriological	Oxoid	Cat# LP0011
Agencourt CleanSEQ	Beckman Coulter	Cat# A29151
Ampicillin	Bio Basic	Cat# AB0028

Antioxidant	Invitrogen	Cat# BT0005
B-27 supplement (50X)	Gibco	Cat# 17504044
BDNF	Invitrogen	Cat# PHC7074
Benzonase nuclease	Sigma-Aldrich	Cat# E1014-25KU
BigDye Terminator v3.1 Cycle Sequencing Kit	Applied Biosystem	Cat# 4337455
Bolt 4-12% Bis-Tris Plus gels	Invitrogen	Cat# NW04120BOX / NW04122BOX
Bolt LDS Sample Buffer (4X)	Invitrogen	Cat# B0007
Bolt MES SDS Running Buffer (20X)	Invitrogen	Cat# B0002
Bolt Transfer Buffer (20X)	Invitrogen	Cat# BT00061
BSA	Bio-Rad	Cat# 500-0007
$CaCl_2 \cdot 2H_2O$	Sigma-Aldrich	Cat# C3306-500G
Chloroform	Sigma-Aldrich	Cat# C2432-500ML
Collagen	Advanced BioMatrix	Cat# 5005-G
Complete, Mini, EDTA-free Protease Inhibitor Cocktail	Roche	Cat# 04693159001
D-Glucose	Sigma-Aldrich	Cat# G5767-500G
DMEM (1X)	Gibco	Cat# 11885-084
DMSO	Sigma-Aldrich	Cat# D4540-100ML
DNA Ladder	New England Biolabs	Cat# N3200S
DPBS	Sigma-Aldrich	Cat# D1408-500G
DTT	Goldbio	Cat# DTT50
EDTA	Sigma-Aldrich	Cat# E5134-500G
Ethanol	Sigma-Aldrich	Cat# E7023-500ML
Fetal Bovine Serum, qualified, Australia origin	Gibco	Cat# 10099141
GlutaMAX supplement	Gibco	Cat# 35050061
Glycine	Sigma-Aldrich	Cat# G8898-1KG
HBSS solution (10X)	Gibco	Cat# 14185052
HCl	Merck	Cat# 1.00319.2500
HEPES	Sigma-Aldrich	Cat# H3375-250G

IGEPAL CA-630	Sigma-Aldrich	Cat# I3021-50ML
Immobilon Western Chemiluminescent HRP Substrate	Millipore	Cat# WBKLS0500
Iodixanol solution	Sigma-Aldrich	Cat# D1556-250ML
Isopropanol	Sigma-Aldrich	Cat# 59304-1L-F
KCl	Sigma-Aldrich	Cat# P9541-500G
KH_2PO_4	Sigma-Aldrich	Cat# P9791-500G
Methanol	Merck	Cat# 1060184000
$MgCl_2 \cdot 6H_2O$	Sigma-Aldrich	Cat# 63068-250G
Molecular Biology Grade Water	Sigma-Aldrich	Cat# W4502-1L
Na_2HPO_4	Sigma-Aldrich	Cat# S3264-500G
NaCl	Sigma-Aldrich	Cat# S7653-5KG
NaOH	Sigma-Aldrich	Cat# S5881-500G
Neurobasal medium	Gibco	Cat# 21103049
Penicillin-Streptomycin solution	Sigma-Aldrich	Cat# P4333-100ML
Phenol red	Sigma-Aldrich	Cat# P3532-5G
PhosSTOP	Roche	Cat# 4906845001
Polyethylenimine (PEI)	Sigma-Aldrich	Cat# 408727-100ML
Poly-L-lysine	Sigma-Aldrich	Cat# P4832-50ML
PVDF, 0.2 µm	Bio-Rad	Cat# 1620177
SDS	Sigma-Aldrich	Cat# L3771-500G
SeeBlue Plus2 Pre-Stained Protein Standard	Invitrogen	Cat# LC5925
Sodium Bicarbonate 7.5% solution	Gibco	Cat# 25080094
Sodium deoxycholate	Sigma-Aldrich	Cat# D6750-25
Sybr Safe DNA gel stain	Invitrogen	Cat# S33102
Tri-Reagent	Sigma-Aldrich	Cat# T9424-100ml
Trizma base	Sigma-Aldrich	Cat# T6066-1KG
Trypan Blue solution	Sigma-Aldrich	Cat# T8154-20ML
TrypLE Express	Gibco	Cat# 12604-013
Trypsin (1:250) powder	Gibco	Cat# 27250018

Tryptone	Oxoid	Cat# LP0042
Tween-20	Sigma-Aldrich	Cat# P2287-500ML
U-73122	Sigma-Aldrich	Cat# U6756
X-tremeGENE 9 DNA Transfection Reagent	Roche	Cat# 06 365 787 001
Yeast Extract	Oxoid	Cat# LP0021
Critical commercial kit/assay		
AAV real-time PCR titration kit	Takara	Cat# 6233
DC Protein Assay Kit II	Bio-Rad	Cat# 500-0112
GenElute HP Plasmid Miniprep Kit	Sigma-Aldrich	Cat# NA0160
Maxima H Minus First Strand cDNA Synthesis Kit	Thermo Scientific	Cat# K1651
PureLink HiPure Plasmid Maxiprep Kit	Invitrogen	Cat# K210007
PureLink HiPure Plasmid Midiprep Kit	Invitrogen	Cat# K210005
RNeasy Mini Kit	Qiagen	Cat# 74104
Zymoclean Gel DNA Recovery Kit	Zymo Research	Cat# D4002
Enzymes for cloning		
AgeI-HF	New England Biolabs	Cat# R3552
BamHI-HF	New England Biolabs	Cat# R3136
BsiWI-HF	New England Biolabs	Cat# R3553
ClaI	New England Biolabs	Cat# R0197
EcoRI-HF	New England Biolabs	Cat# R3101
HindIII-HF	New England Biolabs	Cat# R3104
NheI-HF	New England Biolabs	Cat# R3101
NotI-HF	New England Biolabs	Cat# R3189
Phusion Flash High-Fidelity PCR Master Mix	Thermo Scientific	Cat# F-548
SpeI-HF	New England Biolabs	Cat# R3133
T4 ligase	Invitrogen	Cat# 15224-017

XbaI	New England Biolabs	Cat# R0145
Experimental models: cell lines		
HeLa cells	ATCC	
HEK293A cells	Invitrogen	
Recombinant DNA		
AAV2-oChIEF-tdTomato	Made by Dr John Lin	Cat# 50977 (Addgene)
Oligonucleotides and gBlocks Gene Fragments	IDT	N/A
pcDNA3.1-CMV	Invitrogen	N/A
pcDNA3-CMV	Invitrogen	N/A
pLenti-CMV	University of California, San Diego	N/A
pMDG2.0	Kind gift from Prof Didier Trono	N/A
psPax2	Kind gift from Prof Didier Trono	N/A
PXR8	National Vector Biorepository	
pXX6-80	National Vector Biorepository	
Software		
ApE	M. Wayne Davis, The University of Utah	http://jorgensen.biology.utah.edu/wayned/ape/
ImageJ	Rasband, W.S., NIH, Bethesda, Maryland, USA	https://imagej.nih.gov/ij/
LED Driver Control Panel V3.1.0	Mightex	
Micro-Manager 1.4.22	University of California, San Francisco	doi:10.1002/0471142727.mb1420s92
OriginPro 8	OriginLab, Northampton, MA	https://www.originlab.com

N/A – not applicable

Appendix II: Protein sequences of the main components of the photoactivatable TrkB system.

Table A2 Protein sequences of two main components of the TrkB system.

Name	Sequence
TrkB(kd)-Cry2(535)	MKLARHSKFGMKGPASVISNDDDSASPLHHISNGSNTPSSSEGGPDAVIIG MTKIPVIENPQYFGITNSQLKPDTFVQHIKRHNIVLKRELGEGAFGKVFLAE CYNLCPEQDKILVAVKTLKDASDNARKDFHREAELLTNLQHEHIVKFYGV CVEGDPLIMVFEYMKHGDLNKFLRAHGPDAVLMAEGNPPTELTQSQMLH IAQQIAAGMVYLASQHFVHRDLATRNCLVGENLLVKIGDFGMSRDVYST DYYRVGGHTMLPIRWMPPESIMYRKFTTESDVWSLGVVLWEIFTYGKQP WYQLSNNEVIECITQGRVLQRPRTCPQEVYELMLGCWQREPHTRKNIKNI HTLLQNLAKASPVYLDILGTGGGSGGGSMKMDKKTIVWFRRDLRIEDNPA LAAAAHEGSVFPVFIWCPEEEGQFYPGRASRWWMKQSLAHLSQSLKALG SDLTLIKTHNTISAILDCIRVTGATKVVFNHLYDPVSLVRDHTVKEKLVER GISVQSYNGDLLYEPWEIYCEKGKPFTSFNSYWKKCLDMSIESVMLPPPW RLMPITAAAEAIWACSIEELGLENEAEKPSNALLTRAWSPGWSNADKLLN EFIEKQLIDYAKNSKKVVGNSTSLLSPYLHFGEISVRHVFQCARMKQIIWA RDKNSEGEESADLFLRGIGLREYSRYICFNFPFTHEQSLLSHLRFFPWDADV DKFKAWRQGRTGYPLVDAGMRELWATGWMHNRIRVIVSSFAVKFLLLP WKWGMKYFWDTLLDADLECDILGWQYISGSIPDGHELDRLDNPALQGAK YDPEGEYIRQWLPELARLPTEWIHHPWDAPLTVLKASGVELGTNYAKPIV DIDTARELLAKAISRTREAQIMIGAAPDEIVADSFEALGANTIKEPGLCPSVS SNDQQVPSAV
CIB1(170)-eGFP-CAAX	MNGAIGGDLLLNFPDMSVLERQRAHLKYLNPTFDSPLAGFFADSSMITGG EMDSYLSTAGLNLPMMYGETTVEGDSRLSISPETTLGTGNFKAAKFDTET KDCNEAAKKMTMNRDDLVEEGEEEKSKITEQNNGSTKSIKKMKHKAKKE ENNFSNDSSKVTKELEKTDYIGGGGAGIDMVSKGEELFTGVVPILVELDGD VNGHKFSVSGEGEGDATYGKLTLKFICTTGKLPVPWPTLVTTLTYGVQCF SRYPDHMKQHDFFKSAMPEGYVQERTIFFKDDGNYKTRAEVKFEGDTLV NRIELKGIDFKEDGNILGHKLEYNYNSHNVYIMADKQKNGIKVNFKIRHNI EDGSVQLADHYQQNTPIGDGPVLLPDNHYLSTQSALSKDPNEKRDHMVLL EFVTAAGITLGMDELYKGKKKKKKSKTKCVIM

References

Adolphs, R., Tranel, D., Damasio, H., and Damasio, A. (1994). Impaired recognition of emotion in facial expressions following bilateral damage to the human amygdala. Nature 372, 669-672.

Ahmad, M., Grancher, N., Heil, M., Black, R.C., Giovani, B., Galland, P., and Lardemer, D. (2002). Action spectrum for cryptochrome-dependent hypocotyl growth inhibition in Arabidopsis. Plant Physiol 129, 774-785.

Ahmed, F., and Hristova, K. (2018). Dimerization of the Trk receptors in the plasma membrane: effects of their cognate ligands. Biochem J 475, 3669-3685.

Alfa, R.W., Tuszynski, M.H., and Blesch, A. (2009). A novel inducible tyrosine kinase receptor to regulate signal transduction and neurite outgrowth. J Neurosci Res 87, 2624-2631.

Alger, B.E., and Teyler, T.J. (1976). Long-term and short-term plasticity in the CA1, CA3, and dentate regions of the rat hippocampal slice. Brain research 110, 463-480.

Amaral, M.D., and Pozzo-Miller, L. (2007). TRPC3 channels are necessary for brain-derived neurotrophic factor to activate a nonselective cationic current and to induce dendritic spine formation. The Journal of neuroscience : the official journal of the Society for Neuroscience 27, 5179-5189.

Andero, R., and Ressler, K.J. (2012). Fear extinction and BDNF: translating animal models of PTSD to the clinic. Genes Brain Behav 11, 503-512.

Anggono, V., and Huganir, R.L. (2012). Regulation of AMPA receptor trafficking and synaptic plasticity. Current opinion in neurobiology 22, 461-469.

Annese, J., Schenker-Ahmed, N.M., Bartsch, H., Maechler, P., Sheh, C., Thomas, N., Kayano, J., Ghatan, A., Bresler, N., Frosch, M.P., *et al.* (2014). Postmortem examination of patient H.M.'s brain based on histological sectioning and digital 3D reconstruction. Nature communications 5, 3122.

Ascher, P., and Nowak, L. (1988). The role of divalent cations in the N-methyl-D-aspartate responses of mouse central neurones in culture. The Journal of physiology 399, 247-266.

Atwal, J.K., Massie, B., Miller, F.D., and Kaplan, D.R. (2000). The TrkB-Shc site signals neuronal survival and local axon growth via MEK and P13-kinase. Neuron 27, 265-277.

Banerjee, R., Schleicher, E., Meier, S., Viana, R.M., Pokorny, R., Ahmad, M., Bittl, R., and Batschauer, A. (2007). The signaling state of Arabidopsis cryptochrome 2 contains flavin semiquinone. J Biol Chem 282, 14916-14922.

Bear, M.F., and Malenka, R.C. (1994). Synaptic plasticity: LTP and LTD. Current opinion in neurobiology 4, 389-399.

Beck, G., Munno, D.W., Levy, Z., Dissel, H.M., Van-Minnen, J., Syed, N.I., and Fainzilber, M. (2004). Neurotrophic activities of trk receptors conserved over 600 million years of evolution. J Neurobiol 60, 12-20.

Benito-Gutierrez, E., Garcia-Fernandez, J., and Comella, J.X. (2006). Origin and evolution of the Trk family of neurotrophic receptors. Mol Cell Neurosci 31, 179-192.

Benke, T.A., Luthi, A., Isaac, J.T., and Collingridge, G.L. (1998). Modulation of AMPA receptor unitary conductance by synaptic activity. Nature 393, 793-797.

Berridge, M.J., and Irvine, R.F. (1984). Inositol trisphosphate, a novel second messenger in cellular signal transduction. Nature 312, 315-321.

Bertrand, T., Kothe, M., Liu, J., Dupuy, A., Rak, A., Berne, P.F., Davis, S., Gladysheva, T., Valtre, C., Crenne, J.Y., and Mathieu, M. (2012). The crystal structures of TrkA and TrkB suggest key regions for achieving selective inhibition. J Mol Biol 423, 439-453.

Bleasdale, J.E., Thakur, N.R., Gremban, R.S., Bundy, G.L., Fitzpatrick, F.A., Smith, R.J., and Bunting, S. (1990). Selective inhibition of receptor-coupled phospholipase C-dependent processes in human platelets and polymorphonuclear neutrophils. J Pharmacol Exp Ther 255, 756-768.

Bliss, T.V.P., and Lomo, T. (1973). Long-Lasting Potentiation of Synaptic Transmission in Dentate Area of Anesthetized Rabbit Following Stimulation of Perforant Path. J Physiol-London 232, 331-356.

Bothwell, M. (2006). Evolution of the neurotrophin signaling system in invertebrates. Brain, behavior and evolution 68, 124-132.

Boyden, E.S., Zhang, F., Bamberg, E., Nagel, G., and Deisseroth, K. (2005). Millisecond-timescale, genetically targeted optical control of neural activity. Nature neuroscience 8, 1263-1268.

Brautigam, C.A., Smith, B.S., Ma, Z., Palnitkar, M., Tomchick, D.R., Machius, M., and Deisenhofer, J. (2004). Structure of the photolyase-like domain of cryptochrome 1 from Arabidopsis thaliana. Proceedings of the National Academy of Sciences of the United States of America 101, 12142-12147.

Buard, I., Coultrap, S.J., Freund, R.K., Lee, Y.S., Dell'Acqua, M.L., Silva, A.J., and Bayer, K.U. (2010). CaMKII "autonomy" is required for initiating but not for maintaining neuronal long-term information storage. The Journal of neuroscience : the official journal of the Society for Neuroscience 30, 8214-8220.

Bugaj, L.J., Choksi, A.T., Mesuda, C.K., Kane, R.S., and Schaffer, D.V. (2013). Optogenetic protein clustering and signaling activation in mammalian cells. Nature methods 10, 249-252.

Bugaj, L.J., Spelke, D.P., Mesuda, C.K., Varedi, M., Kane, R.S., and Schaffer, D.V. (2015). Regulation of endogenous transmembrane receptors through optogenetic Cry2 clustering. Nature communications 6, 6898.

Burack, W.R., and Sturgill, T.W. (1997). The activating dual phosphorylation of MAPK by MEK is nonprocessive. Biochemistry-Us 36, 5929-5933.

Carew, T.J., Castellucci, V.F., and Kandel, E.R. (1971). An analysis of dishabituation and sensitization of the gill-withdrawal reflex in Aplysia. Int J Neurosci 2, 79-98.

Carlson, S.M., Chouinard, C.R., Labadorf, A., Lam, C.J., Schmelzle, K., Fraenkel, E., and White, F.M. (2011). Large-scale discovery of ERK2 substrates identifies ERK-mediated transcriptional regulation by ETV3. Sci Signal 4, rs11.

Castellucci, V.F., Carew, T.J., and Kandel, E.R. (1978). Cellular analysis of long-term habituation of the gill-withdrawal reflex of Aplysia californica. Science 202, 1306-1308.

Chang, K.Y., Woo, D., Jung, H., Lee, S., Kim, S., Won, J., Kyung, T., Park, H., Kim, N., Yang, H.W., *et al.* (2014). Light-inducible receptor tyrosine kinases that regulate neurotrophin signalling. Nature communications 5, 4057.

Chao, L.H., Pellicena, P., Deindl, S., Barclay, L.A., Schulman, H., and Kuriyan, J. (2010). Intersubunit capture of regulatory segments is a component of cooperative CaMKII activation. Nature structural & molecular biology 17, 264-272.

Chao, L.H., Stratton, M.M., Lee, I.H., Rosenberg, O.S., Levitz, J., Mandell, D.J., Kortemme, T., Groves, J.T., Schulman, H., and Kuriyan, J. (2011). A mechanism for tunable autoinhibition in the structure of a human Ca2+/calmodulin- dependent kinase II holoenzyme. Cell 146, 732-745.

Che, D.L., Duan, L., Zhang, K., and Cui, B. (2015). The Dual Characteristics of Light-Induced Cryptochrome 2, Homo-oligomerization and Heterodimerization, for Optogenetic Manipulation in Mammalian Cells. ACS Synth Biol 4, 1124-1135.

Chhatwal, J.P., Stanek-Rattiner, L., Davis, M., and Ressler, K.J. (2006). Amygdala BDNF signaling is required for consolidation but not encoding of extinction. Nature neuroscience 9, 870-872.

Choi, J.H., Yu, N.K., Baek, G.C., Bakes, J., Seo, D., Nam, H.J., Baek, S.H., Lim, C.S., Lee, Y.S., and Kaang, B.K. (2014). Optimization of AAV expression cassettes to improve packaging capacity and transgene expression in neurons. Mol Brain 7, 17.

Christie, J.M., Gawthorne, J., Young, G., Fraser, N.J., and Roe, A.J. (2012). LOV to BLUF: flavoprotein contributions to the optogenetic toolkit. Molecular plant 5, 533-544.

Christie, J.M., Salomon, M., Nozue, K., Wada, M., and Briggs, W.R. (1999). LOV (light, oxygen, or voltage) domains of the blue-light photoreceptor phototropin (nph1): binding sites for the chromophore flavin mononucleotide. Proceedings of the National Academy of Sciences of the United States of America 96, 8779-8783.

Chu, N., Salguero, A.L., Liu, A.Z., Chen, Z., Dempsey, D.R., Ficarro, S.B., Alexander, W.M., Marto, J.A., Li, Y., Amzel, L.M., *et al.* (2018). Akt Kinase Activation Mechanisms Revealed Using Protein Semisynthesis. Cell 174, 897-907 e814.

Cohen-Cory, S., Kidane, A.H., Shirkey, N.J., and Marshak, S. (2010). Brain-derived neurotrophic factor and the development of structural neuronal connectivity. Developmental neurobiology 70, 271-288.

Colgan, L.A., Hu, M., Misler, J.A., Parra-Bueno, P., Moran, C.M., Leitges, M., and Yasuda, R. (2018). PKCalpha integrates spatiotemporally distinct Ca(2+) and autocrine BDNF signaling to facilitate synaptic plasticity. Nature neuroscience 21, 1027-1037.

Collingridge, G.L., Kehl, S.J., and McLennan, H. (1983). Excitatory amino acids in synaptic transmission in the Schaffer collateral-commissural pathway of the rat hippocampus. The Journal of physiology 334, 33-46.

Connor, B., Young, D., Yan, Q., Faull, R.L., Synek, B., and Dragunow, M. (1997). Brain-derived neurotrophic factor is reduced in Alzheimer's disease. Brain Res Mol Brain Res 49, 71-81.

Coultrap, S.J., and Bayer, K.U. (2011). Improving a natural CaMKII inhibitor by random and rational design. PloS one 6, e25245.

Crary J. F., Shao Ch. Y., Mirra S. S., Hernandez A. I., and Sacktor T. C. (2006). Atypical Protein Kinase C in Neurodegenerative Disease I: PKMX Aggregates With Limbic Neurofibrillary Tangles and AMPA Receptors in Alzheimer Disease. J Neuropathol Exp Neurol 65, 319-326.

Crick, F. (1999). The impact of molecular biology on neuroscience. Philosophical transactions of the Royal Society of London Series B, Biological sciences 354, 2021-2025.

Crick, F.H. (1979). Thinking about the brain. Sci Am 241, 219-232.

Cunningham, M.E., and Greene, L.A. (1998). A function-structure model for NGF-activated TRK. Embo J 17, 7282-7293.

Cunningham, M.E., Stephens, R.M., Kaplan, D.R., and Greene, L.A. (1997). Autophosphorylation of activation loop tyrosines regulates signaling by the TRK nerve growth factor receptor. J Biol Chem 272, 10957-10967.

Davis, M., Rainnie, D., and Cassell, M. (1994). Neurotransmission in the rat amygdala related to fear and anxiety. Trends Neurosci 17, 208-214.

De Wit, J., Eggers, R., Evers, R., Castren, E., and Verhaagen, J. (2006). Long-term adeno-associated viral vector-mediated expression of truncated TrkB in the adult rat facial nucleus

results in motor neuron degeneration. The Journal of neuroscience : the official journal of the Society for Neuroscience 26, 1516-1530.

Deisseroth, K. (2011). Optogenetics. Nature methods 8, 26-29.

Del Castillo, J., and Katz, B. (1954). Quantal components of the end-plate potential. The Journal of physiology 124, 560-573.

Dikic, I., Schlessinger, J., and Lax, I. (1994). PC12 cells overexpressing the insulin receptor undergo insulin-dependent neuronal differentiation. Current biology : CB 4, 702-708.

Dingledine, R., Borges, K., Bowie, D., and Traynelis, S.F. (1999). The glutamate receptor ion channels. Pharmacol Rev 51, 7-61.

Disatnik, M.H., Hernandez-Sotomayor, S.M., Jones, G., Carpenter, G., and Mochly-Rosen, D. (1994). Phospholipase C-gamma 1 binding to intracellular receptors for activated protein kinase C. Proceedings of the National Academy of Sciences of the United States of America 91, 559-563.

Dombert, B., Balk, S., Luningschror, P., Moradi, M., Sivadasan, R., Saal-Bauernschubert, L., and Jablonka, S. (2017). BDNF/trkB Induction of Calcium Transients through Cav2.2 Calcium Channels in Motoneurons Corresponds to F-actin Assembly and Growth Cone Formation on beta2-Chain Laminin (221). Frontiers in molecular neuroscience 10, 346.

Donnelly, M.L., Luke, G., Mehrotra, A., Li, X., Hughes, L.E., Gani, D., and Ryan, M.D. (2001). Analysis of the aphthovirus 2A/2B polyprotein 'cleavage' mechanism indicates not a proteolytic reaction, but a novel translational effect: a putative ribosomal 'skip'. J Gen Virol 82, 1013-1025.

Douglas, R.M., and Goddard, G.V. (1975). Long-term potentiation of the perforant path-granule cell synapse in the rat hippocampus. Brain research 86, 205-215.

Duan, L., Hope, J.M., Guo, S., Ong, Q., Francois, A., Kaplan, L., Scherrer, G., and Cui, B. (2018). Optical Activation of TrkA Signaling. ACS Synth Biol 7, 1685-1693.

Easton, J.B., Moody, N.M., Zhu, X., and Middlemas, D.S. (1999). Brain-derived neurotrophic factor induces phosphorylation of fibroblast growth factor receptor substrate 2. J Biol Chem 274, 11321-11327.

Ebner, M., Lucic, I., Leonard, T.A., and Yudushkin, I. (2017). PI(3,4,5)P3 Engagement Restricts Akt Activity to Cellular Membranes. Mol Cell 65, 416-431 e416.

Egan, S.E., Giddings, B.W., Brooks, M.W., Buday, L., Sizeland, A.M., and Weinberg, R.A. (1993). Association of Sos Ras exchange protein with Grb2 is implicated in tyrosine kinase signal transduction and transformation. Nature 363, 45-51.

Elgersma, Y., and Silva, A.J. (1999). Molecular mechanisms of synaptic plasticity and memory. Current opinion in neurobiology 9, 209-213.

Emery, P., So, W.V., Kaneko, M., Hall, J.C., and Rosbash, M. (1998). CRY, a Drosophila clock and light-regulated cryptochrome, is a major contributor to circadian rhythm resetting and photosensitivity. Cell 95, 669-679.

English, J.D., and Sweatt, J.D. (1997). A requirement for the mitogen-activated protein kinase cascade in hippocampal long term potentiation. J Biol Chem 272, 19103-19106.

Erdogan, B., Ebbert, P.T., and Lowery, L.A. (2016). Using Xenopus laevis retinal and spinal neurons to study mechanisms of axon guidance in vivo and in vitro. Seminars in cell & developmental biology 51, 64-72.

Errington, M.L., Galley, P.T., and Bliss, T.V. (2003). Long-term potentiation in the dentate gyrus of the anaesthetized rat is accompanied by an increase in extracellular glutamate: real-time measurements using a novel dialysis electrode. Philosophical transactions of the Royal Society of London Series B, Biological sciences 358, 675-687.

Escandon, E., Soppet, D., Rosenthal, A., Mendoza-Ramirez, J.L., Szonyi, E., Burton, L.E., Henderson, C.E., Parada, L.F., and Nikolics, K. (1994). Regulation of neurotrophin receptor expression during embryonic and postnatal development. The Journal of neuroscience : the official journal of the Society for Neuroscience 14, 2054-2068.

Ferrer, I., Goutan, E., Marin, C., Rey, M.J., and Ribalta, T. (2000). Brain-derived neurotrophic factor in Huntington disease. Brain research 866, 257-261.

Forbes, E.M., Thompson, A.W., Yuan, J., and Goodhill, G.J. (2012). Calcium and cAMP levels interact to determine attraction versus repulsion in axon guidance. Neuron 74, 490-503.

Frerking, M., Malenka, R.C., and Nicoll, R.A. (1998). Brain-derived neurotrophic factor (BDNF) modulates inhibitory, but not excitatory, transmission in the CA1 region of the hippocampus. Journal of neurophysiology 80, 3383-3386.

Gartner, A., Polnau, D.G., Staiger, V., Sciarretta, C., Minichiello, L., Thoenen, H., Bonhoeffer, T., and Korte, M. (2006). Hippocampal long-term potentiation is supported by presynaptic and postsynaptic tyrosine receptor kinase B-mediated phospholipase Cgamma signaling. The Journal of neuroscience : the official journal of the Society for Neuroscience 26, 3496-3504.

Gasperini, R., Choi-Lundberg, D., Thompson, M.J., Mitchell, C.B., and Foa, L. (2009). Homer regulates calcium signalling in growth cone turning. Neural Dev 4, 29.

Giese, K.P., Fedorov, N.B., Filipkowski, R.K., and Silva, A.J. (1998). Autophosphorylation at Thr286 of the alpha calcium-calmodulin kinase II in LTP and learning. Science 279, 870-873.

Gomes, R.A., Hampton, C., El-Sabeawy, F., Sabo, S.L., and McAllister, A.K. (2006). The dynamic distribution of TrkB receptors before, during, and after synapse formation between cortical neurons. The Journal of neuroscience : the official journal of the Society for Neuroscience 26, 11487-11500.

Gross, G.G., Junge, J.A., Mora, R.J., Kwon, H.B., Olson, C.A., Takahashi, T.T., Liman, E.R., Ellis-Davies, G.C., McGee, A.W., Sabatini, B.L., *et al.* (2013). Recombinant probes for visualizing endogenous synaptic proteins in living neurons. Neuron 78, 971-985.

Gruart, A., Sciarretta, C., Valenzuela-Harrington, M., Delgado-Garcia, J.M., and Minichiello, L. (2007). Mutation at the TrkB PLC{gamma}-docking site affects hippocampal LTP and associative learning in conscious mice. Learn Mem 14, 54-62.

Grusch, M., Schelch, K., Riedler, R., Reichhart, E., Differ, C., Berger, W., Ingles-Prieto, A., and Janovjak, H. (2014). Spatio-temporally precise activation of engineered receptor tyrosine kinases by light. Embo J 33, 1713-1726.

Guiton, M., Gunn-Moore, F.J., Stitt, T.N., Yancopoulos, G.D., and Tavare, J.M. (1994). Identification of in vivo brain-derived neurotrophic factor-stimulated autophosphorylation

sites on the TrkB receptor tyrosine kinase by site-directed mutagenesis. J Biol Chem 269, 30370-30377.

Guntas, G., Hallett, R.A., Zimmerman, S.P., Williams, T., Yumerefendi, H., Bear, J.E., and Kuhlman, B. (2015). Engineering an improved light-induced dimer (iLID) for controlling the localization and activity of signaling proteins. Proceedings of the National Academy of Sciences of the United States of America 112, 112-117.

Hallett, R.A., Zimmerman, S.P., Yumerefendi, H., Bear, J.E., and Kuhlman, B. (2016). Correlating in Vitro and in Vivo Activities of Light-Inducible Dimers: A Cellular Optogenetics Guide. ACS Synth Biol 5, 53-64.

Han, K.A., Woo, D., Kim, S., Choii, G., Jeon, S., Won, S.Y., Kim, H.M., Heo, W.D., Um, J.W., and Ko, J. (2016). Neurotrophin-3 Regulates Synapse Development by Modulating TrkC-PTPsigma Synaptic Adhesion and Intracellular Signaling Pathways. The Journal of neuroscience : the official journal of the Society for Neuroscience 36, 4816-4831.

Harper, S.M., Neil, L.C., and Gardner, K.H. (2003). Structural basis of a phototropin light switch. Science 301, 1541-1544.

Harward, S.C., Hedrick, N.G., Hall, C.E., Parra-Bueno, P., Milner, T.A., Pan, E., Laviv, T., Hempstead, B.L., Yasuda, R., and McNamara, J.O. (2016). Autocrine BDNF-TrkB signalling within a single dendritic spine. Nature 538, 99-103.

Hayashi-Takagi, A., Yagishita, S., Nakamura, M., Shirai, F., Wu, Y.I., Loshbaugh, A.L., Kuhlman, B., Hahn, K.M., and Kasai, H. (2015). Labelling and optical erasure of synaptic memory traces in the motor cortex. Nature 525, 333-338.

Hebb, D.O. (1949). Neurology, 4th edition. Can J Psychology 3, 241-242.

Heldt, S.A., Zimmermann, K., Parker, K., Gaval, M., Weinshenker, D., and Ressler, K.J. (2014). BDNF deletion or TrkB impairment in amygdala inhibits both appetitive and aversive learning. The Journal of neuroscience : the official journal of the Society for Neuroscience 34, 2444-2450.

Holehonnur, R., Lella, S.K., Ho, A., Luong, J.A., and Ploski, J.E. (2015). The production of viral vectors designed to express large and difficult to express transgenes within neurons. Mol Brain 8, 12.

Holgado-Madruga, M., Moscatello, D.K., Emlet, D.R., Dieterich, R., and Wong, A.J. (1997). Grb2-associated binder-1 mediates phosphatidylinositol 3-kinase activation and the promotion of cell survival by nerve growth factor. Proceedings of the National Academy of Sciences of the United States of America 94, 12419-12424.

Horgan, A.M., and Stork, P.J. (2003). Examining the mechanism of Erk nuclear translocation using green fluorescent protein. Exp Cell Res 285, 208-220.

Huala, E., Oeller, P.W., Liscum, E., Han, I.S., Larsen, E., and Briggs, W.R. (1997). Arabidopsis NPH1: a protein kinase with a putative redox-sensing domain. Science 278, 2120-2123.

Ip, N.Y., Ibanez, C.F., Nye, S.H., McClain, J., Jones, P.F., Gies, D.R., Belluscio, L., Le Beau, M.M., Espinosa, R., 3rd, Squinto, S.P., and et al. (1992). Mammalian neurotrophin-4: structure, chromosomal localization, tissue distribution, and receptor specificity. Proceedings of the National Academy of Sciences of the United States of America 89, 3060-3064.

Jin, W., Lo, T.M., Loh, H.H., and Thayer, S.A. (1994). U73122 inhibits phospholipase C-dependent calcium mobilization in neuronal cells. Brain research 642, 237-243.

Joanne Wang, C., Li, X., Lin, B., Shim, S., Ming, G.L., and Levchenko, A. (2008). A microfluidics-based turning assay reveals complex growth cone responses to integrated gradients of substrate-bound ECM molecules and diffusible guidance cues. Lab Chip 8, 227-237.

Johansen, J.P., Diaz-Mataix, L., Hamanaka, H., Ozawa, T., Ycu, E., Koivumaa, J., Kumar, A., Hou, M., Deisseroth, K., Boyden, E.S., and LeDoux, J.E. (2014). Hebbian and neuromodulatory mechanisms interact to trigger associative memory formation. Proceedings of the National Academy of Sciences of the United States of America 111, E5584-5592.

Kagawa, T., Sakai, T., Suetsugu, N., Oikawa, K., Ishiguro, S., Kato, T., Tabata, S., Okada, K., and Wada, M. (2001). Arabidopsis NPL1: a phototropin homolog controlling the chloroplast high-light avoidance response. Science 291, 2138-2141.

Kanaseki, T., Ikeuchi, Y., Sugiura, H., and Yamauchi, T. (1991). Structural features of Ca2+/calmodulin-dependent protein kinase II revealed by electron microscopy. J Cell Biol 115, 1049-1060.

Kang, H., and Schuman, E.M. (1995). Long-lasting neurotrophin-induced enhancement of synaptic transmission in the adult hippocampus. Science 267, 1658-1662.

Kang, H., Welcher, A.A., Shelton, D., and Schuman, E.M. (1997). Neurotrophins and time: different roles for TrkB signaling in hippocampal long-term potentiation. Neuron 19, 653-664.

Kaplan, D.R., and Miller, F.D. (2000). Neurotrophin signal transduction in the nervous system. Current opinion in neurobiology 10, 381-391.

Katsura, Y., Kubota, H., Kunida, K., Kanno, A., Kuroda, S., and Ozawa, T. (2015). An optogenetic system for interrogating the temporal dynamics of Akt. Sci Rep 5, 14589.

Kawano, F., Suzuki, H., Furuya, A., and Sato, M. (2015). Engineered pairs of distinct photoswitches for optogenetic control of cellular proteins. Nature communications 6, 6256.

Kennedy, M.J., Hughes, R.M., Peteya, L.A., Schwartz, J.W., Ehlers, M.D., and Tucker, C.L. (2010). Rapid blue-light-mediated induction of protein interactions in living cells. Nature methods 7, 973-975.

Khokhlatchev, A.V., Canagarajah, B., Wilsbacher, J., Robinson, M., Atkinson, M., Goldsmith, E., and Cobb, M.H. (1998). Phosphorylation of the MAP kinase ERK2 promotes its homodimerization and nuclear translocation. Cell 93, 605-615.

Kim, H.K., Kim, J.W., Zilberstein, A., Margolis, B., Kim, J.G., Schlessinger, J., and Rhee, S.G. (1991). PDGF stimulation of inositol phospholipid hydrolysis requires PLC-gamma 1 phosphorylation on tyrosine residues 783 and 1254. Cell 65, 435-441.

Kim, N., Kim, J.M., Lee, M., Kim, C.Y., Chang, K.Y., and Heo, W.D. (2014). Spatiotemporal control of fibroblast growth factor receptor signals by blue light. Chemistry & biology 21, 903-912.

Klein, R., Conway, D., Parada, L.F., and Barbacid, M. (1990). The trkB tyrosine protein kinase gene codes for a second neurogenic receptor that lacks the catalytic kinase domain. Cell 61, 647-656.

Klein, R., Nanduri, V., Jing, S.A., Lamballe, F., Tapley, P., Bryant, S., Cordon-Cardo, C., Jones, K.R., Reichardt, L.F., and Barbacid, M. (1991). The trkB tyrosine protein kinase is a receptor for brain-derived neurotrophic factor and neurotrophin-3. Cell 66, 395-403.

Koponen, E., Voikar, V., Riekki, R., Saarelainen, T., Rauramaa, T., Rauvala, H., Taira, T., and Castren, E. (2004). Transgenic mice overexpressing the full-length neurotrophin receptor trkB exhibit increased activation of the trkB-PLCgamma pathway, reduced anxiety, and facilitated learning. Mol Cell Neurosci 26, 166-181.

Korte, M., Carroll, P., Wolf, E., Brem, G., Thoenen, H., and Bonhoeffer, T. (1995). Hippocampal long-term potentiation is impaired in mice lacking brain-derived neurotrophic factor. Proceedings of the National Academy of Sciences of the United States of America 92, 8856-8860.

Korte, M., Griesbeck, O., Gravel, C., Carroll, P., Staiger, V., Thoenen, H., and Bonhoeffer, T. (1996). Virus-mediated gene transfer into hippocampal CA1 region restores long-term potentiation in brain-derived neurotrophic factor mutant mice. Proceedings of the National Academy of Sciences of the United States of America 93, 12547-12552.

Korte, M., Kang, H., Bonhoeffer, T., and Schuman, E. (1998). A role for BDNF in the late-phase of hippocampal long-term potentiation. Neuropharmacology 37, 553-559.

Korte, M., Minichiello, L., Klein, R., and Bonhoeffer, T. (2000). Shc-binding site in the TrkB receptor is not required for hippocampal long-term potentiation. Neuropharmacology 39, 717-724.

Korte, M., and Schmitz, D. (2016). Cellular and System Biology of Memory: Timing, Molecules, and Beyond. Physiol Rev 96, 647-693.

Kovalchuk, Y., Hanse, E., Kafitz, K.W., and Konnerth, A. (2002). Postsynaptic Induction of BDNF-Mediated Long-Term Potentiation. Science 295, 1729-1734.

Kryl, D., Yacoubian, T., Haapasalo, A., Castren, E., Lo, D., and Barker, P.A. (1999). Subcellular localization of full-length and truncated Trk receptor isoforms in polarized neurons and epithelial cells. The Journal of neuroscience : the official journal of the Society for Neuroscience 19, 5823-5833.

Kugler, S., Kilic, E., and Bahr, M. (2003a). Human synapsin 1 gene promoter confers highly neuron-specific long-term transgene expression from an adenoviral vector in the adult rat brain depending on the transduced area. Gene Ther 10, 337-347.

Kugler, S., Lingor, P., Scholl, U., Zolotukhin, S., and Bahr, M. (2003b). Differential transgene expression in brain cells in vivo and in vitro from AAV-2 vectors with small transcriptional control units. Virology 311, 89-95.

Kyriakis, J.M., App, H., Zhang, X.F., Banerjee, P., Brautigan, D.L., Rapp, U.R., and Avruch, J. (1992). Raf-1 activates MAP kinase-kinase. Nature 358, 417-421.

Kyung, T., Lee, S., Kim, J.E., Cho, T., Park, H., Jeong, Y.M., Kim, D., Shin, A., Kim, S., Baek, J., *et al.* (2015). Optogenetic control of endogenous Ca(2+) channels in vivo. Nat Biotechnol 33, 1092-1096.

Lad, S.P., and Neet, K.E. (2003). Activation of the mitogen-activated protein kinase pathway through p75NTR: a common mechanism for the neurotrophin family. J Neurosci Res 73, 614-626.

Lee, S.J., and Yasuda, R. (2009). Spatiotemporal Regulation of Signaling in and out of Dendritic Spines: CaMKII and Ras. Open Neurosci J 3, 117-127.

Leonard, A.S., Lim, I.A., Hemsworth, D.E., Horne, M.C., and Hell, J.W. (1999). Calcium/calmodulin-dependent protein kinase II is associated with the N-methyl-D-aspartate receptor. Proceedings of the National Academy of Sciences of the United States of America 96, 3239-3244.

Leopold, A.V., Chernov, K.G., and Verkhusha, V.V. (2018). Optogenetically controlled protein kinases for regulation of cellular signaling. Chem Soc Rev 47, 2454-2484.

Lessmann, V., Gottmann, K., and Heumann, R. (1994). BDNF and NT-4/5 enhance glutamatergic synaptic transmission in cultured hippocampal neurones. Neuroreport 6, 21-25.

Levine, E.S., Crozier, R.A., Black, I.B., and Plummer, M.R. (1998). Brain-derived neurotrophic factor modulates hippocampal synaptic transmission by increasing N-methyl-D-aspartic acid receptor activity. Proceedings of the National Academy of Sciences of the United States of America 95, 10235-10239.

Levine, E.S., Dreyfus, C.F., Black, I.B., and Plummer, M.R. (1995). Brain-derived neurotrophic factor rapidly enhances synaptic transmission in hippocampal neurons via postsynaptic tyrosine kinase receptors. Proceedings of the National Academy of Sciences of the United States of America 92, 8074-8077.

Li, D., Shatos, M.A., Hodges, R.R., and Dartt, D.A. (2013). Role of PKCalpha activation of Src, PI-3K/AKT, and ERK in EGF-stimulated proliferation of rat and human conjunctival goblet cells. Investigative ophthalmology & visual science 54, 5661-5674.

Li, Y., Wang, D., Li, Y., Chu, H., Zhang, L., Hou, M., Jiang, X., Chen, Z., Su, B., and Sun, T. (2017). Pre-synaptic TrkB in basolateral amygdala neurons mediates BDNF signaling transmission in memory extinction. Cell Death Dis 8, e2959.

Lin, J.Y. (2013). Production and validation of recombinant adeno-associated virus for channelrhodopsin expression in neurons. Methods Mol Biol 998, 401-415.

Lin, J.Y., Lin, M.Z., Steinbach, P., and Tsien, R.Y. (2009). Characterization of engineered channelrhodopsin variants with improved properties and kinetics. Biophys J 96, 1803-1814.

Lin, P.Y., Kavalali, E.T., and Monteggia, L.M. (2018). Genetic Dissection of Presynaptic and Postsynaptic BDNF-TrkB Signaling in Synaptic Efficacy of CA3-CA1 Synapses. Cell Rep 24, 1550-1561.

Lin, S.Y., Wu, K., Levine, E.S., Mount, H.T., Suen, P.C., and Black, I.B. (1998). BDNF acutely increases tyrosine phosphorylation of the NMDA receptor subunit 2B in cortical and hippocampal postsynaptic densities. Brain Res Mol Brain Res 55, 20-27.

Lin, Y.C., Nihongaki, Y., Liu, T.Y., Razavi, S., Sato, M., and Inoue, T. (2013). Rapidly reversible manipulation of molecular activity with dual chemical dimerizers. Angew Chem Int Ed Engl 52, 6450-6454.

Ling, D.S., Benardo, L.S., Serrano, P.A., Blace, N., Kelly, M.T., Crary, J.F., and Sacktor, T.C. (2002). Protein kinase Mzeta is necessary and sufficient for LTP maintenance. Nature neuroscience 5, 295-296.

Lisman, J., Schulman, H., and Cline, H. (2002). The molecular basis of CaMKII function in synaptic and behavioural memory. Nature reviews Neuroscience 3, 175-190.

Lisman, J., Yasuda, R., and Raghavachari, S. (2012). Mechanisms of CaMKII action in long-term potentiation. Nature reviews Neuroscience 13, 169-182.

Liu, H., Liu, B., Zhao, C., Pepper, M., and Lin, C. (2011). The action mechanisms of plant cryptochromes. Trends Plant Sci 16, 684-691.

Liu, H., Yu, X., Li, K., Klejnot, J., Yang, H., Lisiero, D., and Lin, C. (2008a). Photoexcited CRY2 interacts with CIB1 to regulate transcription and floral initiation in Arabidopsis. Science 322, 1535-1539.

Liu, S.J., and Zukin, R.S. (2007). Ca2+-permeable AMPA receptors in synaptic plasticity and neuronal death. Trends Neurosci 30, 126-134.

Liu, Y.F., Chen, H.I., Yu, L., Kuo, Y.M., Wu, F.S., Chuang, J.I., Liao, P.C., and Jen, C.J. (2008b). Upregulation of hippocampal TrkB and synaptotagmin is involved in treadmill exercise-enhanced aversive memory in mice. Neurobiology of learning and memory 90, 81-89.

Liu, Z., Chen, O., Wall, J.B.J., Zheng, M., Zhou, Y., Wang, L., Ruth Vaseghi, H., Qian, L., and Liu, J. (2017). Systematic comparison of 2A peptides for cloning multi-genes in a polycistronic vector. Sci Rep 7, 2193.

Lledo, P.M., Hjelmstad, G.O., Mukherji, S., Soderling, T.R., Malenka, R.C., and Nicoll, R.A. (1995). Calcium/calmodulin-dependent kinase II and long-term potentiation enhance synaptic transmission by the same mechanism. Proceedings of the National Academy of Sciences of the United States of America 92, 11175-11179.

Lombroso, P., and Ogren, M. (2009). Learning and memory, part II: molecular mechanisms of synaptic plasticity. J Am Acad Child Adolesc Psychiatry 48, 5-9.

Lomo, T. (2015). Scientific Discoveries: What Is Required for Lasting Impact. Annu Rev Physiol.

Losi, A., Gardner, K.H., and Moglich, A. (2018). Blue-Light Receptors for Optogenetics. Chem Rev 118, 10659-10709.

Lucic, I., Rathinaswamy, M.K., Truebestein, L., Hamelin, D.J., Burke, J.E., and Leonard, T.A. (2018). Conformational sampling of membranes by Akt controls its activation and inactivation. Proceedings of the National Academy of Sciences of the United States of America 115, E3940-E3949.

Luscher, C., and Malenka, R.C. (2011). Drug-evoked synaptic plasticity in addiction: from molecular changes to circuit remodeling. Neuron 69, 650-663.

Luscher, C., and Malenka, R.C. (2012). NMDA receptor-dependent long-term potentiation and long-term depression (LTP/LTD). Cold Spring Harb Perspect Biol 4.

Lynch, G., Larson, J., Kelso, S., Barrionuevo, G., and Schottler, F. (1983). Intracellular injections of EGTA block induction of hippocampal long-term potentiation. Nature 305, 719-721.

Madden, D.R. (2002). The structure and function of glutamate receptor ion channels. Nature reviews Neuroscience 3, 91-101.

Malenka, R.C., and Bear, M.F. (2004). LTP and LTD: an embarrassment of riches. Neuron 44, 5-21.

Malenka, R.C., and Nicoll, R.A. (1999). Neuroscience - Long-term potentiation - A decade of progress? Science 285, 1870-1874.

Malinow, R., and Miller, J.P. (1986). Postsynaptic hyperpolarization during conditioning reversibly blocks induction of long-term potentiation. Nature 320, 529-530.

Man, H.Y., Wang, Q., Lu, W.Y., Ju, W., Ahmadian, G., Liu, L., D'Souza, S., Wong, T.P., Taghibiglou, C., Lu, J., *et al.* (2003). Activation of PI3-kinase is required for AMPA receptor insertion during LTP of mEPSCs in cultured hippocampal neurons. Neuron 38, 611-624.

Maren, S. (1999). Long-term potentiation in the amygdala: a mechanism for emotional learning and memory. Trends Neurosci 22, 561-567.

Maren, S., and Fanselow, M.S. (1995). Synaptic plasticity in the basolateral amygdala induced by hippocampal formation stimulation in vivo. The Journal of neuroscience : the official journal of the Society for Neuroscience 15, 7548-7564.

Martinez-Galvez, G., Zambrano, J.M., Diaz Soto, J.C., Zhan, W.Z., Gransee, H.M., Sieck, G.C., and Mantilla, C.B. (2016). TrkB gene therapy by adeno-associated virus enhances recovery after cervical spinal cord injury. Exp Neurol 276, 31-40.

Matsuzaki, M., Honkura, N., Ellis-Davies, G.C., and Kasai, H. (2004). Structural basis of long-term potentiation in single dendritic spines. Nature 429, 761-766.

Mauceri, D., Cattabeni, F., Di Luca, M., and Gardoni, F. (2004). Calcium/calmodulin-dependent protein kinase II phosphorylation drives synapse-associated protein 97 into spines. J Biol Chem 279, 23813-23821.

Mayford, M., Siegelbaum, S.A., and Kandel, E.R. (2012). Synapses and memory storage. Cold Spring Harb Perspect Biol 4.

McCarty, J.H., and Feinstein, S.C. (1998). Activation loop tyrosines contribute varying roles to TrkB autophosphorylation and signal transduction. Oncogene 16, 1691-1700.

McKernan, M.G., and Shinnick-Gallagher, P. (1997). Fear conditioning induces a lasting potentiation of synaptic currents in vitro. Nature 390, 607-611.

Mei, F., Nagappan, G., Ke, Y., Sacktor, T.C., and Lu, B. (2011). BDNF facilitates L-LTP maintenance in the absence of protein synthesis through PKMzeta. PloS one 6, e21568.

Meis, S., Endres, T., and Lessmann, V. (2012). Postsynaptic BDNF signalling regulates long-term potentiation at thalamo-amygdala afferents. The Journal of physiology 590, 193-208.

Middlemas, D.S., Lindberg, R.A., and Hunter, T. (1991). trkB, a neural receptor protein-tyrosine kinase: evidence for a full-length and two truncated receptors. Mol Cell Biol 11, 143-153.

Middlemas, D.S., Meisenhelder, J., and Hunter, T. (1994). Identification of TrkB autophosphorylation sites and evidence that phospholipase C-gamma 1 is a substrate of the TrkB receptor. J Biol Chem 269, 5458-5466.

Miller, S.G., and Kennedy, M.B. (1986). Regulation of brain type II Ca2+/calmodulin-dependent protein kinase by autophosphorylation: a Ca2+-triggered molecular switch. Cell 44, 861-870.

Ming, G., Lohof, A.M., and Zheng, J.Q. (1997). Acute morphogenic and chemotropic effects of neurotrophins on cultured embryonic Xenopus spinal neurons. The Journal of neuroscience : the official journal of the Society for Neuroscience 17, 7860-7871.

Minichiello, L. (2009). TrkB signalling pathways in LTP and learning. Nature reviews Neuroscience 10, 850-860.

Minichiello, L., Calella, A.M., Medina, D.L., Bonhoeffer, T., Klein, R., and Korte, M. (2002). Mechanism of TrkB-mediated hippocampal long-term potentiation. Neuron 36, 121-137.

Minichiello, L., Casagranda, F., Tatche, R.S., Stucky, C.L., Postigo, A., Lewin, G.R., Davies, A.M., and Klein, R. (1998). Point mutation in trkB causes loss of NT4-dependent neurons without major effects on diverse BDNF responses. Neuron 21, 335-345.

Minichiello, L., Korte, M., Wolfer, D., Kuhn, R., Unsicker, K., Cestari, V., Rossi-Arnaud, C., Lipp, H.P., Bonhoeffer, T., and Klein, R. (1999). Essential role for TrkB receptors in hippocampus-mediated learning. Neuron 24, 401-414.

Mitchell, C.B., Gasperini, R.J., Small, D.H., and Foa, L. (2012). STIM1 is necessary for store-operated calcium entry in turning growth cones. J Neurochem 122, 1155-1166.

Mizuno, M., Yamada, K., He, J., Nakajima, A., and Nabeshima, T. (2003). Involvement of BDNF receptor TrkB in spatial memory formation. Learn Mem 10, 108-115.

Mizuno, M., Yamada, K., Olariu, A., Nawa, H., and Nabeshima, T. (2000). Involvement of brain-derived neurotrophic factor in spatial memory formation and maintenance in a radial arm maze test in rats. The Journal of neuroscience : the official journal of the Society for Neuroscience 20, 7116-7121.

Molnar, E. (2011). Long-term potentiation in cultured hippocampal neurons. Seminars in cell & developmental biology 22, 506-513.

Murakoshi, H., Shin, M.E., Parra-Bueno, P., Szatmari, E.M., Shibata, A.C.E., and Yasuda, R. (2017). Kinetics of Endogenous CaMKII Required for Synaptic Plasticity Revealed by Optogenetic Kinase Inhibitor. Neuron 94, 690.

Musumeci, G., Sciarretta, C., Rodriguez-Moreno, A., Al Banchaabouchi, M., Negrete-Diaz, V., Costanzi, M., Berno, V., Egorov, A.V., von Bohlen Und Halbach, O., Cestari, V., *et al.* (2009). TrkB modulates fear learning and amygdalar synaptic plasticity by specific docking sites. The Journal of neuroscience : the official journal of the Society for Neuroscience 29, 10131-10143.

Myers, J.B., Zaegel, V., Coultrap, S.J., Miller, A.P., Bayer, K.U., and Reichow, S.L. (2017). The CaMKII holoenzyme structure in activation-competent conformations. Nature communications 8, 15742.

Nabavi, S., Fox, R., Proulx, C.D., Lin, J.Y., Tsien, R.Y., and Malinow, R. (2014). Engineering a memory with LTD and LTP. Nature 511, 348-352.

Nagy, V., Bozdagi, O., Matynia, A., Balcerzyk, M., Okulski, P., Dzwonek, J., Costa, R.M., Silva, A.J., Kaczmarek, L., and Huntley, G.W. (2006). Matrix metalloproteinase-9 is required for hippocampal late-phase long-term potentiation and memory. The Journal of neuroscience : the official journal of the Society for Neuroscience 26, 1923-1934.

Nicoll, R.A. (2003). Expression mechanisms underlying long-term potentiation: a postsynaptic view. Philosophical transactions of the Royal Society of London Series B, Biological sciences 358, 721-726.

Nowak, L., Bregestovski, P., Ascher, P., Herbet, A., and Prochiantz, A. (1984). Magnesium gates glutamate-activated channels in mouse central neurones. Nature 307, 462-465.

Oikawa, K., Odero, G.L., Platt, E., Neuendorff, M., Hatherell, A., Bernstein, M.J., and Albensi, B.C. (2012). NF-kappaB p50 subunit knockout impairs late LTP and alters long term memory in the mouse hippocampus. Bmc Neurosci 13, 45.

Opazo, P., Labrecque, S., Tigaret, C.M., Frouin, A., Wiseman, P.W., De Koninck, P., and Choquet, D. (2010). CaMKII triggers the diffusional trapping of surface AMPARs through phosphorylation of stargazin. Neuron 67, 239-252.

Osborne, A., Wang, A.X.Z., Tassoni, A., Widdowson, P.S., and Martin, K.R. (2018). Design of a Novel Gene Therapy Construct to Achieve Sustained Brain-Derived Neurotrophic Factor Signaling in Neurons. Hum Gene Ther 29, 828-841.

Otani, K., Okada, M., and Yamawaki, H. (2017). Diverse distribution of tyrosine receptor kinase B isoforms in rat multiple tissues. J Vet Med Sci 79, 1516-1523.

Pan, W., Banks, W.A., Fasold, M.B., Bluth, J., and Kastin, A.J. (1998). Transport of brain-derived neurotrophic factor across the blood-brain barrier. Neuropharmacology 37, 1553-1561.

Panja, D., Dagyte, G., Bidinosti, M., Wibrand, K., Kristiansen, A.M., Sonenberg, N., and Bramham, C.R. (2009). Novel translational control in Arc-dependent long term potentiation consolidation in vivo. J Biol Chem 284, 31498-31511.

Paoletti, P., Bellone, C., and Zhou, Q. (2013). NMDA receptor subunit diversity: impact on receptor properties, synaptic plasticity and disease. Nature reviews Neuroscience 14, 383-400.

Parain, K., Murer, M.G., Yan, Q., Faucheux, B., Agid, Y., Hirsch, E., and Raisman-Vozari, R. (1999). Reduced expression of brain-derived neurotrophic factor protein in Parkinson's disease substantia nigra. Neuroreport 10, 557-561.

Park, H., Kim, N.Y., Lee, S., Kim, N., Kim, J., and Heo, W.D. (2017). Optogenetic protein clustering through fluorescent protein tagging and extension of CRY2. Nature communications 8, 30.

Park, H., Popescu, A., and Poo, M.M. (2014). Essential role of presynaptic NMDA receptors in activity-dependent BDNF secretion and corticostriatal LTP. Neuron 84, 1009-1022.

Patterson, S.L., Abel, T., Deuel, T.A., Martin, K.C., Rose, J.C., and Kandel, E.R. (1996). Recombinant BDNF rescues deficits in basal synaptic transmission and hippocampal LTP in BDNF knockout mice. Neuron 16, 1137-1145.

Patterson, S.L., Grover, L.M., Schwartzkroin, P.A., and Bothwell, M. (1992). Neurotrophin expression in rat hippocampal slices: a stimulus paradigm inducing LTP in CA1 evokes increases in BDNF and NT-3 mRNAs. Neuron 9, 1081-1088.

Paul, J., Gottmann, K., and Lessmann, V. (2001). NT-3 regulates BDNF-induced modulation of synaptic transmission in cultured hippocampal neurons. Neuroreport 12, 2635-2639.

Pham, E., Mills, E., and Truong, K. (2011). A synthetic photoactivated protein to generate local or global Ca(2+) signals. Chemistry & biology 18, 880-890.

Pilakka-Kanthikeel, S., Atluri, V.S., Sagar, V., Saxena, S.K., and Nair, M. (2013). Targeted brain derived neurotropic factors (BDNF) delivery across the blood-brain barrier for neuro-protection using magnetic nano carriers: an in-vitro study. PloS one 8, e62241.

Purves, D. (2004). Neuroscience, 3rd edn (Sunderland, Mass.: Sinauer Associates, Publishers).

Rattiner, L.M., Davis, M., French, C.T., and Ressler, K.J. (2004). Brain-derived neurotrophic factor and tyrosine kinase receptor B involvement in amygdala-dependent fear conditioning. The Journal of neuroscience : the official journal of the Society for Neuroscience 24, 4796-4806.

Rattiner, L.M., Davis, M., and Ressler, K.J. (2005). Brain-derived neurotrophic factor in amygdala-dependent learning. The Neuroscientist : a review journal bringing neurobiology, neurology and psychiatry 11, 323-333.

Redchuk, T.A., Omelina, E.S., Chernov, K.G., and Verkhusha, V.V. (2017). Near-infrared optogenetic pair for protein regulation and spectral multiplexing. Nat Chem Biol 13, 633-639.

Reichhart, E., Ingles-Prieto, A., Tichy, A.M., McKenzie, C., and Janovjak, H. (2016). A Phytochrome Sensory Domain Permits Receptor Activation by Red Light. Angew Chem Int Ed Engl 55, 6339-6342.

Rogan, M.T., and LeDoux, J.E. (1995). LTP is accompanied by commensurate enhancement of auditory-evoked responses in a fear conditioning circuit. Neuron 15, 127-136.

Rogan, M.T., Staubli, U.V., and LeDoux, J.E. (1997). Fear conditioning induces associative long-term potentiation in the amygdala. Nature 390, 604-607.

Royo, N.C., Vandenberghe, L.H., Ma, J.Y., Hauspurg, A., Yu, L., Maronski, M., Johnston, J., Dichter, M.A., Wilson, J.M., and Watson, D.J. (2008). Specific AAV serotypes stably transduce primary hippocampal and cortical cultures with high efficiency and low toxicity. Brain research 1190, 15-22.

Saarelainen, T., Pussinen, R., Koponen, E., Alhonen, L., Wong, G., Sirvio, J., and Castren, E. (2000). Transgenic mice overexpressing truncated trkB neurotrophin receptors in neurons have impaired long-term spatial memory but normal hippocampal LTP. Synapse 38, 102-104.

Sakai, T., Kagawa, T., Kasahara, M., Swartz, T.E., Christie, J.M., Briggs, W.R., Wada, M., and Okada, K. (2001). Arabidopsis nph1 and npl1: blue light receptors that mediate both phototropism and chloroplast relocation. Proceedings of the National Academy of Sciences of the United States of America 98, 6969-6974.

Sambrook, J., Fritsch, E.F., and Maniatis, T. (1989). Molecular cloning: a laboratory manual (New York: Cold Spring Harbor Laboratory Press).

Sanhueza, M., Fernandez-Villalobos, G., Stein, I.S., Kasumova, G., Zhang, P., Bayer, K.U., Otmakhov, N., Hell, J.W., and Lisman, J. (2011). Role of the CaMKII/NMDA receptor complex in the maintenance of synaptic strength. The Journal of neuroscience : the official journal of the Society for Neuroscience 31, 9170-9178.

Schildt, S., Endres, T., Lessmann, V., and Edelmann, E. (2013). Acute and chronic interference with BDNF/TrkB-signaling impair LTP selectively at mossy fiber synapses in the CA3 region of mouse hippocampus. Neuropharmacology 71, 247-254.

Schneider, R., and Schweiger, M. (1991). A novel modular mosaic of cell adhesion motifs in the extracellular domains of the neurogenic trk and trkB tyrosine kinase receptors. Oncogene 6, 1807-1811.

Schwartzkroin, P.A., and Wester, K. (1975). Long-lasting facilitation of a synaptic potential following tetanization in the in vitro hippocampal slice. Brain research 89, 107-119.

Shatos, M.A., Hodges, R.R., Bair, J.A., Lashkari, K., and Dartt, D.A. (2009). Stimulatory role of PKCalpha in extracellular regulated kinase 1/2 pathway in conjunctival goblet cell proliferation. Investigative ophthalmology & visual science 50, 1619-1625.

Shen, J., and Maruyama, I.N. (2012). Brain-derived neurotrophic factor receptor TrkB exists as a preformed dimer in living cells. J Mol Signal 7, 2.

Shu, X., Royant, A., Lin, M.Z., Aguilera, T.A., Lev-Ram, V., Steinbach, P.A., and Tsien, R.Y. (2009). Mammalian expression of infrared fluorescent proteins engineered from a bacterial phytochrome. Science 324, 804-807.

Sinnen, B.L., Bowen, A.B., Forte, J.S., Hiester, B.G., Crosby, K.C., Gibson, E.S., Dell'Acqua, M.L., and Kennedy, M.J. (2017). Optogenetic Control of Synaptic Composition and Function. Neuron 93, 646-660 e645.

Slaughter, M. (2002). Basic concepts in neuroscience : a student's survival guide (New York: McGraw-Hill).

Southam, K.A., Stennard, F., Pavez, C., and Small, D.H. (2018). Knockout of Amyloid beta Protein Precursor (APP) Expression Alters Synaptogenesis, Neurite Branching and Axonal Morphology of Hippocampal Neurons. Neurochem Res.

Stephens, R.M., Loeb, D.M., Copeland, T.D., Pawson, T., Greene, L.A., and Kaplan, D.R. (1994). Trk receptors use redundant signal transduction pathways involving SHC and PLC-gamma 1 to mediate NGF responses. Neuron 12, 691-705.

Sutherland, D.J., Pujic, Z., and Goodhill, G.J. (2014). Calcium signaling in axon guidance. Trends Neurosci 37, 424-432.

Szymczak, A.L., and Vignali, D.A. (2005). Development of 2A peptide-based strategies in the design of multicistronic vectors. Expert Opin Biol Ther 5, 627-638.

Taslimi, A., Vrana, J.D., Chen, D., Borinskaya, S., Mayer, B.J., Kennedy, M.J., and Tucker, C.L. (2014). An optimized optogenetic clustering tool for probing protein interaction and function. Nature communications 5, 4925.

Taslimi, A., Zoltowski, B., Miranda, J.G., Pathak, G.P., Hughes, R.M., and Tucker, C.L. (2016). Optimized second-generation CRY2-CIB dimerizers and photoactivatable Cre recombinase. Nat Chem Biol 12, 425-430.

Thiede-Stan, N.K., and Schwab, M.E. (2015). Attractive and repulsive factors act through multi-subunit receptor complexes to regulate nerve fiber growth. J Cell Sci 128, 2403-2414.

Todderud, G., Wahl, M.I., Rhee, S.G., and Carpenter, G. (1990). Stimulation of phospholipase C-gamma 1 membrane association by epidermal growth factor. Science 249, 296-298.

Traverse, S., Seedorf, K., Paterson, H., Marshall, C.J., Cohen, P., and Ullrich, A. (1994). EGF triggers neuronal differentiation of PC12 cells that overexpress the EGF receptor. Current biology : CB 4, 694-701.

Tucker, C.L., Vrana, J.D., and Kennedy, M.J. (2014). Tools for controlling protein interactions using light. Curr Protoc Cell Biol 64, 17 16 11-20.

Varnai, P., Hunyady, L., and Balla, T. (2009). STIM and Orai: the long-awaited constituents of store-operated calcium entry. Trends Pharmacol Sci 30, 118-128.

Vest, R.S., Davies, K.D., O'Leary, H., Port, J.D., and Bayer, K.U. (2007). Dual mechanism of a natural CaMKII inhibitor. Mol Biol Cell 18, 5024-5033.

Vignoli, B., Battistini, G., Melani, R., Blum, R., Santi, S., Berardi, N., and Canossa, M. (2016). Peri-Synaptic Glia Recycles Brain-Derived Neurotrophic Factor for LTP Stabilization and Memory Retention. Neuron 92, 873-887.

Vitureira, N., and Goda, Y. (2013). Cell biology in neuroscience: the interplay between Hebbian and homeostatic synaptic plasticity. J Cell Biol 203, 175-186.

Vojtek, A.B., Hollenberg, S.M., and Cooper, J.A. (1993). Mammalian Ras interacts directly with the serine/threonine kinase Raf. Cell 74, 205-214.

Volk, L.J., Bachman, J.L., Johnson, R., Yu, Y., and Huganir, R.L. (2013). PKM-zeta is not required for hippocampal synaptic plasticity, learning and memory. Nature 493, 420-423.

Wahl, M.I., Jones, G.A., Nishibe, S., Rhee, S.G., and Carpenter, G. (1992). Growth factor stimulation of phospholipase C-gamma 1 activity. Comparative properties of control and activated enzymes. J Biol Chem 267, 10447-10456.

Wang, Y., and Wang, Z. (2003). Regulation of EGF-induced phospholipase C-gamma1 translocation and activation by its SH2 and PH domains. Traffic 4, 618-630.

Welm, B.E., Freeman, K.W., Chen, M., Contreras, A., Spencer, D.M., and Rosen, J.M. (2002). Inducible dimerization of FGFR1: development of a mouse model to analyze progressive transformation of the mammary gland. J Cell Biol 157, 703-714.

Wen, Z., Guirland, C., Ming, G.L., and Zheng, J.Q. (2004). A CaMKII/calcineurin switch controls the direction of Ca(2+)-dependent growth cone guidance. Neuron 43, 835-846.

Whitlock, J.R., Heynen, A.J., Shuler, M.G., and Bear, M.F. (2006). Learning induces long-term potentiation in the hippocampus. Science 313, 1093-1097.

Widmer, H.R., Kaplan, D.R., Rabin, S.J., Beck, K.D., Hefti, F., and Knusel, B. (1993). Rapid phosphorylation of phospholipase C gamma 1 by brain-derived neurotrophic factor and neurotrophin-3 in cultures of embryonic rat cortical neurons. J Neurochem 60, 2111-2123.

Wu, J., Liu, L., Matsuda, T., Zhao, Y., Rebane, A., Drobizhev, M., Chang, Y.F., Araki, S., Arai, Y., March, K., *et al.* (2013). Improved orange and red Ca(2)+/- indicators and photophysical considerations for optogenetic applications. ACS Chem Neurosci 4, 963-972.

Wu, Y.I., Frey, D., Lungu, O.I., Jaehrig, A., Schlichting, I., Kuhlman, B., and Hahn, K.M. (2009). A genetically encoded photoactivatable Rac controls the motility of living cells. Nature 461, 104-108.

Xu, B., Gottschalk, W., Chow, A., Wilson, R.I., Schnell, E., Zang, K., Wang, D., Nicoll, R.A., Lu, B., and Reichardt, L.F. (2000). The role of brain-derived neurotrophic factor receptors in the mature hippocampus: modulation of long-term potentiation through a presynaptic mechanism involving TrkB. The Journal of neuroscience : the official journal of the Society for Neuroscience 20, 6888-6897.

Yang, H.W., Shin, M.G., Lee, S., Kim, J.R., Park, W.S., Cho, K.H., Meyer, T., and Heo, W.D. (2012). Cooperative activation of PI3K by Ras and Rho family small GTPases. Mol Cell 47, 281-290.

Ying, S.W., Futter, M., Rosenblum, K., Webber, M.J., Hunt, S.P., Bliss, T.V., and Bramham, C.R. (2002). Brain-derived neurotrophic factor induces long-term potentiation in intact adult hippocampus: requirement for ERK activation coupled to CREB and upregulation of Arc synthesis. The Journal of neuroscience : the official journal of the Society for Neuroscience 22, 1532-1540.

Yumerefendi, H., Dickinson, D.J., Wang, H., Zimmerman, S.P., Bear, J.E., Goldstein, B., Hahn, K., and Kuhlman, B. (2015). Control of Protein Activity and Cell Fate Specification via Light-Mediated Nuclear Translocation. PloS one 10, e0128443.

Zahavi, E.E., Steinberg, N., Altman, T., Chein, M., Joshi, Y., Gradus-Pery, T., and Perlson, E. (2018). The receptor tyrosine kinase TrkB signals without dimerization at the plasma membrane. Sci Signal 11.

Zakharenko, S.S., Patterson, S.L., Dragatsis, I., Zeitlin, S.O., Siegelbaum, S.A., Kandel, E.R., and Morozov, A. (2003). Presynaptic BDNF required for a presynaptic but not postsynaptic component of LTP at hippocampal CA1-CA3 synapses. Neuron 39, 975-990.

Zhang, F., Wang, L.P., Brauner, M., Liewald, J.F., Kay, K., Watzke, N., Wood, P.G., Bamberg, E., Nagel, G., Gottschalk, A., and Deisseroth, K. (2007). Multimodal fast optical interrogation of neural circuitry. Nature 446, 633-639.

Zhang, H., Zhang, C., Vincent, J., Zala, D., Benstaali, C., Sainlos, M., Grillo-Bosch, D., Daburon, S., Coussen, F., Cho, Y., *et al.* (2018). Modulation of AMPA receptor surface diffusion restores hippocampal plasticity and memory in Huntington's disease models. Nature communications 9, 4272.

Zhang, K., Duan, L., Ong, Q., Lin, Z., Varman, P.M., Sung, K., and Cui, B. (2014). Light-mediated kinetic control reveals the temporal effect of the Raf/MEK/ERK pathway in PC12 cell neurite outgrowth. PloS one 9, e92917.

Zheng, F., Soellner, D., Nunez, J., and Wang, H. (2008). The basal level of intracellular calcium gates the activation of phosphoinositide 3-kinase-Akt signaling by brain-derived neurotrophic factor in cortical neurons. J Neurochem 106, 1259-1274.

Zhou, X.X., Pan, M., and Lin, M.Z. (2015). Investigating neuronal function with optically controllable proteins. Frontiers in molecular neuroscience 8, 37.